Experimental and analytical investigations on flashing-induced instabilities in natural circulation two-phase systems

- applications to the startup of Boiling Water Reactors -

Annalisa Manera

The research described in this thesis was performed at the Department of Reactor Physics of the Interfaculty Reactor Institute, Delft University of Technology, Mekelweg 15, 2629 JB, Delft, The Netherlands.

Part of this work was carried out within the framework of the Natural Circulation and Stability Performance of Boiling Water Reactors (NACUSP) project, which is financed by the Fifth Framework Program of the European Community.

Experimental and analytical investigations on flashing-induced instabilities in natural circulation two-phase systems

- applications to the startup of Boiling Water Reactors -

Proefschrift

ter verkrijging van de graad van doctor
aan de Technische Universiteit Delft,
op gezag van de Rector Magnificus prof. dr. ir. J.T. Fokkema,
voorzitter van het College van Promoties,
in het openbaar te verdedigen op maandag 8 september 2003 om 10.30 uur
door

Annalisa Manera

Ingegnere Nucleare
geboren te Bari (Italië)

Dit proefschrift is goedgekeurd door de promotoren:
Prof. dr. ir. H. van Dam
Prof. dr. ir. T.H.J.J. van der Hagen

Samenstelling promotiecommissie:

Reactor Magnificus, voorzitter	
Prof. dr. ir. H. van Dam	Technische Universiteit Delft, promotor
Prof. dr. ir. T.H.J.J. van der Hagen	Technische Universiteit Delft, promotor
Prof. dr. ir. A.H.M. Verkooijen	Technische Universiteit Delft
Prof. dr. R.F. Mudde	Technische Universiteit Delft
Prof. dr. ir. Th.H. van der Meer	Universiteit Twente
Prof. dr. G. Yadigaroglu	Swiss Federal Institute of Technology (ETH), Zurich

ISBN: 90-73861-44-6

Printed in The Netherlands

This thesis consists of an extended summary and the following papers:

I. A. Manera, H.-M. Prasser, T.H.J.J. van der Hagen, R.F. Mudde and W.J.M. de Kruijf, "A comparison of void-fraction measurements during flashing-induced instabilities obtained with a wire-mesh sensor and a gamma-transmission set-up", *Proc. 4th International Conference on Multiphase Flow (ICMF-2001)*, May 27 - June 1, New Orleans, USA (2001).

II. A. Manera, H.-M. Prasser, U. Rohde, T.H.J.J. van der Hagen, "Assessment of void-fraction correlations and drift-flux models applied to stationary and transient flashing flow in a vertical pipe", to be submitted to *International Journal of Heat and Mass Transfer*.

III. A. Manera, H.-M. Prasser, D. Lucas, T.H.J.J. van der Hagen, "Flow pattern visualization and bubbles size distributions during stationary and transient flashing flow in a vertical pipe", to be submitted to *International Journal of Multiphase Flow.*

IV. A. Manera, T.H.J.J. van der Hagen, "Stability of natural-circulation-cooled Boiling Water Reactors during startup: experimental results", *Nuclear Technology*, **143**, pp. 77-88 (2003).

V. A. Manera, U. Rohde, H.-M. Prasser, T.H.J.J. van der Hagen, "Modelling of flashing-induced instabilities in the start-up phase of natural circulation BWRs using the two-phase flow code FLOCAL", to be submitted to *Nuclear Technology.*

VI. D.D.B. van Bragt, W.J.M. de Kruijf, A. Manera, T.H.J.J. van der Hagen, H. van Dam, "Analytical modelling of flashing-induced instabilities in a natural circulation cooled boiling water reactor", *Nuclear Engineering and Design*, **215**, pp. 87-98 (2002).

Contents

SUMMARY **III**

SAMENVATTING **V**

PUBLICATIONS NOT INCLUDED IN THIS THESIS **VII**

CHAPTER 1 INTRODUCTION **1**
1.1. THE DESIGN OF SIMPLIFIED BWRS 1
1.2. THE START-UP PHASE AND THE FLASHING PHENOMENON 2
1.3. LITERATURE SURVEY ON FLASHING-INDUCED INSTABILITY 3
1.3.1. Experimental work 3
1.3.2. Analytical and numerical work 3
1.4. MOTIVATIONS FOR FURTHER WORK 4
1.5. OUTLINE OF THIS THESIS 5

CHAPTER 2 THE EXPERIMENTAL FACILITY CIRCUS **7**
2.1. DESIGN CHARACTERISTICS OF THE FACILITY 7
2.2. INSTRUMENTATION 7
2.2.1. The conductivity needle-probes with integrated thermocouple 8
2.2.2. The gamma set-up for chordal void fraction measurements 8
2.2.3. The wire-mesh sensor 9
2.2.4. The lda set-up 12
2.2.5. Signals acquisition system and synchronization 13

CHAPTER 3 CHARACTERISTICS OF VOID-FRACTION PRODUCTION DURING FLASHING **15**
3.1. SUITABILITY OF DRIFT-FLUX MODELS FOR VOID-FRACTION PREDICTION DURING FLASHING 15
3.1.1. Stationary conditions 16
3.1.2. Transient conditions 16
3.2. FLOW PATTERN VISUALIZATION 19

CHAPTER 4 EXPERIMENTS ON FLASHING-INDUCED FLOW INSTABILITIES **21**
4.1. PHENOMENOLOGY OF FLASHING-INDUCED INSTABILITIES 21
4.2. CHARACTERISTICS OF FLASHING-INDUCED INSTABILITIES AND STABILITY MAPS 22

CHAPTER 5 MODELLING OF FLASHING-INDUCED FLOW INSTABILITIES **25**
5.1. CHARACTERISTICS OF THERMAL-HYDRAULIC CODES (FROM HEM TO 6-EQUATIONS MODELS) 25
5.2. FLOCAL: A 4-EQUATIONS TWO-PHASE FLOW CODE 26
5.2.1. Main code improvements 27

CHAPTER 6 CODE VALIDATION **31**
6.1. NODALIZATION ADOPTED 31
6.2. COMPARISON WITH EXPERIMENTAL DATA 31
6.2.1. Void-fraction evolution in the adiabatic section 32
6.2.2. Quantitative comparison with the experimental results 33
6.2.3. Effect of turbulent diffusion caused by temperature gradients 35

CHAPTER 7 START-UP PROCEDURES **37**
7.1. INTRODUCTION 37
7.2. THE START-UP PROCEDURE OF THE DODEWAARD REACTOR 37
7.3. BRIEF LITERATURE SURVEY ON START-UP PROCEDURES FOR NATURAL-CIRCULATION BWRS 38
7.4. OPTIMAL START-UP PROCEDURES 39

CONCLUSIONS **45**

NOMENCLATURE **47**

ABBREVIATIONS **48**

REFERENCES **49**

ACKNOWLEDGMENT **53**

CURRICULUM VITAE **55**

PAPERS I-VI

Summary

In this thesis the phenomena of flashing and flashing-induced instabilities in natural circulation two-phase systems are discussed. Special emphasis is given to the natural circulation Boiling Water Reactor (BWR), a new reactor design that has been chosen by General Electric as one of the upcoming workhorses of the nuclear industry.

It is shown both experimentally and by means of thermal-hydraulic models that flashing, i.e. steam production in adiabatic conditions, plays an important role during the start-up phase of this type of reactor. In particular, it is demonstrated that under specific conditions (at low power and low pressure) flashing may trigger self-sustained flow oscillations. To tackle the problem of flashing-induced instability and gain experimental insight in the phenomenon, a dedicated facility (CIRCUS) was designed and optimised.

Two experimental campaigns carried out at the CIRCUS facility are discussed. The first addresses the characteristics of flashing-induced instabilities. Flow oscillations were recorded at different conditions (controlling parameters being the power, the inlet subcooling and the pressure) and stability maps were derived. It is shown that an unstable region has to be traversed to transit from the stable single-phase to two-phase operation. Increasing pressure has a stabilizing effect on the instability, decreasing both the amplitude of the flow oscillations and the extension of the operational unstable region. Also, decreasing the compressible volume in the steam dome has a stabilizing effect, but this is not as pronounced as the effect of the pressure. In addition, experimental evidence was found of the thermal non-equilibrium between liquid and vapour phase in the first phase of the flow oscillations.
The second experimental campaign is focused on the characteristics of flashing flows in a vertical pipe. Such a study is unique in this field since no study is reported in literature dealing with this topic. Special emphasis is given to the prediction of the void production during flashing and to the suitability of drift-flux models when applied to stationary and transient flashing flows. Such a study requires the measurement of local void fraction and steam velocity. These quantities are evaluated on the basis of wire-mesh sensor data. Methods based on cross-correlation techniques and drift-flux models are used to estimate the time-dependent steam velocity during flashing-induced flow oscillations. The void-fraction data obtained with wire-mesh sensors, combined with the steam velocity measurements, are used to achieve a complete three-dimensional reconstruction of the flow pattern during transient flashing flow. The evolution of bubble size distributions is studied. The experimental radial distribution of steam bubbles in stationary flow is compared with the results obtained by means of an equilibrium model. The good agreement obtained suggests that radial equilibrium of bubbles can establish even in flows which are not fully developed in axial direction.

Flashing-induced flow oscillations are simulated by means of a four-equation model, with the code FLOCAL, developed at the Forschungszentrum Rossendorf (FZR, Germany). The code is able to consider thermal non-equilibrium between the liquid and vapour phases and different phases velocity via a drift-flux model. The code is improved by introducing new models to take into account additional physical phenomena that play an important role in the low-pressure low-power operational region of natural circulation two-phase systems (among others, the impact of thermal structures and turbulent diffusion induced by temperature gradients).
The code is benchmarked successfully against the experimental data collected at the CIRCUS facility and helps increasing the physical insight into the complex process of flashing-induced instabilities.

Finally, a novel start-up procedure is proposed for natural circulation BWRs. The suggested procedure does not require external pressurization of the reactor vessel. A simplified quasi-static model is developed to check whether a significant flow rate can be ensured during the entire start-

up phase and whether the rate of steam production is sufficient to pressurize the system in a reasonable time.

In conclusion, flashing is found to play a fundamental role in natural circulation two-phase systems when operated at low pressures. The physical origin of flow oscillations induced by flashing is understood and clarified and the applicability of one-dimensional models is proven to be satisfactory in the geometrical scales examined. However, the problem of scalability remains open, since three-dimensional effects cannot be neglected if information for industrial applications (large scale problems) is desired.

Samenvatting

In dit proefschrift worden de verschijnselen van “flashing” en “flashing-geïnduceerde” instabiliteiten in natuurlijke-circulatie tweefasen systemen bestudeerd. Speciale aandacht wordt besteed aan natuurlijke-circulatie kokendwaterreactoren (BWRs), een nieuw reactorontwerp dat door General Electric is gekozen als een van de mogelijke toekomstige werkpaarden voor de nucleaire industrie.

Er wordt zowel experimenteel als met thermohydraulische modellen aangetoond dat flashing, stoomproductie in adiabatische condities, een belangrijke rol speelt tijdens de opstartfase van dit type reactoren. Tevens wordt aangetoond dat onder bepaalde condities (bij laag vermogen en lage druk) zichzelf instandhoudende oscillaties kunnen ontstaan. Om het probleem van flashing-geïnduceerde instabiliteit aan te pakken en om experimenteel inzicht in dit verschijnsel te verkrijgen is voor dit doeleinde een opstelling (CIRCUS genaamd) ontworpen en geoptimaliseerd.

Twee experimentele programma’s, uitgevoerd met de CIRCUS opstelling, worden besproken. Het eerste richt zich op de karakteristieken van flashing-geïnduceerde instabiliteiten. Stromingsoscillaties zijn opgemeten bij verschillende condities (met variërend vermogen, inlaat subcooling en druk) en stabiliteitsdiagrammen zijn daaruit afgeleid. Het is aangetoond dat een gebied van instabiliteit wordt doorkruist om van stabiele eenfase stroming tot het tweefasen operationele gebied te komen. Verhogen van de druk heeft een stabiliserend effect wat leidt tot een verkleining van de amplitude van stromingsoscillaties als ook een vergroting van het stabiele gebied. Een verkleining van het samendrukbaar volume in de stoomketel heeft ook een stabiliserend effect maar dit effect is niet zo sterk als het voornoemde effect van drukverhoging. Verder is experimenteel bewijs gevonden voor het thermisch niet-evenwicht tussen de vloeistof- en dampfase gedurende het eerste stadium van stromingsoscillaties. Het tweede experimentele programma richt zich op de karakteristieken van flashing stromingen in een verticale buis. Een dergelijke studie is uniek in zijn soort in dit vakgebied. Speciale aandacht is gegeven aan de voorspelling van de dampfractie tijdens flashing en aan de geschiktheid van driftflux modellen wanneer toegepast op stationaire en transiënte flashing stromingen. Een dergelijke studie vereist meting van de lokale dampfractie en stoomsnelheid. Deze grootheden zijn geëvalueerd op basis van gemeten data afkomstig van een “wire-mesh” sensor. Methoden op basis van cross-correlatie technieken en driftflux modellen zijn gebruikt om de tijdafhankelijke stoomsnelheid tijdens flashing-geïnduceerde stromingsoscillaties te schatten. De dampfractie data verkregen via de wire-mesh sensor, gecombineerd met de stoomsnelheidsmetingen, zijn gebruikt om een complete driedimensionale reconstructie te maken van het stromingspatroon gedurende transiënte flashingstroming. De ontwikkeling van de belgrootteverdeling is bestudeerd. De experimentele radiale distributies van stoombellen in stationaire stroming zijn vergeleken met de resultaten verkregen uit een evenwichtsmodel. De goede overeenkomst suggereert dat radiaal evenwicht van de belverdeling kan ontstaan zelfs in stromingen die niet volledig in axiale richting ontwikkeld zijn.

Flashing-geïnduceerde stromingsoscillaties zijn gesimuleerd d.m.v. een vier-vergelijkingen model met de code FLOCAL, ontwikkeld door het Forschungszentrum Rossendorf (FZR, Duitsland). De code verdisconteert thermisch niet-evenwicht tussen de vloeistof- en dampfasen en de verschilsnelheid tussen de fasen d.m.v. een driftflux model. De code is verbeterd door het introduceren van nieuwe modellen die belangrijke fysische verschijnselen beschrijven in het operationele regime van natuurlijke-circulatie tweefasen systemen onder lage druk en met laag vermogen (o.a. de invloed van thermische structuren en temperatuurgradiënt-geïnduceerde turbulente diffusie). De resultaten van de code zijn vergeleken met experimentele resultaten verkregen van de CIRCUS opstelling en helpt tot het verkrijgen van inzicht in het complexe proces van flashing-geïnduceerde instabiliteiten.

Ten slotte is een nieuwe opstartprocedure voor kokendwaterreactoren voorgesteld. De voorgestelde procedure vereist geen extern opgelegde drukopbouw in het reactorvat. Een versimpeld quasi-statisch model is ontwikkeld om te controleren of voldoende stroming gegarandeerd kan worden tijdens de opstartfase en of de mate van stoomproductie voldoende groot is om het systeem in redelijke tijd op druk te brengen.

Samenvattend speelt flashing een belangrijke rol in natuurlijke-circulatie tweefasen systemen indien deze bij lage druk bedreven worden. De fysische oorzaak van flashing-geïnduceerde stromingsoscillaties is bestudeerd en verduidelijkt. De toepasbaarheid van eendimensionale modellen blijkt toereikend op de bestudeerde schaal. Het probleem van schaalbaarheid blijft echter open, daar driedimensionale effecten niet verwaarloosd kunnen worden indien men informatie wil verkrijgen voor industriële toepassingen (op grote schaal).

PUBLICATIONS NOT INCLUDED IN THIS THESIS

INTERNATIONAL JOURNALS

1. A. Manera, T.H.J.J. van der Hagen, H. van Dam, "On the determination of transit times during flow oscillation by means of noise analysis techniques", submitted to *Ann. Nucl. Energy*.

2. A. Manera, R. Zboray, T.H.J.J. van der Hagen, "Assessment of linear and nonlinear auto-regressive methods for BWR stability monitoring", *Progress in Nuclear Energy* **43**, pp.321-327 (2003).

3. T.H.J.J. van der Hagen, A. Manera, and W.J.M. de Kruijf, "Experiments on flashing and flashing induced instabilities during the start-up of natural-circulation-cooled Boiling Water Reactors", *Archives of Thermodynamics* **23,** 3, 105-118 (2002).

4. W.J.M. de Kruijf, K.C.J. Ketelaar, G. Avakian, P. Gubernatis, D. Caruge, A. Manera, T.H.J.J. van der Hagen, G. Yadigaroglu, G. Dominicus, U. Rohde, H.-M. Prasser, F. Castrillo, M. Huggenberger, D. Hennig, J.L. Munoz-Cobo, C. Aguirre, "Planned experimental studies on natural circulation and stability performance of boiling water reactors in four experimental facilities and first results (NACUSP)", *Nuclear Engineering and Design*, **221**, 241-250 (2003).

5. M. Furuya, A. Manera, D.D.B. van Bragt, T.H.J.J. van der Hagen, W.J.M. de Kruijf, "Effect of liquid density differences on boiling two-phase flow stability", *Journal of Nuclear Science and Technology*, **39**, 10 (2002).

INTERNATIONAL CONFERENCE PROCEEDINGS

1. A. Manera, H.-M. Prasser, T.H.J.J. van der Hagen, "Suitability of drift-flux models, void-fraction evolution and 3D flow pattern visualization during stationary and transient flashing flow in a vertical pipe", *Proc. 10th Int.Topical Meetg. On Nuclear Reactor Thermal Hydraulics*, NURETH-10, October 5-9, Seoul, Korea (2003).

2. A. Manera, U. Rohde, H.-M. Prasser, T.H.J.J. van der Hagen, "Modelling of flashing-induced instabilities in the start-up phase of natural circulation BWRs using the code FLOCAL", *Proc. of 10th Int.Topical Meetg. On Nuclear Reactor Thermal Hydraulics*, NURETH-10, October 5-9, Seoul, Korea (2003).

3. A. Manera, T.H.J.J. van der Hagen, U. Rohde, H.-M. Prasser, "Overview on stability of natural-circulation-cooled Boiling Water Reactors during start-up – an experimental and modeling analysis", *Proc. of Int. Conf. on Global Environment and Advanced Nuclear Power Plants,* GENES4/ANP2003, September 15-19, Kyoto, Japan (2003).

4. F. Schäfer, A. Manera, "Investigation of flashing-induced instabilities at the CIRCUS test facility using the code ATHLET", *Proc. 10th Int.Topical Meetg. On Nuclear Reactor Thermal Hydraulics*, NURETH-10, October 5-9, Seoul, Korea (2003).

5. A. Manera, F. Schäfer, "Experimental and theoretical investigations of flashing induced instabilities at the CIRCUS test facility", *Proc. Jahrestagung Kerntechnik 2003*, Annual Meeting on Nuclear Technology, 20-22 May, Berlin, Germany (2003).

6. K.C.J. Ketelaar, W.J.M. de Kruijf, T. van der Hagen, A. Manera, G. Avakian, P. Gubernatis, D. Caruge, G. Yadigaroglu, G. Dominicus, U. Rohde, H.-M. Prasser, F. Castrillo, M. Huggenberger, D. Hennig, J.L. Munoz-Cobo, C. Aguirre, "Natural Circulation and Stability Performance of BWRs (NACUSP)", in *Proc. FISA 2001 EU Research in reactor safety*, November 12-15, Luxembourgh, EUR 20281, European Communities, pp. 535-546 (2001).

7. H.-M. Prasser, A. Manera, A. Böttger, J. Zschau, "Flow structure during flashing in the CIRCUS test facility modelling the start-up of a Boiling Water Reactor", Institute of Safety Research, Annual Report 2001, Forschungszentrum Rossendorf e.V., Wissenschaftlich-Technische Berichte, FZR-342, pp. 26-34 (2002).

8. T.H.J.J. van der Hagen, A. Manera, and W.J.M. de Kruijf , "Experiments on flashing and flashing induced instabilities during the start-up of natural-circulation-cooled Boiling Water Reactors", *Proc. of HEAT 2002 "3rd International Conference on Transport Phenomena in Multiphase Systems*, June 24-27, Baranów Sandomierski, Poland, Editor: M.E. Poniewski, pp.149-159 (2002). Also in journal.

9. A. Manera, T.H.J.J. van der Hagen, "On stability of natural-circulation-cooled BWRs during start-up (experimental results)", *Proc. of International Conference on Advanced Nuclear Power Plants (ICAPP-2002)*, June 9-13, Hollywood, Florida, on CD, 10 pp (2002). Also in journal.

10. A. Manera, R. Zboray, T.H.J.J. van der Hagen, "Assessment of linear and nonlinear auto-regressive methods for bwr stability monitoring", *Proc. SMORN-8 Symposium on Nuclear Reactor Surveillance and Diagnostics*, May 27-31, Göteborg, Sweden , 2002. Also in journal.

11. A. Manera, H. Hartmann, W.J.M. de Kruijf, T.H.J.J. van der Hagen, R.F. Mudde and D.W. de Haas, "Experimental observations on flashing-induced oscillations in a water/steam natural-circulation loop", *Proc. 4th International Conference on Multiphase Flow (ICMF-2001)*, May 27 - June 1, New Orleans (2001).

12. A. Manera, H. Hartmann, W.J.M. de Kruijf, T.H.J.J. van der Hagen and R.F. Mudde, "Low-pressure dynamics of a natural-circulation two-phase flow loop", *Proc. of the 4th Workshop on Measurement techniques of stationary and transient multiphase flow*, November 16-17, 2000, Rossendorf, Germany, FZR-320 (2001).

13. A. Manera, T.H.J.J. van der Hagen, W.J.M. de Kruijf and H. van Dam, "On the Determination of Transit Times During Flow Oscillations", *Proc. Of IMORN-28*, October 11-13, Athens, Greece, 301-318 (2000).

14. A. Manera, W.J.M. de Kruijf, T.H.J.J. van der Hagen, and R.F. Mudde, "Experiments with the CIRCUS Facility on Flashing-Induced Instabilities During Start-up of Natural-Circulation-Cooled BWRS", *Proc. Int. Top. Meetg. on Advances in Reactor Physics and Mathematics and Computation into the Next Millennium (PHYSOR 2000)*, May 7-11, Pittsburg, USA (paper 27), 12 pages (2000).

15. W.J.M. de Kruijf, T.H.J.J. van der Hagen, R. Zboray, A. Manera and R.F. Mudde, "CIRCUS and DESIRE: Experimental facilities for research on natural-circulation-cooled Boiling Water Reactors", *Proc. IAEA TCM on Natural Circulation Data and Methods for Innovative Nuclear Power Plant Design*, July 18-21, Wenen, IAEA-TECDOC-1281 (2000).

16. W.J.M. de Kruijf, R. Zboray, A. Manera, T.H.J.J. van der Hagen, H. van Dam and R.F. Mudde, "Non-linear characteristics of thermohydraulic instabilities in innovative BWRs", *Proc. of ICENES 2000, 10th International Conference on Emerging Nuclear Energy Systems*, September 25-28, Petten, The Netherlands, pp. 467-476 (2000).

17. M. Furuya, A. Manera, D.D.B. van Bragt, T.H.J.J. van der Hagen and W.J.M. de Kruijf, "Effect of Liquid Density Differences on Two-Phase Flow Instability", *Proc. of 9-th Int. Topical Mtg. On Nuclear Reactor Thermal Hydraulics (NURETH-9)*, October 3-8, San Francisco, USA (1999). Also in Journal.

18. Zboray, A. Manera, W.J.M. de Kruijf, T.H.J.J. van der Hagen, D.D.B. van Bragt and H. van Dam, "Experiments on Non-linear Density-Wave Oscillations in the DESIRE Facility", *Proc. of 9-th Int. Topical Mtg. On Nuclear Reactor Thermal Hydraulics (NURETH-9)*, October 3-8, San Francisco, USA (1999).

19. T.H.J.J. van der Hagen and A. Manera, "The Influence of Carry Under on Natural-Circulation BWR Statics and Dynamics", *Proc. of 9-th Int. Topical Mtg. On Nuclear Reactor Thermal Hydraulics (NURETH-9)*, October 3-8, San Francisco, USA (1999).

20. R. Zboray, A. Manera, T.H.J.J. van der Hagen and W.J.M. de Kruijf, "Destabilizing the DESIRE facility by increasing the riser exit pressure drop", *Proc. of Jahrestagung Kerntechnik '99, Annual meeting on nuclear technology '99*, May 18-21, Karlsruhe, Germany, 79-82 (1999).

REPORTS

1. A. Manera, W.J.M. de Kruijf, "Listing of equations used in DAVID_LP, version 99_2", Interfaculty Reactor Instute, The Netherlands, report by order of Electricité de France, IRI-131-99-009 (2000).

2. A. Manera, W.J.M. de Kruijf, "User manual time domain model for low pressures, DAVID_LP, version 99_2", Interfaculty Reactor Instute, The Netherlands, report by order of Electricité de France, IRI-131-99-010 (2000).

3. W.J.M. de Kruijf, A. Manera, R. Zboray, T.H.J.J. van der Hagen, "ESBWR stability analyses", Interfaculty Reactor Instute, The Netherlands, report by order of Electricité de France, IRI-131-2000-001 (2000).

4. W.J.M. de Kruijf, A. Manera, D.W. de Haas, J.G.F. Schut, T.H.J.J. van der Hagen, R.F. Mudde, H.-M. Prasser, "Description of CIRCUS including test matrix", EU project NACUSP, FIKS-CT2000-00041, D8a (2000).

5. M. Huggenberger, T.H.J.J. van der Hagen, A. Manera, U. Rohde, "Work-package plan WP2", EU project NACUSP, FIKS-CT2000-00041, D07 (2003).

6. T. Sengstag, A. Manera, W.J.M. de Kruijf, "Definition of pre-test calculations for the CIRCUS NACUPS tests", EU project NACUSP, FIKS-CT2000-00041, D9d (2002).

Chapter 1

INTRODUCTION

The modern development of nuclear power plants (NPPs) is characterized by the demand for more economical and reliable reactors, in order to improve the competitiveness of nuclear energy. The economy of existent NPP designs suffers for the complexity of the safety systems (which have to be redundant and diversified). Nuclear reactors can be made more competitive and reliable by adopting a simpler design and passive safety systems. Following this philosophy, the design of natural-circulation BWRs was developed. In this type of reactors the coolant circulation is gravity-driven and is ensured as long as heat is produced in the core (if a sufficient water level is maintained) without the need of any active system. In addition, the main safety systems are based on passive components.
It is expected that the simplicity and passive features of the natural circulation BWRs design might also increase the public acceptance of such type of reactors.

1.1. THE DESIGN OF SIMPLIFIED BWRS

Among the natural-circulation BWRs, the 1.190 MWe ESBWR (European Simplified Boiling Water Reactor) [1] is the most promising candidate. This reactor is based on the design of the 670 MWe SBWR by General Electric (GE).
The pressure vessel of the ESBWR has a diameter of about 7 m and a height of approximately 25 m. The active core length is about 3 m. A scheme of the reactor is presented in Fig. 1. As in forced-circulation BWRs, the steam that is produced in the RPV (reactor pressure vessel) is sent directly to the turbine to produce electricity (direct cycle).

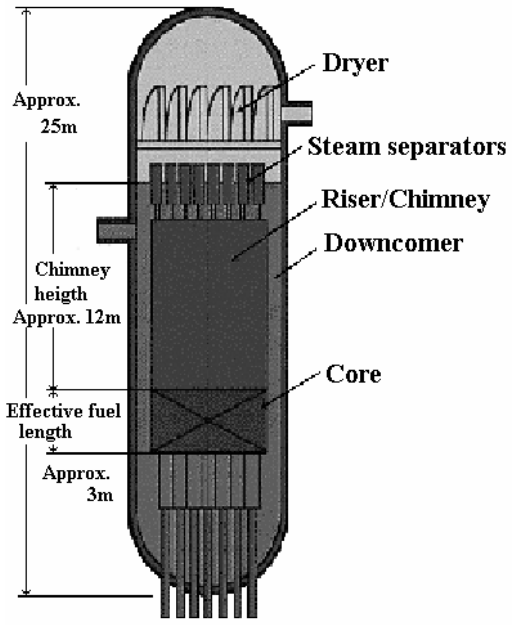

Fig. 1. Scheme of a typical natural circulation BWR. This design refers, in particular, to the ESBWR. Other designs can differ for the dimensions and for the absence of steam separators.

To enhance the flow rate, a long adiabatic pipe (so-called riser or chimney) is needed above the core. In this way the flow and power rates that can be obtained make the reactor still economically interesting. The riser may be partitioned. High flow rate is achieved also by designing a shorter core, to reduce the pressure drops over the fuel assemblies, and by using low pressure loss steam separators. In this way it is possible to reach an average flow rate per fuel bundle two to three times higher than that of a forced-circulation BWR when operated under natural-circulation conditions. However, at nominal conditions the flow rate is lower with respect to forced circulation BWRs, so that a lower power density (~48 kW/l) has to be employed. Consequently, the number of fuel assemblies is increased to ensure the same power output of typical forced circulation BWRs. On the other hand the lower power density allows for longer fuel cycles.
The elimination of the recirculation systems (pumps and related piping and components) simplifies the design and excludes a whole series of transients and initiating events that can lead to accidents (pump trips, LOCAs due to failures of the recirculation piping, etc.). Moreover, the simplicity of the design contributes in shortening significantly the time needed for the reactor construction.
The large RPV volume provides a large reservoir of water above the core. This gives longer periods of time before the action of automatic systems and of the reactor operators is needed during

transients caused by loss of feed-water or LOCAs. In addition, the rate at which the system pressure increases in conditions of isolated reactor (main steam valve closed) is lower.
The main safety systems based on passive components are the isolation condenser system (ICS) that removed the decay-heat when the reactor is isolated, the gravity driven cooling system (GDCS) that provides emergency core cooling in case of LOCAs and the passive containment cooling system (PCCS) that maintains the pressure of the containment within its pressure limits in any situation.

Unfortunately, the innovation of the design has introduced operational uncertainties, especially related to the start-up phase of the reactor, when the system has to pass from single-phase to two-phase operation. In fact, natural circulation systems may exhibit thermal-hydraulic instabilities under low-power and low-pressure conditions. The instabilities in the region between single-phase and stable two-phase natural-circulation mode are mainly induced by flashing in the riser section (i.e. steam[1] production in adiabatic conditions). The feedback between steam generation in the riser and buoyancy of the natural-circulation loop may give rise, under specific conditions, to flow oscillations. These oscillations are undesired, since they make the start-up of the reactor rather difficult and may lead to thermal fatigue and vibrations of the internal structures of the pressure vessel.
The flashing phenomenon and the flow instabilities that it induces in natural-circulation loops are the main object of this thesis.

1.2. THE START-UP PHASE AND THE FLASHING PHENOMENON

Flashing refers to steam production that takes place without the need of an external heat source. Steam production occurs due to superheating of the liquid phase (for instance if the local pressure decreases or if hot liquid is transported from a higher to a lower pressure region).

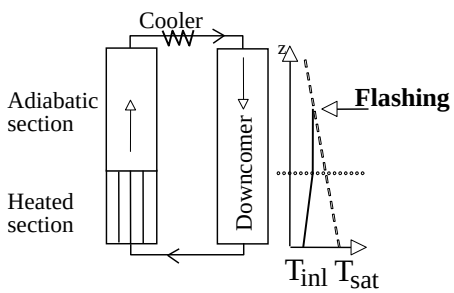

Fig. 2. Flashing in the riser section. Flashing (steam production) occurs when the coolant reaches saturation conditions in the adiabatic section. Note that the saturation temperature decreases considerably along the vertical axis when the system operates at low pressures.

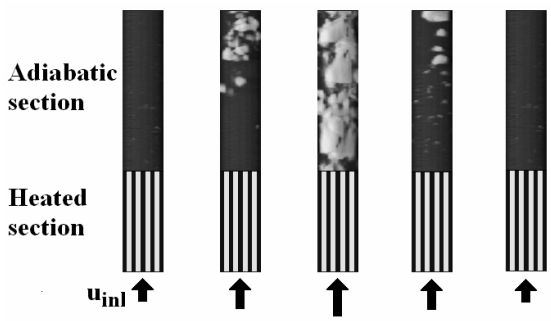

Fig. 3 Flashing in dynamic conditions. The steam production in the adiabatic section causes an increase of flow rate which in turn will lead to a decrease of the coolant temperature. If the coolant temperature drops below saturation, flashing is suppressed and the flow rate decreases.

At start-up conditions both system pressure and heating power are low. The low system pressure implies large differences in saturation temperature between the inlet and the outlet of the adiabatic section (in a natural circulation BWR this difference can easily exceed 10 K). At low powers the coolant, which is heated up in the heated section of the natural circulation loop, may not reach saturation conditions in the core itself. However, due to the strong variation of saturation temperature along the system, flashing can occur in the adiabatic section (see Fig. 2), leading to an enhancement of the natural circulation flow rate. In dynamic conditions this phenomenon can cause self-sustained flow oscillations, as schematically illustrated in Fig. 3: if only single-phase is present in the system, the natural-circulation flow rate is low. If the temperature of the coolant entering the adiabatic section is high enough, flashing takes place, as shown in Fig. 3. The occurrence of

[1] A more general expression widely used in literature to indicate the gas-phase of a two-phase mixture is *void*. Correspondently, the steam fraction present in a steam/liquid mixture is also referred to as *void fraction*.

flashing will cause a decrease of the pressure below the location of bubbles formation. The decrease in local pressure will trigger additional steam formation, leading to a large variation of the flow rate in the system. The increase of flow rate will cause a subsequent decrease of the coolant temperature entering the adiabatic section, so that the process of flashing may eventually stop and the flow rate will be low again. The coolant temperature entering the adiabatic section will therefore increase, leading to a new flashing cycle. In this way a self-sustained flow oscillation will take place.
The occurrence of flashing will also cause an increase of the water level in the steam dome, leading to an increase of the system pressure due to the compression of the steam cushion present in the steam dome. This will result in a decrease of the steam production in the riser. Hence, the presence of the steam dome has a feedback effect that reduces the amplitude of the flow oscillations.
The fluid travelling time in the heated section and the travelling time of enthalpy perturbations in the adiabatic section of the loop play an important role in determining the period of the oscillation.
A detailed analysis of the mechanism and characteristics of the instability is reported in Paper IV.

1.3. LITERATURE SURVEY ON FLASHING-INDUCED INSTABILITY

1.3.1. EXPERIMENTAL WORK

Flashing-induced flow oscillations were first pointed out by the pioneering work of Wissler and colleagues [2], who reported about flashing-induced instabilities[2] in a natural circulation steam/water loop in 1956. Since then, several experimental studies have addressed stability of natural circulation two-phase flow systems at low pressure [3-8] emphasizing that well-defined start-up procedures are needed to cross the instability region during the transition from single-phase to two-phase flow operation. In particular, experiments performed on the DANTON facility [3] have shown that the pressure increase caused by the steam produced in the reactor vessel is not sufficient to suppress completely the flow oscillations and that without external pressurization an instability region between single-phase and two-phase operation has necessarily to be crossed. Unstable behaviour at low power and low pressure has also been encountered at specific conditions explored in an experimental campaign at the Dutch natural circulation BWR Dodewaard [9].

1.3.2. ANALYTICAL AND NUMERICAL WORK

Generally, simplified models are developed in order to gain more insight in the physics of a given process. However, not many of these models have been reported in literature, which can deal with flashing-induced instabilities. Inada et al. [10] reported a simplified model based on HEM (Homogeneous Equilibrium Model) formulation, which includes pressure-dependent thermodynamic properties along the vertical axis of the system but excludes single-phase natural circulation (i.e. in their model the flow rate is different from zero only when steam is present in the system). Though the model is able to predict stability boundaries fairly well compared with experimental data, the code cannot be used to simulate start-up procedures since it has been developed in frequency domain. Van Bragt et al. [11] extended the model by Inada et al. in time-domain, but the energy balance is linearised to derive a simple differential equation for the dynamics of the boiling boundary. In this way, important non-linear effects might be excluded. Moreover, single-phase circulation is not taken into account as in the original model from Inada et el. Consequently, far from the stability boundary, where alternation between single- and two-phase flow circulation and non-linear effects become important, the code cannot reproduce correctly flashing-induced instabilities.
Sawai et al. [12] developed a time-domain model also based on HEM formulation. Despite the authors claim that the model was developed for low-pressure conditions, they do not consider pressure changes along the axis of the system, which are fundamental for the reproduction of

[2] These oscillations are in reality *stable limit cycles*, i.e. the state variables vary periodically and their amplitude remains bounded. Strictly speaking thus, they cannot be regarded to as *instabilities*. Nevertheless they are undesired and in literature are commonly referred to in this way.

flashing-induced instabilities. As a consequence of the strong simplification Sawai et al. do not find any flashing-type flow oscillations, but they find unstable behaviour related to flow pattern transition from churn/annular to slug flow. This transition however is not observed experimentally during the start-up phase of natural-circulation systems [5, 13].
Chatoorgoon [14] developed a simple time-domain code, SPORT, also based on HEM formulation, which includes single-phase circulation and pressure-dependent thermodynamic properties along the axis of the system. Chatoorgoon shows that the code is able to reproduce flashing instabilities at low pressure and low power, but no systematic parametric study is performed and no comparison with experimental results is shown.
Even state-of-the-art thermal-hydraulic codes have often given unsatisfactory and sometimes even contradictory results. Cheng et al. reported on RAMONA-4B [15] applied to the start-up transient of the SBWR and did not find flashing-induced instabilities. The inability of finding flashing-induced oscillations is not surprising since in this code local physical properties are evaluated on system averaged transient pressure without taking into account the effect of local pressure. Paniagua et al. [16] developed a modified version of RAMONA-4B that includes local pressure dependencies and an explicit numerical scheme to avoid numerical damping of the solution. Their simulations with the improved code show occurrence of geysering-type instabilities, but the quantitative comparison with experimental results from Wang et al. [17] gives an under-prediction of the flow-rate oscillation amplitude. They do not report about flashing-induced instabilities.
The 7-equations thermal-hydraulic code MONA-2.2 developed by Studsvik-Scandpower [18] has been proven to be unable to reproduce any flashing at low pressure due to numerical problems [19]. Cheung and Rao [20] performed simulations of the start-up of the ESBWR with TRACG code and claim that no instabilities are found during the entire start-up procedure. Andersen et al. [21] reproduced flashing-induced instabilities with TRACG and found excellent qualitative agreement with the different kinds of flow oscillations obtained experimentally at the CRIEPI (Central Research Institute of Electric Power Industry, Japan) test facility. In the cases they examined the amplitude of flow oscillations is always underestimated, but no systematic quantitative comparison is reported. Moreover, they do not find any unstable region at low power in contradiction with experimental results.
Tiselj and Cerne [22] showed that RELAP5 cannot deal with flashing, since the results become strongly dependent on the integration time step used for the simulations. On the contrary, Analytis and Lübbesmeyer [23] managed to reproduce instabilities at low pressure with TRAC-BF1/v2001.2 and RELAP5/MOD3.3, but the two codes give completely different predictions and the reason for the discrepancy is not found.

1.4. MOTIVATIONS FOR FURTHER RESEARCH

The phenomena involved during the start-up of natural circulation BWRs are not yet fully understood and there is a need for more experimental investigations. In addition it is necessary to develop and test models for the low-power low-pressure operational region of natural circulation two-phase systems, if reliable simulations of start-up procedures for the ESBWR are to be achieved and if guidelines for the operation of the reactor have to be set up. No computer code has been proven to be reliable enough at low-pressure and low-power conditions to predict the behaviour of the ESBWR during the start-up procedure with reasonable confidence. As a matter of fact, very few codes have been found to be able to reproduce the physics behind flashing-induced flow oscillations and to resemble the available experimental data.
To cope with the lack of experiments and models, a project (NACUSP) was started in December 2000 within the European-Union Fifth Framework Program. One of the main aims of the NACUSP project is the understanding of the physics of the phenomena involved during the start-up phase of natural-circulation BWRs, providing a large experimental database and validating state-of-the-art thermal-hydraulic codes in the low-pressure, low-power operational region of these reactors. The work presented in this thesis has been carried out within this project.

1.5. OUTLINE OF THIS THESIS

A brief description of the experimental set-up CIRCUS and its instrumentation is presented in Chapter 2. Special attention is given to the wire-mesh sensor, an advanced two-phase flow instrumentation by which most of the experimental results reported in this thesis have been obtained. A comparison of this measuring technique with gamma-transmission set-ups is the main subject of Paper I.
In Chapter 3 the characteristics of spatial and time evolution of void-fraction during flashing in upward flow are discussed. Both stationary and transient flows are considered for the analysis. The chapter is based on the results reported in Paper II and Paper III.
Chapter 4 deals with the mechanism and characteristics of flashing-induced instabilities in two-phase natural circulation systems. More details can be found in Paper IV.
The modelling problems and needs are discussed in Chapter 5, where the FLOCAL code is presented. The model, originally developed at the Forschungszentrum Rossendorf (FZR, Germany), has been improved to take into account all the phenomena that play an important role during flashing instabilities. A detailed comparison with the experiments performed at the CIRCUS facility is shown in Chapter 6 and in Paper V.
Finally, in Chapter 7 start-up procedures for the natural circulation Boiling Water Reactors are discussed and suggestions are given for further improvements.

Briefly, the achievements presented in this thesis can be summarized in three main groups:
1. Analysis of steam production during flashing in upward flow (Papers II and III).
2. Experimental analysis of flashing-induced instabilities and clarification of the instability mechanism (Paper I and Paper IV).
3. Modelling of flashing-induced instabilities (Papers V and VI).

Note that the model described in Paper VI has been developed by D.D.B. van Bragt. My personal contribution to the model consisted in correcting the equation resulting from the integration of the energy balance (eq. 6) and in implementing the analytical model in FORTRAN in order to perform numerical simulations.
In addition, I could benefit of the software for the visualization and treatment of the wire-mesh data. In order to allow further developments, the source codes of such software were made available by dr. H.-M. Prasser.

Chapter 2

THE EXPERIMENTAL FACILITY CIRCUS

In this chapter a brief introduction on the experimental facility CIRCUS and its instrumentation is presented. All the experimental work reported in this thesis has been carried out on the above mentioned set-up. A more detailed description of the facility can be found in Ref. [24].

2.1. DESIGN CHARACTERISTICS OF THE FACILITY

The experimental facility (CIRCUS) is a natural-circulation water/steam loop. The heated section (1.95 m) consists of four parallel heated channels and four bypass channels. On top of the heated channels a long adiabatic section (length of 3m) is present. This part will be referred to as "riser section". The steam produced in the heated channels and in the riser section is condensed in the heat exchangers.

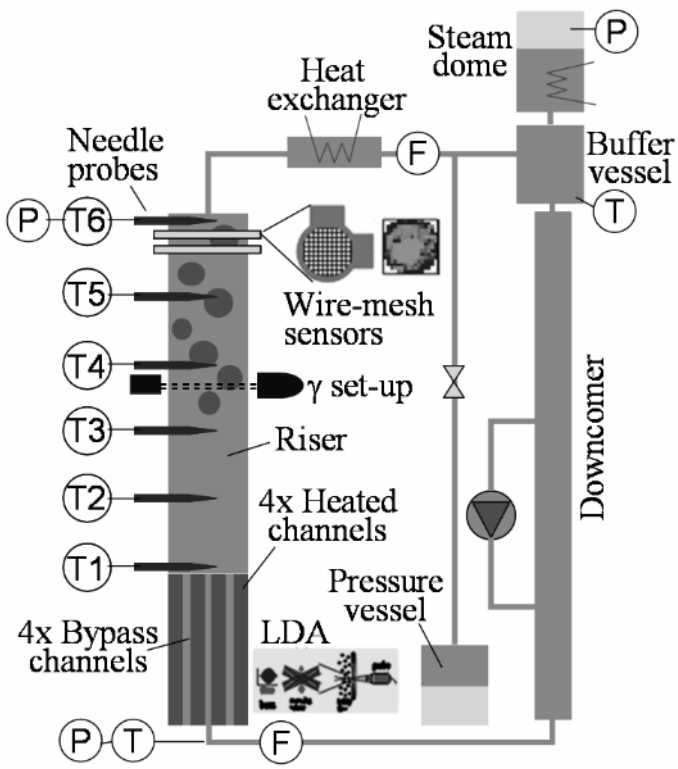

Fig. 4. Scheme of the CIRCUS facility.

A pressure vessel containing air and water separated by a membrane is used to pressurize the loop before starting the set of experiments. A vessel, in which a mixture of water and steam is at saturation conditions, is used to simulate the steam dome of a reactor; here a small heater compensates for heat losses. A buffer vessel is used to damp temperature oscillations at the outlet of the heat exchanger in order to ensure a constant temperature at the inlet of the heated section.

Table 1 Characteristics of the test facility

Power range per rod	0 - 3 kW
Pressure range	1 - 5 bar
Fuel channel diameter	20.4 mm
Fuel rod diameter	12.5 mm
Heated section length	1.95 m
Adiabatic section diameter	47 mm
Adiabatic section length	3 m

A simplified scheme of the facility is shown in Fig. 4 and the main characteristics are reported in Table 1. The instrumentation with which the facility is equipped is described in paragraph 2.2.

2.2. INSTRUMENTATION

The instrumentation in CIRCUS is schematically illustrated in Fig. 4. The flow rate at the inlet of the heated section and before the steam dome is measured by means of magnetic flow-meters (accuracy of ± 0.01 l/s). Thermocouples (accuracy of ± 0.5 ^{o}C) are located at the inlet and outlet of each heated channel, along the riser section, in the heat exchanger and in the steam dome. PT100 sensors are located at the inlet of the heated section and in the steam dome for more accurate temperature measurements. Pressure sensors are used to measure the absolute pressure at the inlet of the heated section, at the outlet of the riser and in the steam dome. Differential pressure sensors are mounted across the steam dome (for water level measurements) and across the valves at the inlet of the heated section. Beside standard instrumentation, advanced measuring techniques are used for detailed void-fraction measurements and for high sampling rate velocity measurements.

2.2.1. THE CONDUCTIVITY NEEDLE-PROBES WITH INTEGRATED THERMOCOUPLE

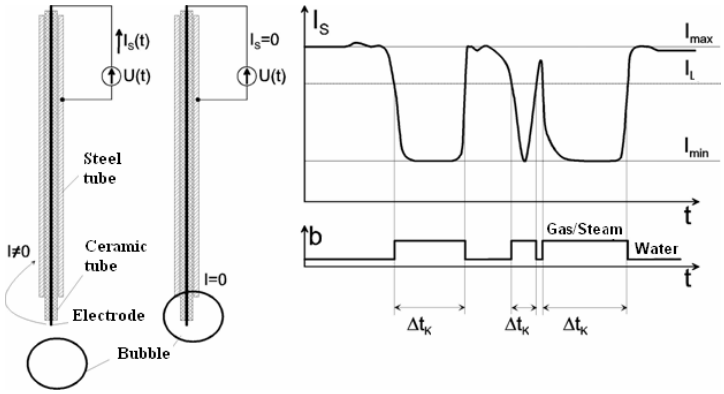

Fig. 5 Working principle of the needle probe sensors. When a steam bubble comes in touch with the tip of the probe a sudden drop of the current is registered. In this way it is possible to discriminate between liquid and vapour phase.

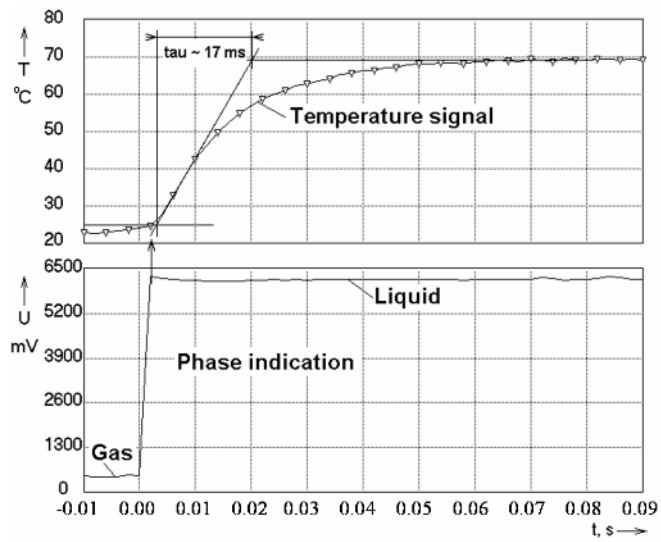

Fig. 6 Time response of needle probe sensors. The fluid temperature can be measured with a time constant of 17 ms. The discrimination between liquid and vapour phase done on the basis of the current signal is practically instantaneous.

The needle-probe sensors used at the CIRCUS facility have been developed at the Forschungzentrum Rossendorf (FZR, Germany). The innovation of these sensors with respect to standard conductivity probes widely used in test facilities is in the integrated fast thermocouple [25]. The sensors are located at six axial positions along the central axis of the riser section (see positions T1 to T6 in Fig. 4). Four probes are located at the exit of each heated channel.

The measuring principle is based on the local conductivity of the fluid touching the probe. The electric current, which is sampled with a rate of 500 Hz, drops considerably if a gas/steam bubble touches the tip of the probe, giving rise to bubble pulses (see Fig. 5). The bubble pulses are discriminated in order to get a binary signal and the time-dependent void-fraction is successively obtained by averaging the binary signal on a given time interval (in the present work a time interval of 0.5 s is used).

In Fig. 6 the time response of the probe, obtained by dropping the sensor from ambient air into hot water, is shown with regard both to the temperature and the conductivity measurements. Both signals are sampled with 500 Hz.

The current signal, on the basis of which the discrimination between liquid and vapour phase is done, changes practically instantaneously when the probe reaches the water surface. The temperature measurement can be approximated as the response of a first-order system, with a time constant of about 17 ms.

2.2.2. THE GAMMA SET-UP FOR CHORDAL VOID FRACTION MEASUREMENTS

The γ-transmission set-up mounted in the riser of the CIRCUS facility consists of a 100mCi ^{51}Cr source and of a NaI(Tl) scintillator detector. ^{51}Cr has been chosen because the energy of the gamma rays that it emits (320 keV) requires small amount of shielding material (about 3.5 cm of lead) and at the same time allows enough resolution to distinguish between steam and liquid phase. Moreover, this type of source is cheap and easy to produce in the reactor facilities of the Interfaculty Reactor Institute (IRI).

The source is collimated by means of a collimator with a window of 2 mm width and 8 mm height. A similar collimator is present in front of the detector as well. Source and detector are joined together to preserve their relative alignment.

By means of this set-up the chordal void fraction along the γ-beam crossing the riser section is measured. Only the photo-peak (320 keV) of the gamma-spectrum is selected for the void-fraction measurements. To convert the measurements into chordal void fraction a calibration procedure is

needed, in which the attenuation of the γ-beam is measured in conditions of "empty pipe" and "pipe completely filled with water", in order to obtained the detector count-rates I_G and I_L respectively. The chordal void fraction α_C is then evaluated on the basis of the measured time-dependent count-rate I according to:

$$\alpha_C = \frac{\ln(I) - \ln(I_L)}{\ln(I_G) - \ln(I_L)} \tag{1}$$

Due to the relatively short half-life (27.7 days) of ^{51}Cr, a correction has to be made to take into account the decay of the source.

2.2.3. THE WIRE-MESH SENSOR

Two wire-mesh sensors are used in the CIRCUS facility. This type of sensor has been developed at the Forschungszentrum Rossendorf (FZR, Germany); it measures the two-dimensional void-fraction distribution over the cross-section of a pipe on the basis of the local instantaneous conductivity of the fluid flowing in the pipe itself. The sensor has a diameter of 47 mm (equal to the diameter of the adiabatic section on which it is mounted) and is made up of two electrode grids of 16 wires each placed at an axial distance of 1.5 mm. The two grids are positioned perpendicularly to each other in order to form a matrix of 16x16 cross-points (see Fig. 7). The distance between two successive parallel wires is equal to 2.8 mm, this being also the spatial resolution of the sensor. Details on the working principles of the sensor are given by Prasser et al. [26]. The sampling frequency of the new generation sensors can be up to 10000 Hz. The wires have a diameter of 120 μm and occupy approximately 4 % of the total cross-section, so that the flow resistance introduced by the sensor is not significant.

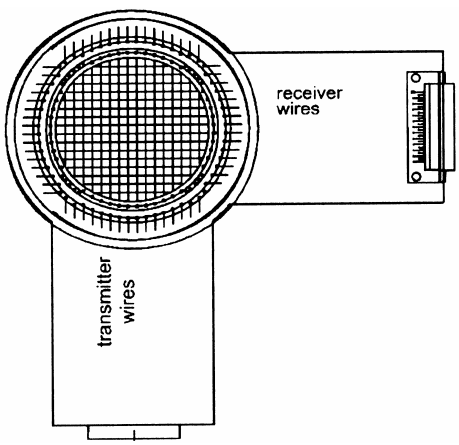

Fig. 7. Wire-mesh sensor.

A maximum sampling frequency of 1200 Hz can be achieved with the sensors available at the CIRCUS facility. The time-dependent fluid conductivity measured by the sensor on a matrix of 16x16 points is converted into void fraction assuming a linear dependence of the void fraction with respect to the fluid conductivity. For the conversion to void fraction it is necessary to calibrate the sensor in conditions of "tube completely filled with liquid" and "tube completely filled with gas". The calibration data are stored and used successively for the conversion of the measurement data. Additional corrections are needed if variations of the fluid temperature occur during the measurements.

A linear dependence is assumed between void fraction and fluid conductivity, so that the local void fraction $\alpha[i,j]$ at a given point [i,j] of the 16x16 measurement matrix can be expressed as:

$$\alpha[i,j] \simeq 1 - \frac{u[i,j] - u_G[i,j]}{u_L[i,j] - u_G[i,j]} \tag{2}$$

where $u[i,j]$ is the measured mixture conductivity at the position [i,j] of the 16x16 points matrix, $u_G[i,j]$ the gas conductivity and $u_L[i,j]$ the water conductivity. The latter two quantities are obtained during the calibration procedure for each matrix point [i,j]. Appropriate weighting of the local void fractions $\alpha[i,j]$ is performed to evaluate the cross-section averaged void fraction. Details are given in Paper I.

TEMPERATURE CORRECTION FOR VOID-FRACTION MEASUREMENTS

During flashing-induced flow oscillations the amplitude of local temperature oscillations in the riser can be of several degrees, so that assuming a constant liquid conductivity $u_L[i,j]$ as in eq. (2) can lead to an erroneous evaluation of the void fraction. An example of the effect of temperature changes on the cross-section averaged void fraction is given in Fig. 8 (left). Here the average void fraction evaluated on the basis of eq. (2) is shown during typical flashing-induced flow instability. The large fluctuations of the void fraction are due to the fast alternation of water and steam.

During a flashing cycle the void fraction exhibits also negative values, while it shows positive values between two successive flashing cycles even though only liquid is present in the riser. This is due to the fact that the liquid temperature varies in time and exhibits a local maximum during a flashing cycle and a local minimum between two successive cycles. Since the liquid conductivity decreases with decreasing temperature, a decrease (increase) of temperature is erroneously interpreted as an increase (decrease) of void fraction.

To take fluid temperature variations into account, calibration data for the liquid conductivity $u_L[i,j]$ have been stored at different liquid temperatures and a linear regression has been used to describe the dependence of the conductivity as function of temperature:

$$\frac{u_L[i,j]-u_G[i,j]}{u_L^0[i,j]-u_G[i,j]} \simeq \frac{aT+b}{aT_0+b} \tag{3}$$

where $u_L[i,j]$ is the measured liquid conductivity at a given temperature T, $u_L^0[i,j]$ the liquid conductivity measured at a reference temperature T_0, and a and b the coefficients of the linear regression. Applying the linear regression of eq. (3), the local void fraction becomes:

$$\alpha[i,j] \simeq 1-\frac{u[i,j]-u_G[i,j]}{u_L^0[i,j]-u_G[i,j]}\frac{aT_0+b}{aT+b} \tag{4}$$

The fluid temperature T is measured by means of a thermocouple positioned at the axial location of the wire-mesh sensor in the centre of the cross section (in between the two layers of electrodes).

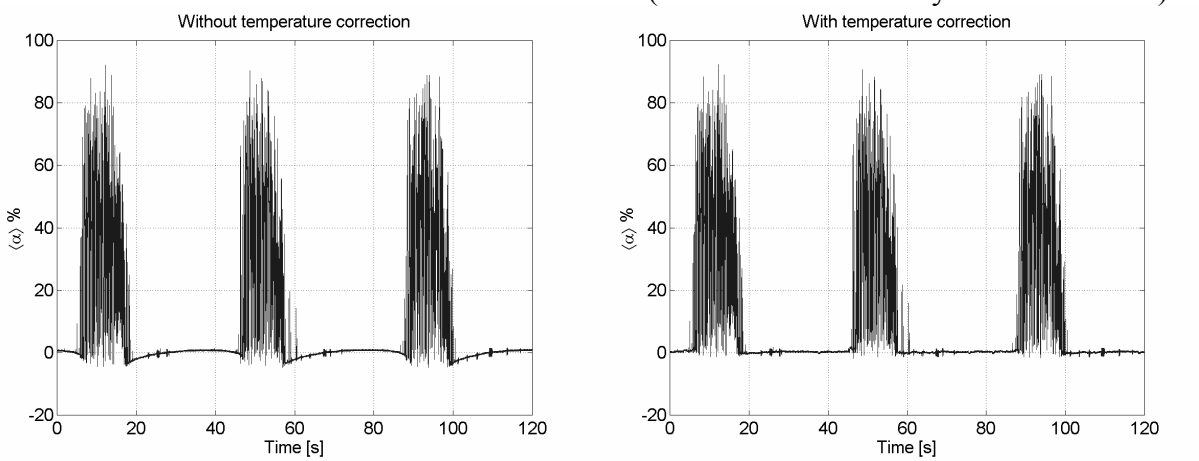

Fig. 8. Average void fraction without (left) and with (right) temperature correction.

The artefact shown in Fig. 8 (left) vanishes when the temperature correction as stated in eq. (4) is applied (see Fig. 8, right).

COMPARISON WITH GAMMA-TRANSMISSION TECHNIQUES

The sensor has been successfully applied to measure gas fractions, flow-pattern transitions and bubble-size distributions in air-water flows [27], for boron dilution measurements during transients occurring in Pressurized Water Reactors [28] and for cavitation experiments during rapid valve closure in pipelines [29]. However, it had never been applied in water/steam flows and in conditions of variable mixture temperature.

To assess the performances of the wire-mesh sensor in water/steam flows, two gamma-transmission set-ups positioned respectively just below and above the wire-mesh sensor were used for a comparison of void fraction measurements. The γ-beams were aligned to the central wire of the wire-mesh sensor. In this way the chordal void fraction measured by the gamma-transmission set-ups can be directly compared with the chordal void fraction measured by the wire-mesh sensor along the same path. The chordal void-fraction measured by the γ-transmission set-ups is evaluated according to eq. (1). A time constant τ_R of 0.3 s is used for the rate-meters of the two set-ups, corresponding to a statistical error on the count-rate of about 2%.

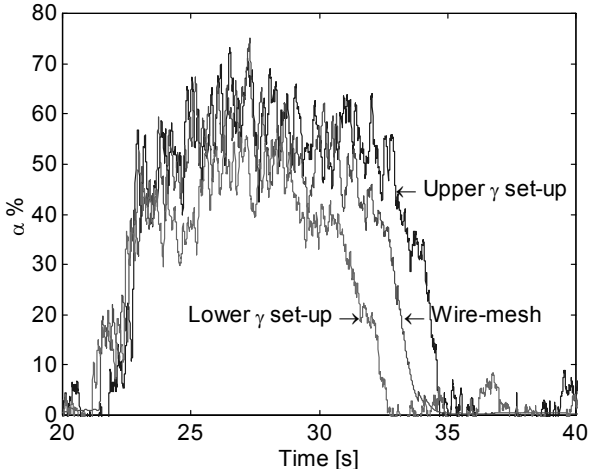

Fig. 9. Chordal void fraction measured by the gamma-transmission set-ups and simulated chordal void fraction at the wire-mesh sensor (τ_R = 0.3 s, cross-section central line).

The chordal void fraction α_i measured by the wire-mesh sensor along the central wire *i* is evaluated as the sum of the void fraction $\alpha_{i,j}$ in each node belonging to the wire *i* weighted by a factor w_j, that takes into account whether the [i,j]-mesh contributes totally (central mesh) or only partially (mesh at periphery) to the total area intercepted by the sensor along the wire *i*.

To compare the signals of the wire-mesh sensor and of the gamma-transmission set-ups it has to be taken into account that the wire-mesh sensor measures instantaneous void fraction, while the gamma-transmission set-ups behave like first-order integrators with a time constant τ_R set on the rate-meter used to digitise the count-rate. Thus, the signal of the wire-mesh has been properly filtered to simulate the response of a hypothetical gamma-transmission set-up located at the wire-mesh position. The comparison with the two gamma-transmission set-ups is shown in Fig. 9.

Taking into account the gamma-transmission filtering effect, the time series of gamma-transmission and wire-mesh sensor measurements present a comparable structure. The chordal void fraction measured by the wire-mesh sensor is in between the chordal void fractions measured by the gamma-transmission set-ups. Despite the fact that the wire-mesh sensor is axially located in the middle between the two gamma-transmission set-ups, the average chordal void fraction measured by the wire-mesh sensor is closer to the one measured by the upper gamma-transmission set-up than to the chordal void fraction measured by the lower gamma-transmission set-up. This is consistent with the non-linear axial-profile of void-fraction production during flashing [30].

In addition, from Fig. 9 it can be seen that the steam production due to flashing starts almost simultaneously at the different locations occupied by the gamma-transmission set-ups and by the wire-mesh sensor. A delay of a few seconds exists at the end of the flashing process, before all the measuring devices register a zero void fraction. This delay is about the time needed for the flashing front (being the location below which one-phase flow is present) to move upwards along the adiabatic section as a consequence of the increased flow rate. A more detailed comparison is reported in Paper I.

EFFECT ON INSTABILITIES

The electrodes of the wire-mesh sensor may provide extra nucleation sites for steam bubbles production. To investigate the significance of this effect, measurements were repeated after the wire-mesh sensor was removed from the experimental loop.

The measurements with and without wire-mesh sensor were carried out keeping the same temperature at the inlet of the heated section, the same initial pressure at the outlet of the adiabatic section and the same water level in the steam dome. In Fig. 10 two of the main state variables of the system during flashing-induced instability are shown before and after the wire-mesh sensor removal (the time shift between the two measurements is arbitrary and it is used only to facilitate the

comparison). No appreciable differences are found between the two series of measurements. Also the period of the oscillation remains unchanged.

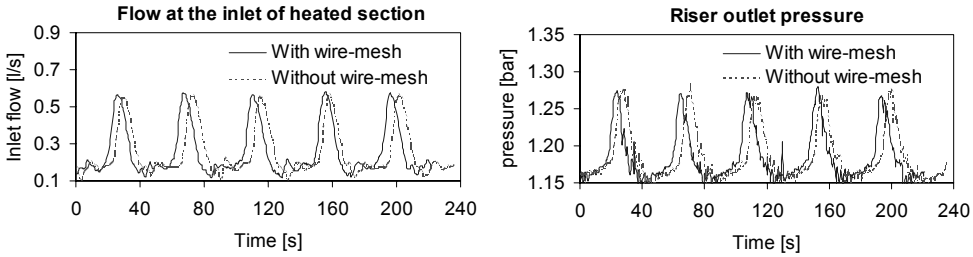

Fig. 10. Inlet flow and outlet-riser pressure with and without wire-mesh sensor.

The void fraction measured by the gamma set-ups does not change significantly as it can be seen in Fig. 11, in which the chordal void fractions measured by the lower and upper se-ups are shown for the two measurements. In the figure, the time-averaged chordal void fractions during a flashing cycle are also reported.

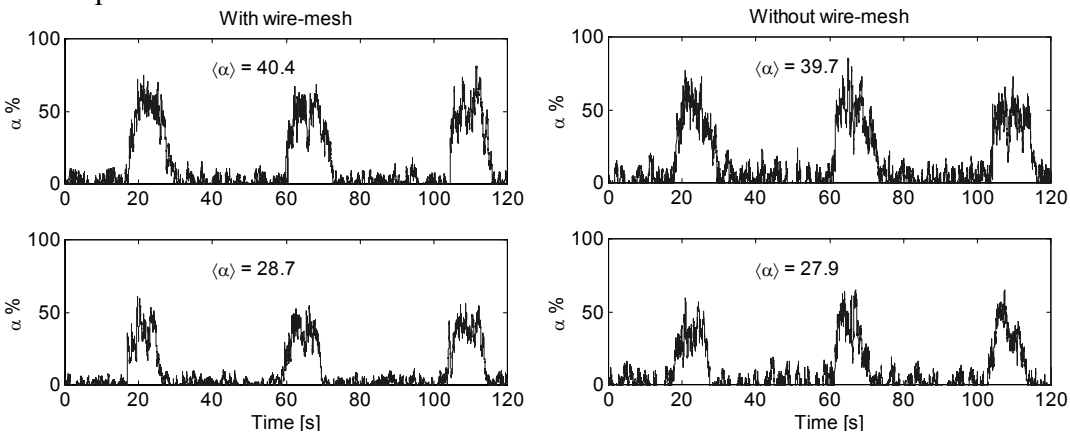

Fig. 11. Void fraction measured by the gamma-transmission set-ups with (left) and without (right) the presence of a wire-mesh sensor. No significance difference can be observed between the two cases.

2.2.4. THE LDA SET-UP

A Laser-Doppler-Anemometry (LDA) set-up is used to measure the flow velocity with a high sampling rate. The technique, which is non-intrusive, is based on the Doppler shift that occurs when a beam of light is scattered by a moving particle [31].

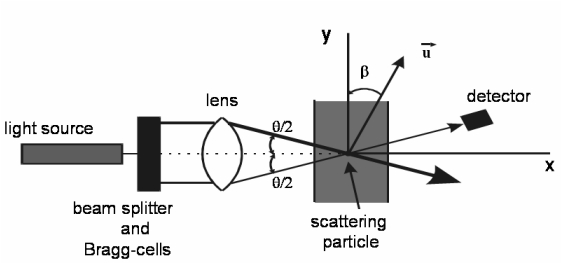

Fig. 12: Simplified scheme of the LDA set-up.

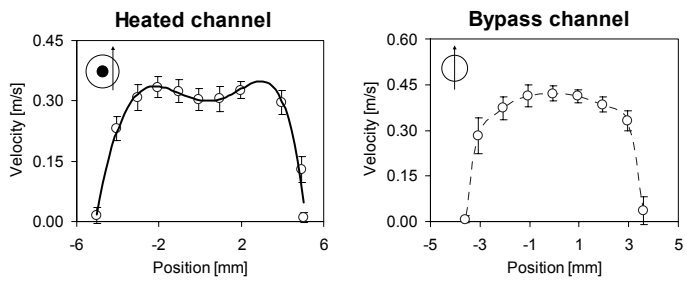

Fig. 13: Velocity profile in the heated channel and in the bypass channel. The direction in which the profile has been measured in the two cases is schematically illustrated.

Since the velocities of interest are much smaller than the velocity of light, the Doppler shift would be too small to be detected. The problem is solved by splitting the original laser beam by means of a beam splitter before sending the beam through the flow and by letting the shifted beam interfere with the non shifted beam (so-called reference beam). In this way, the signal that reaches the detector contains the frequency difference between the two beams.

A simplified scheme of the LDA set-up is reported in Fig. 12. A 532 nm wavelength green laser is applied at CIRCUS. To have the highest possible light intensity at the detector surface the forward mode is used, which means that light source and detector have to be aligned. The alignment needed between the set-up components (lens, beam splitter and Bragg cells) makes the technique extremely difficult to be realized.
The velocity of the fluid in the control volume intercepted by the two beams in the flow is linearly dependent on the frequency difference measured by the detector. To allow the measurement of negative velocities, i.e. to detect negative Doppler frequency shifts, the frequency of the reference beam is shifted by means of a Bragg cell. The frequency measured by the detector is related to the local fluid velocity according to the relation:

$$f = f_{Shift} + \frac{2\sin\frac{\theta}{2}}{\lambda_0}\left|\vec{u}\right|\cos\beta \tag{5}$$

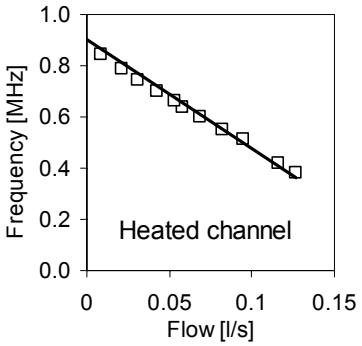

Fig. 14: Calibration fit for flow measurements.

where f_{shift} is the frequency shift generated by the Bragg cell. From eq. (5) it is clear that only the vertical component of the fluid velocity is measured in the applied configuration. Thanks to the frequency shift f_{shift} negative velocities produce still a positive frequency f measured by the detector. An example of velocity profiles measured in one of the heated channels and in one of the bypass channels is presented in Fig. 13. For flow measurements, a calibration is performed in stationary conditions taking the flow-meter at the inlet of the heated section as reference. The calibration for the heated channel is reported in Fig. 14 (with the control volume equidistantly located between the pipe walls and the heated rod surface).

2.2.5. SIGNALS ACQUISITION SYSTEM AND SYNCHRONIZATION

Six PCs are used at CIRCUS to monitor the facility, to control the measurement devices and for the signals acquisition. A scheme is shown in Fig. 15.
PC1 acquires the signals from the conductivity probes unit with a sampling frequency of 500 Hz. PC2 and PC3 control the two wire-mesh sensors respectively and store the corresponding measurements. The sampling frequency can be set up to 1200 Hz.
PC4 hosts the monitor program that is used to monitor and control the CIRCUS facility. The monitor program receives all signals with the exception of conductivity probes, wire-mesh and LDA set-up. The sampling frequency for the monitoring system is set to 2 Hz.
The signals acquisition at higher sampling frequency is done by means of a SCADAS unit that provides a system of amplifiers and filters. This unit is controlled by means of PC5. On this PC the SCADAS measurements are also stored.
PC6 allows the control of the LDA set-up and the storage of the corresponding measurements.
When performing a measurement, all the different systems need to be synchronized. For this scope a signal is generated when the acquisition is started on PC1. This signal triggers the LDA measurements on PC6 and the wire-mesh measurement on PC2. PC2 is then connected to PC3 to synchronize PC2 and PC3 during the entire acquisition time of the two wire-mesh sensors. The trigger signal is stored by PC4 and PC5, which are started before the trigger signal from PC1 is activated. In this way, all the measurements files can be synchronized.

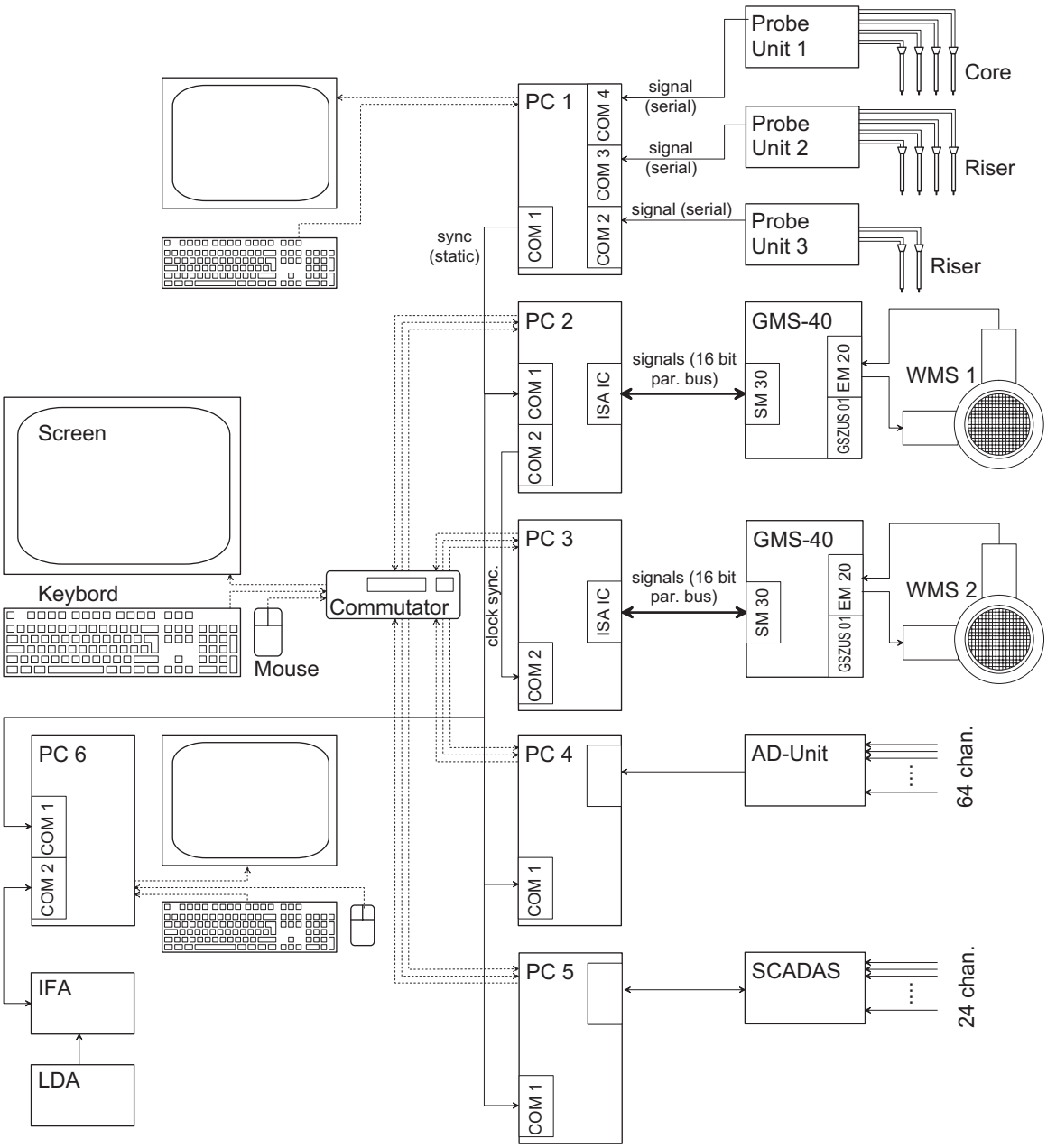

Fig. 15: Scheme of the acquisition system.

Chapter 3

CHARACTERISTICS OF VOID-FRACTION PRODUCTION DURING FLASHING

Subject of this chapter is the flashing phenomenon in a vertical upward flow. Special attention is given to the assessment of void-fraction correlations and drift-flux models. Stationary and transient flashing flow is covered. Visualization of the flow pattern evolution is treated as well. More details can be found in Papers II and III.

3.1. SUITABILITY OF DRIFT-FLUX MODELS FOR VOID-FRACTION PREDICTION DURING FLASHING

Drift-flux models have been and are still widely used in thermal-hydraulic codes for nuclear and other industrial applications. These models are applied to study the behaviour of two-phase flow in stationary as well as transient conditions and for void-fraction prediction. Despite the strong empirical nature of drift-flux models, their simplicity and robustness make them often preferable to complete two-fluid models in which several closure relations are needed to couple the set of balance equations for the two phases.

Since the first drift-flux model was proposed in 1965 by Zuber and Findlay [32], large experience has been gained regarding air-water flows, in which air and liquid are supplied separately, and steam-water flows where the steam is produced by heated rods. Very little is known about flashing flows, in which steam is produced in the super-heated liquid due to a decrease of the gravitational head along the system. The experiments and models available in literature mainly refer to flashing in horizontal pipes as a consequence of pipe rupture (during blow-down) and cannot be directly applied to flashing flows in vertical pipes caused by variations of gravitational pressure head.

To cope with this lack, an experimental campaign has been carried out at the CIRCUS facility. Both transient flow, during flashing-induced instabilities in natural-circulation conditions, and stationary flow conditions have been addressed in the study. In the latter case the facility was operated in forced circulation in order to increase the operational parameters range for constant flow experiments. The measurements were carried out at atmospheric pressure, with the steam dome open to the environment. During each experiment the power level and the temperature at the inlet of the heated section are kept constant. Two wire-mesh sensors located in the upper part of the riser section at an axial distance between each other of 27.5 mm are used to carry out void-fraction and steam-velocity measurements.

To test drift-flux models and void-fraction correlations the following quantities are needed (local quantities are referred to the height H of the test section where the lower wire-mesh sensor is located):

a) local cross-section-averaged void fraction $<\alpha_H>$;
b) local superficial liquid velocity $J_{L,H}$;
c) local superficial steam velocity $J_{G,H}$.

Only the first of these quantities can be measured directly. In the general case of transient flow, the steam and liquid superficial velocities are derived from the following relation:

$$\begin{cases} J_{G,H}(t) = \langle \alpha_H \rangle (t) \langle u_{G,H} \rangle (t) \\ J_{L,H}(t) = J_{L,inl}(t) - J_{G,H}(t)\dfrac{\rho_G}{\rho_L} + \dfrac{\rho_L - \rho_G}{\rho_L}\dfrac{d}{dt}\displaystyle\int_0^H \langle \alpha \rangle (z,t)\,dz \end{cases} \tag{6}$$

where the liquid flow rate $J_{L,inl}$ at the inlet of the heated section is measured by means of a magnetic flow meter and LDA set-up. The void fraction $<\alpha_H>$ is measured by means of the lower wire-mesh

sensor, the steam bubbles velocity $u_{G,H}$ is derived by cross-correlating the cross-section-averaged void-fractions measured by the two wire-mesh sensors. The integral spatial-averaged void-fraction on the right-hand side of eq. (6) is calculated on the basis of the needle-probes signals, assuming linear interpolation between two successive axial locations. Before the integration is performed, the needle-probe signals have to be properly corrected to take into account the radial void-fraction profile in the pipe cross-section, as described in Paper II.

3.1.1. STATIONARY CONDITIONS

For the experiments carried out at constant flow rate, the liquid superficial velocity ranges from about 0.08 to 0.2 m/s, while the steam superficial velocity ranges from about 0.03 to 1.5 m/s. This approximately covers the parameters range at atmospheric pressure at which flashing-induced instabilities may occur during the start-up phase of natural circulation BWRs. Both bubbly and slug/churn flow regimes were encountered. For each measurement, point signals are recorded for 200 s and average values are derived for all the quantities needed (the local cross-section-averaged void fraction $<\alpha_H>$ and the local superficial velocities $J_{L,H}$ and $J_{G,H}$).

Several drift-flux models and void-fraction correlations have been selected from the literature. All the correlations used in thermal-hydraulics codes developed for nuclear applications have been taken into account.

The performances of the different models with respect to the experimental results are discussed in details in Paper II. Here only a few conclusions will be reported (see also Table 2): the GE-Ramp and Nabizadeh correlations perform best, followed by Dix, modified Sonnenburg and Takeuchi models. Takeuchi, Nabizadeh and Sonnenburg relations perform better with the churn-flow data points. Liao-Parlos-Griffith, Hughmark, Labuncov and the original Sonnenburg correlations perform extremely poorly (for a comprehensive list of references see Paper II). The findings on flashing flow are in line with the results on steam-water flows by Chexal et al. [33] who found GE-Ramp and Dix correlations to provide the best performances with regard to all experimental sets, with the exception of large-diameter pipe data.

Table 2 Statistical comparison of void-fraction predictions for stationary flow

Correlation	$<\varepsilon>$	$<\lvert\varepsilon\rvert>$	$\sigma_{\lvert\varepsilon\rvert}$
Zuber-Findlay (churn flow)	-0.036	0.042	0.037
Ishii	-0.037	0.042	0.042
Liao-Parlos-Griffith	0.213	0.213	0.113
Maier-Coddington	0.090	0.090	0.044
GE-Ramp	0.012	0.026	0.026
Dix	0.031	0.033	0.035
Rouhani	0.008	0.045	0.033
Hughmark	-0.261	0.261	0.120
Labuncov	0.153	0.153	0.077
Sonnenburg	0.117	0.117	0.061
Modified Sonnenburg	-0.030	0.039	0.029
Chexal-Lellouche	0.089	0.089	0.040
Nabizadeh	-0.003	0.029	0.019
Takeuchi	-0.028	0.034	0.028

mean error
$<\varepsilon> \equiv <\alpha_{Measured} - \alpha_{Calculated}>$

mean of the absolute error
$<\lvert\varepsilon\rvert>$

standard deviation
$\sigma_{\lvert\varepsilon\rvert}$.

3.1.2. TRANSIENT CONDITIONS

Nine measurements were performed in conditions of natural circulation during flashing-induced instabilities. The heating power and inlet temperature for each case are indicated in Table 3. The first six measurements were performed at a power of 10.8 kW. The inlet subcooling was varied in order to cover all the unstable conditions from stable single-phase to stable two-phase operation. The last three measurements were performed at different powers and subcooling.

The assessment of drift-flux models during transient flashing flows needs careful analysis. In transient conditions time-dependent liquid and steam velocities and void-fraction are needed. While there is no problem with regards to liquid velocity and cross-section-averaged void fraction due to the high time sampling rate at which the relative measurements can be performed (by LDA and wire-mesh sensors respectively), problems arise for the estimation of the steam velocity. Previously it has been explained that the steam velocity is evaluated by cross correlating the signals of two wire-mesh sensors located one on top of each other. The cross correlation has to be calculated over a limited time window if the temporal variations of the velocity have to be derived. It is recommendable that ensemble-averaged quantities are evaluated with a time step not larger than 0.5 - 1 s. Thus the same limitation holds for the time window over which the cross correlation is evaluated. Unfortunately a small time window goes at the expenses of the accuracy of the cross-correlation. To overcome the problem and reduce the uncertainty on the estimation of the steam velocity, longer measurements (600 s) are performed in comparison with the stationary measurements in order to record a significant number of flashing cycles for each operational condition.

For each measurement, first individual flashing cycles are discriminated on the basis of the signal of the lower wire-mesh. The beginning of a flashing cycle is determined as the time instant at which the wire-mesh sensor measures a cross-section-averaged void fraction of at least 10%.

Table 3 Measurements for transient flashing flow

Case	Power [kW]	Inlet Temperature [°C]
1	10.8	72.8
2	10.8	78.2
3	10.8	82.1
4	10.8	84.8
5	10.8	88.1
6	10.8	96.0
7	10.0	91.5
8	8.0	91.5
9	6.0	90.5

For each flashing cycle, the cross-section-averaged void fraction (from wire-mesh signal) and the integral void fraction in the adiabatic section (from needle-probes signals) are determined with a time-step of 0.5 s. The steam bubbles velocity is calculated every 0.5 s by cross-correlating the instantaneous cross-section-averaged void fractions measured by the two wire-mesh sensors. Ensemble averaging is performed over all flashing cycles in order to guarantee sufficient statistical accuracy. The steam velocity is calculated on the basis of the ensemble-averaged cross-correlation.

Ensemble averaging is also done for the liquid velocity and for the void fraction, in order to obtain at a given parameters combination (power, inlet subcooling, pressure, etc.) a representative time-dependent flashing cycle. An example is reported in Fig. 16 and Fig. 17.

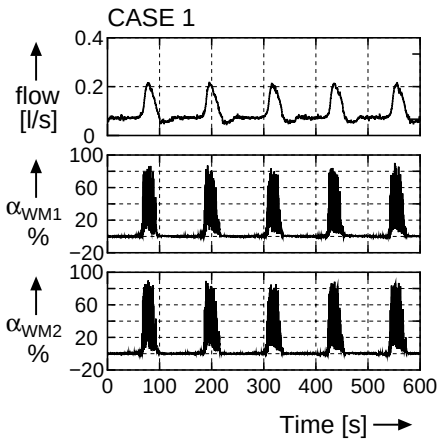

Fig. 16: Examples of flow-rate and instantaneous cross-section averaged void-fraction signals during flashing-induced flow oscillations.

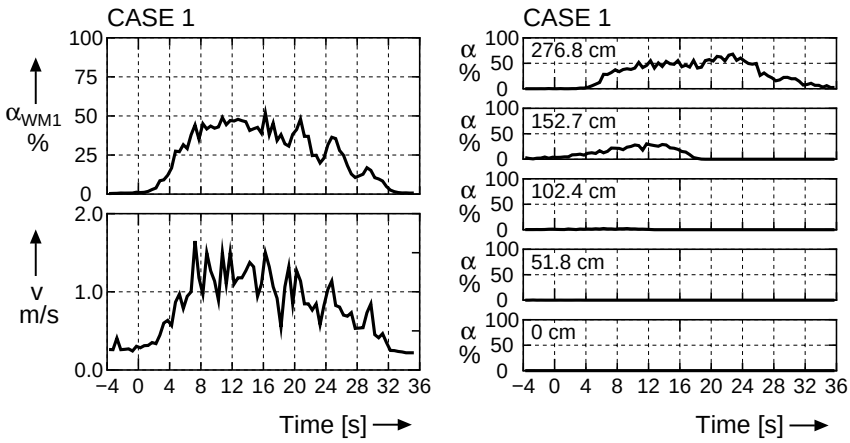

Fig. 17. Example of ensemble-average flashing cycles. The local cross-section averaged void fraction α_{WM1}, the steam velocity v (left) and the void-fraction evolution along the adiabatic section (right) are reported. A time step of 0.5 s was used.

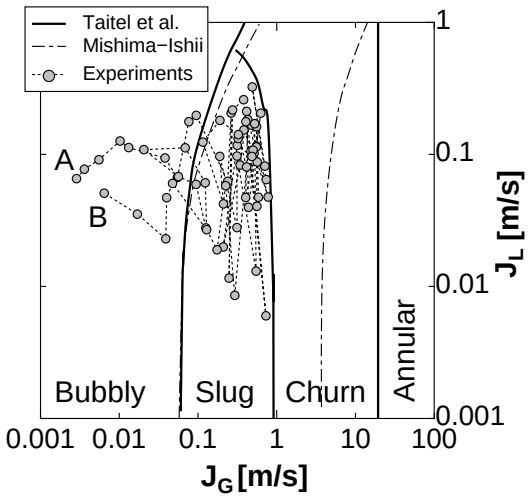

Fig. 18 Localization of transient working point in the J_G-J_L flow map for Case 1 of Table 3. The time increases from point A to point B.

In Fig. 16 the time-trace of the flow rate at the inlet of the heated section is reported together with the cross-section-averaged void fraction measured at the locations of the two wire-mesh sensors (at a power of 10.8 kW and an inlet temperature of 72.8 ^{o}C, case 1 of Table 3). The corresponding ensemble-averaged flashing cycle is reported in Fig. 17. In particular, the cross-section-averaged void fraction at the position of the lower wire-mesh sensor and the steam velocity are shown.

The case presented in Fig. 16 and Fig. 17 is characterized by the fact that the adiabatic section is only partially occupied by flashing flow (considerable void production is observed only in the upper part of the adiabatic section, as shown in Fig. 17 right). This is because the operational point is quite close to the stable single-phase region.

Increasing the inlet temperature, the height at which the onset of flashing occurs shifts toward the inlet of the adiabatic section. A case in which flashing starts from the inlet of the riser is shown in Paper II.

The transient working point for the case presented in Fig. 16 and Fig. 17 is shown in Fig. 18 in the J_G-J_L phase-space (the time increases from point A to point B). The flow maps according to Taitel et al. [34] and to Mishima-Ishii [35] are also reported. As it can be seen, during a flashing cycle the flow pattern transits from bubbly-flow to slug/churn flow and ends as bubbly flow again. This can be also seen by visual inspection of the test section and by bubbles reconstruction and flow pattern visualization, as it is demonstrated in paragraph 3.2 and in Paper III.

The application of drift-flux models to all the transient cases show similar trends as observed for the stationary data-set (see Table 4 and Paper II for details). As a conclusion it can be stated that, in view also of their relative simplicity, GE-Ramp and Dix models are to be recommended for application to flashing flows. A further assessment would be needed in case of large-diameter pipes.

Table 4 Statistical comparison of void-fraction predictions for transient flow

Correlation	$\langle\varepsilon\rangle$	$\langle\lvert\varepsilon\rvert\rangle$	$\sigma_{\lvert\varepsilon\rvert}$
Zuber-Findlay (churn flow)	-0.066	0.073	0.056
Ishii	-0.067	0.074	0.056
Liao-Parlos-Griffith	0.186	0.186	0.104
Maier-Coddington	0.078	0.079	0.051
GE-Ramp	-0.007	0.034	0.031
Dix	0.008	0.029	0.029
Rouhani	-0.033	0.049	0.043
Hughmark	-0.325	0.326	0.161
Labuncov	0.138	0.138	0.077
Sonnenburg	0.098	0.098	0.058
Modified Sonnenburg	-0.040	0.054	0.048
Chexal-Lellouche	0.113	0.114	0.068
Nabizadeh	-0.046	0.075	0.071
Takeuchi	-0.054	0.062	0.053

mean error
$\langle\varepsilon\rangle \equiv \langle\alpha_{Measured} - \alpha_{Calculated}\rangle$

mean of the absolute error
$\langle\lvert\varepsilon\rvert\rangle$

standard deviation
$\sigma_{\lvert\varepsilon\rvert}$.

3.2. FLOW PATTERN VISUALIZATION

For the three-dimensional reconstruction of the flow pattern the time-dependent bubble velocity is needed. This can be estimated in several ways, as illustrated in Paper III. Once the bubble velocity is known, it is possible to transform the time coordinate of the wire-mesh data in the spatial coordinate perpendicular to the measurements plane. For visualization purposes, the velocity evaluated on the basis of the cross-correlation between the two wire-mesh signals as described in paragraph 3.1.2 will be considered.

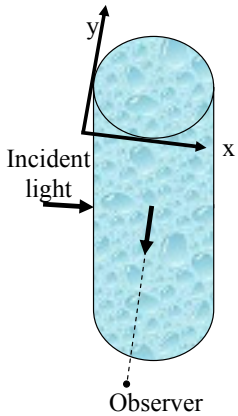

Fig. 19 Schematic representation for the 3D flow visualization.

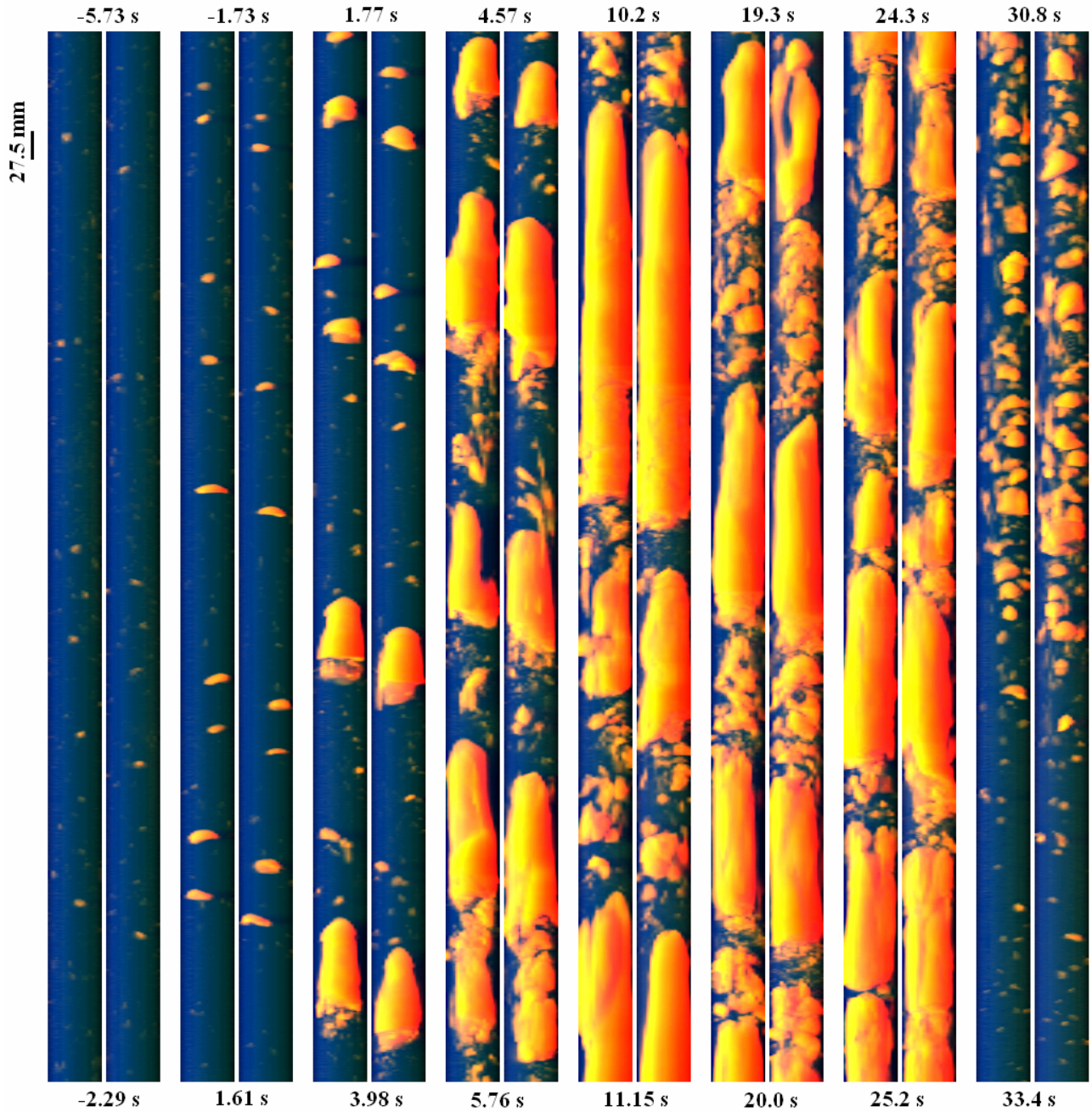

Fig. 20 Flow pattern visualization reconstructed from wire-mesh data. The transient flow pattern for case 1 of Table 3 is visualized at different time instants (same time axis as in Fig. 17). Two successive columns correspond to the measurements extracted from the two wire-mesh sensors respectively. The columns have a length of 20 times the pipe diameter, the latter being 47 mm. The time corresponding to the beginning and the end of each column is indicated. The scaled distance between the two wire-mesh sensors (27.5 mm) is reported as well.

To visualize the flow a simplified ray-tracing algorithm is used (see ref. [36] and Paper III). This technique is applied here for the first time to visualize flow patterns in which the superficial steam velocity changes with time.
The data column is assumed to be illuminated from the left side by parallel white light, as schematically indicated in Fig. 19, and the light intensity departing in the direction of the observer is calculated. For this purpose virtual absorption and dispersion coefficients for the three light components (red, green and blue) are assigned to the liquid and vapour phase respectively. These coefficients are chosen in order to optimise the visualization.
A clear advantage of the visualization method described above is the achievement of a more realistic picture of the three-dimensional flow pattern that contains information of the entire three-dimensional void-fraction distribution. Such information would be lost if only a cross-section in the centre of the pipe is shown.
The flow visualization at different time instants for the flashing cycle of Case 1 treated in paragraph 3.1.2 is shown in Fig. 20. The same time axis as in Fig. 17 is used. Two successive columns correspond to the measurements performed by the two wire-mesh sensors respectively. The picture is in scale, the length of the column being twenty times the pipe diameter (20 *47 = 940 mm). The time instants corresponding to the beginning and the end of different columns are indicated for each column separately.
As mentioned in paragraph 3.1.2 on the basis of the flow map presented in Fig. 18 and from visual inspection of the test section, the flow pattern transits from bubbly to slug/churn flow and back to bubbly flow in the last instants of the flashing cycle.
Note that if the “correct” bubble velocity is used for each bubble, the distance between the bubble fronts of a given bubble as seen from the two wire-mesh sensors should be exactly equal to the distance of 27.5 mm existing between the two sensors (the distance between the two wire-mesh sensors is reported in scale in Fig. 20). Thus, a larger or smaller distance gives an idea of the velocity under-estimation or over-estimation respectively that is caused by the use of an approximate velocity.
A detailed analysis of the flow structure in stationary and transient conditions is presented in Paper III. There the evolution of bubble size distributions is discussed. In addition, a model is applied to study the equilibrium of bubbles radial distribution according to bubbles size classes.

Chapter 4

EXPERIMENTS ON FLASHING-INDUCED FLOW INSTABILITIES

In this chapter the mechanism and the main characteristics of flashing-induced instabilities are explained. The content of this chapter is based on the results reported in Paper IV.

4.1. PHENOMENOLOGY OF FLASHING-INDUCED INSTABILITIES

Chapter 1 describes the mechanism of self-sustained flow oscillations triggered by flashing occurring in the adiabatic section of a natural-circulation two-phase system. Typical time-traces of the flow rate that can be observed in such a system are presented in Fig. 21. The time-traces have been recorded at the CIRCUS facility at a power of 8 kW and a pressure of 1 bar. Increasing the inlet temperature, four main types of behaviour can be observed: stable single-phase circulation (Fig. 21.a), intermittent natural circulation (Fig. 21.b through Fig. 21.f), unstable two-phase circulation (Fig. 21.g) and stable two-phase circulation (Fig. 21.h).

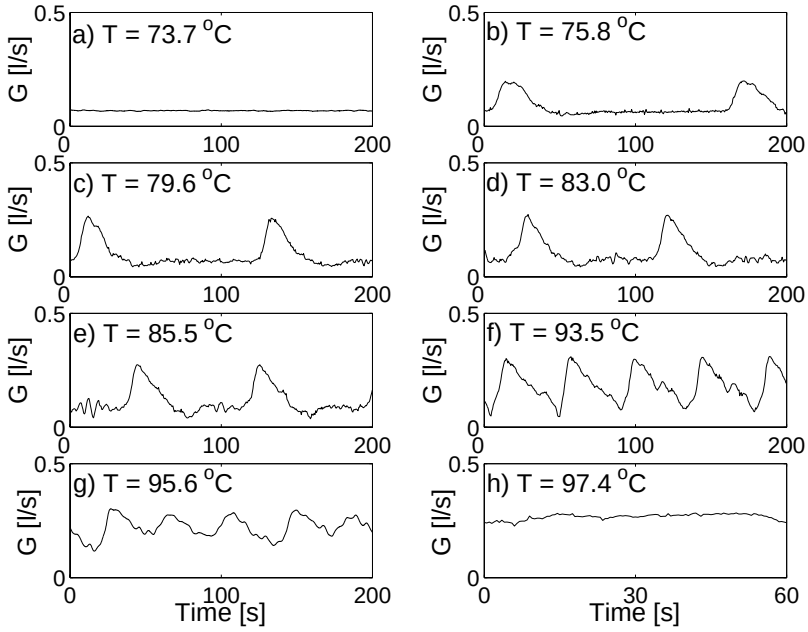

Fig. 21 Typical experimental flow time traces. All cases are recorded at a power of 8 kW and a pressure of 1 bar. The inlet temperature is indicated separately for each case.

At single-phase circulation, the liquid temperature always remains below saturation. The intermittent natural circulation occurs as soon as the system passes from single-phase to two-phase operation and is characterized by an alternate presence of liquid and two-phase mixture in the riser section. Within a cycle an incubation period is present before the flow-rate increases, needed to the liquid to reach saturation.

The incubation period becomes shorter and shorter with increasing inlet temperature and disappears in the unstable two-phase natural-circulation region. In the latter condition, two-phase mixture is always present in the riser section due to flashing, but the location at which flashing starts (the flashing boundary) oscillates, giving rise to an oscillatory driving force in the system and consequently to a flow oscillation. Finally, when the flashing boundary stabilizes, stable two-phase circulation takes place; in this case a much higher flow rate is achieved than with single-phase natural circulation due to the considerable density difference between liquid in the downcomer and two-phase mixture in the riser. Similar trends appear when the inlet temperature is kept constant and the power is increased instead.

A better insight is achieved if the evolution of the void fraction in the adiabatic section is analysed as well. Typical time-traces of the void-fraction evolution in the adiabatic section are shown in Fig. 22. At high subcooling (Fig. 22.a) flashing starts relatively high in the riser and expands successively upwards and downwards. When the inlet temperature is increased (Fig. 22.b) vapour starts to be generated in the heated section below the riser inlet. These steam bubbles collapse in the riser but contribute to the heating up of the liquid phase. Their contribution becomes stronger with increasing inlet temperature (Fig. 22.c and Fig. 22.d) so that flashing is triggered soon after the

condensation of steam bubbles coming from the heated section. At even lower subcooling (Fig. 22.e) the temperature in the riser is high enough that bubbles coming from the heated section are able to trigger flashing starting at the riser inlet without being condensed first.

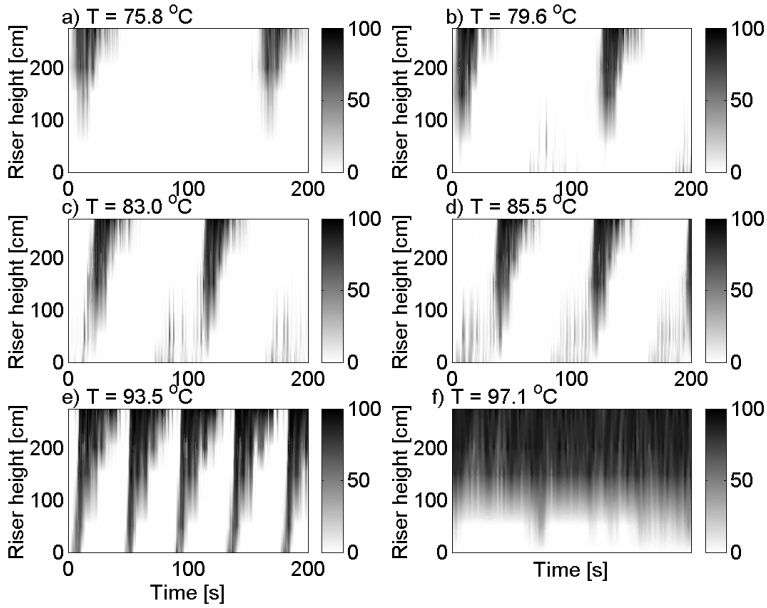

Fig. 22 Evolution of void fraction in the adiabatic section for different inlet subcoolings at a power of 8 kW and a pressure of 1 bar. Vertical bars give the grey-scale coding for void fraction (in percent). The measurements have been performed by means of needle-probes.

In Fig. 22.f a stable case is reported; in this case the position of the flashing boundary does not change significantly. Bubbles formation and condensation continue to take place in the riser, and local void fraction fluctuations with a frequency between 2 and 4 Hz (see Paper I) are observed. These fluctuations are related to the lengths, frequencies and velocities of the steam bubbles. A more detailed analysis of the temporal and spatial void-fraction development during flashing instabilities can be found in Paper IV.

The findings discussed above are in contrast with results reported in literature, stating that flashing starts first at the riser exit [6] and flashing instabilities occur only when the void fraction is produced in the very vicinity of the riser exit [37].

4.2. CHARACTERISTICS OF FLASHING-INDUCED INSTABILITIES AND STABILITY MAPS

Several experiments have been carried out at the CIRCUS facility to derive so-called stability maps. These maps are represented in the power-subcooling plane in the present discussion since power and subcooling are the variables directly controlled during the measurements.

Stability maps have been constructed at a pressure of 1 bar and 2 bar. In the former case, two different compressible volumes in the steam dome have been considered. The results are shown in Fig. 23. These maps clearly indicate that, keeping the subcooling constant and increasing the power, the system transits from stable single-phase to stable two-phase circulation passing through a region of instabilities. The same happens when the power is kept constant and the subcooling is decreased.

In agreement with other experimental results reported in literature [5, 38, 39], the range of inlet subcoolings for which instabilities occur increases with power and decreases with pressure. Increasing system pressure has a stabilizing effect also because it reduces the relative amplitude of flow oscillations (see Fig. 24).

The effect of compressible steam volume in the steam dome does not influence the behaviour of the system in steady state conditions since in this case no variation of the compressible volume in the steam dome occurs. In dynamic conditions, however, flashing in the riser will cause a larger pressure increase when a smaller compressible volume is available in the steam dome (smaller H in Fig. 23 and Fig. 24). The pressure increase in its turn will lead to vapour collapse and to an increase of saturation temperature. This feedback limits the amplitude of the flow oscillation. This can be seen in Fig. 24: at a given subcooling, the relative amplitude of flow oscillations corresponding to a steam cushion height of 18 cm (corresponding to about 40 % of the total steam dome volume) is smaller than with a height of 26 cm (corresponding to about 56 % of the total steam dome volume). The reason why at lower subcooling (i.e. close to the stable two-phase operational region) the difference is less significant is not straightforward and is explained in details in Paper IV. The compressible volume in the steam dome has in any case a very small effect. Also Jiang et al. [6] did

not observed significant differences varying the compressible volume from 40% to 50% of the total steam volume. They observed appreciable differences when the compressible volume was further decreased to 30% of the steam dome volume.

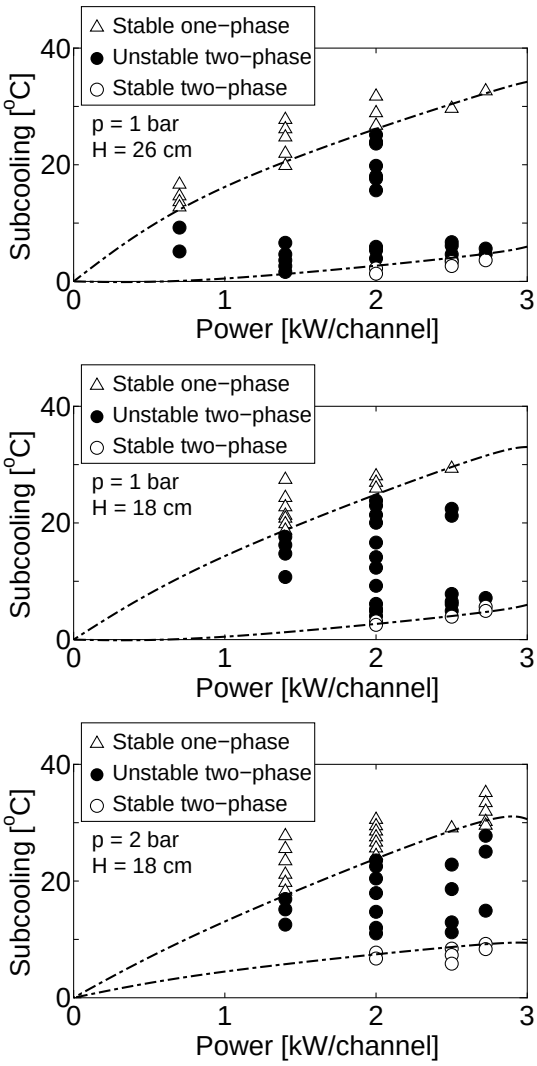

Fig. 23 Stabilities boundary for different pressures p and steam dome volumes in the steam dome. H indicates the height of the steam cushion in the steam dome.

The physical origin of the observed instability suggests that the propagation time of enthalpy perturbations, i.e. the transit time of the mixture through the core and riser is a dominant factor in determining the oscillation period. This transit time is inversely proportional to the coolant flow rate. Therefore the oscillation period should be expected to be inversely proportional to the coolant flow rate as well. The relation between oscillation period and coolant flow rate is shown in Fig. 25. The oscillation period decreases monotonously with increasing average flow rate, although cases with different subcooling, heating power and system pressure have been considered. Clearly, the relation between oscillation period and average flow rate depends only on the geometrical characteristics of the system. The relation also supports the idea that the faster the propagation of enthalpy perturbations, the shorter the period of the oscillation. The importance of enthalpy propagation for the establishment of flashing-induced instabilities can be deduced also by observing that variations of the coolant temperatures at the inlet and outlet of the adiabatic section have about 180° phase shift (see Paper I and Paper IV).

Furuya et al. [5] have shown that the relationship between the kinetic pressure $\rho_L\langle u^2\rangle/2$ and the so-called driving pressure (i.e. the pressure difference that originates from the density difference between fluid in the downcomer and in the core/riser sections) can be approximated by a straight line passing through the origin and that

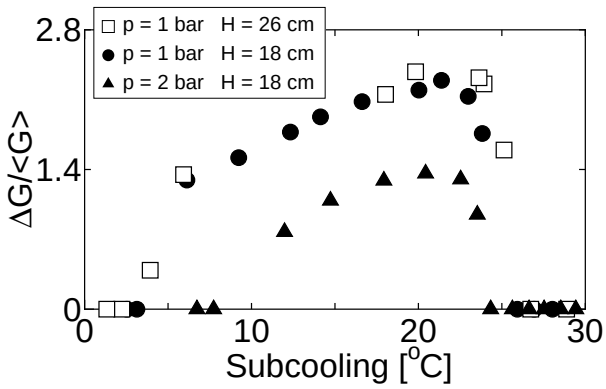

Fig. 24 Relative amplitude of flow oscillation as a function of inlet subcooling. All cases reported correspond to a power of 8 kW and a pressure of 1 bar.

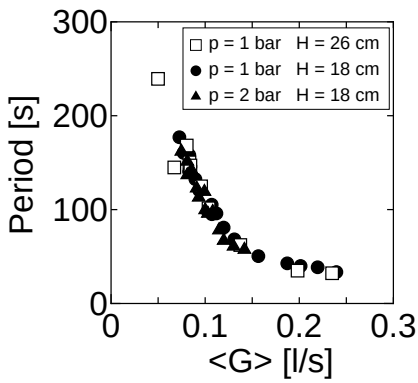

Fig. 25 Oscillation period as a function of the average flow rate. Operational points at different powers and inlet subcoolings are reported.

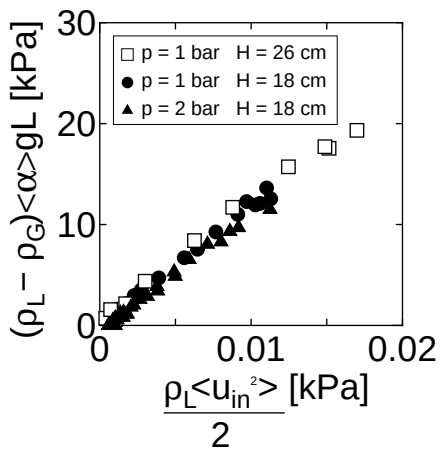

Fig. 26 Average driving pressure as a function of average kinetic pressure. Both stable and unstable operational conditions are represented, at different powers and inlet subcoolings.

the static characteristics are well correlated regardless of whether the flow condition is stable or unstable. This is also found for the experimental set presented in this work (see Fig. 26). Both stable and unstable cases are reported in the picture.

The fact that stable points lie on a straight line supports the idea that driving pressure and friction are the major terms in the momentum balance of the loop. Since also unstable points lie on the same line it means that, in average, during an oscillation period inertia plays a small role in the determination of flow magnitude. The slope of the line can thus be interpreted as a measure of an effective k-factor of the total frictional pressure drops in the entire loop. Furuya et al. [41] finds such a linear dependence with slopes down to ~ 33.

Chapter 5

MODELLING OF FLASHING-INDUCED FLOW INSTABILITIES

An introduction to the modelling of two-phase flow is presented in this chapter. Special emphasis is given to the physics that needs to be modelled to correctly reproduce flashing-induced instabilities at low-pressure and low-power conditions. The two-phase flow code FLOCAL, which is used in this thesis for the simulation of flashing-induced instabilities, is described.

5.1. CHARACTERISTICS OF THERMAL-HYDRAULIC CODES (FROM HEM TO 6-EQUATIONS MODELS)

There are different ways to model two-phase flow with different levels of approximations. Generally the quantities of interest are:

a) the void fraction α, defined as the ratio A_G/A between the area occupied by the steam and the total area of the cross-section;
b) the quality x, defined as the ratio M_G/M between the steam mass flow rate and the total mass flow rate through the cross section;
c) the pressure p;
d) the internal energy (or enthalpy) of steam and liquid phase (U_G and U_L respectively or h_G and h_L);
e) the steam and liquid velocities (u_G and u_L respectively).

The void fraction can be determined on the basis of the quality, once the pressure and the ratio between the velocities of the two phases (so-called *slip-ratio*) are known. Thus the problem reduces to a total of six unknowns.

One of the major difficulties in modelling two-phase flow is the fact that the geometry of the interface between the two phases (i.e. steam and water) is not known a priori, since the way in which the phases are going to distribute with respect to each other (i.e. the flow pattern) is also part of the solution. Three- or two-dimensional two-phase models based on a Computational Fluid Dynamics (CFD) approach are extremely time-consuming and their application is limited to bubbly flows with low void-fraction, their development being still underway, hence only one-dimensional models will be discussed here.

The most general approach in 1-D geometry is based on 6-equations models where the two phases are treated as two separated fluids for which mass, momentum and energy balances are solved separately. This type of model is implemented in the so-called state-of-the-art or best-estimate codes (RELAP5, TRAC, MONA, etc.) and allows considering thermal non-equilibrium and slip between the phases. The disadvantage of this approach lies, beside the complexity of the numerical schemes and the computational efforts required, in the need of several closure relations to couple the balance equations for the two phases. Closure relations are mostly empirical and flow-pattern dependent. The complexity of this type of models makes it difficult if not impossible to determine cause-effect relationships in the results of the simulations. On the other hand, state-of-the-art codes have the advantage of being quite general, so that they can be used to simulate a wide range of geometrical configurations and a large variety of thermal-hydraulic problems.

Simpler approaches consider, with decreasing level of complexity, five, four or three balance equations. In the latter case, referred to as HEM (Homogeneous Equilibrium Model), the two-phase mixture is modelled as one single fluid and thermal equilibrium is assumed between the two phases (i.e. the two phases are assumed to be at the same temperature, equal to the saturation temperature). A drift velocity may be considered in the void-fraction/quality relation by means of drift-flux models.

To simulate flashing-induced instabilities the essential factors to be considered are:

1. Pressure dependency on the axial location along the system and evaluation of the fluid thermodynamic properties as function of the local pressure. If the local pressure is not considered, the model cannot predict the occurrence of flashing. Hence, this effect is fundamental for the model. For this a HEM model would be sufficient.
2. Velocity slip between the phases. It is of great importance for a reliable prediction of the void fraction, which is one of the most important variables in flashing systems because it determines the buoyancy of the natural circulation loop. In principle, to evaluate the velocity slip, the liquid and vapour velocities should be calculated separately on the basis of two momentum balance equations. However, drift-flux models can be used to assess the phase slip on the basis of other state variables (void fraction, pressure, flow rate, etc.) so that the slip between the phases could be taken into account even with a HEM model.
3. Thermal non-equilibrium between liquid and steam phases. This includes subcooled boiling in the heated section and liquid in superheating conditions in the adiabatic section. Experimental evidence of both superheating and subcooled boiling has been found (see Paper IV and Paper V). They are especially important during the incubation phase between two successive flashing cycles. Thermal non-equilibrium cannot be taken into account with a HEM model.

Though a HEM model combined with correlations for phase slip and subcooled boiling could reproduce the instabilities reasonably well, a 4-equations model seems to be a good compromise (in terms of model complexity) in order to achieve not only qualitative but also quantitative agreement with experimental data.

5.2. FLOCAL: A 4-EQUATIONS TWO-PHASE FLOW CODE

A 4-equations model has enough complexity to fully take into account the essential physics that is recognized during flashing instabilities at low pressures. On the other hand this type of model has the advantages of being still simple enough to allow relatively easy modifications and implementations of new models without drastic changes to the structure of the code. Small computational efforts are needed giving the possibilities to perform, among others, parametric studies and computation of stability boundaries. Moreover, the number of empirical correlations needed is quite limited, so that clear cause-effect relationships can be assessed in the simulations.

FLOCAL [42] is a 1-D 4-equations two-phase thermal-hydraulic code originally developed to model the dynamic behaviour of the AST-500 reactor, a Russian design of a district reactor based on natural circulation. The core is modelled as a series of parallel coolant channels associated to one or more fuel assemblies. On top of the core both individual (parallel) risers and a common riser can be modelled. The parallel channels are coupled by a boundary condition of equal pressure drops over their total length.

The system of partial differential equations (PDEs) consists of a momentum balance, an energy balance and a mass balance equation for the two-phase mixture with in addition a separate mass balance equation for the vapour phase:

$$\begin{cases} \text{mixture mass balance} & \frac{\partial}{\partial t}\left[\alpha\rho_G+(1-\alpha)\rho_L\right]+\frac{\partial}{\partial z}\left[u_G\rho_G\alpha+u_L\rho_L(1-\alpha)\right]=0 \\ \text{vapour mass balance} & \frac{\partial}{\partial t}(\rho_G\alpha)+\frac{\partial}{\partial z}(u_G\rho_G\alpha)=\mu \\ \text{mixture energy balance} & \frac{\partial}{\partial t}\left[\alpha h_G\rho_G+(1-\alpha)h_L\rho_L\right]+\frac{\partial}{\partial z}\left[h_Gu_G\rho_G\alpha+h_Lu_L\rho_L(1-\alpha)\right]=Q \\ \text{mixture momentum balance} & \frac{\partial}{\partial t}\left[\alpha\rho_Gu_G+(1-\alpha)\rho_Lu_L\right]+\frac{\partial}{\partial z}\left[u_G^2\rho_G\alpha+u_L^2\rho_L(1-\alpha)\right]+ \\ & +\frac{\partial p_R}{\partial z}+g\left[\alpha u_G+(1-\alpha)u_L\right]+\frac{\partial p}{\partial z}=0 \end{cases} \tag{7}$$

where Q is the source term of power density and μ is the evaporation/condensation rate. The coupling between the two mass balance equations is done by means of additional evaporation and condensation models, allowing thermodynamic non-equilibrium between the two phases (the steam temperature is assumed to be always equal to the saturation temperature, while no restriction is put on the liquid temperature). The difference in velocity between steam and liquid phase is taken into account by means of a drift-flux model.
The four balance equations are completed by a quasi-stationary relation for the phase-slip and by the thermodynamic state equations $h_G=h''(p)$, $\rho_G=\rho''(p)$, $\rho_L=\rho(h_L, p)$. Constitutive relations are used for the distributed and concentrated friction pressure drops p_R and for the evaporation/condensation rate μ. The homogeneous two-phase friction multiplier is used to evaluate two-phase frictional pressure drops.
To evaluate the heat transfer between fuel and coolant the heat balance for the fuel and the cladding is solved:

$$\rho c \frac{\partial T}{\partial t} = \frac{1}{r}\frac{\partial}{\partial r}\left(\lambda r \frac{\partial T}{\partial r}\right) + Q_B \tag{8}$$

where Q_B is the source term of power density in the fuel. Constant values are assumed for the density ρ, the heat capacity c, and the conductivity λ of fuel and cladding. More details about the model and the constitutive relations used can be found in Ref. [42] and in Paper V. Also the iterative schemes implemented for the spatial and temporal integration of the set of PDEs are discussed in these documents.

5.2.1. MAIN CODE IMPROVEMENTS

After some pre-test calculations and a detailed analysis of the experimental data collected at CIRCUS, improvements have been made to the code to include other physical effects that, though not fundamental to simulate flashing instabilities, are important for a good quantitative agreement between experiments and simulations. Here, the major additions to the original model are described.

HEAT STRUCTURES

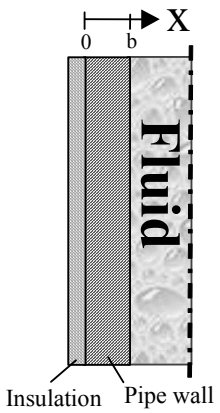

Fig. 27 Scheme of an axial node of the adiabatic section.

During the analysis of flashing-induced instabilities, it has been found that heat structures play an important role in the determination of the oscillation period (this issue is discussed in Chapter 6 and in Paper V). To consider the dynamics of the heat structures of core and adiabatic sections, a model for pipe walls has been included in the FLOCAL code. The glass pipes of the CIRCUS facility are approximated as flat walls (slab model). This approximation is acceptable because the ratio between wall thickness and pipe radius is small (< 0.1). A scheme of an axial node of the adiabatic section is illustrated in Fig. 27. The heat conduction equation expressed by:

$$\frac{\partial T}{\partial t} = \frac{\lambda}{\rho\, c_p}\frac{\partial^2 T}{\partial x^2} \tag{9}$$

is solved with the following boundary conditions:

$$\begin{cases} \lambda \dfrac{\partial T}{\partial x} = -q''_{wall} & x = b \\ \dfrac{\partial T}{\partial x} = 0 & x = 0 \end{cases} \tag{10}$$

A zero heat flux is assumed as boundary condition for the external wall surface ($x=0$) because of the presence of insulation material in the experimental set-up. For the surface at contact with the fluid ($x=b$) it holds:

$$q''_{wall} = H_{WF}\left(T_{wall} - T_{fluid}\right) \tag{11}$$

For the heat transfer coefficient H_{WF} between fluid and wall the Guerrieri's model [43] is used, which is basically a Dittus-Bolter type correlation extended to the case of two-phase mixture.
To solve the PDE (9) the temperature distribution in the wall is expanded in eigenfunctions. After appling the boundary conditions (10) and truncating the expansion to N for practical applications, the PDE can be expressed as a system of $N+1$ ODEs:

$$\begin{cases} \dfrac{\partial \Delta T_{wall,0}}{\partial t} = \dfrac{q''}{b\,\rho\,c_p} \\ \dfrac{\partial \Delta T_{wall,n}}{\partial t} = \dfrac{2q''}{b\,\rho\,c_p} - \dfrac{\lambda}{\rho\,c_p}\left(\dfrac{n\pi}{b}\right)^2 \Delta T_{wall,n} \quad \text{n=1,2,...N} \end{cases} \tag{12}$$

with

$$T_{wall}(t) = T_{wall}(t=0) - \sum_{n=0}^{N} \Delta T_{wall,n}(t) \tag{13}$$

The system of equations (12) is solved for each axial node of the adiabatic and heated sections. An explicit Euler scheme is used for the numerical integration. To ensure numerical stability a much smaller time step is needed with respect to the one used for the solution of the PDEs in (7). Therefore a separate time-step controlled routine has been added to the code.
At the beginning of the dynamic calculation, it is assumed that walls and fluid are at the same temperature as calculated from the steady-state module of the code FLOCAL.

TURBULENT DIFFUSION

During the incubation period that precedes the occurrence of flashing, liquid at higher temperature coming from the heated section moves upward toward a region at lower temperature in the riser. The negative temperature gradient can cause turbulent mixing between the temperature layers because of buoyancy effects. This phenomenon is more significant at low velocities when the turbulent diffusive processes play an important role with respect to convective processes. In Chapter 6 it will be shown that this phenomenon may have strong influence on the duration of the incubation period.
Experimental evidence of the smearing of the temperature front during flashing experiments at the CIRCUS facility can be deduced by analysing thermocouples signals. As shown in Fig. 4, the temperature is measured at six axial locations along the riser section. To study how the temperature front propagates along the riser a virtual z axis is defined for each i-th temperature measurement:

$$z_i^*(t) = \int_{t_0}^{t} u_{inl}(t')\,dt' - z_i \tag{14}$$

where $u_{inl}(t)$ is the liquid velocity at the inlet of the test section and z_i is the distance of the i-th thermocouple from the inlet of the riser (where the temperature T1 is measured. See Fig. 4). The time t_0 can be chosen arbitrarily. Assuming the liquid to be incompressible, the fluid velocity can be considered only time-dependent so that the virtual axis z^* in eq. (14) represents the space that would be travelled by a temperature wave moving with a velocity $u_{inl}(t)$. In Fig. 28 the temperatures measured along the riser section during a flashing cycle are presented (left) together with the corresponding void fraction (right) measured by means of needle-probes. Instead of the time-axis, the virtual z^*-axis is used. In case of pure transport, all the temperatures in the new reference system

should rise and decrease in the same way (since the time shift due to transport has been eliminated by means of the change of coordinate system). On the contrary, from Fig. 28 (left) it is observed that the slope of the temperature rise is progressively decreasing along the riser (from T1 to T6). This slope change is observed when the temperature gradient is negative. During the temperature drop instead, when the temperature gradient is positive and the buoyancy does not cause additional mixing, all the temperature measurements are superimposed with the exception of measurements T5 and T6 and in minor extent of T4. This is due to the fact that at location *4* to *6* steam has been produced (see void fraction measurements in Fig. 28 right) in which case the assumption of space-independent velocity does not hold and the definition of the virtual axis z^* loses its usefulness.

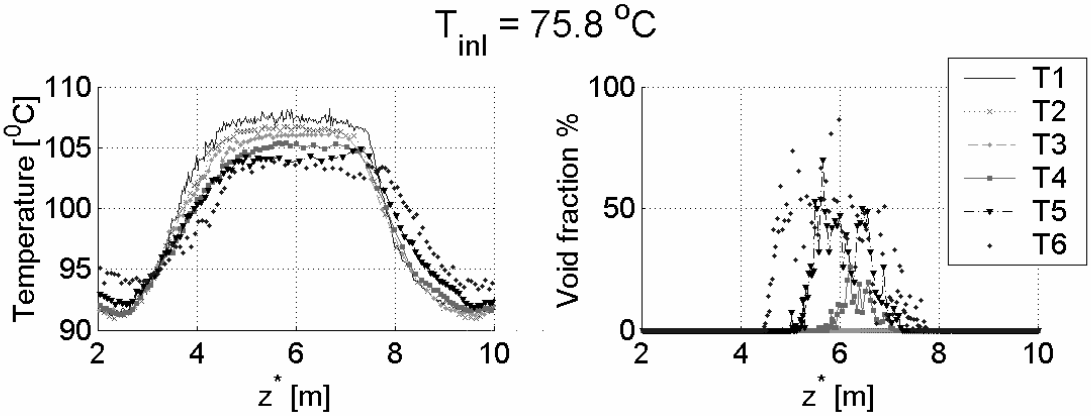

Fig. 28 Experimental evidence of mixing between temperature layers (power of 8 kW, pressure of 1 bar). The fluid temperature rises with decreasing slope along the axis of the riser section. In the decreasing phase, the temperature decreases with the same velocity at all location, with the exception of the ones were void fraction is present.

The effect of turbulent mixing due to buoyancy effects in presence of a negative temperature gradient has been found also by CFD simulations performed at conditions representative of the measurements carried out at the CIRCUS facility.
The energy balance in the original FLOCAL model has the form:

$$\frac{\partial \rho h}{\partial t} + \frac{\partial \rho u h}{\partial z} = q \tag{15}$$

In the adiabatic section $q=0$ (if heat transfer to the structures is not considered), thus in the single-phase region the temperature front is simply transported upward with velocity u. A very simple way to model the effect of turbulent mixing on the temperature field is to include a diffusive term in the energy balance (15) as follows:

$$\frac{\partial \rho h}{\partial t} + \frac{\partial \rho u h}{\partial z} = q + \frac{\partial}{\partial z}\left(\nu \frac{\partial h}{\partial z} \right) \tag{16}$$

The diffusive term will cause a smearing of the temperature front moving from the heated to the adiabatic section, causing a time delay in the flashing occurrence. The effect should become negligible when the convective term in the equation plays a major role.
A simple estimation for the diffusivity coefficient ν is given by [44]:

$$\nu \approx L^2 \sqrt{\frac{1}{T}\frac{\partial T}{\partial z} g} \tag{17}$$

where L is an appropriate scale length. At conditions typical of the CIRCUS facility the diffusivity is of the order of about $5*10^{-3}$ m^2/s.
The diffusivity is not constant, being a function of the temperature gradient, but an exact modelling of this effect goes beyond the scope of this work. Thus, a constant value of $5*10^{-3}$ m^2/s has been used in the FLOCAL model to study the effect of diffusivity on the period of flashing-induced flow oscillations. Results are discussed in Chapter 6. The coefficient is set to zero when void is present

(in this case the diffusion term can be neglected with respect to the transport term) or when the temperature gradient is positive. In the latter case, low-density fluid is on top of high-density fluid and the mixing of temperature layers will not occur because of density differences.

DRIFT-FLUX MODELS

The drift-flux models originally implemented in FLOCAL were Zuber-Findlay, Bankoff and Labuncov. As shown in Chapter 3, none of these models produces satisfactory predictions of the void-fraction in a flashing flow at low pressure. On the basis of the findings reported in Chapter 3, the GE-Ramp model was included in the code and selected to carry out the comparison with experimental results. Since in this model the drift velocity and the distribution parameter are function of the void fraction, the latter one has to be evaluated iteratively. Apart from the GE-Ramp model, other drift-flux models have been implemented in FLOCAL to check whether the same trends observed in the experimental work described in Chapter 3 are also seen in the simulation. The results obtained with FLOCAL in combination with different drift-flux models are reported in Paper II.

Chapter 6

CODE VALIDATION

In this chapter the simulations carried out with the code FLOCAL are qualitatively and quantitatively compared with the experimental data obtained from the CIRCUS facility. The dominant physical effects during flashing-induced instabilities are discussed.

6.1. NODALIZATION ADOPTED

The nodalization used to simulate the CIRCUS facility is schematically represented in Fig. 29. Both heated and riser sections have been divided into 30 axial nodes for the spatial integration of the system of PDEs.

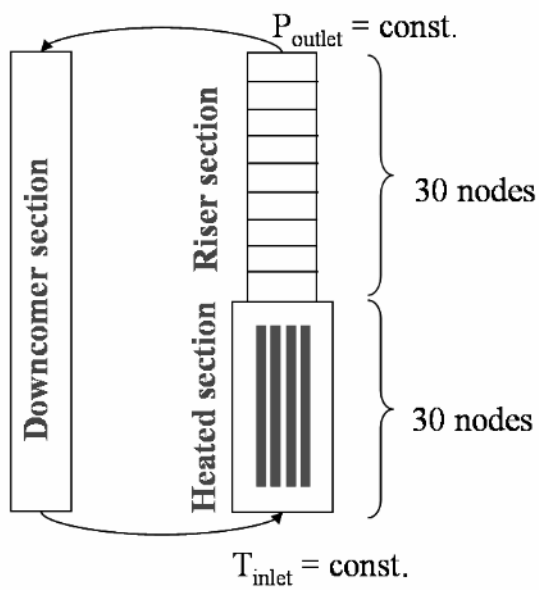

Fig. 29 CIRCUS nodalization adopted for the FLOCAL simulations. The heated section and the riser are both discretized in 30 axial nodes. For the downcomer a lumped parameters model is used. Boundary conditions are supplied for the inlet temperature and the outlet pressure.

As boundary conditions, the coolant temperature at the inlet of the heated section and the pressure at the outlet of the adiabatic section are kept constant. The boundary condition on the coolant temperature is exact, since the inlet temperature is kept constant also during the experiments. This is not the case for the condition on the outlet pressure. In the experimental set-up the loop is connected to a steam dome, where a mixture of steam and water is present. During flow instabilities, the production of steam in the adiabatic section causes an equivalent volume of water to enter the steam dome leading to a compression (and partially condensation) of the steam cushion in the steam dome itself. This has as effect a temporary increase of the system pressure that limits the steam production and expansion in the adiabatic section and therefore the amplitude of the flow oscillations. Since the feedback of the steam dome is not considered in this analysis with the code FLOCAL, one should expect higher amplitude of the flow oscillations in the simulations. In any case, neglecting the feedback of the steam dome does not affect the reproducibility of the phenomenology of flashing-induced instabilities.

The friction factors that define the concentrated frictional pressure drops have been evaluated on the basis of standard geometry-based correlations [45]. The friction factor of the valve at the inlet of the heated section has been determined experimentally.

6.2. COMPARISON WITH EXPERIMENTAL DATA

The predictions of FLOCAL are first compared with stationary experimental results in single-phase conditions at a pressure of 1 and 2 bar to check whether the geometry and frictional pressure drops in the loop are well estimated. The comparison shows good agreement (see Paper V). Time-dependent cases are reported in Fig. 30, where the time traces of the flow rate calculated with FLOCAL are compared with the experimental time-traces recorded at the CIRCUS facility. The time-traces were collected at a total heating power of 8 kW and a system pressure of 1 bar. The temperature at the inlet of the heated section is gradually increased. As expected, FLOCAL slightly over-estimates the maximum flow rate achieved during the flow oscillations. As mentioned previously, this is due to the neglect of the feedback from the compressible volume in the steam

dome. Despite this approximation, the general phenomenology and trends seem to be reproduced very well, with the exception of the oscillation period that appears to be in general under-estimated.

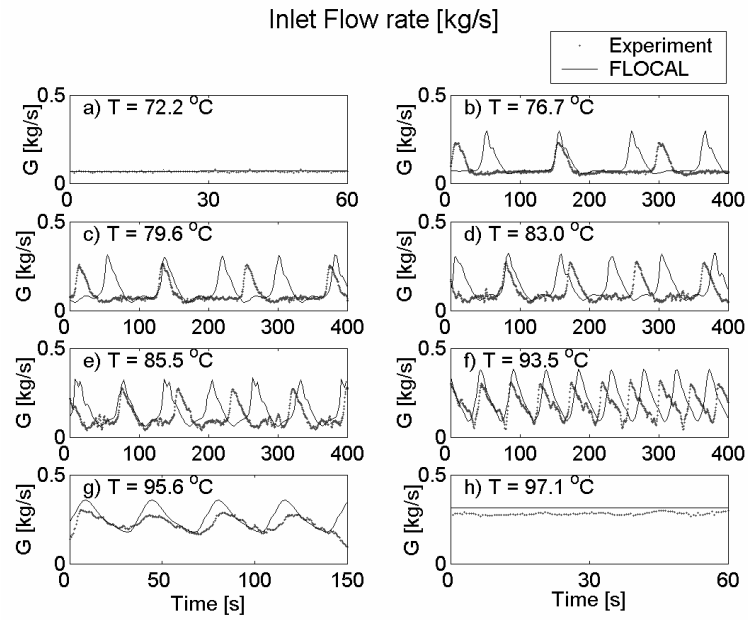

Fig. 30 Comparison between experimental flow-rate time traces and FLOCAL simulations (8 kW, 1 bar). The coolant temperature at the inlet of the heated section is increased from case to case.

Increasing the inlet temperature, the model correctly predicts the transition from stable single-phase circulation (Fig. 30.a) to stable two-phase circulation (Fig. 30.h) passing through an intermediate unstable region (Fig. 30.b through Fig. 30.g). As from the experiments, two main types of instabilities are predicted by the code: a first type, that can be called intermittent natural circulation, in which single-phase and two-phase natural circulation alternate periodically (Fig. 30.b through Fig. 30.f) and a second type of oscillation, that can be called unstable two-phase circulation, during which the two-phase mixture is always present in the system and a symmetrical flow oscillation that approximate the sinusoidal shape is established (Fig. 30.g).

The existence of an incubation period between two successive flow-rate peaks (Fig. 30.b through Fig. 30.e) is also predicted by the model, though its duration is under-estimated. This issue will be discussed in more details in paragraph 6.2.2. In agreement with the experimental trend, the period of the oscillation decreases with decreasing inlet temperature.

6.2.1. VOID-FRACTION EVOLUTION IN THE ADIABATIC SECTION

In Fig. 31 the time evolution of the void fraction along the vertical axis of the riser section is reported. Again the time traces were recorded at a total heating power of 8 kW and a system pressure of 1 bar. Different cases are shown corresponding to different temperatures at the inlet of the heated section. The magnitude of the void fraction is represented by means of contour plots. Both simulated (left picture) and experimental (right picture) time traces are reported.

Also with regard to the void fraction good agreement is found between the model predictions and the experiments and the phenomenology is reproduced very well. At low inlet temperatures (Fig. 31.a) flashing starts relatively high in the riser and later on the flashing front expands and propagates both in upward and downward directions. As soon as the inlet temperature increases, steam bubbles are generated first in the heated section (subcooled boiling) below the riser inlet. These bubbles collapse in the riser (contributing to the heating up of the fluid) before flashing starts (Fig. 31.b and Fig. 31.c). Increasing the inlet temperature, flashing in the riser is directly triggered by the voids coming from the heated section (Fig. 31.d and Fig. 31.e).

Experimental evidence of thermal non-equilibrium between liquid and vapour phase, as shown in (Fig. 31.b through Fig. 31.d), can be verified even better by a careful analysis of the needle-probes' signals. In Fig. 32 the instantaneous local void fractions measured by the needle-probes along the vertical axis of the riser section are presented together with the corresponding temperatures. From the enlargement at the right side of the picture it is evident that temperature peaks occur concurrent with the passage of steam bubbles (detected as peaks in the void fraction).

Steam bubbles transported upwards encounter liquid which can be even more than 2°C colder than the steam. The thermal non-equilibrium between liquid and vapour phase is very pronounced when flashing is not yet developed. The magnitude of the temperature difference between liquid and vapour decreases during the development of steam production until thermal-equilibrium is reached.

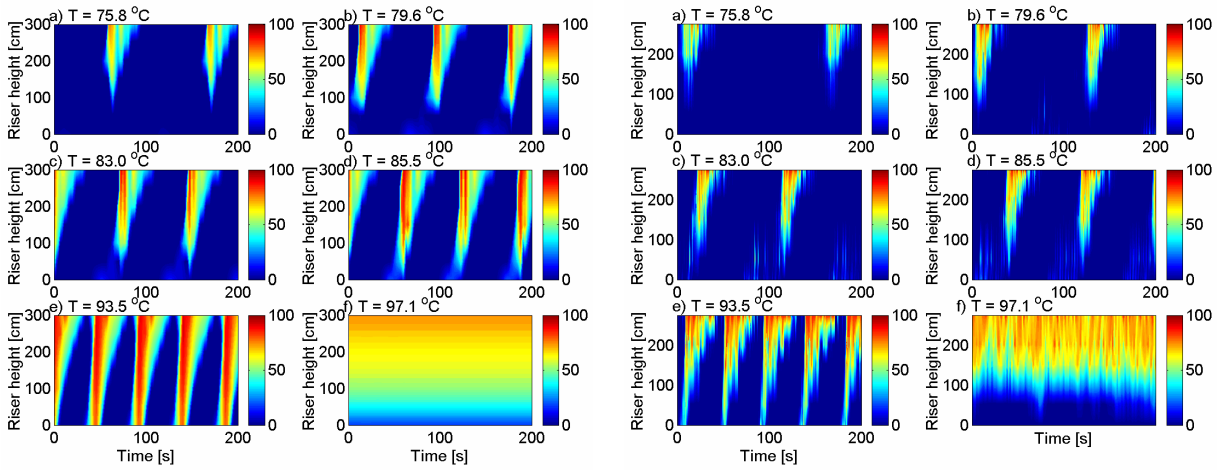

Fig. 31 Void-fraction evolution from FLOCAL simulations (left) and as measured with needle-probes at the CIRCUS facility (right). Vertical bars give the colour-scale coding for the void fraction (in percent). The needle-probes signals have been corrected to take into account the radial void-fraction profile, as described in Paper II.

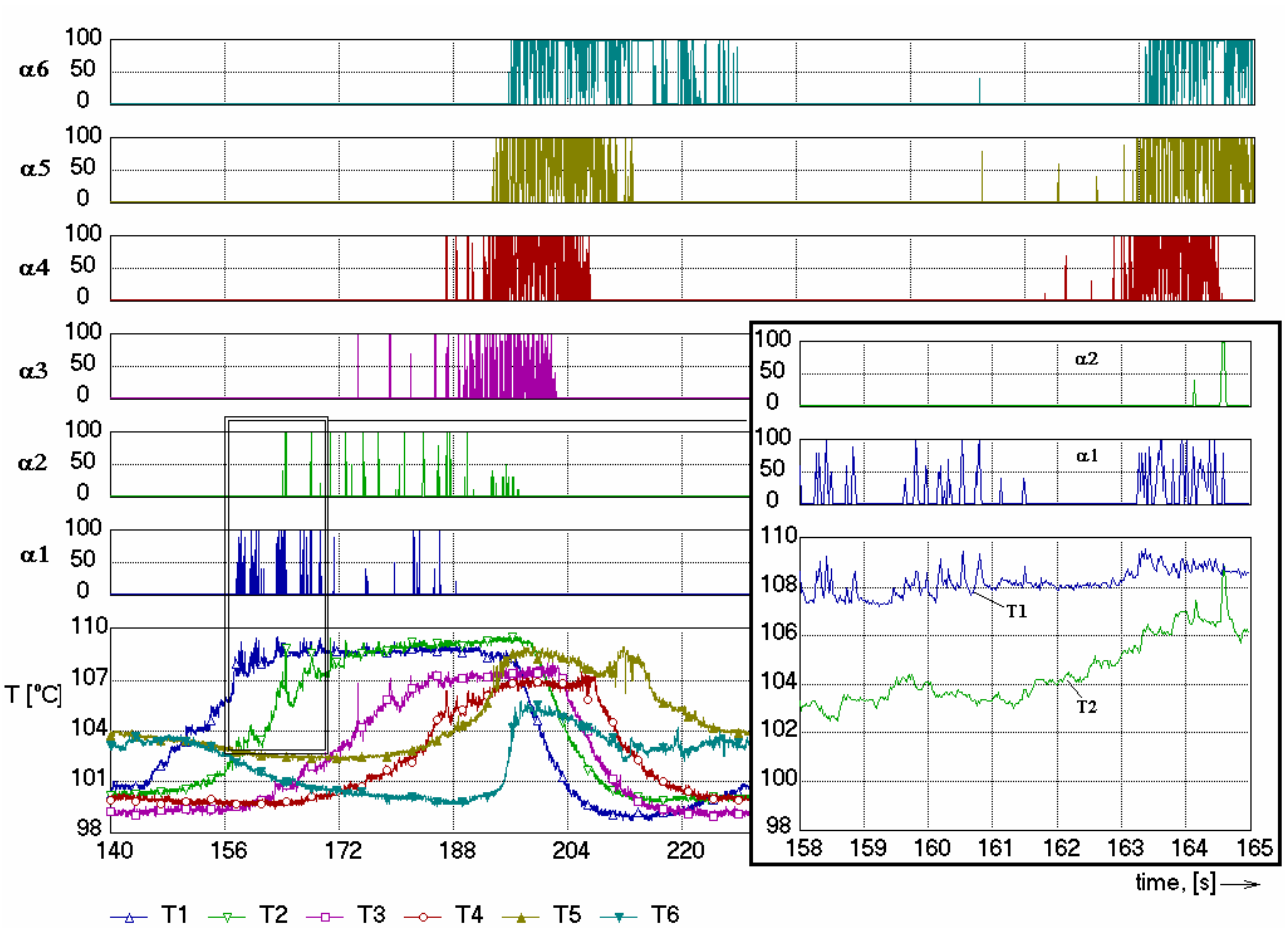

Fig. 32 Experimental evidence of thermal non-equilibrium between liquid and vapour phase. The void fraction and the fluid temperature measured along the axis of the riser section by means of the needle-probes with integrated thermocouples are shown. From the enlarged detail it can be seen that, in the first phase of flashing, temperature peaks occur at the passage of steam bubbles.

6.2.2. QUANTITATIVE COMPARISON WITH THE EXPERIMENTAL RESULTS

A quantitative comparison between experimental and model results is shown in Fig. 33 to Fig. 36. In Fig. 33.a the oscillation period is reported against the average flow rate. Fair agreement is found. The findings of the experimental campaign at the CIRCUS facility supported the idea that the

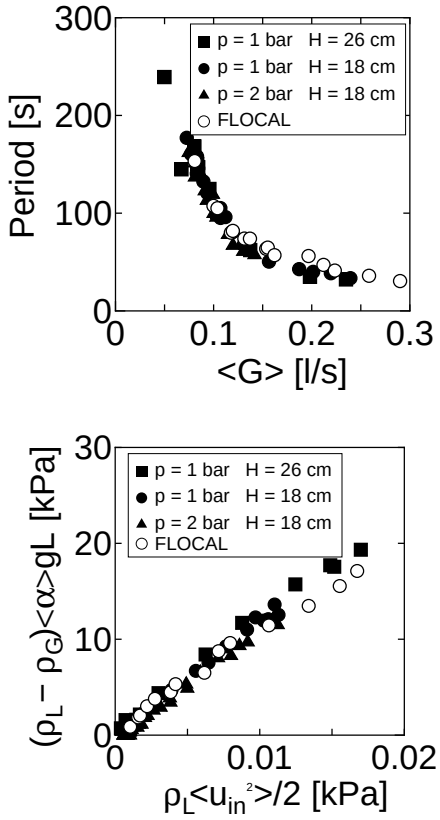

(a)

(b)

Fig. 33 Relation between oscillation period and average flow rate (a) and between driving and kinetic pressure (b). Measurements and calculations (FLOCAL).

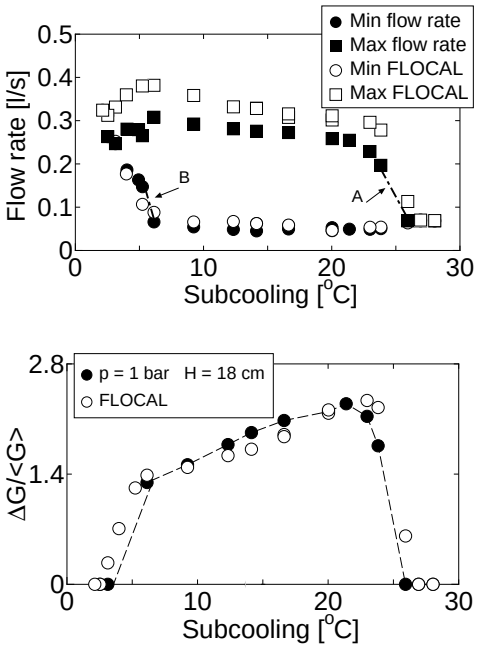

(a)

(b)

Fig. 34 Relation between maximum and minimum flow rate vs inlet subooling (a) and between relative amplitude of the flow oscillation and inlet subcooling (b). Measurements and calculations (FLOCAL).

relation between the two variables is merely a function of the geometry of the system and it is not influenced by pressure, heating power or inlet subcoolings. This trend seems to be confirmed by the FLOCAL calculations. In Fig. 33.b the relation between the driving pressure in the loop and the kinetic pressure is shown. All experimental points, both stable and unstable, lie approximately on a straight line passing through the origin. In Chapter 4 and in Paper IV it is argued that the reason for this behaviour is the fact that driving pressure and friction are the major terms in the momentum balance of the loop, while inertia and acceleration pressure drops play a small role in the determination of flow magnitude. This argument has been confirmed by the FLOCAL calculations, since it is found that inertia and acceleration pressure drops are orders of magnitude smaller than frictional and gravitational pressure drops. This effect is even more prominent at low inlet subcooling (i.e. high void fraction).

In Fig. 34.a the relation between minimum and maximum flow rate during a flashing-induced flow oscillation and the inlet subcooling is shown for the experiments and the model results (8 kW power, 1 bar system pressure). The calculated minimum flow rate matches very well the experimental values. The maximum flow rate is overestimated, this effect being caused by the boundary condition of constant pressure at riser outlet used in FLOCAL. Nevertheless, the transition A, from stable single-phase to unstable circulation, and the transition B, from intermittent circulation to unstable two-phase circulation, are well reproduced.

In Fig. 34.b the relation between the relative amplitude of the flow oscillation and the inlet subcooling is reported, always for a total power of 8 kW and a system pressure of 1 bar. The subcooling range of instabilities (from ~3°C to ~25°C) is predicted perfectly. On the other hand, the very good agreement in predicting the relative amplitude of oscillation $\Delta G/\langle G\rangle$ is misleading since it is due to the combination of the overestimation of maximum flow rate and underestimation of the oscillation period.

The relation between oscillation period and inlet subcooling is presented in Fig. 35 (8 kW, 1 bar). As already pointed out, in many cases the model under-estimates the oscillation period (from Fig. 30 it can be seen that it is mainly the incubation period which is under-estimated rather than the duration of the flow peak caused by the flashing transient).

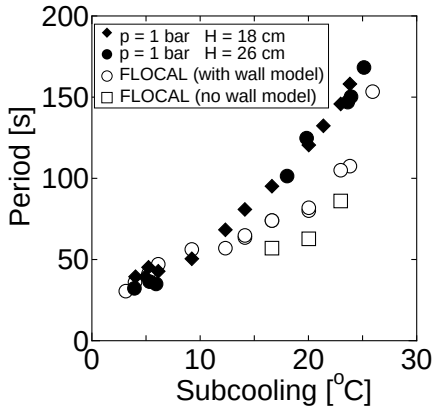

Fig. 35 Oscillation period vs subcooling.

The oscillation period is very well predicted at low subcoolings (i.e. high flow rates and absence of single-phase circulation) and underestimated at high subcoolings (i.e. at low flow rates and presence of alternate single-phase/two-phase circulation). The reason could lie on both heat losses to the environment, neglected in the calculation presented here, and on the smearing of the temperature front during the single-phase circulation. Calculations including heat losses have been performed with FLOCAL but, though they cause an increased incubation period, they do not justify the extent of under-estimation of the incubation period. The smearing of the temperature front has already been discussed in Chapter 5 and seems to be caused by turbulent diffusion in presence of a negative temperature gradient along the vertical axis of the adiabatic section. Its effect will be discussed in paragraph 6.2.3.

The strong effect of the energy accumulated in the heat structures, namely the walls of riser and heated section is clearly visible (Fig. 35, "no wall" calculations). Finally, in Fig. 36 the comparison between experimental and calculated stability boundaries in the subcooling-power plane is reported. Good agreement is found.

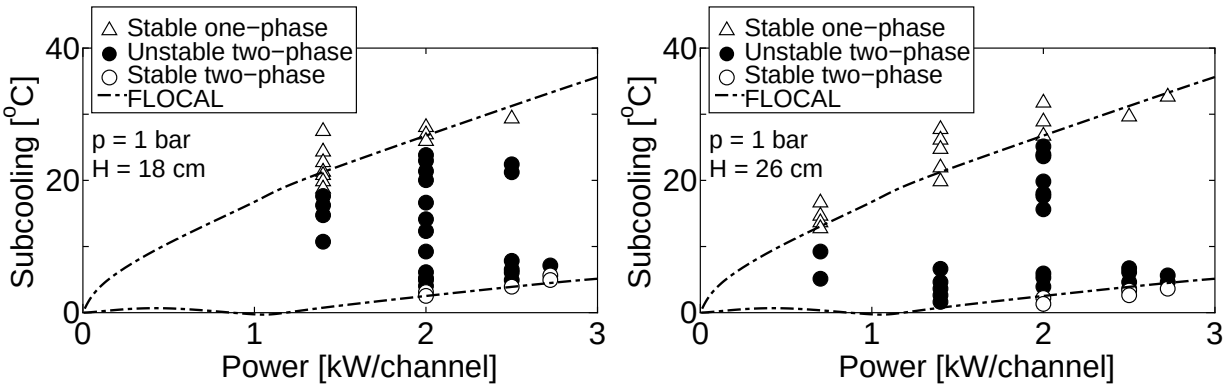

Fig. 36 Comparison between experimental and FLOCAL stability boundary.

6.2.3. EFFECT OF TURBULENT DIFFUSION CAUSED BY TEMPERATURE GRADIENTS

The effect of turbulent diffusion on the oscillation period is shown in Fig. 37 for simulations at high and low inlet subcooling. As it can be seen, at high subcooling (Fig. 37 left) a considerable increase of the incubation period (i.e. of the oscillation period) is achieved if the diffusion term is considered in the energy balance. At low subcooling (Fig. 37 right) the effect is negligible.

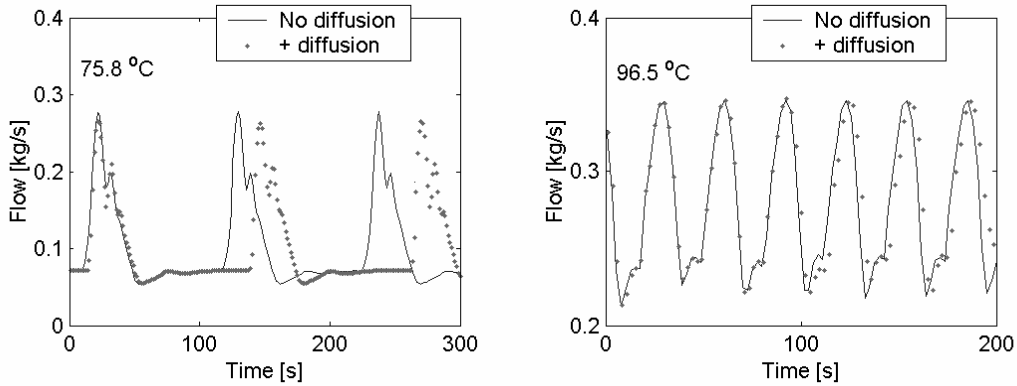

Fig. 37 Effect of diffusive term in the energy balance equation. Two FLOCAL simulations are shown at low and high inlet temperature respectively.

Thus, this phenomenon explains why the original FLOCAL model under-estimates the oscillation period at high inlet subcoolings, while it gives good predictions at low inlet subcoolings (Fig. 35).

Chapter 7

START-UP PROCEDURES

In this chapter a literature review is presented on start-up procedures that have been suggested for natural circulation BWRs. Moreover, a novel start-up procedure is proposed that does not need external pressurization of the reactor vessel.

7.1. INTRODUCTION

The elimination of recirculation pumps and associated systems allows a great simplification of the design of BWRs. On the other hand it has been shown, both experimentally and analytically, that such a new reactor configuration makes the system susceptible to thermal-hydraulic instabilities during the start-up phase. Up till now there has been no discussion whether or not the reactor could stand flow oscillations and, in this case, what are the limits within which the amplitudes and frequencies of the oscillations (of flow, temperatures, etc.) are still acceptable. As a matter of fact the reactor power is very low, so there are large margins with respects to thermal limits and power peaking factors; the core is in single-phase conditions, so the flow oscillation does not turn into a power oscillation; the periods of the oscillations are relatively large and the amplitudes of temperature fluctuations are about 10 ^{o}C or lower. It should be examined if such oscillations could initiate thermal fatigue of the reactor internals. A serious problem could be related to the mechanical vibrations of the structures that might be induced by the flow oscillations. The vibrations depend not only on the geometry of the structures but also on how and where the structures are fixed, so that a detailed description of the reactor is needed to perform any assessment.

However, since it is not clear whether flashing-induced oscillations are acceptable for the reactor safety or not, appropriate start-up procedures have to be planned to avoid instabilities.

Before going through the different proposals present in literature, it seems appropriate to first describe the start-up procedure realized at the Dodewaard reactor [46]. This procedure was proven to be successful during the almost 30 years of operation of the reactor.

7.2. THE START-UP PROCEDURE OF THE DODEWAARD REACTOR

The start-up of Dodewaard is described by Nissen et al. [46] and develops as follows (for a scheme of the reactor it is suggested to refer to Fig. 1, keeping in mind that no steam separators are present in Dodewaard):

a) first the vessel contains water at about 95 ^{o}C with a water level of 2.54 m above riser exit (the value at nominal power is 0.54 m). The water is circulated and heated up by means of the RAS (Reactor Shutdown Cooling System) heaters up to 100 ^{o}C;
b) the reactor is made critical and an heat-up rate of 45 to 55 ^{o}C/h (by fission power) is maintained. The pressure rises. When a pressure of 5 bar is reached the RWCU (Reactor Water Clean-up System) is started to keep the water level at the desired value;
c) while the pressure rises, the water level above the riser is decreased by means of the RWCU till the nominal level is reached at a pressure of 20 bar. Later on the water level is kept constant by regulating the FW (feed water) flow. Meanwhile, the turbine bypass is used to control the pressure increase;
d) at 30 bar the turbine is started, while pressure and power are continuously increased until nominal values.

Measurements during start-up conditions of the Dodewaard reactor are available, though the lack of instrumentation makes the assessment of the results rather difficult. In fact, during the start-up only reactor pressure and power measurements are available and it is not clear when the transition from single- to two-phase circulation occurs. If steam production takes place only in the riser section at

low power, noise analysis of the in-core neutron detectors will probably not detect significant fluctuations if flow oscillations are generated, especially in transient conditions (flow oscillations in Dodewaard were deduced by neutron flux fluctuations induced via the void-reactivity feedback).
Whether flow oscillations took place or not during the start-up of the Dodewaard reactor, it is striking that no problems (mechanical vibrations, thermal stresses and fatigue) have ever been encountered during the life of the reactor.

7.3. BRIEF LITERATURE SURVEY ON START-UP PROCEDURES FOR NATURAL-CIRCULATION BWRS

Not many proposals of start-up procedures are reported in literature, but all authors [3, 20, 40, 47, 48] agree on the fact that the system should be pressurized before the transition to two-phase circulation is allowed.
Nayak [48] and Jiang et al. [40] propose to externally pressurize the system by injecting in the pressure vessel respectively steam produced in a separate boiler or nitrogen. Once the pressure in the vessel is high enough, the reactor power can be increased to achieve two-phase natural circulation. Unfortunately the procedure suggested by Nayak needs an external boiler of adequate volume and power and the related connecting piping to the reactor vessel, while the one suggested by Jiang et al. requires an additional system for the nitrogen storage and the related connecting piping to the reactor vessel. The external pressurization does not accomplish to the requirements of simplicity that are at the base of the natural circulation BWRs design and is thus not recommendable.
Cheung and Rao [20], from the General Electric (GE) developers team of the ESBWR concept, suggest a start-up procedure in which the reactor is first filled with water at 80 ^{o}C at a pressure of 0.55 bar (such pressure is achieved by opening the connection to the condenser and by operating for a while the vacuum pumps). The reactor is made critical and is pressurized in conditions of single-phase circulation up to a pressure of 63 bar. At this pressure the transition to two-phase operation is achieved by opening the MSIVs (Main Steam Isolation Valves). A simulation by means of TRACG shows that no flow oscillations occur during the transition from single- to two-phase operation.
A similar start-up procedure is simulated by Cheng et al. [15] by means of the code RAMONA-4B. Contrary to Cheung and Rao, Cheng et al. [15] find that the system pressure increases considerably only after net vapour generation takes place in the reactor core. Two points are of particular interest: 1) the simulation does not produce any instability, even if two-phase circulation is reached at low pressure (5 bar); 2) steam starts to be produced in the core and at the inlet of the riser section, i.e. no flashing occurs in the upper part of the riser. Further literature research on RAMONA-4B reveals that in this code thermodynamics properties are evaluated on the basis of the transient average pressure in the system! The observations at point (1) and (2) are thus not surprising at all in view of the fact that the occurrence of flashing cannot be predicted by this code.
Schuster et al. [3], though they do not propose any start-up procedure, on the basis of experimental results collected at the DANTON facility they state that “without external pressurization there exists no other way to reach the stable two-phase operation mode. In all cases a range of instability has to be passed”. A careful analysis of the DANTON facility reveals that the free volume above the riser (5 m length) and the downcomer is only 10 cm high. This means that it is practically not possible to create a steam cushion in this volume without producing steam also in the riser section. Thus it is indeed impossible to start-up the facility without incurring in flow instabilities if external pressurization is not supplied. The start-up procedure for DANTON is described in Ref. [49]. The facility is filled with cold water until a water level of 5 cm above the riser is achieved. The power supplies for the heated section (3 m length) are switched on and single-phase circulation starts. During this time the valve in the steam dome is kept open. When the water in the steam dome reaches saturation conditions the valve is closed and the pressure increases as a result of steam production. Since flashing takes place also in the riser section, flow instabilities are observed.
However, due to the strong limitations on the water level above the riser exit, the DANTON facility is not representative of a natural circulation BWR. In fact, in the design of natural circulation BWRs

a nominal water level of about 0.5-1 m is intended above the riser exit and probably, like in the Dodewaard reactor, it is possible to achieve an even higher water level during the start-up phase, depending on the design of the steam separators.

7.4. OPTIMAL START-UP PROCEDURES

On the basis of the experimental results presented in Chapter 4, we want to develop an optimal start-up procedure keeping in mind that such a procedure should not introduce further complexity in the reactor design, since *simplicity* is the principle on which this new design of BWRs is founded.
It has been shown experimentally and numerically that with increasing pressure the operational region in which a flashing-induced instability can occur becomes smaller.

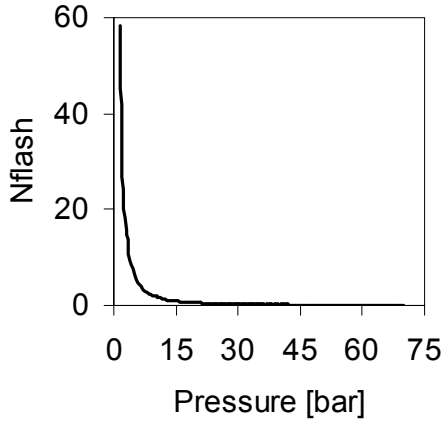

Fig. 38 Flashing number as function of pressure. It is a measure of the importance of the flashing phenomenon.

A measure of the importance of flashing can be deduced also by analyzing the behaviour of the flashing number N_{flash} as a function of pressure. This number appears in the dimensionless form of the system of PDEs for a two-phase flow system when the variation of saturation temperature as function of the local pressure is taken into account, as shown in Paper VI.
The flashing number is a function of the difference between the saturation temperatures at the inlet of the core and at the outlet of the riser. As can be seen in Fig. 38, at pressures higher than 20 bar flashing becomes negligible. Still, care should be taken for so-called low-quality instabilities caused by the fact that at low pressures small variations of the quality induce large variations of the void fraction. In this sense, this second type of instability is very close to flashing-induced instabilities, since the mechanism is based on the propagation of enthalpy perturbations.

It is clear that the system has to be pressurized in order to eliminate the possibility of flashing-induced flow instabilities. It was already mentioned that pressurization by means of nitrogen is not desirable, since an appropriate system would be needed for the storage of the nitrogen itself and care would have to be taken to release the nitrogen out of the pressure vessel, once steam is created in the reactor. Pressurizing by means of steam created in an external vessel is also not desirable, since this would mean to include in the design extra components and piping at the expenses of the economics and the simplicity of the reactor design. Thus, the first problem to solve is how to create a steam cushion in the steam dome, without using external components to pressurize the system.
It is supposed that at the beginning the reactor is filled with water around 80-100 ^{o}C. Such a coolant temperature is consistent with the start-up of the Dodewaard reactor and with the proposal from GE for the start-up of the ESBWR.
Two ways are, at least in principle, possible to create a steam cushion in the steam dome:

1. <u>In conditions of pool boiling</u>
   a) The water level in the reactor vessel is below the riser exit. The MSIVs are closed.
   b) The reactor is made critical at low power. No natural circulation can establish, since downcomer and riser section are not connected by a water level. Due to the temperature gradient, if the power is low enough, it is possible to allow flashing at the top of the riser section so that steam will be produced in the upper part of the riser. Since there is no flow circulation, instabilities cannot take place. Changes in the water level in the riser can be corrected, if needed, via the FW line or by the RWCU system. Eventually, the MSIVs can be opened to let the air out.
   c) Once steam is created at 1 bar, the reactor is made subcritical, the MSIVs are closed and FW is injected in the reactor vessel to increase the water level above the riser exit. Single-phase natural circulation will establish due to the density difference between downcomer and core/riser sections. The process will continue until the temperature field in core/riser

sections and downcomer reaches equilibrium. Though at the beginning of this process colder water enters the core, this will not create reactivity problems if the reactor is made subcritical enough before the water level is increased (a decrease of 1 ^{o}C of the coolant temperature will introduce a positive reactivity of about 3 pcm).

d) After the flow transient stops, the reactor can be made critical again without problems of reactivity excursion. The power has to be kept low enough to operate the reactor in single-phase circulation conditions and it should be high enough to allow flashing outside the riser section (see Fig. 39 for reference. Steam separators are not reported for the sake of simplicity). The pressure in the vessel will increase due to level swell, heating and the production of steam. To enhance the single-phase natural circulation the RWCU may be employed to extract warm water from the vessel bottom and inject colder water in the downcomer. No FW flow is supplied during this phase.

e) When the pressure in the vessel is high enough the MSIVs can be opened and the power can be increased to allow transition from single- to two-phase circulation.

2. <u>In conditions of single-phase circulation</u>

a) The water level in the reactor vessel is above the riser exit (see Fig. 39 for a simplified scheme).

b) The reactor is made critical and the power level is adjusted to allow flashing above the riser exit. In this way single-phase circulation can take place in the reactor vessel. Again the RWCU system can be used to enhance the extent of natural circulation. No FW flow is supplied.

c) Once steam is created, the reactor can be kept at atmospheric pressure by keeping the MSIVs open if the system has to be deareated.

d) After closing the MSIVs, the system is operated in single-phase circulation, allowing flashing above the riser exit and the procedure continues as from point d) of previous case.

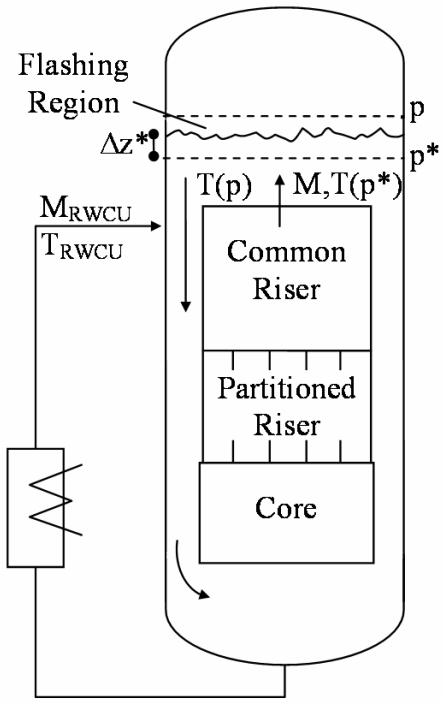

Fig. 39 Scheme of the flow paths in the reactor vessel. The RWCU system extracts water from the bottom of the vessel and release water at a lower temperature through the feed-water line.

During the operation in single-phase circulation it has to be checked that significant flow rate can be kept, even at higher pressures, and that the steam production rate is sufficient to increase the system pressure. For the assessment the geometry of the ESBWR is taken as reference, in view of the fact that this design has been selected by GE for future commercialization.

In the start-up procedure suggested in this chapter, a certain water level is present above the riser outlet and flashing is supposed to take place in a confined region above the riser exit, as indicated in Fig. 39. GE does not give any indication about the water level above the riser exit. From the design specification however, it can be deduced that the steam separators extend for about 2.5 m above the riser exit. It is then reasonable to suppose that during start-up a collapsed water level of about 1-1.5 m is admissible (in Dodewaard a level of 2.54 m was used) above the riser. Flashing could be allowed in the last 0.5 m to produce steam.

From the specification of GE, it is possible to use the RWCU system to recirculate 21 kg/s of coolant during the start-up procedure. The heat exchanger connected to the RWCU system lowers the coolant temperature by about 50 ^{o}C before injecting the coolant back to the vessel (even higher cooling can be achieved, but a value of 50 ^{o}C will be used here for a conservative assessment).

For the calculations, the flow paths indicated in Fig. 39 are considered. We would like that water exits the riser with a temperature such that saturation conditions are reached at $\Delta z^* = 0.5$ m below the collapsed water level. Water will recirculate in the downcomer with a temperature equal to the saturation temperature corresponding at the system pressure p.
The driving pressure that will originate can then be expressed as:

$$\Delta p^*_{drv} \approx \left(L_{core} + L_{riser}\right) g \left.\frac{\partial \rho_F}{\partial T}\right|_{sat} \Delta T^* \tag{18}$$

For the ESBWR specifications $L_{core} = 2.743$ m and $L_{riser} = 10$ m.
The temperature difference ΔT^* can be approximated with:

$$\Delta T^* = T_{sat}\left(p^*\right) - T_{sat}\left(p\right) \approx \rho_F\left(p\right) g \Delta z^* \left.\frac{\partial T}{\partial p}\right|_{sat} \tag{19}$$

The driving pressure can be increased by using the RWCU system. In this case, the temperature difference between core inlet and riser exit would be:

$$\Delta T = \Delta T^* + \Delta T_0 \frac{M_{RWCU}}{M_T} \tag{20}$$

where M_{RWCU} is the flow rate recirculated by the RWCU system (21 kg/s according to GE specifications), M_T is the total flow rate circulation in the reactor and ΔT_0 is temperature decrease achieved by the cooling of the RWCU system (~50 ^oC). The driving pressure results equal then to:

$$\Delta p_{drv} \approx \Delta p^*_{drv} + \left(L_{core} + L_{riser}\right) g \left.\frac{\partial \rho_F}{\partial T}\right|_{sat} \Delta T^* \tag{21}$$

For the evaluation of single-phase circulation at different conditions the total frictional pressure drop in the loop has to be known:

$$\Delta p_f = \frac{M_T^2}{2\rho_F} \sum_i \left(\frac{k_i}{A_i^2}\right) \qquad \mathrm{K} = \sum_i \left(\frac{k_i}{A_i^2}\right) \tag{22}$$

In single-phase conditions the factor K of eq. (22) can be assumed to be constant. This factor can be estimated by considering the data published by Cheung and Rao [20] stating that, using the RCWU system, a flow rate of about 800 kg/s is established in the reactor at a pressure of 1 bar.
Once the friction factor is known, the flow rate M_T circulating in the reactor is calculated by combining eqs. (18) to (22). This yields an equation of the third degree in M_T that can be solved exactly.

$$\begin{cases} M_T^3 + qM_T + r = 0 \\ q = -\dfrac{2\rho_F}{K}\Delta p_{drv}; \;\; r = -\dfrac{2\rho_F}{K} g\left(L_{core} + L_{riser}\right) M_{RWCU} \Delta T_0 \left.\dfrac{\partial \rho_F}{\partial T}\right|_{sat} \end{cases} \tag{23}$$

The equation admits only one real solution given by [50]:

$$\begin{cases} M_T = \sqrt[3]{-\dfrac{r}{2} + \sqrt{D}} + \sqrt[3]{-\dfrac{r}{2} - \sqrt{D}} \\ D = \dfrac{q^3}{27} + \dfrac{r^2}{4} > 0 \end{cases} \tag{24}$$

In Fig. 40 (left) the estimated temperature difference between core inlet and riser outlet is reported as function of the system pressure with and without operation of the RWCU system. It is assumed that the collapsed water level above the riser and the position at which onset of flashing occurs

remain constant. Without making use of the RWCU system, the temperature difference ΔT drops rapidly to values close to zero, since at higher pressures the variation of saturation temperature becomes smaller (this is the reason why the flashing number is negligible after 20 bar). On the contrary, if the RWCU system is used the temperature difference ΔT remains always above 1°C. The corresponding flow rate that establishes in the reactor in the two cases is reported in Fig. 40 (right). If the RWCU system is used significant recirculation is established at all pressures. The values obtained are in perfect agreement with the calculations performed by GE [20].

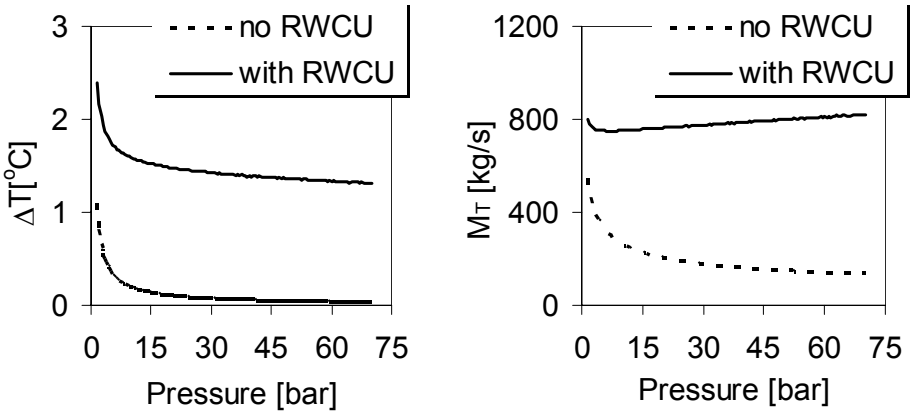

Fig. 40 Temperature difference between downcomer and riser with and without RWCU system (left) and corresponding mass flow rate circulating in the reactor (right).

The power needed to heat up the system at the desired temperatures is given in Fig. 41 as function of the pressure. The values obtained are lower than the ones predicted by GE (17 MW) [20] due to the fact that heat structures and heat losses have not been considered in this evaluation. The system could be operated at constant power by regulating the RCWU system.

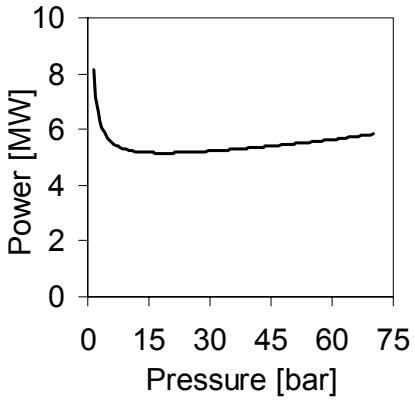

Fig. 41 Power as function of pressure. This power level is needed to keep the position of the flashing onset independent of the system pressure.

The steam produced can be approximated with:

$$M_G = \frac{M_T c_P}{h_{FG}} \Delta T^*_{sub} \tag{25}$$

and the variation of system pressure with time can be evaluated from:

$$\frac{dp}{dt} = \frac{M_T \left.\frac{\partial h_F}{\partial p}\right|_{sat} \rho_F g \Delta z^* + M_G h_F}{V_{SD}\left(h_G \left.\frac{\partial \rho_G}{\partial p}\right|_{sat} + \rho_G \left.\frac{\partial h_G}{\partial p}\right|_{sat} - 1\right)} \tag{26}$$

where V_{SD} indicates the free volume in the steam dome, above the collapsed water level. For simplification swelling of the level is not considered in the calculations, i.e. V_{SD} is assumed to be constant. In principle the volume V_{SD} can be kept constant by controlling the flow re-circulated by the RCWU system. If the level is allowed to increase, this will yield a faster increase of the system pressure due to the compression of the steam cushion in the steam dome.

The right hand side of eq. (26) is only a function of the pressure *f(p)* (quasi-static solution). For the time integration, the function *f(p)* can be fitted (see Fig. 42) and the integration in time can be performed analytically. The free volume of the steam dome is evaluated considering a free height of 6 m above the riser and a diameter of 6 m. The volume occupied by the structures (steam separators and dryers) is not known, thus the pressure increase will be underestimated.

The time evolution of the system pressure is shown in Fig. 43. The pressure reaches 63 bar in 28 h against the 22 h of the GE start-up procedure. In reality, as already mentioned, the pressure is

underestimated due to the larger free volume in the steam dome and the neglect of the level swelling.

From this simple evaluation it seems possible to operate the reactor in single-phase circulation with significant flow rates at all pressures, creating at the same time enough steam to allow increase of the pressure in the reactor vessel.

In addition, it was shown that the use of the RWCU system is fundamental if a significant flow rate has to be ensured during the entire start-up procedure.

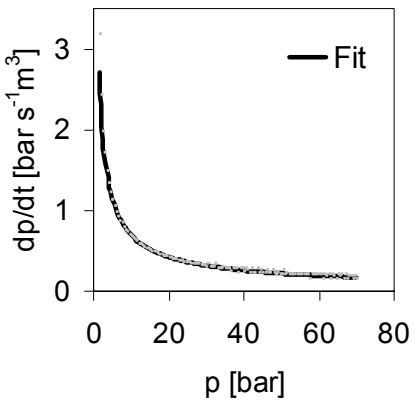

Fig. 42 Right hand side of eq. (26).

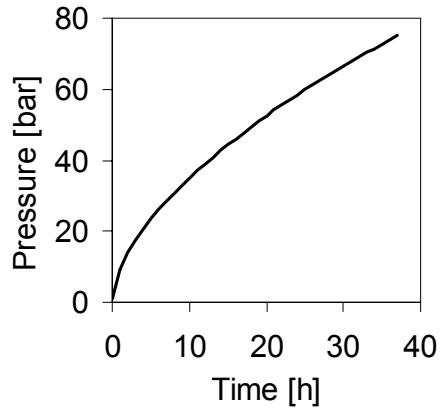

Fig. 43 Time evolution of the reactor pressure.

Conclusions

The flashing phenomenon, of importance during the start-up phase of natural circulation BWRs, was studied in details experimentally and analytically. To perform experimental investigations a two-phase natural circulation loop, CIRCUS, was built at the Delft University of Technology and equipped with advanced instrumentations.

By means of a simplified model, it was shown that an unstable operational region exists between stable single-phase and two-phase operation. This finding was confirmed by the results of an experimental campaign carried out at the CIRCUS facility. In particular, it was found that flashing is the main cause of the instability and that the propagation of enthalpy waves is important for the determination of the frequency of the instability. The thermal non-equilibrium character of the flashing phenomenon was shown as well.
It was demonstrated that increasing pressure has a stabilizing effect on the instability. Also decreasing the compressible volume in the steam dome has a stabilizing effect, but this is not as pronounced as the effect of the pressure. In contrast with results reported in literature, it was shown that instabilities can occur independently of the position of the flashing boundary in the adiabatic section.
Further research is needed to investigate how a partitioned riser would affect the instabilities characteristics. It is believed that out-of-phase oscillations between parallel risers may occur and render even more complicated the start-up of natural circulation BWRs.

A second experimental campaign was performed to gain qualitative and quantitative information on flashing flows in a vertical pipe. The applicability of drift-flux models to predict the void fraction in stationary and transient conditions was studied and the GE-Ramp model was proven to perform very well. It was shown that appropriate treatment of the data delivered by two wire-mesh sensors allows a complete three-dimensional reconstruction of the steam bubbles. This was further used both for bubbles size analysis and for flow pattern visualization during stationary and transient flashing flow. In the latter condition it was demonstrated that flow pattern transition from bubbly to slug/churn flow takes place. The experimental void-fraction radial profile was decomposed according to bubble size classes and the results were compared with calculations carried out with an equilibrium model. The good agreement found suggests the idea that equilibrium in the radial direction is reached rapidly, even in not fully developed flows.

A 4-equations model, FLOCAL, was used to gain physical insight in the process of flashing-induced flow oscillations. This code allows the liquid and vapor phases to be in thermal non-equilibrium and, by means of a drift-flux model, to have different velocities (so-called phase slip). The GE-Ramp drift-flux model was implemented to evaluate the phase slip, since this model was proven to perform very well when applied to flashing flows. In addition, it was found that thermal structures and turbulent diffusion due to temperature gradients play an important role in the determination of the incubation period at high subcoolings.
In full agreement with experimental results it was found that:

- the flashing front propagates simultaneously upward and downward, but with decreasing subcooling the downward propagation becomes less significant;
- temperature propagation in the riser section has a wavy character and inlet and outlet temperature in the riser are out-of-phase;
- two main types of instabilities occur: the first in which two-phase flow alternates with single-phase flow; the second in which two-phase flow is always present in the system, but the axial location of flashing onset changes periodically;
- the relation between oscillation period and average flow rate is geometry-dependent and independent of inlet subcooling, power or pressure. The relation found with FLOCAL is in agreement with the experimental one;

- the relation between gravitational pressure head and inlet kinetic pressure is linear; the relation is also in good agreement with the experiments.

The onset of instability between single-phase and two-phase operation and the onset of two-phase flow stable circulation was well predicted. Since the feedback mechanism of the steam dome was not taken into account in the simulations, the maximum flow rate during flashing-induced oscillations was slightly overestimated. Gravitational and frictional pressure drops were found to be the major terms in the momentum balance for the determination of the amplitude of the flow oscillations, the acceleration and inertia pressure drops being orders of magnitude smaller. The incubation period, which occurs at high subcoolings between two consecutive flashing cycles, was underestimated. The error was significantly reduced if heat structures were modeled for the core and the riser section and if turbulent diffusion due to negative temperature gradients was taken into account.

Finally, a novel start-up procedure for natural circulation BWRs was proposed, in which the pressurization of the reactor takes place while the reactor is operated in single-phase circulation and steam is created above the riser exit. By means of a quasi-static model it was shown that the pressurization of the system occurs in a reasonable time. It was proven that, when the reactor is operated in single-phase circulation, the use of the RWCU system is fundamental if a significant flow rate has to be ensured at all pressures.
The procedure could not be simulated with FLOCAL because in this code a lumped parameters model is used for the steam dome. In other words, flashing in the water level above the riser exit could not be modelled. Including this effect requires only a slight modification of the code and does not involve changes in the numerical schemes (i.e. it will not affect the validity of the code as proved in this work). Such a modification and a time-dependent simulation of the proposed start-up procedure are highly recommended for future work.

However, the problem of scalability remains open since three-dimensional effects cannot be neglected if information for industrial applications is desired. This opens the way, among others, to fundamental studies on flow pattern evolution in large pipes and on the effect of radial temperature and velocity profiles. Surely, one of the biggest challenges to be tackled is the derivation of microscopic constitutive laws (i.e. geometry independent) for the further development of three-dimensional two-phase models.

Nomenclature

A	flow area	m^2
c_p	heat capacity	$J\ kg^{-1}\ K^{-1}$
C_0	distribution parameter	-
f	frequency	Hz
g	gravity acceleration	$m\ s^{-2}$
G	mass flux	$kg\ m^{-2}\ s^{-1}$
h	enthalpy	$J\ kg^{-1}$
H	height	m
H_{WF}	heat transfer coefficient	$W\ m^{-2}\ s^{-1}$
I	count rate	s^{-1}
J	superficial velocity	$m\ s^{-1}$
L	length	m
m	mass flow	$kg\ s^{-1}$
p	pressure	$kg\ m^{-1}\ s^{-2}$
Q	source of power density	$W\ m^{-3}$
S	slip-ratio	-
t	time	s
T	temperature	^oC
u	velocity	$m\ s^{-1}$
x	quality	-
z	spatial coordinate	m

Greek symbols

α	void fraction	-
α_C	chordal void fraction	-
ε	void-fraction error	-
λ	thermal conductivity	$W\ m^{-1}\ K^{-1}$
μ	condensation/evaporation rate	$kg\ m^{-3}\ s^{-1}$
ν	thermal diffusivity	$m^{-2}\ s^{-1}$
ρ	density	$kg\ m^{-3}$
σ	standard deviation	-

Subscripts

G	vapour
inl	inlet
L	liquid
R	riser
W	wall

Abbreviations

BWR	Boiling Water Reactor
ESBWR	European Simplified Boiling Water Reactor
GDCS	Gravity Driven Cooling System
GE	General Electric
HEM	Homogeneous Equilibrium Model
ICS	Isolation Condenser System
LDA	Laser Doppler Anemometry
LOCA	Loss of Coolant Accident
NPP	Nuclear Power Plant
MSIV	Main Steam Isolation Valve
PCCS	Passive Containment Cooling System
RPV	Reactor Pressure Vessel
RWCU	Reactor Water Clean Up System
SBWR	Simplified Boiling Water Reactor

References

1. Y.K. CHEUNG, B.S. SHIRALKAR, A.S. RAO, "Design Evolution of Natural circulation in ESBWR," *6th Int. Conf. on Nuclear Engineering ICONE-6*, May 10-15, San Diego, USA (1998).

2. E. WISSLER, H.S. ISBIN, N.R. AMUDSON, "Oscillatory Behavior of a Two-phase Natural-circulation Loop," *A.I.Ch.E.J.* Vol. **2**, No. 2, pp. 157-162 (1956).

3. C. SCHUSTER, A. ELLINGER, J. KNORR, "Analysis of Flow Instabilities at the Natural Circulation Loop DANTON with regards to Non-linear Effects," *Heat and Mass Transfer,* **36**, 557 (2000).

4. M. ARITOMI, J.H. CHIANG, T. NAKAHASHI, M. WATARUM, M. MORI, "Fundamental Study on Thermo-hydraulics During Start-up in Natural Circulation Boiling Water Reactors (I)," *J. Nucl. Sci. Technol.,* **29**, *7*, 631 (1992).

5. M. FURUYA, F. INADA, A. YASUO, "A Study on Thermalhydraulic Instability of a Boiling Natural Circulation Loop with a Chimney (Part II. Experimental Approach to Clarify the Flow Instability in Detail)," *Heat Transfer - Japanese Research,* **24**, *7*, 577 (1995).

6. S.Y. JIANG, YAO, J.H. BO, S.R. WU, "Experimental Simulation Study on Start-up of the 5 MW Nuclear Heating Reactor," *Nucl. Eng. Des.,* **158**, 111 (1995).

7. J.M. KIM, S.Y. LEE, "Experimental Observation of Flow Instability in a Semi-closed Two-phase Natural Circulation Loop," *Nucl. Eng. Des.,* **196**, 359 (2000).

8. S.R. WU, H.J. JIA, S.Y. JIANG, Y.J. ZHIANG, "Investigation on Two-phase Flow Stability in a Natural Circulation System," *Kerntechnik.,* **65**, *5-6*, 222 (2000).

9. T.H.J.J. VAN DER HAGEN, A.J.C. STEKELENBURG, "The Low-Power Low-Pressure Flow Resonance in a Natural Circulation Boiling Water Reactor," *Nucl. Eng. Des.,* **177**, 229 (1997).

10. F. INADA, M. FURUYA, A. YASUO, "Thermo-hydraulic instability of boiling natural circulation loop induced by flashing (analytical consideration)," *Nucl. Eng. Des.,* **200**, 187-199 (2000).

11. D.D.B. VAN BRAGT, W.J.M. DE KRUIJF, A. MANERA, T.H.J.J. VAN DER HAGEN, H. VAN DAM, "Analytical modeling of flashing-induced instabilities in a natural circulation cooled boiling water reactor," *Nucl. Eng. Des.*, **215**, 87-98 (2002).

12. T. SAWAI, M. KAJI, S. NAKANISHI, S. YAMAUCHI, "Stability and non-linear dynamics in natural circulation loop at low pressure condition," 2nd *Int. Symp. on Two-Phase Flow Modelling and Experimentation*, May 23-26, Pisa, Italy, 363-369 (1999).

13. A. MANERA, H.-M. PRASSER, U. ROHDE, T.H.J.J. VAN DER HAGEN, "Assessment of void-fraction correlations and drift-flux models applied to stationary and transient flashing flow in a vertical pipe," *to be submitted* (2003).

14. V. CHATOORGOON, "SPORTS – A simple non-linear thermalhydraulic stability code," *Nucl. Eng. Des.*, **93**, 51-67 (1986).

15. H.S. CHENG, H.J. KHAN, U.S. ROHATGI, "Simulation of SBWR Startup Transient and Stability," BNL-65535 (1998).

16. J. PANIAGUA, U.S. ROTHAGI, V. PRASAD, "Modeling of Thermal Hydraulic Instabilities in Single Heated Channel Loop During Startup Transients," *Nucl. Eng. Des.*, **193**, 207 (1999).

17. S.B. WANG, J.Y. WU, C. PAN, W.K. LIN, "Thermal-hydraulic Oscillations in a Low Pressure Two-phase Natural Circulation Loop at Low Pressures and High Inlet Subcoolings," *Proc. of 4th Int. Topical Meetg. Nuclear Thermal Hydraulics, Operations and Safety*, April 5-8, Taipei, Taiwan (1994).

18. N. HOYER, 1994, "MONA, a 7-Equation Transient Two-Phase Flow Model for LWR Dynamics," *Proc. of Int. Conf. on New Trends in Nuclear System Thermohydraulics,* May 30-June 2, Pisa, Italy (1994).

19. T. SENGSTAG, "Pre-test calculations MONA-2-2 on the CIRCUS tests," NACUSP FIKS-CT-2000-00041, report D9a (2002).

20. Y.K. CHEUNG, A.S. RAO, "Startup Simulation of a Natural Circulation Plant - ESBWR," *Proc. of 8th Int. Conf. on Nucl. Eng. ICONE-8*, April 2-6, Baltimore, MD, USA (2000).

21. J.G.M. ANDERSEN, F. INADA, L.A. KLEBANOV, "TRACG Analyses of Flashing Instability During Start-up," *Proc. of 3rd Int. Conf. on Nucl. Eng. ICONE-3*, April 23-27, Kyoto, Japan (1995).

22. I. TISELJ, G. CERNE, "Some Comments on the Behaviour of RELAP5 Numerical Scheme at Very Small Time Step," *Nucl. Eng. Des.*, **134**, 3 (2000).

23. G. TH. ANALYIS, D. LÜBBESMEYER, "Pre-test calculations on flashing-induced instability experiments in PANDA with TRAC-BF1/v2001.2 and RELAP5/MOD3.3./beta," EU project NACUSP, FIKS-CT-2000-00041, D09c (2002).

24. W.J.M. DE KRUIJF, A. MANERA, D.W. DE HAAS, J.G.F. SCHUT, T.H.J.J. VAN DER HAGEN, R.F. MUDDE, H.-M. PRASSER, "Description of CIRCUS including test matrix," EU project NACUSP, FIKS-CT2000-00041, D08a (2000).

25. H.-M. PRASSER, A. BÖTTGER, J. ZSCHAU, T. GOCHT, "Needle-shape conductivity probes with integrated micro-thermocouple and their application in rapid condensation experiments with non-condensable gases," *Kerntechnik*, **68**, 114 (2003).

26. H.-M. PRASSER, A. BÖTTGER, J. ZSCHAU, "A new electrode-mesh tomograph for gas-liquid flows," *Flow Measurement and Instrumentation* **9**, 111-119 (1998).

27. A.K. KRÜSSENBERG, H.-M. PRASSER, A. SCHAFFRATH , "A new criterion for identification of the bubble slug transition in vertical tubes," *Kerntechnik* **65**, 1 (2000).

28. G. GRUNWALD, T. HÖNHE, H.-M. PRASSER, "Experimental investigations on the four-loop test facility ROCOM," *Kerntechnik* **65**, 5-6 (2000).

29. A. DUDLIK, H.-M. PRASSER, S. SCHLÜTER, "Visualization of cavitating liquid flow behind fast acting valves," *Second European Congress of Chemical Engineering,* 5-7 October, Montpellier (1999).

30. E. ELIAS, P.L. CHAMBRÉ, "Bubble transport in flashing flow," *Int. J. Multiphase flow* **26**, 191-206 (2000).

31. L. E. DRAIN, "The Laser Doppler Technique," John Wiley & Sons Ltd (1980).

32. N. ZUBER, J.A. FINDLAY, "Average volumetric concentration in two-phase flow systems," *J. Heat Transfer*, **87** (1965).

33. B. CHEXAL, J. HOROWITZ, G.S. LELLOUCHE, "An assessment of eight void fraction models," *Nucl. Eng. Des*., **126**, pp. 71-88 (1991).

34. Y. TAITEL, D. BORNEA, A.E. DUKLER, "Modelling flow pattern transitions for upward gas-liquid flow in vertical tubes," *AIChE J.,* **26**,345-354 (1980).

35. K. MISHIMA, M. ISHII, "Flow regime transition criteria for upward two-phase flow in vertical tubes," *Int. J. Heat Mass Transfer,* **27**, 723-737 (1984).

36. H.-M. PRASSER, M. BEYER, A. BÖTTGER, H. CARL, D. LUCAS, A. SCHAFFRATH, P. SCHÜTZ, F.-P. WEISS, J. ZSCHAU, "Influence of the pipe diameter on the structure of the gas-liquid interface in a vertical two-phase pipe flow," *Proc. of the 10th International Topical Meeting on Nuclear Reactor Thermal Hydraulics (NURETH-10)*, October 5-9, Seoul, Korea (2003).

37. F. INADA, M. FURUYA, A. YASUO, "Thermo-hydraulic Instability of a Boiling Natural Circulation Loop with a Chimney (an Analytical Study of Instability at Low and High Pressure," *Proc. of 7th Int. Conf. on Nucl. Eng. ICONE-7*, April 19-23, Tokyo, Japan (1999).

38. S.R. WU, H.J. JIA, S.Y. JIANG, Y.J. ZHIANG, "Investigation on Two-phase Flow Stability in a Natural Circulation System," *Kerntechnik.,* **65**, *5-6*, 222 (2000).

39. F. INADA, Y. YASUO, "The Boiling Flow Instability of a Natural Circulation BWR with a Chimney at Low Pressure Start-up," *Proc. of ANP'92, Int. Conf. on Design and Safety of Advanced Nuclear Power Plants*, October 25-29, Tokyo, Japan, Vol. 3, p. 25.3.1 (1992).

40. S.Y. JIANG, Y.J. ZHANG, J.H. BO, F. WANG, "Conversion from single to two-phase operation in a natural circulation nuclear reactor," *Kerntechnick*, **63**, 132-138 (1998).

41. M. FURUYA, F. INADA, Y. YASUO, "Inlet throttling effect on the boiling two-phase flow stability in a natural circulation loop with a chimney," *Heat and Mass Transfer*, **37**, 111-115 (2001).

42. U. ROHDE, "Ein teoretisches Modell fur Zweiphasen-stromungen in wassergekulthen Kernreaktoren und seine Anwendung zur Analyse des Naturumlaufs im Heizreaktor AST-500," Ph.D. dissertation, Akademie der Wissenschaften der DDR, Dresden (1986).

43. J.HUHN, J.WOLF, "Zweiphasenströmung," VEB Fachbuchverlag Leipzig (1975).

44. E.E.. ZUKOSKI, "A review of flows driven by natural convection in adiabatic shafts," NIST-GCR-95-679, Caltech (1995).

45. I.E. IDELCHIK, "Handbook of hydraulic resistance," 2nd ed., Washington Hemisphere (1986).

46. W.H.M. NISSEN, J. VAN DER VOET, J. KARUZA, "The startup of the Dodewaard natural circulation Boiling Water Reactor – experiences," *Nucl. Technol.*, **107**, 93-102 (1994).

47. J.H. CHIANG, M. ARITOMI, M. MORI, M. HIGUCHI, "Fundamental study on thermo-hydraulics during start-up in natural circulation Boiling Water Reactors (III)," *J. Nucl. Sci. Technol*. **31**, 9, 883-893 (1994).

48. A. NAYAK, "Study on the stability of natural circulation for the design of Advanced Heavy Water Reactor," Doctoral dissertation, Tokyo Institute of Technology, Japan (2000).

49. C. SHUSTER, J. KNORR, "Analysis of experiments at the natural circulation loop DANTON with the code ATHLET," *Proc. Jahrestagung Kerntechnik 2003*, Annual Meeting on Nuclear Technology 2003, May 20-22, Berlin, Germany (2003).

50. N. PATEL, A. TEJA, "The calculation of thermodynamic properties and phase equilibria using a new cubic equation of state," Ph.D. Thesis, Loughborough University of Technology (1980).

Acknowledgment

I would like to thank prof.dr.ir. H. van Dam for giving me the opportunity to pursue this research in first place and for his help in the difficult moments.

I would like to express my gratitude to prof.dr.ir. T.H.J.J. van der Hagen for giving me the opportunity to work in an international environment, for the freedom he gave me during my Ph.D. period, for introducing me to the world of noise-analysis and for his continuous and contagious enthusiasm.

Many thanks to prof.dr. R.F. Mudde for the enjoyable discussions on two-phase flow during the BWR meetings and for his support during the installation of the LDA set-ups.

I would like to thank dr. U. Rohde for giving me the opportunity to work with the code FLOCAL and for his support during the three months I spent at the Rossendorf Research Center.

Dr. H.-M. Prasser is deeply acknowledged for supporting me in all the activities related to the wire-mesh sensors and the needle-probes and for the very useful discussions on experimental and theoretical matters of two-phase flow research.

I wish to thank all the NACUSP team for the interesting collaboration and for the nice time spent during the meetings.

I would like to thank Riny Purmer, not only for the everyday help in all administrative matters, but also for her friendship and trust, for the continuous support and for her efforts to teach me the Dutch language. Regarding this last matter I also have to thank Kees, Robert and Marianne for the turbo-Dutch training.

Thanks to Ine Olsthoorn and Sonja Jobse for helping with all the small and big problems of everyday “department-life”.

I would like to address a special thank to the technicians for modifying the experimental facility every time I needed, with high efficiency and precision and always at a record time. Without their support this work would have never seen an end! In particular, I would like to thank: Dick de Haas for his help with the electronics and the data acquisition system. I will never forget the long days at the beginning of my Ph.D. period spent together at the facility when, not without some fear, we were trying to start-up the system and to create steam; Jelle Schut (beroemd als de liefste technicus ter wereld. Ik zal de keer dat je mijn leven hebt gered, zeker niet vergeten), for building the facility and for coming up with a fast solution every time I had a technical problem; August Winkelman and Camiel Kaaijk for their help with computer matters (and I do not forget the idea of the “bier-vat”!); Jaap Beekman for his patience and assistance to make the LDA set-ups working properly.

I wish to thank my room-mates Róbert Zboray, Masahiro Furuya and Arun Nayak for their help and for the fruitful discussions.

Many thanks to my friends Dávid Légrády, Máté Szieberth and Róbert and Nóra Zboray for giving me a taste of the Hungarian culture and for the interesting discussions about all kind of subjects; Niels Boerema is deeply acknowledged for helping with the Dutch translation of my propositions (and thanks for giving the final strike to dissolve our band…we would have not got far anyway). Thanks also to Danny Lathouwers for listening to me (almost) all the time, for encouraging me to go on in the no-working-mood days and for his assistance in the Dutch translation of the summary of this thesis.

I wish to thank the RF group and the “Spanish group” (Antonio, Cristina, Alfonso, Ramon and the Spanish-of-adoption Sasha, Marijn and Daniele) for the very nice atmosphere during these years in Holland.

I would like to thank my music teacher Karen Reuter for helping me accomplish my dream of playing the piano.

Ringrazio infine i miei genitori, Marco, Ileana e Michael per il loro sostegno e per il tentativo di compensare la lontananza con lunghe telefonate.

Curriculum vitae

Annalisa Manera

Born:	February 6, 1974 in Bari, Italy
1992	Maturita' scientifica (60/60) Award: 2nd prize Chemistry Olympics Games, Basilicata, Italy, 1991
1999	M.Sc. in Nuclear Engineering (110/110 cum laude) University of Pisa, Italy
2001	Patent of "Qualified Expert in Radiation Protection of the 3rd Level" The Netherlands
May 1999- May 2003	Ph.D. student at the Department of Reactor Physics Interfaculty Reactor Institute Delft University of Technology, The Netherlands
Since May 2003	Researcher at the Department of Reactor Physics Interfaculty Reactor Institute Delft University of Technology, The Netherlands

Proc. 4th International Conference on Multiphase Flow (ICMF-2001),
May 27 - June 1, 2001, New Orleans, USA.

A COMPARISON OF VOID-FRACTION MEASUREMENTS DURING FLASHING-INDUCED INSTABILITIES OBTAINED WITH A WIRE-MESH SENSOR AND A GAMMA-TRANSMISSION SET-UP

A. Manera[1,*], H.-M. Prasser[2], T.H.J.J. van der Hagen[1,3], R.F. Mudde[3] and W.J.M. de Kruijf[1]

[1]Interfaculty Reactor Institute (IRI), Delft University of Technology, The Netherlands
[2]Institute of Safety Research, Forschungszentrum Rossendorf (FZR), Dresden, Germany
[3]Kramers Laboratorium voor Fysische Technologie, Delft University of Technology, The Netherlands

ABSTRACT

The void fraction produced in an adiabatic section (riser) during flashing-induced instabilities in a natural-circulation steam/water loop is measured by means of a wire-mesh sensor and two gamma-transmission set-ups located just above and below the wire-mesh sensor respectively. In this paper a comparison between the two different measuring techniques is given. The wire-mesh sensor is capable of measuring the time-dependent two-dimensional void-fraction distribution on a grid of 16x16 points equally distributed over a cross section of the riser, while the gamma-transmission set-ups measure the chordal void fraction along a collimated beam through the riser at a certain height.

The high sampling rate of the wire-mesh sensor (up to 1200 Hz) allows to detect both the frequencies characteristic of the flashing process (between 2 and 4 Hz) and the frequencies characteristic of the flashing-induced flow oscillation (below 0.05 Hz). The former frequencies are less visible in the spectrum of the gamma-transmission signal due to the lower signal-to-noise ratio.

The effect of the wire-mesh sensor on the triggering of void production due to the provision of extra nucleation sites is also studied; no significant differences are observed in the main parameters of the instability if the wire-mesh sensor is removed from the experimental loop.

INTRODUCTION

Steam/water-flow natural-circulation systems are widely applied in chemical industry and in electricity production; examples of such systems can be found in boilers, steam generators and new-generation nuclear power plants (e.g. natural-circulation Boiling Water Reactors). These systems can undergo instabilities (so-called flashing-induced instabilities) if operated at low pressures and low powers, which are typical start-up conditions.

The state-of-the-art thermalhydraulic codes have not been qualified yet for natural-circulation water/steam systems operating at low pressures and low powers (Ishii 1997) and the analytical models available are poor in void-fraction predictions, since

[*] Corresponding author. Tel. + 31-15-2786962; fax: +31-15-2786422
E-mail address: manera@iri.tudelft.nl

simple homogeneous equilibrium models are implemented (Inada et al. 1997, Van Bragt et al. 1999).

Experimental data are therefore needed in order to provide a suitable database against which models and codes can be validated. For this reason, an experimental facility (CIRCUS) has been built at the Delft University of Technology (Manera et al. 2000). For a successful development of analytical and numerical models, a good prediction of the void production during flashing is of fundamental importance. In this paper the focus is on void-fraction measurements during flashing-induced instabilities.

For detailed and high-frequency void-fraction measurements a wire-mesh sensor is used; the sensor has been developed to measure two-dimensional void-fraction distributions in two-phase flow systems (Prasser et al. 1998). The sensor has been successfully applied to measure gas fractions, flow-pattern transitions and bubble-size distributions in air-water flows (Krüssenberg et al. 2000), for boron dilution measurements during transients occurring in Pressurized Water Reactors (Grunwald et al. 2000) and for cavitation experiments during rapid valve closure in pipelines (Dudlik et al. 1999). Nevertheless, it has never been applied in water/steam flows and in condition of variable mixture temperature. Therefore, a set of measurements has been performed with the CIRCUS facility to study the performance of the wire-mesh sensor. Two gamma-transmission set-ups positioned just below and above the wire-mesh sensor respectively have been used to make the comparison.

The accuracy of the void-fraction measurements performed with the wire-mesh sensor (± 5%) has been determined in steady-state conditions over a wide range of void fractions and gas superficial velocities (Prasser et al. 1998, Krüssenberg et al. 2000).

In this study it is investigated whether the wire-mesh sensor can provide additional information on the dynamics of the flashing phenomenon.

In addition, to study the possible undesired effect of the wire-mesh sensor on triggering of void production, a set of experiments has been performed after removing the wire-mesh sensor from the experimental loop.

In the following section a brief introduction on flashing-induced instabilities is given, before presenting the experimental set-up and the results obtained.

FLASHING-INDUCED INSTABILITIES IN A NATURAL-CIRCULATION LOOP

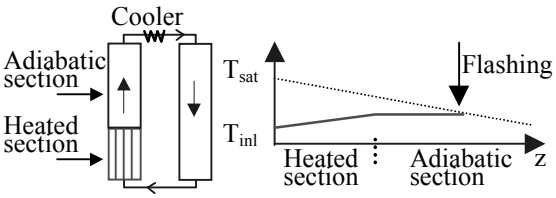

Fig. 1. Flashing in the adiabatic section.

During operation of steam/water-flow natural-circulation systems characterised by a heated section and an adiabatic section (see scheme in Fig. 1), void production (flashing) can take place in the adiabatic vertical section of the loop even if no boiling occurs in the heated section. The process is schematically illustrated in Fig. 1: the coolant enters the heated section with a given temperature T_{inl} and it is heated-up. In the adiabatic section the fluid temperature remains constant (if no heat losses are considered), but flashing can occur due to the decrease of saturation temperature along the axis of the system. The fluid temperature at the exit of the

heated section must be higher than the saturation temperature at the exit of the adiabatic section to allow flashing to occur. The process is more important at low pressures because the difference in saturation temperature between the heated and the adiabatic section of the loop is more significant and the ratio between liquid and vapour density is larger.

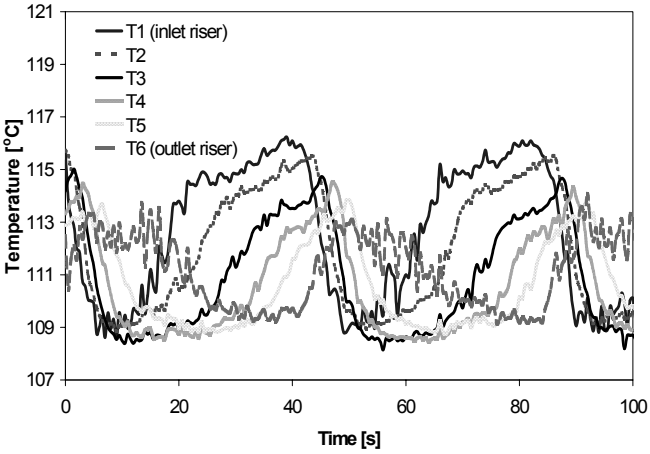

Fig. 2. Temperature time traces along the riser section.

As a consequence of flashing, the natural-circulation flow rate will increase as a result of the increased buoyancy of the loop. The increase of the flow rate will lead to a decrease of the temperature of the fluid coming into the adiabatic section to values that can be low enough to suppress flashing. The suppression of flashing will cause a decrease of the flow rate in the loop, leading to a subsequent increase of the fluid temperature. Therefore, flashing can again take place in the riser causing a self-sustained flow oscillation characterised by periodical void production in the adiabatic section of the loop.

The amplitude of the temperature oscillations can be several degrees, as it can be seen from Fig. 2, in which typical temperature time traces registered at different heights of the adiabatic section in CIRCUS are reported. The positions at which the temperatures are measured along the adiabatic section are illustrated in Fig. 3.

CIRCUS

A scheme of the experimental facility CIRCUS is shown in Fig. 3. The heated section consists of four electrically heated channels and four parallel bypass channels. On the top of the heated section a cylindrical adiabatic section is present. The steam produced in the loop is condensed by means of a heat exchanger.

A steam dome, in which a mixture of steam and water is kept at saturation conditions, is used to control the pressure of the system, while a buffer vessel assures a constant temperature at the inlet of the heated section during experiments. The main characteristics of the facility are reported in Table 1.

Power range per rod	0 - 3 kW
Pressure range	1 - 5 bar
Fuel channel diameter	20.4 mm
Fuel rod diameter	12.5 mm
Bypass channel diameter	10 mm
Heated section length	1.95 m
Riser diameter	47 mm
Riser length	3 m

Table 1. Main characteristics of the CIRCUS facility.

The facility is equipped with thermocouples, flowmeters, pressure sensors and pressure-drop sensors. Two Laser-Doppler-Anemometry set-ups are used to measure the flow velocity fluctuations in two parallel channels simultaneously. In addition, the void fraction in the riser is measured by means of a wire-mesh sensor (two-dimensional void-fraction measurements) and by two gamma-transmission set-ups (chordal void-fraction measurements). Details on the wire-mesh sensor and on the two gamma-transmission set-ups are given in the following sections.

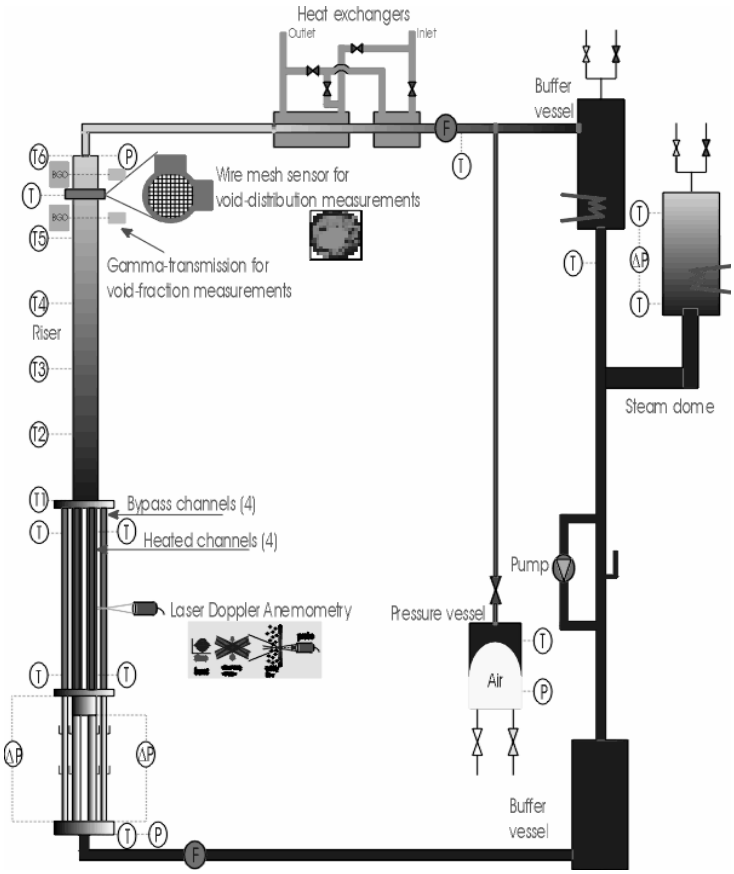

Fig. 3. Scheme of the CIRCUS facility.

Experimental procedure

To perform the experiments, first the facility is pressurised to the desired value of pressure by means of the pressure vessel and the required amount of steam is created in the steam dome. Then, the pressure vessel is disconnected from the loop and the measurement is started after a stationary limit-cycle oscillation is reached. For the study presented in this paper the temperature at the inlet of the heated section has been kept constant at about 98.5 ^{o}C and an initial pressure of 1.2 bar has been set at the exit of the adiabatic section.

THE WIRE-MESH SENSOR

The wire-mesh sensor used in the CIRCUS facility has been developed at the Forschungszentrum Rossendorf (FZR) in Germany; it measures the two-dimensional

void-fraction distribution over the section of a pipe on the basis of the local instantaneous conductivity of the fluid flowing in the pipe.

The sensor has a diameter of 47 mm (equal to the diameter of the adiabatic section on which it is mounted) and is made up of two electrode grids of 16 wires each placed at an axial distance of 1.5 mm. The two grids are positioned perpendicularly to each other in order to form a matrix of 16x16 cross-points (see Fig. 4). The distance between two successive parallel wires is equal to 2.8 mm, this being the spatial resolution of the sensor. Details on the working principles of the sensor are given by Prasser (Prasser et al. 1998).

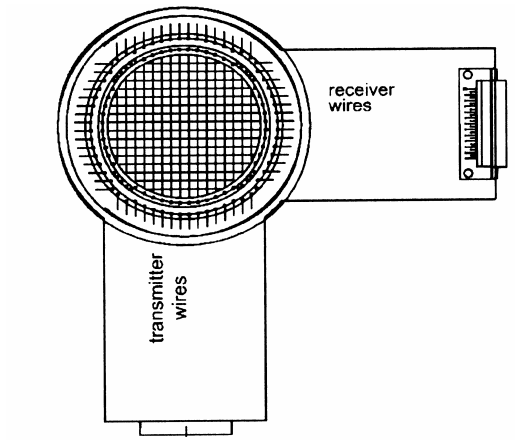

Fig. 4. Wire-mesh sensor.

The sampling frequency can be up to 1200 Hz. In the present study a sampling frequency of 500 Hz has been used.

The wire-mesh sensor measures the time-dependent fluid conductivity on a matrix of 16x16 points. The conversion to void fraction is performed assuming a linear dependence of the void fraction with respect to the fluid conductivity. For the conversion to void fraction it is necessary to calibrate the sensor in conditions of "tube completely filled with liquid" and "tube completely filled with gas". The calibration data are stored and used successively for the conversion of the measurement data. Additional corrections are needed if variations of the fluid temperature occur during the measurements.

To take fluid-temperature variations into account, calibration data of the wire-mesh sensor have been stored at different liquid temperatures and a linear regression has been used to describe the dependence of the conductivity as function of the temperature:

$$\frac{u_{lq}[i,j]-u_g[i,j]}{u_{lq}^0[i,j]-u_g[i,j]} \simeq \frac{aT+b}{aT_0+b}, \tag{1}$$

where $u_{lq}[i,j]$ is the measured liquid conductivity at the position [i,j] of the 16x16 points matrix, $u_g[i,j]$ the gas conductivity (from calibration data), $u_{lq}^0[i,j]$ the water conductivity measured at the reference temperature T_0, T the actual fluid temperature and a and b the coefficients of the linear regression. Applying the linear regression of equation (1), the void fraction is evaluated by:

$$\alpha[i,j]=1-\frac{u[i,j]-u_g[i,j]}{u_{lq}^0[i,j]-u_g[i,j]}\frac{aT_0+b}{aT+b}, \tag{2}$$

where $\alpha[i,j]$ is the local void fraction at the [i,j] position and $u[i,j]$ the mixture conductivity. The fluid temperature is measured by means of a thermocouple positioned at the location of the wire-mesh sensor.

An example of the influence of the temperature correction on the spatial-averaged void fraction measured by the wire-mesh sensor during a flashing-induced oscillation is shown in Fig. 5. Without taking into account fluid-temperature variations, a non-zero void fraction is measured by the wire-mesh sensor even when one-phase flow is

present in the section. This artefact vanishes when temperature correction is being applied.

The large fluctuations of the void fraction in Fig. 5 are due to the fast alternation of water and steam occurring during flashing.

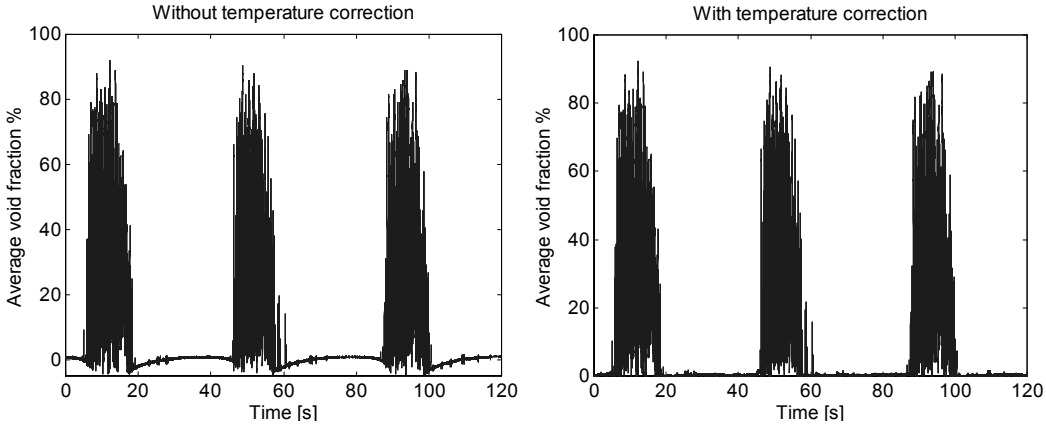

Fig. 5. Average void fraction without (left) and with (right) temperature correction.

THE TWO GAMMA-TRANSMISSION SET-UPS

Two gamma-transmission set-ups are mounted 17 cm above and below the wire-mesh sensor respectively. A 100mCi Cr-51 is used as gamma-source (one for each gamma-transmission set-up); this choice allows relatively small dimensions of the measuring device since only 3.5 cm lead are necessary for shielding purposes. NaI(Tl) scintillator detectors are used and only the Cr-51 gamma-peak (320 keV) is selected.

A top view of one of the two gamma-transmission set-ups and the wire-mesh sensor is schematically given in Fig. 6.

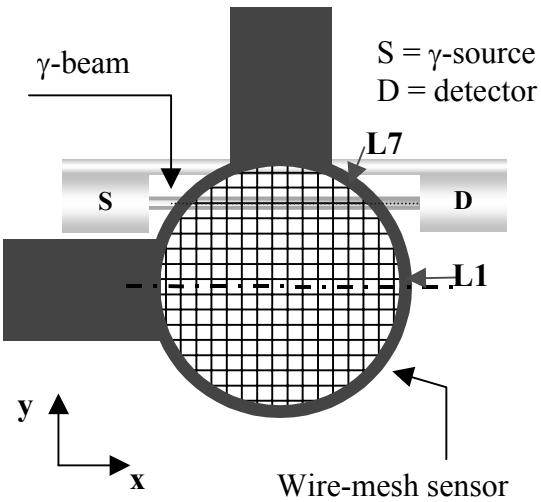

Fig. 6. Scheme of the experimental set-up (top view).

The gamma-source **S** emits a collimated γ-beam of 2 mm width (height equal to 8 mm). A collimator is present in front of the detector in order to measure the chordal void fraction along the 2 mm wide beam crossing the section from the source to the detector. Source and detector are joined together to preserve their relative alignment.

They can be moved perpendicularly to the wires of one of the two grids of the wire-mesh sensor (always parallel to the x-direction as indicated in Fig. 6).

During each measurement the gamma beam is centred along a single wire of the wire-mesh sensor; an example is illustrated in Fig. 7. In this way the chordal void fraction measured by the gamma-transmission set-ups along a given path can be directly compared to the chordal void fraction measured by the wire-mesh sensor along the same path.

The chordal void fraction α_i measured by the wire-mesh sensor along the i-th wire is evaluated as the sum of the void fraction $\alpha_{i,j}$ in each node belonging to the i-th wire weighted by a factor w_j, that takes into account whether the [i,j]-mesh contributes totally (central mesh) or only partially (mesh at periphery) to the total area intercepted by the sensor along the i-th wire.

Note that the spatial resolution of the wire-mesh sensor (2.8 mm) is somewhat larger than the beam width (2 mm).

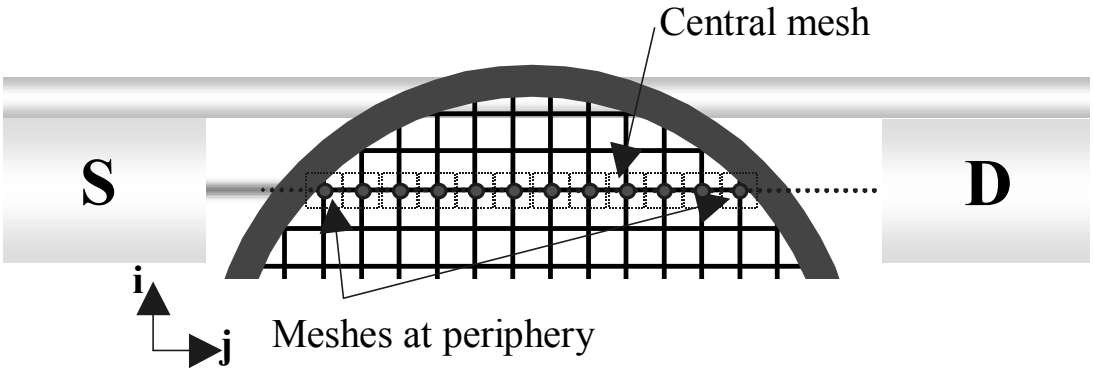

Fig. 7. Determination of chordal void fraction.

EXPERIMENTAL RESULTS

Comparison between gamma-transmission and wire-mesh sensor

Two sets of measurements have been performed setting the time constant τ_R of the rate-meter of the gamma-transmission set-ups equal to 0.3 and 0.03 seconds respectively, leading to statistical error on the count-rate ranging from less than 2% (for τ_R = 0.3 s) to less than 6% (for τ_R = 0.03 s).

The measurements have been carried out placing the gamma beams along different wires of the wire-mesh sensor, going from the centre of the section (central wire of the wire-mesh sensor L1) to the periphery (wire L7), as indicated in Fig. 6.

A trigger is used to synchronise the wire-mesh sensor with the gamma-transmission measurements.

For simplicity, the chordal void fractions measured by the gamma-transmission set-ups are indicated in the text as α_{LW} for the lower set-up and as α_{UP} for the upper set-up respectively. The chordal void fraction measured by the wire-mesh sensor is indicated as α_{WM}.

In Fig. 8 the chordal void fractions α_{LW}, α_{UP} and α_{WM} are shown for the measurement performed at position L1 (see Fig. 6) and with a rate-meter time constant τ_R equal to 0.3 seconds.

The highly detailed structure of the wire-mesh sensor measurement, due to the high sampling frequency, makes a direct comparison with the gamma-transmission measurements difficult.

To compare the wire-mesh sensor and the gamma-transmission set-ups signals, it has to be taken into account that the wire-mesh sensor measures instantaneous void fraction, while the gamma-transmission set-ups behave like a first-order integrator with a time constant τ_R set on the rate-meter used to digitalise the count-rate.

The relation between the count-rate and the voltage output of the rate-meter is expressed by:

$$V_\gamma(t_0) = \frac{1}{B\tau_R}\int_{-\infty}^{t_0} R_\gamma(t)\, e^{\frac{t-t_0}{\tau_R}}\, dt, \qquad (3)$$

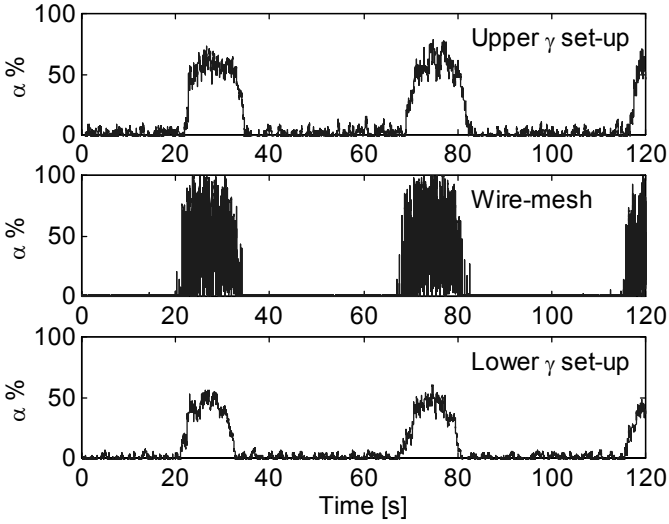

Fig. 8. Chordal void fraction measured by the two gamma-transmission set-ups (τ_R = 0.3 s) and by the wire-mesh sensor at position L1.

where R_γ is the count-rate measured by the gamma-transmission set-up and V_γ the corresponding rate-meter voltage output. B is a proportionality factor (depending on physical characteristics of the rate-meter as resistance, capacitance, etc.). If the count-rate is constant eq. (3) becomes:

$$V_\gamma = \frac{1}{B} R_\gamma . \qquad (4)$$

Therefore, for the calibration values it is possible to write:

$$\begin{cases} V_{\gamma,lq} = \dfrac{1}{B} R_{\gamma,lq} \\ V_{\gamma,g} = \dfrac{1}{B} R_{\gamma,g} \end{cases} \qquad (5)$$

where 'lq' refers to liquid calibration and 'g' to air calibration.

For a hypothetical gamma-transmission set-up placed at the location of the wire-mesh sensor the following relation holds:

$$\alpha_{WM}(t_0) = \frac{ln\left(R_{WM}(t_0)\right) - ln\left(R_{\gamma,lq}\right)}{ln\left(R_{\gamma,g}\right) - ln\left(R_{\gamma,lq}\right)}, \qquad (6)$$

where $\alpha_{WM}(t_0)$ is the chordal void fraction measured by the wire-mesh sensor at the time t_0 and $R_{WM}(t_0)$ the count-rate measured by the hypothetical gamma-transmission set-up. Inverting eq. (6):

$$\begin{cases} R_{WM}(t_0) = R_{\gamma,lq} e^{G\alpha_{WM}(t_0)} = B V_{\gamma,lq} e^{G\alpha_{WM}(t_0)} \\ G = \ln\left(V_{\gamma,g}\right) - \ln\left(V_{\gamma,lq}\right) \end{cases} \qquad (7)$$

The voltage output $V_{WM}(t_0)$ of the rate-meter of the hypothetical gamma-transmission set-up positioned at the location of the wire-mesh sensor is expressed by:

$$V_{WM}(t_0) = \frac{1}{B\tau_R}\int_{-\infty}^{t_0} R_{WM}(t)\, e^{\frac{t-t_0}{\tau_R}}\, dt = \frac{V_{\gamma,lq}}{\tau_R}\int_{-\infty}^{t_0} e^{G\alpha_{WM}(t)} e^{\frac{t-t_0}{\tau_R}}\, dt\,. \tag{8}$$

Using eq. (8), the chordal void fraction as measured by the hypothetical gamma-transmission set-up is given by:

$$\alpha_{WMsim}(t_0) = \frac{ln\left(V_{WM}(t_0)\right) - ln\left(V_{\gamma,lq}\right)}{ln\left(V_{\gamma,g}\right) - ln\left(V_{\gamma,lq}\right)}\,. \tag{9}$$

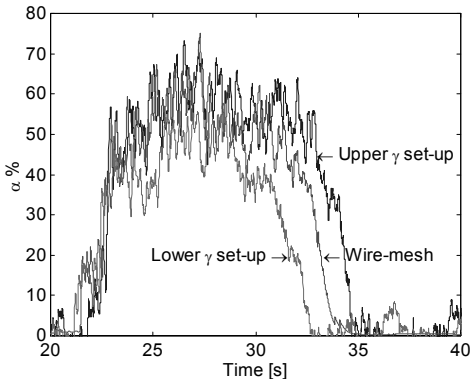

Fig. 9 Chordal void fraction measured by the gamma-transmission set-ups and simulated chordal void fraction at the wire-mesh sensor (τ_R = 0.3 s, position L1).

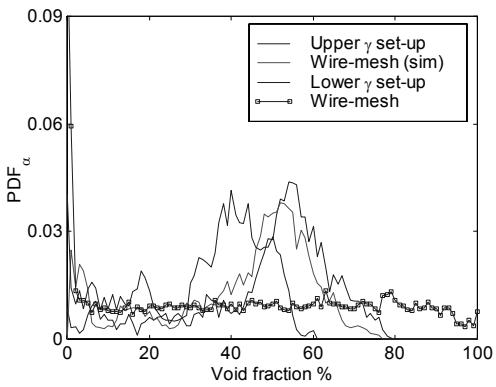

Fig. 10 PDF of chordal void fraction measured by the gamma-transmission set-ups and simulated chordal void fraction at the wire-mesh sensor (position L1, τ_R = 0.3 s).

In this paper this quantity will be referred to as *simulated chordal void fraction*.

The dynamic structures of the signals given by the gamma-transmission set-ups and the simulated chordal void fraction at the wire-mesh sensor appear to be very similar, as it can be seen in Fig. 9. In the figure, the simulated chordal void fraction at the wire-mesh sensor is reported together with the chordal void fraction measured by the gamma-transmission set-ups (shown also in Fig. 8).

From Fig. 9 it can be noticed that the void production due to flashing starts almost simultaneously at the different locations occupied by the gamma-transmission set-ups and by the wire-mesh sensor. A delay of a few seconds exists at the end of the flashing process before all the measuring devices register a zero void fraction. This delay is about the time needed for the flashing front (being the location below which one-phase flow is present) to move upwards along the adiabatic section as a consequence of the increased flow rate.

In Fig. 10 the probability density functions (PDFs) of the chordal void fractions α_{LW}, α_{UP}, α_{WM} and of the simulated chordal void fraction α_{WMsim} are presented. No direct comparison can be done between the PDF of the chordal void fractions measured by the two gamma-transmission set-ups and the PDF of the chordal void fraction measured by the wire-mesh sensor. This is due to the high rate-meter time constant (0.3 s) with respect to the frequency at which water and steam alternate during a flashing process (as it will be shown in the range of 2-4 Hz). The PDF of α_{WMsim} presents the same structure as

the PDFs of α_{LW} and α_{UP}. As expected, the maximum of the void fraction PDF moves to higher void-fraction values proceeding upward in the adiabatic section (from the lower gamma-transmission set-up to the upper one).

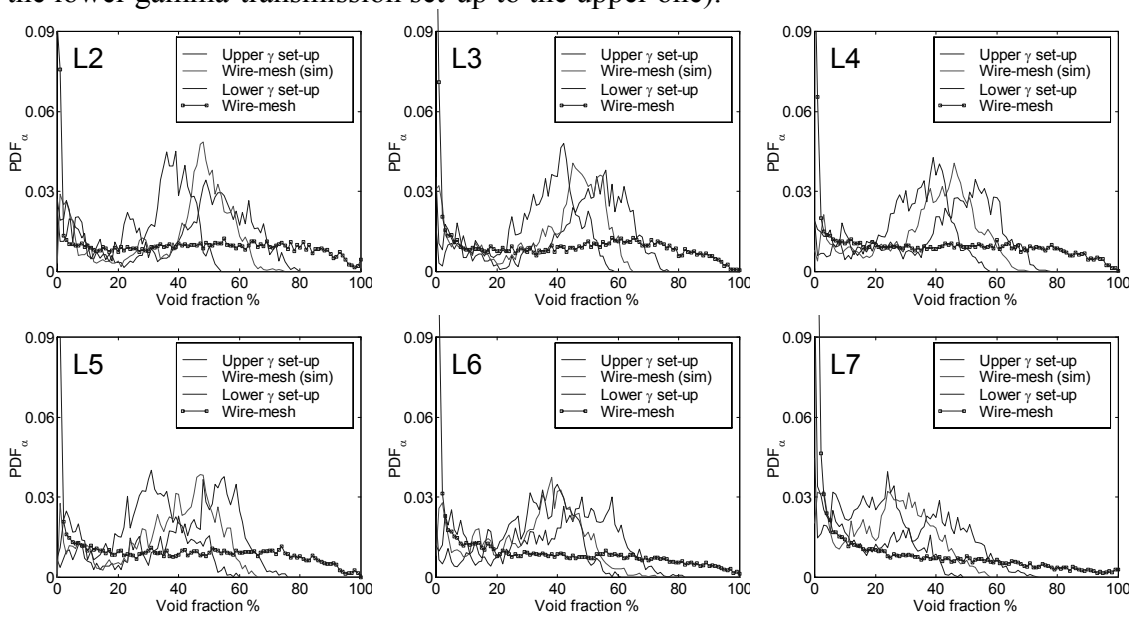

Fig. 11. PDFs of chordal void fractions measured at different positions (τ_R = 0.3 s).

In Fig. 11 the void-fraction PDFs for the other measurements carried out at positions L2 to L7 (from centre to periphery of the cross section) are reported. The maxima of the PDFs move to lower void-fraction values proceeding from the centre of the section (L1) to the periphery (L7).

	τ_R = 0.3 s				τ_R = 0.03 s			
	Upper γ	WM_{sim}	Lower γ	WM	Upper γ	WM_{sim}	Lower γ	WM
L1	48	42	32	42	46	41	31	42
L2	43	39	28	41	45	37	31	38
L3	45	37	32	37	45	37	28	38
L4	42	37	29	37	40	34	28	35
L5	43	36	27	36	42	33	22	34
L6	40	31	29	31	41	29	27	30
L7	30	23	16	23	30	24	20	25

Table 2. Average chordal void fraction during flashing process.

In Table 2 the time average (over the flashing process) of the chordal void fractions α_{LW}, α_{UP}, α_{WM} and α_{WMsim} are reported for the two sets of experiments performed. No remarkable difference is found between the time average of the chordal void fractions α_{WM} (measured at a sampling frequency of 500 Hz) and α_{WMsim}, even in the case of higher rate-meter time constant. This indicates that a sound filtering-method has been used.

The time-averaged chordal void fraction measured by the wire-mesh sensor is always in between the time-averaged chordal void fractions measured by the gamma-transmission set-ups. Despite the fact that the wire-mesh sensor is axially located in the middle between the two gamma-transmission set-ups, the average chordal void fraction measured by the wire-mesh sensor is closer to the chordal void fraction measured by the upper gamma-transmission set-up than to the one measured by the

lower gamma-transmission set-up. This is consistent with the non-linear build-up of void-fraction production during flashing (Elias and Chambré 2000).

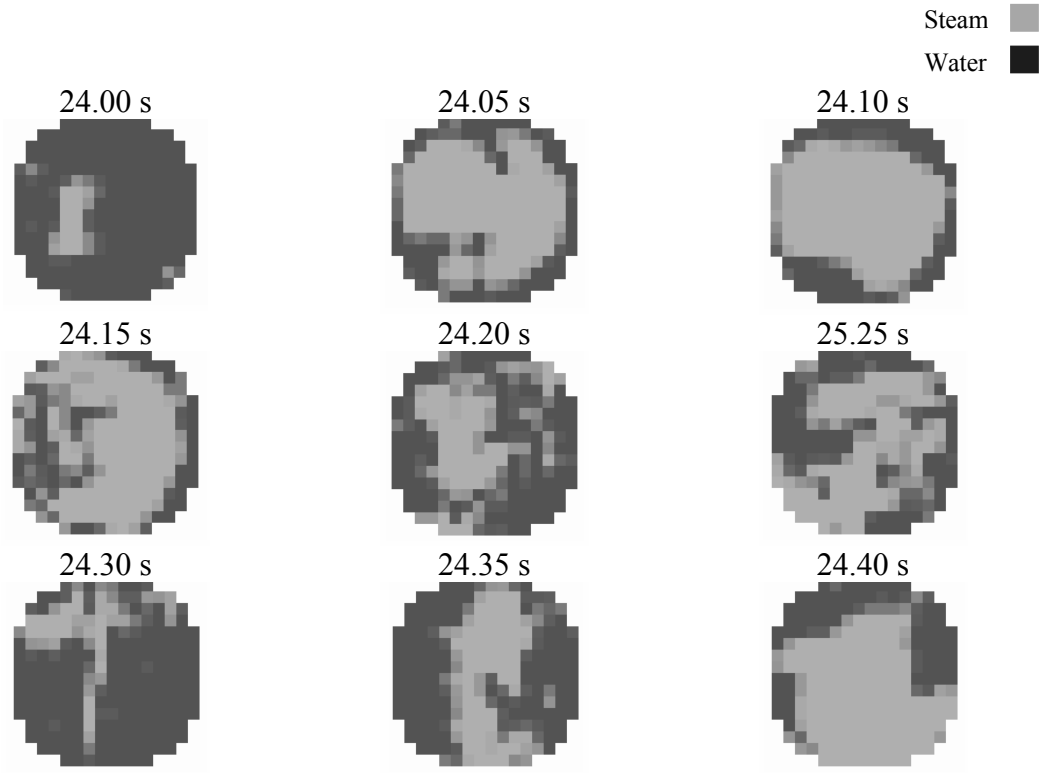

Fig. 12. Series of two-dimensional void-fraction distributions measured by the wire-mesh sensor over a time interval of 0.4 seconds.

The tendency of the maxima of the void fraction PDFs to move toward lower void fraction values when going from L1 to L7 (i.e. from the centre to the periphery of the cross-section) suggests that the steam tends to concentrate in the centre of the cross section during flashing. Detailed information on the void fraction distribution over the cross section can be extracted from the wire-mesh measurements. In Fig. 12 a series of wire-mesh two-dimensional void fraction distributions is shown over a time interval of 0.4 seconds; the correspondent time series of the cross-section-averaged void fraction is reported in Fig. 13. From Fig. 12 it can be seen that lower values of void fraction should be expected at the periphery of the section. This is confirmed by the trend found after analysing the results reported in Table 2.

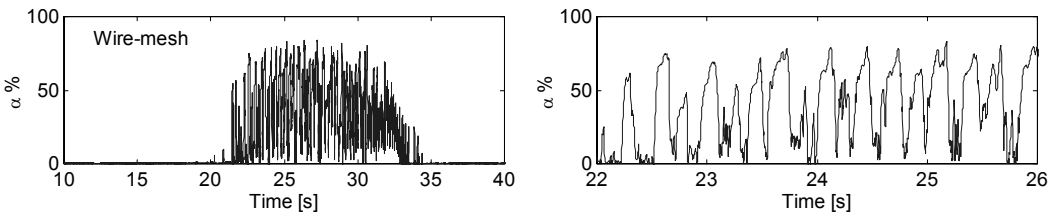

Fig. 13. Cross-section-averaged void fraction measured by the wire-mesh sensor during a flashing peak (left) and zoomed over 4 s (right).

From Fig. 12 it can be also noticed that almost no steam is present at the time instant t = 24 s and t = 24.3 s, giving an idea of the frequency at which water and steam alternate in the cross-section during flashing. This can be furthermore examined in Fig. 13, in which an enlargement of the time series of the cross-section-averaged void fraction is reported over a time interval of 4 s. Water and steam alternate in the section

at frequencies around 2-4 Hz. The frequency content of the flashing process can be also seen in the auto-power-spectral-density (APSD) of the signals measured by the wire-mesh sensor and by the gamma-transmission set-ups (τ_R = 0.03 s), as illustrated in Fig. 14-(a). The frequency of the flashing process is less visible in the spectrum of the gamma-transmission signal due to the lower signal-to-noise ratio. Below 0.1 Hz, the characteristic frequency of the flashing-induced flow oscillation is shown together with higher harmonics in Fig. 14-(b).

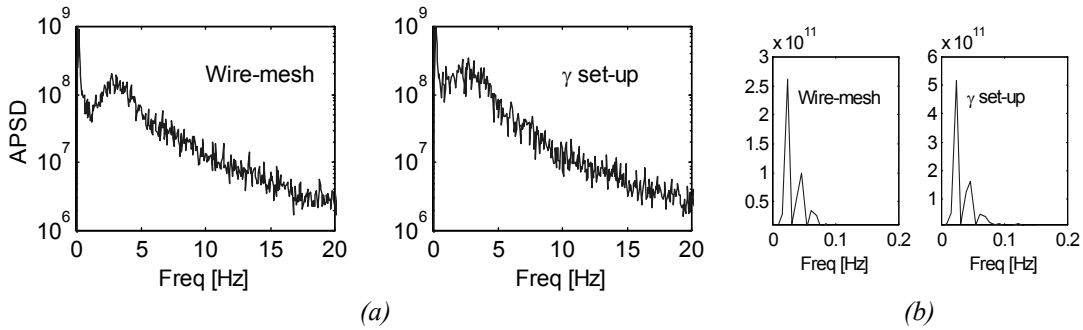

Fig. 14. APSD of wire-mesh sensor and gamma-transmission (τ_R = 0.03 s) signals (a) and zoomed over 0.2 Hz (b).

Effect of the wire-mesh sensor on the void fraction production

To investigate the effect of the wire-mesh sensor on the triggering of void-fraction production due to the possible provision of extra nucleations sites, measurements have been carried out after the wire-mesh sensor has been removed from the experimental loop.

The measurements have been done setting the temperature at the inlet of the heated section, the initial pressure at the outlet of the adiabatic section and the condensed-water level in the steam dome at the same values at which the measurements presented in the previous section have been performed.

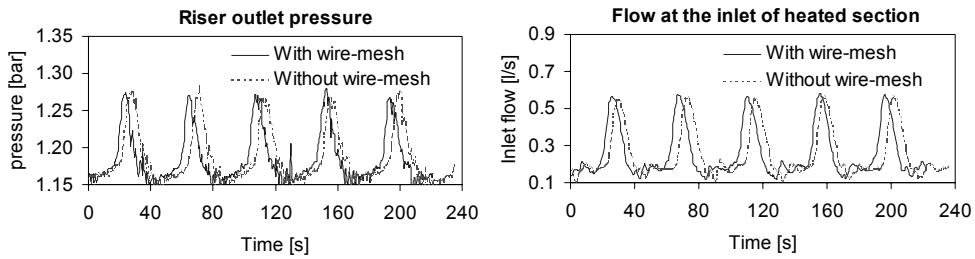

Fig. 15. Inlet flow and outlet-riser pressure with and without wire-mesh sensor.

In Fig. 15 two of the main parameters of the flashing-induced instability are shown before and after the wire-mesh sensor removal. No appreciable differences have been found between the measurements performed with and without the wire-mesh sensor. Also the period of the oscillation remains unchanged. The void fraction measured by the gamma set-ups does not change significantly as it can be seen, for example, in Fig. 16, in which the chordal void fractions α_{LW} and α_{UP} are shown before and after the removal of the wire-mesh sensor from the experimental loop. In the figure, the time-averaged chordal void fractions are also reported.

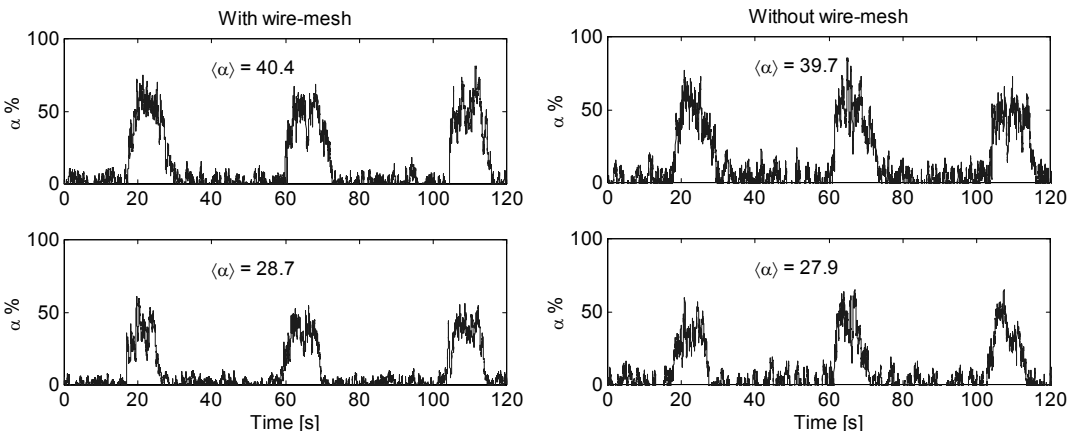

Fig. 16. Void fraction measured by the gamma-transmission set-ups with (left) and without (right) wire-mesh sensor.

Conclusions

A comparison is presented between void-fraction measurements carried out with a wire-mesh sensor (for instantaneous two-dimensional void-fraction distributions) and two gamma-transmission set-ups (for chordal void fraction measurements) in a natural-circulation loop. The two gamma-transmission set-ups were positioned just above and below the wire-mesh sensor, respectively. All measurements were carried out during flashing-induced flow oscillations. For a direct comparison between the two measuring techniques the filtering effect of the gamma-transmission system on the void fraction measurements has been considered. It has been found that:

- taking into account the gamma-transmission filtering effect, the time series of gamma-transmission and wire-mesh sensor measurements present a comparable structure;
- the time-averaged chordal void fraction measured by the wire-mesh sensor is always in between the time-averaged chordal void fractions measured by the two gamma-transmission set-ups; it is closer to the chordal void fraction measured by the upper gamma-transmission set-up than to the one measured by the lower gamma-transmission set-up due to the non-linear build-up of void-fraction production during flashing;
- steam tends to concentrate in the centre of the cross-section during flashing. This trend is confirmed by the two-dimensional void-fraction distribution measured by the wire-mesh sensor;
- void production due to flashing starts almost simultaneously at the different locations occupied by the gamma-transmission set-ups and by the wire-mesh sensor, but a delay of a few seconds exists at the end of the flashing process before all the measuring devices register a zero void fraction, this delay being about the time needed for the flashing front to move upwards along the adiabatic section as a consequence of the increased flow rate;
- the characteristic frequencies at which water and steam alternate in the section during flashing are about 2-4 Hz. These frequencies are clearly visible in the wire-mesh sensor signal thanks to the high sampling frequency (500 Hz in this study) and the high signal-to-noise ratio.

In addition, experiments have been performed after removing the wire-mesh sensor from the experimental loop to study the possible undesired effect of the wire-mesh sensor on triggering of void production. No appreciable differences have been found between the measurements performed with and without the sensor in the main characteristics of the flashing-induced instability (i.e. oscillation period, flow rate oscillation, pressure, etc.) and in the void-fraction measurements carried out with the two gamma-transmission set-ups.

References

Dudlik, A., Prasser, H.-M., Schlüter, S., 1999, "Visualization of cavitating liquid flow behind fast acting valves", *Second European Congress of Chemical Engineering - Montpellier 5-7 October (on CD-ROM), 1999*.

Krüssenberg, A.-K., Prasser, H.-M., Schaffrath, A., 2000, "A new criterion for identification of the bubble slug transition in vertical tubes", *Kerntechnik* **65**, 1.

Grunwald, G., Hönhe, T., Prasser, H.-M., 2000, "Experimental investigations on the four-loop test facility ROCOM", *Kerntechnik* **65**, 5-6.

Elias, E., Chambré, P.L., 2000, "Bubble transport in flashing flow", *Int. J. Multiphase flow* **26**, 191-206.

Inada, F., Furuya, M., Yasuo, A., 1997, "Thermo-hydraulic instability of boiling natural circulation loop induced by flashing (analytical consideration)", *Proc. Eighth Int. Top. Meetg. on Nucl. Reactor Thermal-hydraulics*, *Kyoto, Japan, September 30 – October 4, 1997*.

Ishii, M., 1997, "Views on the future of thermal hydraulic modeling", *Proc. OECD/CSNI Workshop on Transient Thermal-Hydraulic and Neutronic Code Requirements, November 5-8, 1996, Annapolis, Maryland, USA, NUREG/CP-0159, NEA/CSNI/R(97)4.*

Manera, A., De Kruijf, W. J. M., and Van der Hagen, T. H. J. J., 2000, "Experiments with the CIRCUS-facility on flashing-induced instabilities during start-up of natural-circulation-cooled BWRs," *Proceedings PHYSOR 2000, May 7-11, 2000, Pittsburgh, Pennsylvania, USA (on CDROM)*, 2000.

Prasser, H.-M., Böttger, A., Zschau, J., 1998, "A new electrode-mesh tomograph for gas-liquid flows", *Flow Measurement and Instrumentation* **9**, 111-119.

Van Bragt, D. D. B., De Kruijf, W. J. M., Van der Hagen, T. H. J. J., and Van Dam, H., 1999, "Analytical modeling of flashing-induced instabilities in a natural circulation cooled boiling water reactor," *Eurotherm Seminar No. 63, 6-8 September 1999, Genoa, Italy* (to be published in *Nucl. Eng. Des).*

Assessment of void-fraction correlations and drift-flux models applied to stationary and transient flashing flow in a vertical pipe

A. MANERA[1], H.-M. PRASSER[2], U. ROHDE[2], T.H.J.J. VAN DER HAGEN[1,3]
[1]Interfaculty Reactor Institute, Delft University of Technology, Mekelweg 15, 2629 JB, Delft, The Netherlands
[2]Forschungzentrum Rossendorf e.V., Institute of Safety Research, P.O.B. 510119, D-01314 Dresden, Germany
[3]Kramers Laboratorium voor Fysische Technologie, Delft University of Technology, The Netherlands

An assessment of void-fraction correlations and drift-flux models applied to stationary and transient flashing flows in a vertical pipe has been performed. Experiments have been carried out on a steam/water loop that can be operated both in forced and natural-circulation conditions. Advanced instrumentation has been used to obtain a detailed picture of the void-fraction development in the system. The stationary data have been compared with the results obtained by the two-phase fluid dynamics code FLOCAL.

1. INTRODUCTION

Drift-flux models have been and still are widely used in thermal-hydraulic codes both for nuclear and other industrial applications. They are applied to study two-phase flow behaviour in steady as well transient conditions and for void-fraction prediction. Despite the strong empirical nature of drift-flux models, their simplicity and robustness make them often preferable to complete two-fluid models in which several closure relations are needed to couple the set of balance equations for the two phases. Since the first drift-flux model was proposed in 1965 by Zuber and Findlay [1], large experience has been gained regarding air-water flows, in which air and liquid are supplied separately, and steam-water flows where the steam is produced by heated rods. Very little is known about flashing flows, in which steam is produced in the super-heated liquid due to a decrease of the gravitational head along the system. This topic has gained great interest in the last years since it appears to be of fundamental importance for the start-up phase of natural-circulation-cooled Boiling Water Reactors (BWRs). In these systems, at low-pressure and low-power conditions, flashing[1] occurs in the long adiabatic section (riser) which is built above the core to enhance natural circulation. The occurrence of flashing may lead to limit cycle oscillations characterized by a periodically oscillating flow rate.

Knowledge of the flashing phenomenon is therefore of fundamental importance for the determination and assessment of models to be implemented in the thermal-hydraulic codes that will be used for the design of optimal start-up procedures of natural circulation BWRs (and in general of natural circulation two-phase flow systems).

The experiments and models available in literature mainly refer to flashing in horizontal pipes as a consequence of pipe rupture (during blow-down) and cannot be directly applied to flashing flows in vertical pipes caused by variations of gravitational pressure head.

In this paper an experimental campaign is presented to study the suitability of drift-flux models for the prediction of void fraction when applied to flashing flow in vertical pipes as a consequence of variation of the gravitational pressure head. Both cases of stationary (in conditions of forced circulation) and transient flashing flow (in conditions of natural circulation) are treated. The experiments are carried out on the steam/water natural circulation loop CIRCUS [2], built at the Delft University of Technology to study the start-up phase of natural circulation Boiling Water Reactors.

Advanced instrumentation (wire-mesh sensors [3]) is used to measure two-dimensional void-fraction distributions and to estimate steam velocity.

The void fraction along the adiabatic test

[1] Flashing is very likely to occur at low pressures since at these conditions the coolant saturation temperature can vary of several degrees even with a few percent of pressure variation.

section measured by means of needle-probes sensors [4] is compared (after appropriate correction to take into account the void fraction profile in the pipe) with predictions obtained by the 4-equations two-phase flow model FLOCAL [5]. In this code different drift-flux models have been implemented.
In the next paragraphs first the experimental set-up, the instrumentations and the treatment of the measured signals is illustrated. Then, the analysis of stationary and transient experiments is presented.

2. THE EXPERIMENTAL SET-UP

The test facility CIRCUS (see scheme in Fig. 1) is a steam/water loop that can be operated both in forced and natural circulation conditions. The test section consists of an adiabatic pipe (3 m length, 47 mm diameter) built on top of four parallel heated channels.

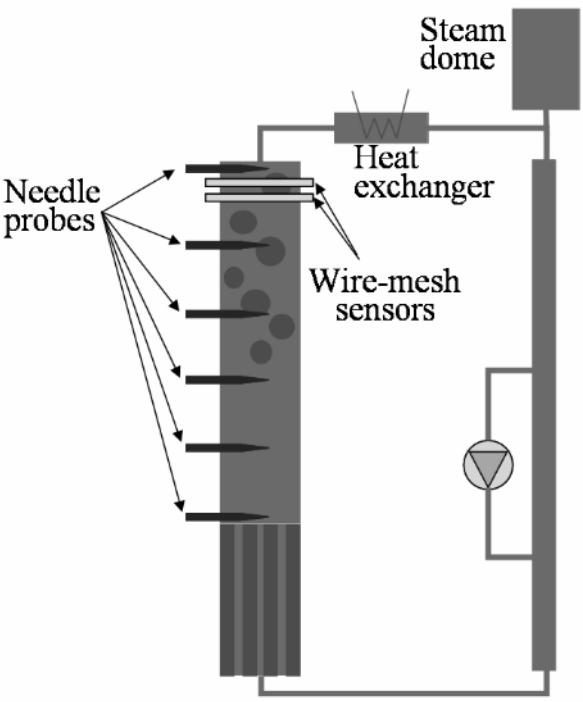

Fig. 1 Scheme of the test facility CIRCUS.

The steam produced in the heated and in the adiabatic sections is condensed by means of a heat exchanger. The pressure can be set higher than atmospheric pressure by means of a steam dome where liquid and steam are kept at saturation conditions. The measurements presented in this paper have been carried out at atmospheric pressure, with the steam dome open to the environment. During each experiment the power level and the temperature at the inlet of the heated section are kept constant.

Table 1 Characteristics of the test facility

Power range per rod	0 - 3 kW
Pressure range	1 - 5 bar
Fuel channel diameter	20.4 mm
Fuel rod diameter	12.5 mm
Heated section length	1.95 m
Adiabatic section diameter	47 mm
Adiabatic section length	3 m

3. INSTRUMENTATION

3.1. Flow measurements

The liquid velocity at the inlet of the heated section is measured by a magnetic flow-meter. Since this type of flow-meter has a time response of about 1-2 s, a Laser-Doppler-Anemometry set-up is used during transient measurements. This set-up measures the local velocity in one of the heated channels. The measured velocity is converted to flow rate on the basis of a calibration curve derived in stationary conditions using the magnetic flow-meter as a reference.

3.2. Local void fraction measurements

The local void fraction is measured at six positions along the central vertical axis of the adiabatic section by means of needle probes [4].

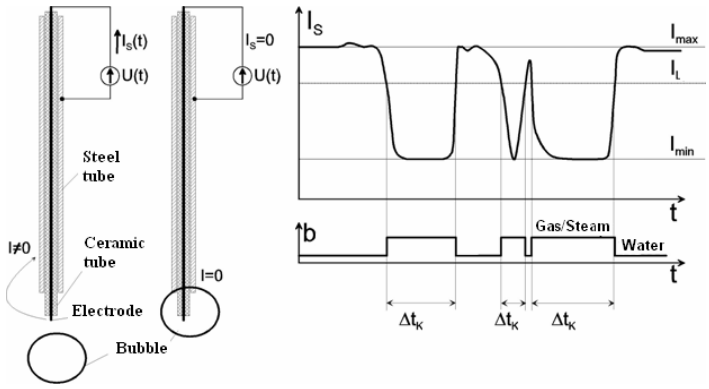

Fig. 2 Working principle of the needle probe sensors.

The measuring principle is based on the local conductivity of the fluid touching the probes. The electric current, which is sampled with a rate of 500 Hz, drops considerably if a gas/steam bubble touches the tip of the probe, giving rise to bubble pulses (see Fig. 2). The bubble pulses are discriminated in order to get a binary signal and the void fraction is

successively obtained by averaging the binary signal on a given time interval (0.5 s is used in the present study).

3.3. Two-dimensional void fraction measurements and steam-bubbles' velocity

In the upper part of the adiabatic section two wire-mesh sensors are present, positioned at an axial distance from each other of 27.5 mm. A wire-mesh sensor measures the two-dimensional void-fraction distribution over the section of a pipe on the basis of the local instantaneous conductivity of the fluid flowing in the pipe. Details on the working principle of the sensors are given by Prasser [4].

The inner diameter of the sensors used is 47 mm (equal to the inner diameter of the adiabatic section in which it is mounted). Each sensor consists of two electrode grids of 16 wires each placed at an axial distance of 1.5 mm. The two grids are positioned perpendicularly to each other (see Fig. 3) in order to form a matrix of 16x16 cross points. The distance between two successive parallel wires is 2.8 mm, this being the spatial resolution of the sensor. The sampling frequency is equal to 1200 Hz. The sensor measures the time-dependent fluid conductivity on the matrix of 16x16 points. The conversion to void fraction is performed assuming a linear dependence of the void fraction with respect to the fluid conductivity. For the conversion to void fraction it is necessary to calibrate the sensor in conditions of "tube completely filled with liquid" and "tube completely filled with gas". The calibration data are stored for each point of the 16x16 matrix and used successively for the conversion of the measured data. Additional corrections are needed if variations of the fluid temperature occur during the measurements. To take fluid temperature variations into account, calibration data of the wire-mesh have been stored at different liquid temperatures and a linear regression has been used to describe the dependence of the conductivity as function of the temperature [6]. The calibration coefficients are determined for each measuring point of the sensor individually. The fluid temperature is measured by means of a thermocouple positioned at the location of the wire-mesh sensor (see Fig. 3). Without taking into account fluid temperature variations, a non-zero void fraction may be measured by the wire-mesh even when one-phase flow is present in the section [6]. The decrease of the conductivity of the sub-cooled water between two consecutive flashing cycles results in an erroneous increase of the void fraction if this is calculated assuming a constant liquid conductivity. This effect vanishes when the described temperature calibration is applied.

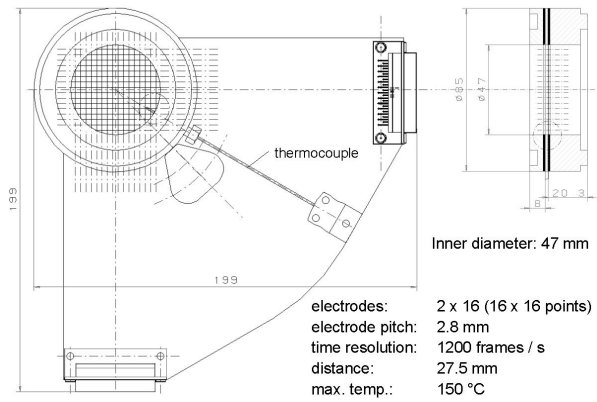

Fig. 3 Scheme of the wire-mesh sensor.

4. TREATMENT OF MEASURED SIGNALS

To test drift-flux models and void-fraction correlations the following quantities are needed (local quantities are referred to the height H of the test section where the lower wire-mesh sensor is located):

a) local cross-section-averaged void fraction $\langle\alpha_H\rangle$;

b) local superficial liquid velocity J_L;

c) local superficial steam velocity J_G.

Of these only the first quantity can be measured directly. In the general case of transient flow, the steam and liquid superficial velocities are derived from the following relation:

$$\begin{cases} J_G(t) = \langle\alpha_H\rangle(t)\langle w_G\rangle(t) \\ J_L(t) = J_{L,inl}(t) - J_G(t)\dfrac{\rho_G}{\rho_L} + \dfrac{\rho_L-\rho_G}{\rho_L}\dfrac{d}{dt}\displaystyle\int_0^H \langle\alpha\rangle(z,t)\,dz \end{cases} \tag{1}$$

where the liquid flow rate $J_{L,inl}$ at the inlet of the heated section is measured by means of a magnetic flow meter and LDA set-up. The void fraction $<\alpha_H>$ is measured by means of the lower wire-mesh sensor, the steam-bubbles' velocity w_G is derived by cross-correlating the spatial-averaged void-fractions measured by the two wire-mesh sensors. The integral spatial-averaged void-fraction on the right-hand side of eq. (1) is calculated on the basis of the needle-probes signals, assuming linear interpolation between two successive axial locations. Before the integration is performed, the needle-probe signals have to be properly corrected to take into account the radial void-fraction profile in the pipe cross-section, as described in the next paragraph.

4.1. Correction to take into account radial void-fraction profiles

In the parameters' range in which the measurements are performed the radial void-fraction profile is centre-peaked as shown in Fig. 4, where examples of two-dimensional void-fraction distributions as measured by the wire-mesh sensor are reported.

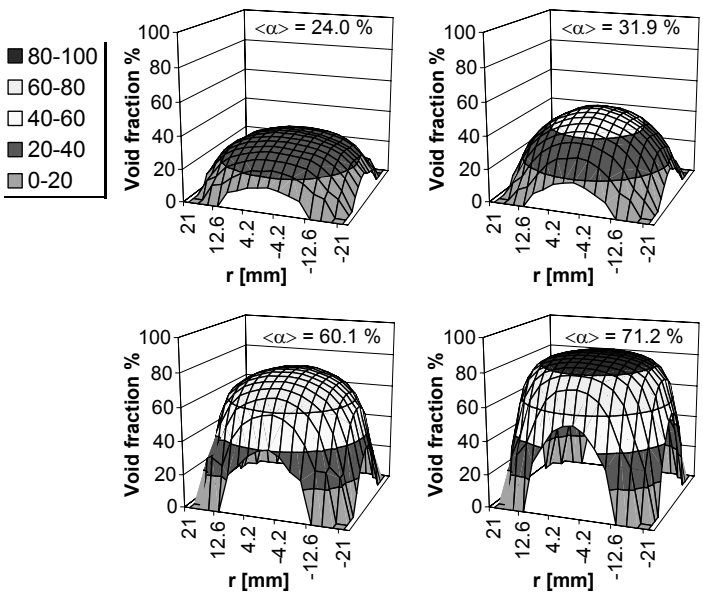

Fig. 4. Void fraction profiles measured by the wire-mesh sensor.

Measurements of void fraction by means of probes situated in the centre of the pipe will lead thus to an overestimation of the void fraction in the section. The overestimation is the highest for void fractions around 50 %, as shown in Fig. 5, where the central void-fraction α_C is plotted against the cross-section-averaged void-fraction $<\alpha>$. The data for the comparison are obtained by means of the wire-mesh sensor.

The following relation is proposed for the correction:

$$\frac{\langle \alpha \rangle}{\alpha_C} = A\alpha_C + B \qquad (2)$$

with A = 0.37 and B = 0.496. Note that no boundary condition is imposed for the case of α_C equal to unity.

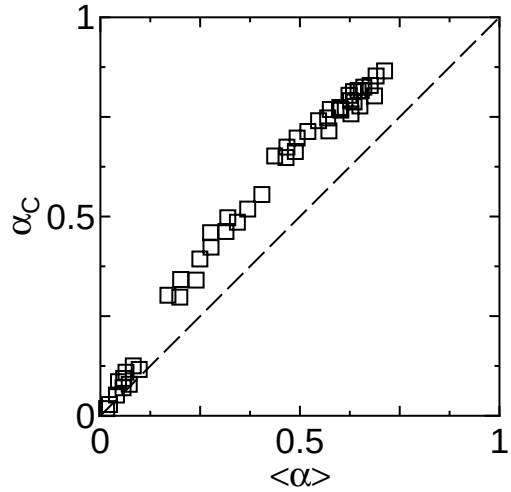

Fig. 5. Relation between cross-section-averaged and central void fraction (wire-mesh sensor data).

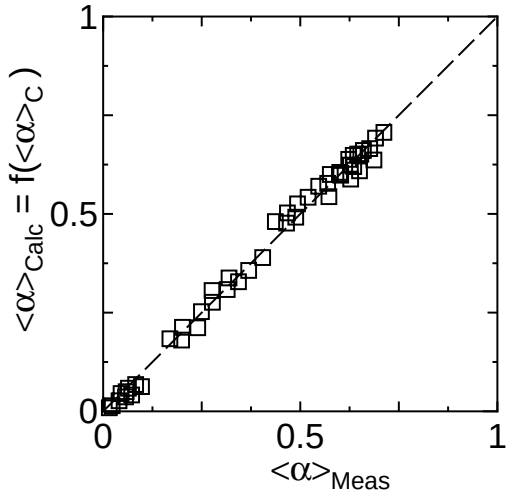

Fig. 6. Comparison between calculated (using the measured central void fraction and the empirical relation (2)) and measured cross-section-averaged void fraction.

Good agreement is found for the comparison between the measured cross-section-averaged void fraction $<\alpha>_{Meas}$ and the calculated

$<\alpha>_{Calc}$, evaluated on the basis of α_C according to relation (2). This relation will be used to treat the needle-probes data for the evaluation of the liquid superficial velocity in transient flashing flow and for the comparison in stationary conditions between experimental void-fraction profiles along the axis of the test section and the one-dimensional two-phase code FLOCAL [5].

5. RESULTS AND DISCUSSION

Only few assessments of void-fraction correlations are reported in literature. A review of all published assessments can be found in ref. [7]. Dukler et al. [8] compare only three hold-up correlations, respectively Hoogendoorn [9], Hughmark [10], and Martinelli [11] correlations. Despite the Hoogendoorn correlation is judged to have the best agreement with the experimental data, all three correlations perform quite poorly. The assessment by Friedel [12] takes into account 18 correlations, but only 3 among them, namely Hughmark [10] and Rouhani I and II [13], are found to give satisfactory agreement with the experimental data for individual ranges as well as for the total range of parameters. The Nabizadeh correlation [14] is also found to perform adequately, but gives unreliable predictions for some of the experimental sets analyzed by Friedel. Unfortunately in Friedel's assessment, a quantitative comparison in terms of statistical parameters is reported only for the three best relations and no distinction is made between different parameters' ranges. More extensive comparisons are reported by Vijayan et al. [15], Chexal et al. [16], and by Coddington and Macian [17]. In these three independent assessments the statistical parameters are reported for all the considered correlations and in the latter two assessments an explicit distinction is made between correlations' performances at low- and high-pressure conditions.

All the reviews mentioned above refer only to stationary measurements and do not take specifically into account flashing flows. In the following paragraphs, the application of void-fraction correlations to flashing flow in a vertical pipe consequent to the decrease of gravitational pressure head will be presented. The assessment is made both in conditions of stationary and transient flashing flow.

Attention should be paid to the fact that most of the models are implicitly dependent on the void fraction itself. In these cases the void fraction has to be evaluated iteratively.

5.1. Assessment of void-fraction correlations in stationary conditions

Experiments to study stationary flashing flow have been carried out in forced circulation conditions. For each experiment the power level in the heated section and the liquid flow rate and the temperature at the inlet of the test section are kept constant.

The liquid superficial velocities ranges from about 0.08 to 0.2 m/s, while the steam superficial velocity ranges from about 0.03 to 1.5 m/s. This approximately covers the parameters range at atmospheric pressure at which flashing-induced instabilities may occur during the start-up phase of natural circulation BWRs. In Fig. 7 the experimental points are reported together with the transition boundaries between bubbly, slug and churn flow according to Mishima and Ishii [18] and Taitel et al. [19].

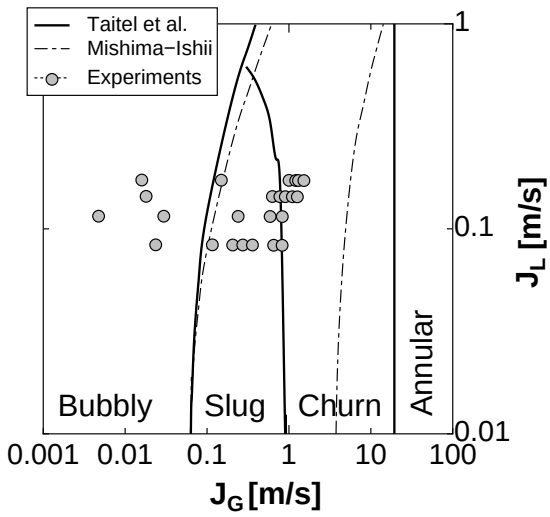

Fig. 7. Experimental conditions with respect to flow map.

In the following a brief comment is given for all the void-fraction correlations considered in this assessment. The performances of the different correlations are discussed on the basis of the comparison between predicted and experimental void-fraction data shown in Fig. 8.

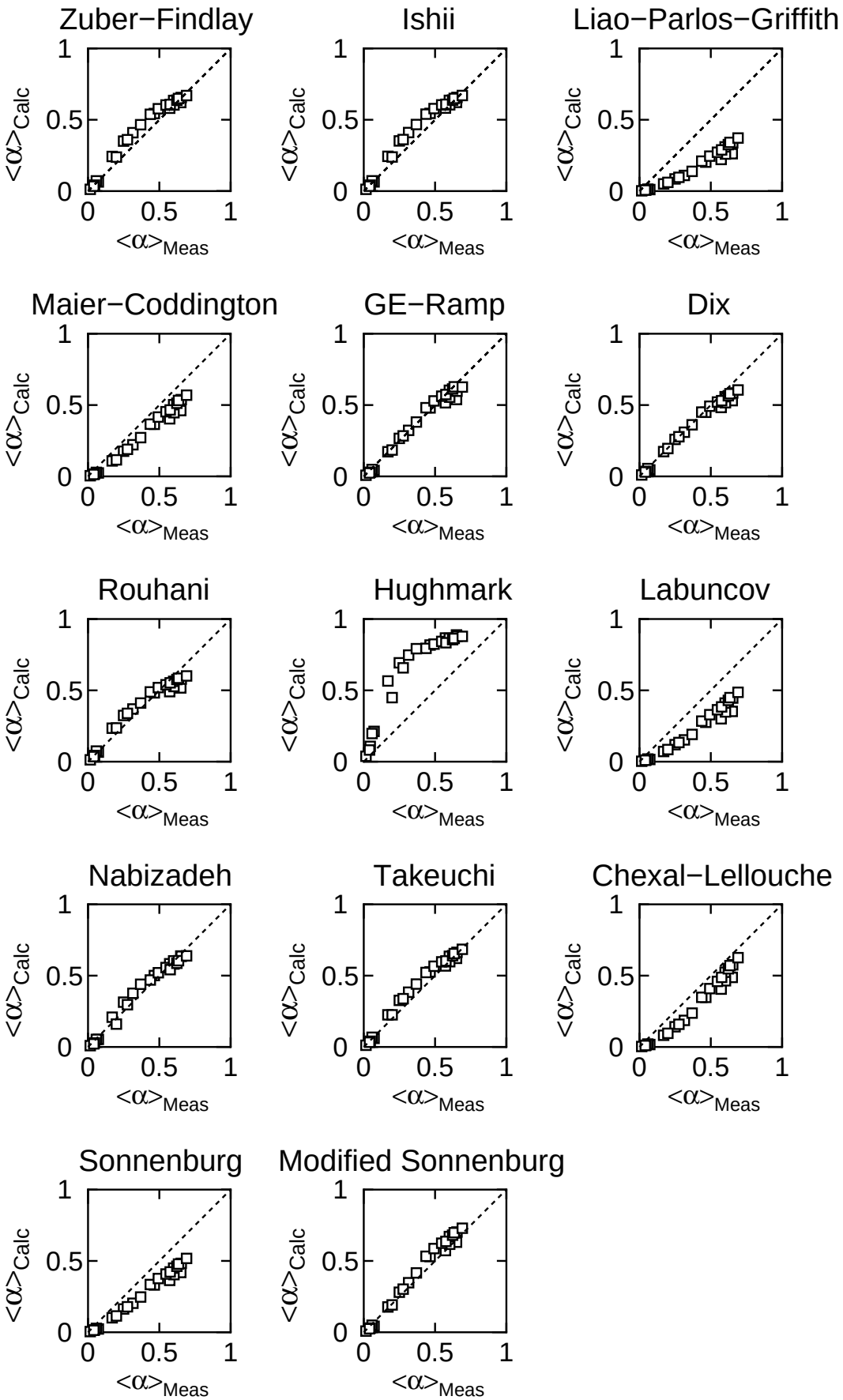

Fig. 8 Performances of void-fraction correlations (stationary data).

Zuber-Findlay [20]
Both the churn-turbulent and slug models were tested on the experimental data set. As in the assessment by Coddington and Macian, who considered the churn-turbulent model only, this drift-flux model over-estimates the void fraction at low pressure. Use of the slug-flow model yields similar results. In Fig. 8 only the results relative to the churn-turbulent model are reported.

Ishii model [21]
Both the distribution parameter and the drift velocities are flow-pattern dependent. It is found that the correlation over-estimates the void fraction in the slug flow-pattern region and under-estimates the void fraction in the churn-turbulent region. This could explain why in previous assessments at low-pressure conditions, Chexal et. al. found the correlation to over-estimate the void fraction and Coddington and Macian found the correlation to under-estimate the void fraction.

Liao, Parlos, Griffith [22]
This correlation strongly under-estimates the void fraction. Poor performances are found also by Coddington and Macian; they find under-estimation at low pressure. Chexal finds over-estimation. The difference between the two reviews may lay on the application to different flow regimes (bubbly or slug/churn flow).

Maier-Coddington [23]
This correlation was developed by least square fit of all experimental data used for their review on void-fraction correlations, thus it was extended to a large range of pressures and flow conditions and not specifically meant for low pressure. Applied to flashing flow at atmospheric pressure, it leads to a significant under-estimation of the void fraction.

GE-Ramp [7]
The GE-Ramp model has been developed for application in all vertical flow conditions. Both the distribution parameter and the drift velocity are function of the void fraction. In accordance with the previous assessment of Chexal et al. it is found that the relation, together with the Dix's model, is the best correlation for low-pressure conditions. However, Chexal et. al do not suggest its application for large-diameter pipes.

Dix model [24]
The model was developed for upward and counter-current flows in vertical pipes. Despite the fact that this model was developed for pressures higher than 10 bar, very good agreement is found even if applied at atmospheric pressure. As for the Ge-Ramp relation, Chexal. et al. do not suggest its use in case of large-diameter pipes.

Rouhani [13]
In the slug-flow region this correlation leads mainly to an over-estimation of the void fraction. In the churn-flow region the void fraction is strongly under-estimated.

Hughmark [10]
The model was intended for air/water flow at atmospheric pressure and for steam/water flows up to 140 bar. Applied to the flashing-flow measurements it strongly over-predicts the void fraction.

Labuncov [25, 26]
The model was developed for upward steam/water and air/water flows in vertical pipes on a wide range of pressures (from 1 up to 196 bar) and pipe-diameters (from 17 up to 748 mm). Even if the field of application covers the parameters' range of the measurements reported in the present work, a strong under-estimation of the void fraction is found.

Chexal-Lellouche [27]
This correlation has been developed as a universal correlation independent on the flow pattern condition, in order to guarantee continuity for all parameters' ranges. It can be applied to vertical, horizontal as well as to inclined flows and to counter-current flows. A clear disadvantage of the correlation lays in its complexity. Vijayan et al. [15] found that this correlation leads to erroneous results when applied in the low flow rate regime, typical for natural-circulation loops during start-up. The same conclusion has to be drawn

Table 2 Statistical comparison of void-fraction predictions for stationary flow

Correlation	$<\varepsilon>$	$<\lvert\varepsilon\rvert>$	$\sigma_{\lvert\varepsilon\rvert}$
Zuber-Findlay (churn flow)	-0.036	0.042	0.037
Ishii	-0.037	0.042	0.042
Liao-Parlos-Griffith	0.213	0.213	0.113
Maier-Coddington	0.090	0.090	0.044
GE-Ramp	0.012	0.026	0.026
Dix	0.031	0.033	0.035
Rouhani	0.008	0.045	0.033
Hughmark	-0.261	0.261	0.120
Labuncov	0.153	0.153	0.077
Sonnenburg	0.117	0.117	0.061
Modified Sonnenburg	-0.030	0.039	0.029
Chexal-Lellouche	0.089	0.089	0.040
Nabizadeh	-0.003	0.029	0.019
Takeuchi	-0.028	0.034	0.028

in the present assessment. For all experimental data points the relation clearly under-estimates the void fraction.

Sonnenburg [28]
This model has been developed to take into account all flow situations, including CCFL. A modified version of the model was also developed by Sonnenburg to improve the prediction of the model in case of low flow rates and low pressures. Undeniably, it is found that the modified version of Sonnenburg's model performs better than the original model for the low-pressure data reported in the present study.

Nabizadeh [14]
This correlation is an extension of the Zuber-Findlay model which includes a better description of the distribution parameter. It reproduces the experimental data better than the GE-Ramp and Dix's models when applied to the churn-flow region.

Takeuchi [29]
It was developed on the basis of experimental data from a scaled steam-generator facility. Both the distribution parameter and the drift velocity are continuous functions of the void fraction. This correlation leads to over-estimation of the void fraction for most of the data analyzed. As the Nabizadeh correlation, when applied to the churn-flow region it reproduces the experimental data better than the GE-Ramp and Dix's models.

In Table 2 the performances of the different void-fraction correlations are reported in terms of the mean error $<\varepsilon> = <\alpha_{Measured} - \alpha_{Calculated}>$, the mean of the absolute error $<|\varepsilon|>$ and its standard deviation $\sigma_{|\varepsilon|}$.
As was already clear from Fig. 8, the GE-Ramp and Nabizadeh correlations perform the best, followed by Dix, modified Sonnenburg and Takeuchi models. Takeuchi and Nabizadeh and Sonnenburg relations perform better with the churn-flow data points. Liao-Parlos-Griffith, Hughmark, Labuncov and original Sonnenburg correlations perform extremely poorly.
The findings on flashing flow are in line with the results on steam-water flows by Chexal's et al. who find GE-Ramp and Dix correlations to provide the best performances with regards to all experimental sets, with the exception of large-diameter pipe data.

5.2. Assessment of void-fraction correlations during transient conditions
When a two-phase loop is operated in natural-circulation conditions it may exhibit flow instabilities induced by flashing in the adiabatic section of the loop. This phenomenon is of particular interest since it can take place during the start-up phase of natural circulation BWRs. Typical measured flashing-induced flow-instabilities are shown in Fig. 9. For each of the two cases presented, the flow rate and the cross-section averaged void fractions measured by the two wire-mesh sensors are reported.

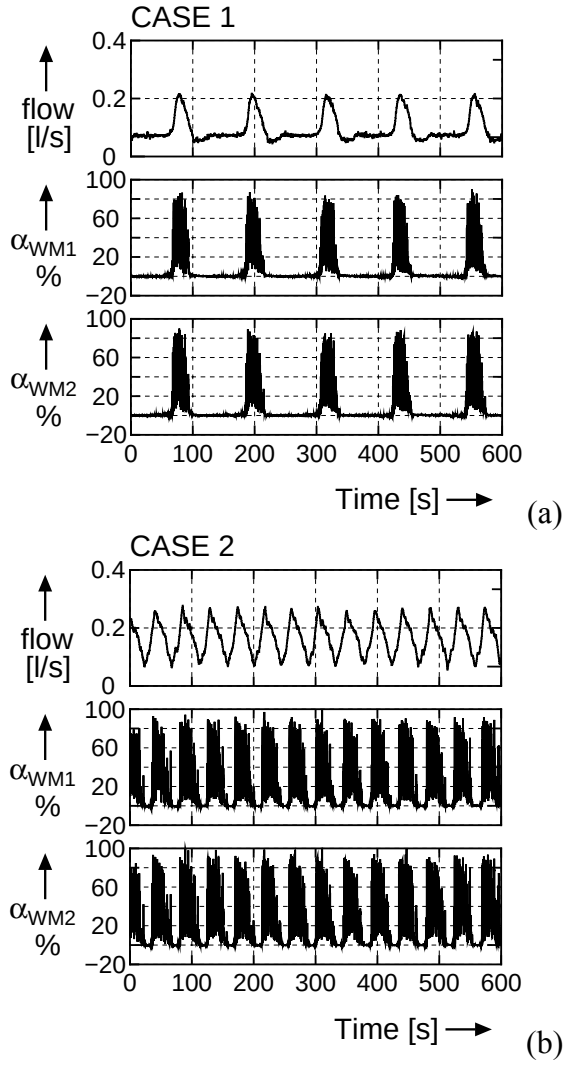

Fig. 9. Examples of flow-rate and instantaneous cross-section averaged void fraction signals during flashing-induced instabilities.

For the assessment of void-fraction correlations during transient flashing flow, first flashing cycles are discriminated on the basis of the signal of the lower wire-mesh sensor. The beginning of a flashing cycle is determined as the time instant at which the wire-mesh sensor measures a cross-section-averaged void fraction of at least 10%. For each flashing cycle the gas and liquid superficial velocities, the cross-section-averaged void fraction and the integral void fraction in the adiabatic section are determined with a time-step of 0.5 s. The steam-bubbles' velocity was determined every 0.5 s by cross-correlating the instantaneous cross-section averaged void fractions measured by the two wire-mesh sensors. Then, ensemble averaging is performed over all flashing cycles in order to guarantee sufficient statistical accuracy. In this way, for a given parameters' combination (power, subcooling, pressure, etc.) it is possible to obtain a representative time-dependent flashing cycle.

The corresponding ensemble-averaged flashing cycles for the two example cases 1 and 2 are shown in Fig. 10, which reports the cross-section averaged void fraction α_{WM1} measured at the lower wire-mesh sensor location, the gas velocity v and the corrected void-fraction measured by the needle-probes at different heights in the adiabatic test section.

Case 1 is characterized by the fact that the adiabatic section is only partially occupied by flashing flow (considerable void production is observed only in the upper part of the adiabatic section, as shown in Fig. 10). Case 2, instead, is characterized by the fact that flashing occurs in the all adiabatic section.

During a flashing-induced instability both J_G and J_L are time-dependent. The behaviour of the working point with time is shown in Fig. 11 (both for case 1 and case 2). The flow pattern varies from bubbly-flow to slug/churn flow and ends as bubbly flow again (the time increases from point A to B in Fig. 11). This can be also seen by visual inspection of the test section and by bubbles' reconstruction and flow pattern visualization on the basis of the wire-mesh sensor data [30].

Several measurements were carried out during flow oscillations induced by flashing and for all cases an ensemble-averaged flashing cycle was derived, before the assessment of drift-flux models was performed. The comparison between transient experimental and predicted void fractions for all the correlations considered in this study is shown in Fig. 12. More than 500 data-points are used for the comparison.

The performances of the different void-fraction correlations with respect to the transient data are summarized in Table 3. Similar trends as for the stationary data-set are observed. In view also of their relative simplicity, GE-Ramp and Dix models are to be recommended for application to flashing flows. A further assessment would be needed for the cases of large-diameter pipes.

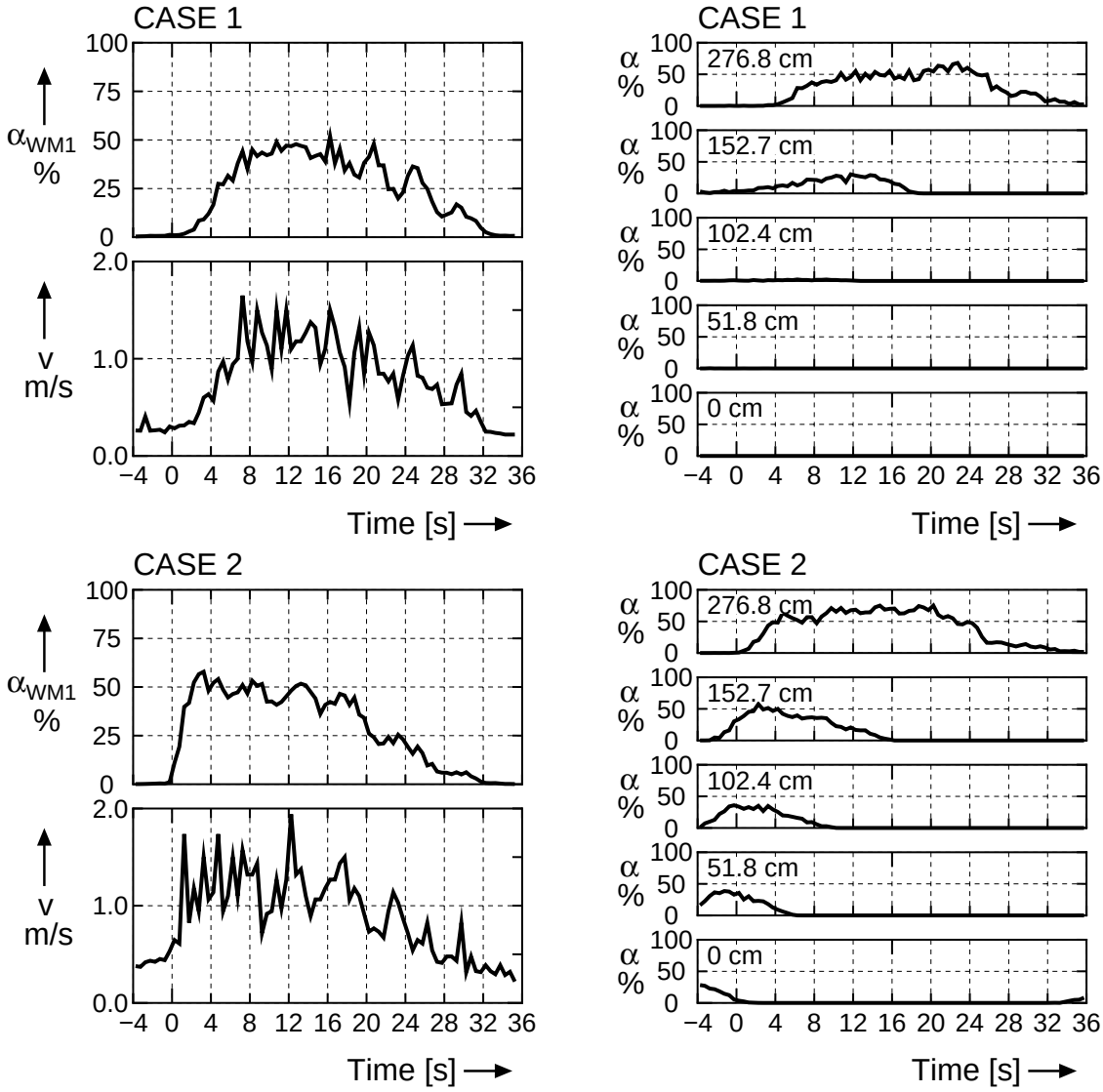

Fig. 10. Examples of ensemble-average flashing cycles: local cross-section averaged void fraction α_{WM1}, steam velocity v and void fraction evolution along the adiabatic section.

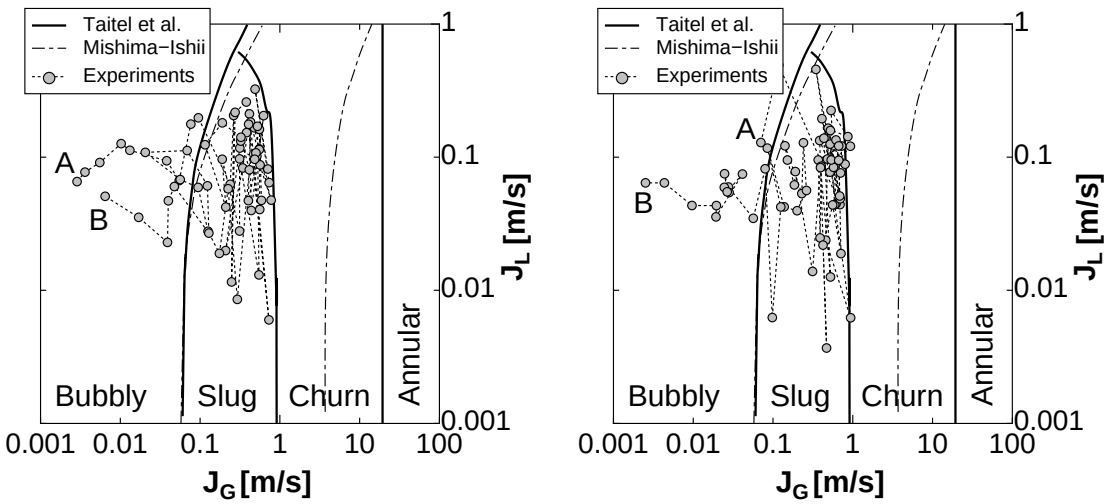

Fig. 11 Localization of transient working points in the J_G-J_L flow map for Case 1 (left) and Case 2 (right).

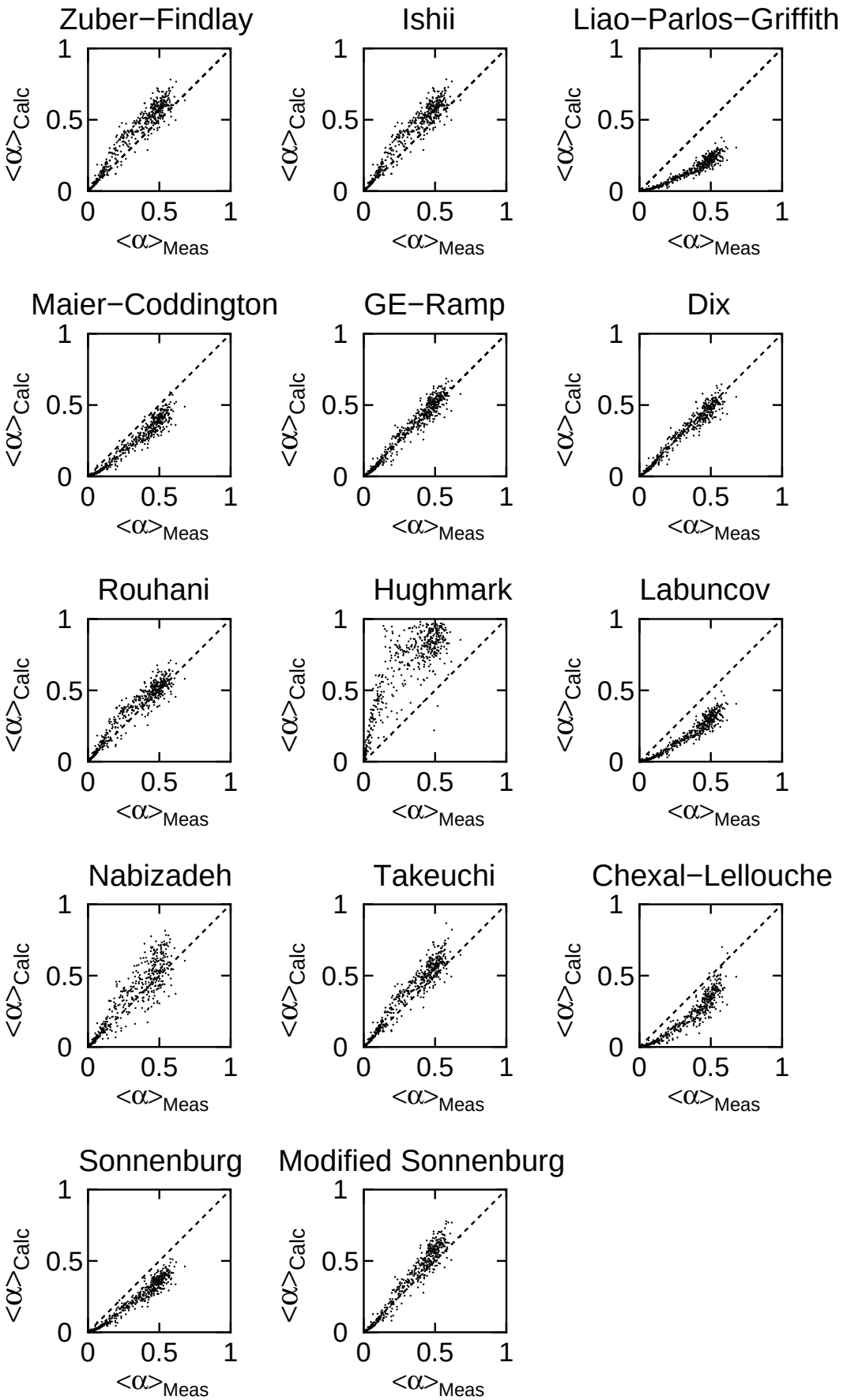

Fig. 12 Performances of void-fraction correlations (transient data)

Table 3 Statistical comparison of void-fraction predictions for transient flow

Correlation	<ε>	<|ε|>	$\sigma_{\|\varepsilon\|}$
Zuber-Findlay (churn flow)	-0.066	0.073	0.056
Ishii	-0.067	0.074	0.056
Liao-Parlos-Griffith	0.186	0.186	0.104
Maier-Coddington	0.078	0.079	0.051
GE-Ramp	-0.007	0.034	0.031
Dix	0.008	0.029	0.029
Rouhani	-0.033	0.049	0.043
Hughmark	-0.325	0.326	0.161
Labuncov	0.138	0.138	0.077
Sonnenburg	0.098	0.098	0.058
Modified Sonnenburg	-0.040	0.054	0.048
Chexal-Lellouche	0.113	0.114	0.068
Nabizadeh	-0.046	0.075	0.071
Takeuchi	-0.054	0.062	0.053

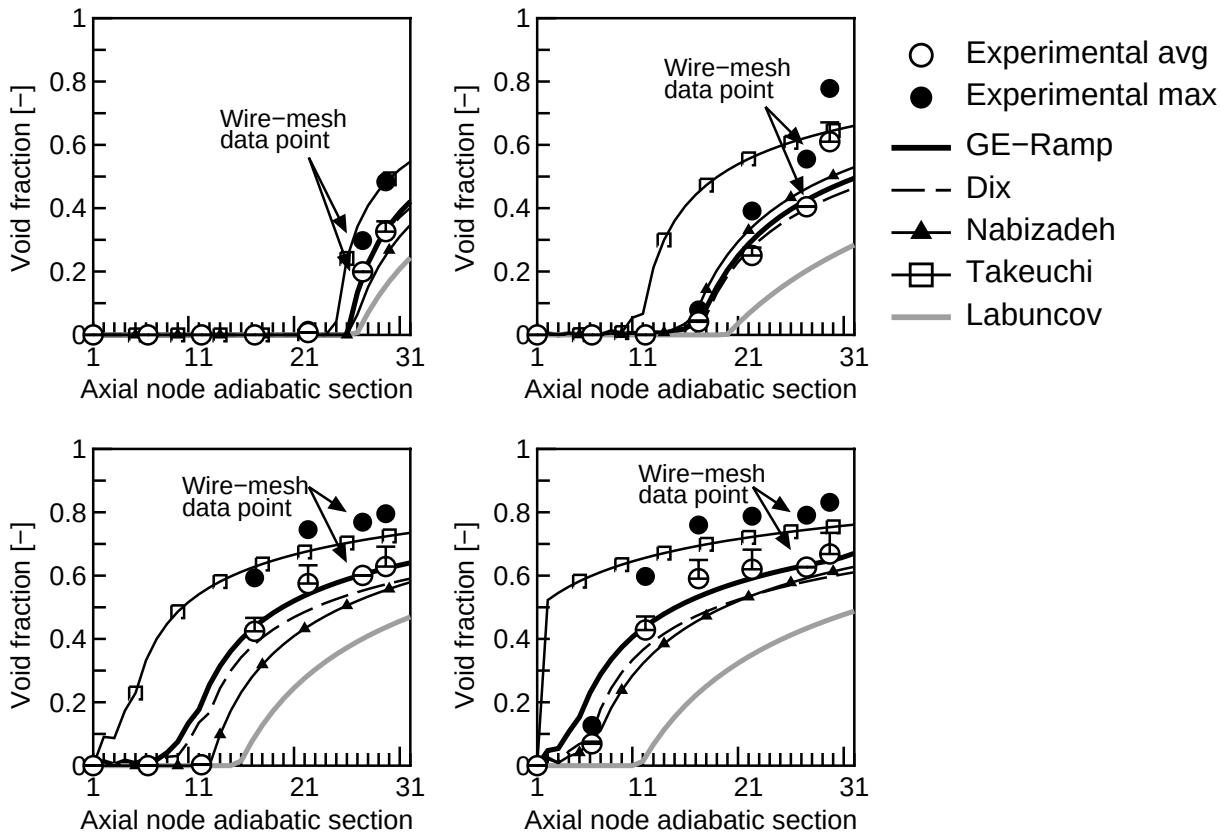

Fig. 13. Axial void-fraction profile predicted by FLOCAL compared with experimental data.

6. SIMULATIONS WITH THE TWO-PHASE FLOW CODE FLOCAL

The 4-equations two-phase code FLOCAL [5] has been used to predict the void fraction profile along the adiabatic test section in stationary conditions. For this purpose different drift-flux models and void-fraction correlations have been implemented in the code. The results are compared with the experimental data. For the calculations, both the heated and the adiabatic sections of the test loop were modelled using 30 axial nodes. Boundary conditions are the heating power, the temperature and the liquid flow rate at the inlet of the test section, the pressure at the outlet of the adiabatic section.

In Fig. 13 the comparison between simulations and experimental data is reported for four cases. For each case, the axial void-fraction profile in the adiabatic section of the experimental loop is calculated using different void-fraction correlations. As mentioned

earlier in this paper, the void fraction profile is measured by means of needle-probes located at six different axial positions in the adiabatic section. To get the cross-section-averaged void-fraction the correction described in paragraph 4.1 has been applied. The central and cross-section-averaged void-fraction measured by the lower wire-mesh sensor are also reported in Fig. 13. The trends regarding the soundness of the void-fraction predictions for the different void-fraction correlations are in full agreement with the conclusions drawn above in the previous paragraph. Namely: the GE-Ramp and Dix models give the best overall predictions, the Labuncov model strongly under-estimate the void fraction in the all range of void fractions. The Takeuchi model mainly over-estimates the void fraction. The Nabizadeh model over-predicts the void fraction below 50 % and under-predicts the void fraction above 50 %.

CONCLUSIONS

An assessment of void-fraction correlations applied to flashing flows at atmospheric pressure was carried out. The experimental data were obtained from a two-phase flow loop. The study focused both on stationary (in conditions of forced circulation) and transient (in conditions of natural circulation) flashing flows. In case of transient flashing flow, it is found that flow pattern transition between bubbly and slug/churn flow occurs.

It is found that GE-Ramp and Dix model give very good predictions of the void-fraction both for the stationary and the transient data set. The simulations performed with the two-phase flow code FLOCAL lead to the same conclusion with regards to the best void-fraction correlations.

The findings on flashing flow are in line with the results on steam-water flows obtained by Chexal's et al., who found GE-Ramp and Dix correlations to provide the best performances with regards to all experimental sets, with the exception of large-diameter pipe data.

AKNOWLEDGMENT

The work presented has been partially sponsored within the EU 5th Framework Program, NACUSP project, FIKS-CT2000-00041.

NOMENCLATURE

H	height	m
J	superficial velocity	$m\ s^{-1}$
t	time	s
w	velocity	$m\ s^{-1}$
z	axial coordinate	m
Greek symbols		
α	void fraction	-
ε	error	-
Subscripts		
G	vapour	
inl	inlet	
L	liquid	

REFERENCES

1. N. ZUBER, J.A. FINDLAY, "Average volumetric concentration in two-phase flow systems," *J. Heat Transfer*, **87** (1965).
2. A. MANERA, T.H.J.J. VAN DER HAGEN, "Stability of Natural-circulation-cooled Boiling Water Reactors during Startup: Experimental Results," *Nuclear Technology*, **143** (2002).
3. H.-M. PRASSER, A. BÖTTGER, J. ZSCHAU, "A New Electrode-Mesh Tomograph for Gas-Liquid Flows," *Flow Measurement and Instrumentation,* **9**, 111 (1998).
4. H.-M. PRASSER, R. LOTZMANN, G. UHLMANN, L. MAROTI, P. WINDBERG, "Beobachtung des Loop-Seal-Clearings in der Integralanlage PMK-NVH des KFKI Budapest mit Nadelsonden," *Kernenergie*, **34** (1991).
5. U. ROHDE, "Theoretische Untersuchung dynamischer Naturumlaufinstabilitäten im Kernheizreaktor AST-500," *Kernenergie* **30** (1987).
6. A. MANERA, H.-M. PRASSER, T.H.J.J. VAN DER HAGEN, R.F. MUDDE AND W.J.M. DE KRUIJF, "A comparison of void-fraction measurements during flashing-induced instabilities obtained with a wire-mesh sensor and a gamma-transmission set-up," *Proc. 4th International Conference on Multiphase Flow (ICMF-2001)*, May 27 - June 1, New Orleans (2001).
7. "Thermal-hydraulic relationships for advanced water cooled rectors", IAEA-TECDOC-1203 (2001).

8. A.E. DUKLER, MOYE WICKS III, R.G. CLEVELAND, "Frictional Pressure Drop in Two-Phase Flow: A. A comparison of Existing Correlations for Pressure Loss and Holdup", *A.I.Ch.E. J.* **10**, pp. 38-53 (1964).
9. C.J. HOOGENDOORN, "Gas-liquid flow in horizontal pipes", *Chem. Eng. Sci.*, **9**, pp. 205-217 (1959).
10. G.A. HUGHMARK, "Holdup and heat transfer in horizontal slug gas-liquid flow", *Chem. Eng. Sci.*, **20**, pp. 1007-1010 (1965).
11. R.W. LOCKHART, R.C. MARTINELLI, "Proposed correlation of data for isothermal two-phase, two-component flow in pipes", *Chem. Eng. Prog.*, **45**, pp. 39-48 (1949).
12. L. FRIEDEL, "Pressure drop during gas/vapour-liquid flow in pipes", *Int. Chem. Eng.*, **20**, 3, pp. 352-367 (1980).
13. S.Z. ROUHANI, "Subcooled void fraction", AB Atomenergi Rep., AWE-RTV-841 (1969).
14. H. NABIZADEH, "Modellgesetze and Parameteruntersuch fur den volumetrichen Dampfgehalt in einer zweiphasen Stroemung", EIR-Bericht, Nr. 323 (1977).
15. P.K. VIJAYAN, A.P. PATIL, D.S. PILKHWAL, V. VENKAT RAY, "An assessment of pressure drop and void fraction correlations with data from two-phase natural circulation loops", *Heat and Mass Transfer*, **36**, pp. 541-548 (2000).
16. B. CHEXAL, J. HOROWITZ, G.S. LELLOUCHE, "An assessment of eight void fraction models", *Nucl. Eng. Des.*, **126**, pp. 71-88 (1991).
17. P. CODDINGTON, R. MACIAN, "A study of the performances of void fraction correlations used in the context of drift-flux two-phase flow models", *Nucl. Eng. Des.*, **215**, pp. 199-216 (2002).
18. K. MISHIMA, M. ISHII, "Flow regime transition criteria for upward two-phase flow in vertical tubes," *Int. J. Heat Mass Transfer,* **27**,723-737 (1984).
19. Y. TAITEL, D. BORNEA, A.E. DUKLER, "Modelling flow pattern transitions for upward gas-liquid flow in vertical tubes," *AIChE J.,* **26**,345-354 (1980).
20. N. ZUBER, J.A. FINDLAY, "Average volumetric concentration in two-phase flow systems", *J. Heat Transfer*, ASME **87**, pp. 453-468 (1965).
21. M. ISHII, "One-dimensional drift-flux Model and Constitutive Equations for Relative Motion Between Phases in Various Two Phase Flow Regimes", ANL-77-47 (1977).
22. L.H. LIAO, A. PARLOS, P. GRIFFITH, "Heat Transfer Carryover and Fall Back in PWR Steam Generators During Transients", NUREG/CR-4376, EPRI NP-4298 (1985).
23. D. MAIER, P. CODDINGTON, "Review of wide range void correlations against an extensive data base of rod bundle void measurements", *Proc.5th Int. Conf. on Nucl. Eng. ICONE-5*, May 25-29, Nice, France (1997).
24. G.F. DIX, "Vapor Void Fraction for Forced Convection with Subcooled Boiling t Low Flow Rates", NEDO-10491 (1971).
25. D.A. LABUNCOV, "Parosoderzanie druchfaznogo adiabatnogo potoka vertikla'nych kanalach", *Teploenergetika* **7** (1960).
26. J. HUNH, J. WOLF, "Zweiphasen-stromung", VEB Fachbuchverlag Leipzig (1975).
27. B. CHEXAL, J. HOROWITZ, G.S. LELLOUCHE, "A void fraction correlation for generalized applications", *Progress in Nuclear Energy*, **27**, 4, pp. 255-295 (1992).
28. H.G. SONNENBURG, "Berechnung der Phasendifferenzgeschwindigkeit von Wasser und Dampf in geometrisch unterschiedlich berandeten Kanälen", Dissertation, TU Berlin, Fachbereich 6 (1994).
29. K. TAKEUCHI, M.Y. YOUNG, L.E. HOCHREITER, "Generalized drift flux correlation for vertical flow", *Nucl. Sci. Eng.*, **112**, pp. 170-180 (1992).
30. A. MANERA, H.-M. PRASSER, D. LUCAS, T.H.J.J. VAN DER HAGEN, "Flow pattern visualization and bubble size distributions during stationary and transient flashing flow in a vertical pipe", *to be submitted*.

Flow pattern visualization and bubbles size distributions during stationary and transient flashing flow in a vertical pipe

A. MANERA[1], H.-M. PRASSER[2], D. LUCAS[2], T.H.J.J. VAN DER HAGEN[1]
[1]Interfaculty Reactor Institute, Delft University of Technology, Mekelweg 15, 2629 JB, Delft, The Netherlands
[2]Forschungzentrum Rossendorf e.V., Institute of Safety Research, P.O.B. 510119, D-01314 Dresden, Germany

An experimental three-dimensional reconstruction and visualization of stationary and transient flashing flow in a vertical pipe (47 mm diameter) is presented. The measurements have been performed by means of wire-mesh sensors. This type of sensor delivers two-dimensional void fraction distributions in the pipe cross-section where it is mounted with a maximum sampling rate of 10,000 frames per second. A sampling rate of 1200 frames per second has been used in this work. Steam bubbles have been identified from the wire-mesh data and their complete three-dimensional reconstruction has been performed by taking into account the steam bubble velocity. For the estimation of the bubble velocity, two wire-mesh sensors positioned at a small axial distance from each other have been used. The velocity has been determined by cross-correlation of the two wire-mesh signals, by direct identification of the travelling time of the steam bubbles between the two sensors and by means of a drift-flux model. A comparison between the three methods of bubbles velocity measurement is reported. Stationary and time-dependent bubble size distributions have been derived. The stationary radial void-fraction profiles have been decomposed according to bubble size classes and compared with the results obtained with an equilibrium model.

1. INTRODUCTION

Flashing flows in vertical pipes have found great interest in the last years since they might appear during the start-up phase of natural-circulation-cooled Boiling Water Reactors (BWRs). In these systems the coolant flow is driven by natural circulation instead of using pumps and a long adiabatic section (riser or chimney) is present above the reactor core to enhance the flow rate.

It has been demonstrated theoretically [1, 2] and experimentally [3-8] that under specific conditions flashing[1](i.e. void production) in the adiabatic section may trigger undesired self-sustained flow oscillations. To avoid such instabilities, optimal start-up procedures are needed. Such procedures are tested by means of so-called best-estimate codes (TRACG, ATHLET, RELAP, etc.). These codes are based on the one-dimensional two-fluid model approach and necessitate a set of constitutive relations to couple the balance equations for the liquid and vapour phase. These relations have not been derived specifically for flashing flow subsequent to a decrease of gravitational head. On the contrary, computer simulations [9-15] of natural circulation BWRs systems at low pressure (when the flashing phenomenon plays a key-role) have often given unsatisfactory and sometimes even contradictory results.

Knowledge of the characteristics of flashing flows is therefore of fundamental importance for the determination and assessment of models to be implemented in best-estimate codes for the design of optimal start-up procedures for the natural circulation BWRs (and in general of natural circulation two-phase flow systems).

The experiments and models available in literature [16-20] mainly refer to flashing in horizontal pipes as a consequence of sudden depressurization (i.e. blow down transients, for instance due to a pipe rupture) or close to a pipe restriction and cannot be directly applied to flashing flows in vertical pipes caused by variations of gravitational pressure head.

Many authors report about air-water flows, in which air and liquid are supplied separately, and scarce literature can be found focused on

[1] Flashing is very likely to occur at low pressures since at these conditions the coolant saturation temperature can vary of several degrees even with a few percent of pressure variation.

steam-water flows where the steam is produced by heaters placed below an adiabatic test section.

In summary, very little is known about flashing flows, in which steam is produced in the super-heated liquid due to a decrease of the gravitational head along the system. In particular, the structure of a flashing flow in a vertical pipe has never been analyzed before.

In this paper, a characterization of flashing flows in a vertical pipe is presented. The determination of the prevailing flow patter regime is usually the first step in the study of a two-phase flow. Further steps include quantitative information necessary for the assessment of constitutive relations. Stationary as well as transient (during flashing-induced flow oscillations) flashing flows are studied. Advanced instrumentation, namely wire-mesh sensors, is used for this task. Appropriate treatment of the data delivered by the wire-mesh sensors gives the possibility to derive stationary and transient bubbles size distributions and a complete 3D visualization of the flow pattern.

2. THE EXPERIMENTAL SET-UP

The test facility (see scheme in Fig. 1) is a steam/water loop built at the Delft University of Technology to simulate the behaviour of a natural-circulation BWR at low-pressure conditions. Demineralised water is used as working fluid. The test section consists of an insulated adiabatic pipe (3 m length, 47 mm diameter), so-called riser, made of glass built on top of four parallel heated channels. The steam produced in the heated and in the adiabatic sections is condensed by a heat exchanger. The pressure can be set higher than the atmospheric pressure by means of a steam dome where liquid and steam are kept at saturation conditions (in this case the loop is pressurised by means of a pressure vessel containing air and water separated by a membrane. After the pressurization the vessel is disconnected from the loop). A buffer vessel is used to damp temperature oscillations at the outlet of the heat exchanger in order to ensure a constant temperature at the inlet of the heated section. The facility can be operated both in forced and natural circulation conditions. The main characteristics of the test facility are reported in Table 1.

The measurements presented in this paper have been carried out at atmospheric pressure, with the steam dome open to the environment. During each experiment, the power level and the temperature at the inlet of the heated section are kept constant.

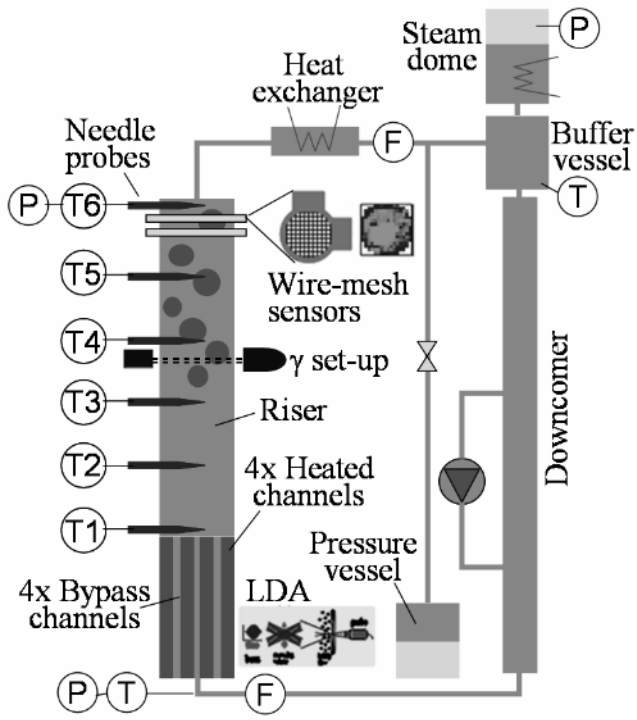

Fig. 1 Scheme of the test facility.

Table 1 Characteristics of the test facility

Power range per rod	0 - 3 kW
Pressure range	1 - 5 bar
Fuel channel diameter	20.4 mm
Fuel rod diameter	12.5 mm
Heated section length	1.95 m
Adiabatic section diameter	47 mm
Adiabatic section length	3 m

2.1 Instrumentation

The instrumentation of the test facility is schematically illustrated in Fig. 1. The flow rate at the inlet of the heated section and before the steam dome is measured by means of magnetic flow-meters. Thermocouples are located at the inlet and outlet of each heated channel, along the adiabatic section, in the heat exchanger and in the steam dome. The temperature at the inlet of the heated section is measured by a PT100 for higher accuracy. Pressure sensors are used to measure the absolute pressure at the inlet of the heated

section, at the outlet of the riser and in the steam dome. Differential pressure sensors are mounted across the steam dome (for water level measurements) and across the valves at the inlet of the heated section. Beside standard instrumentation, advanced measuring techniques are used for detailed void-fraction measurements and for velocity measurements at high sampling rate. The latter measurements are performed by means of Laser-Doppler Anemometry set-ups. The void-fraction measurements are performed by means of local conductivity needle-probes [21] equidistantly distributed along the axis of the adiabatic section, and by wire-mesh sensors. Two of such sensors are mounted in the upper part of the adiabatic section, positioned at an axial distance from each other of 27.5 mm. Details are given in the next paragraph.
Further information about the set-up and its instrumentation can be found in Ref. [22].

3. THE WIRE-MESH SENSOR

The wire-mesh sensor, developed at the Forschungzentrum Rossendorf (FZR, Germany) allows the measurement of the instantaneous two-dimensional void-fraction distribution over the cross-section of a pipe. The measurement is based on the local instantaneous conductivity of the fluid flowing in the pipe. Details on the working principle of the sensors are given by Prasser et al. [23].

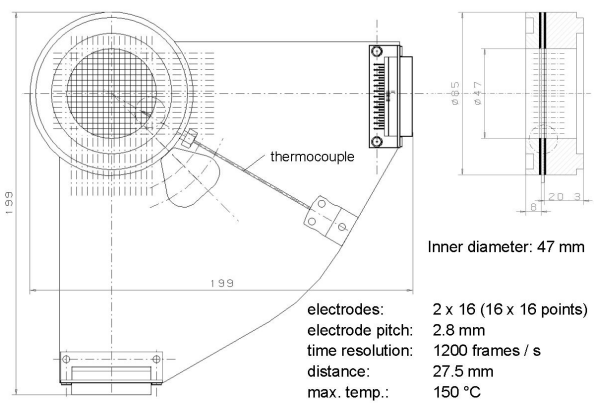

Fig. 2 Scheme of the wire-mesh sensor.

The inner diameter of the two sensors used in the CIRCUS set-up is 47 mm (equal to the inner diameter of the adiabatic section in which it is mounted). Each sensor consists of two electrode grids that are positioned perpendicularly to each other (see Fig. 2) in order to form a matrix of 16x16 crossing points. The distance between two successive parallel wires is 2.8 mm, this being the spatial resolution of the sensor. The sampling frequency of such a device can be set up to 10 kHz. A sampling frequency of 1200 Hz has been used in the present study.

3.1. Treatment of the measured signal

It has been previously mentioned that the wire-mesh sensor delivers a matrix of 16x16 instantaneous local conductivity measurements at each wires crossing point. Defining a rectangular coordinate system having its origin in the centre of the sensor, the temporal- and spatial- coordinates are expressed as:

$$t = i \cdot \Delta t = \frac{i}{f_m};\ x = j \cdot \Delta x;\ y = k \cdot \Delta y\,,$$

with the spatial pitches $\Delta x = \Delta y = 2.8$ mm and the sampling frequency $f_m = 1200$ Hz.
Assuming a linear dependency between local instantaneous conductivity and void fraction (this assumption has been proven to be satisfactory in previous works [23, 24]), the local fluid conductivity $u_{i,j,k}$ measured at the time instant $i\Delta t$ at the crossing point identified by the indexes j and k can be converted into void fraction $\varepsilon_{i,j,k}$ according to:

$$\varepsilon_{i,j,k} = \frac{u_{i,j,k} - u_{G_{j,k}}}{u_{L_{j,k}} - u_{G_{j,k}}} \qquad (1)$$

where $u_{Gj,k}$ and $u_{Lj,k}$ are the fluid conductivity that would be measured if the area around the crossing point *(j, k)* would be completely filled with gas or liquid respectively. These data are retrieved during a calibration procedure in which measurements are performed in conditions of “tube completely filled with liquid” and “tube completely filled with gas”. The data are stored for each of the 16x16 crossing points of the sensor.
A special correction is needed if the temperature of the fluid is expected to vary during the experiments. In this case a decrease of the liquid temperature, for example, will cause a decrease of the liquid conductivity u_L that would be interpreted as an increase of void fraction, if the relation (1) is adopted. To take into account temperature variations, the liquid conductivity is measured

by the wire-mesh sensor at different liquid temperatures and a linear regression is derived [25] for each crossing point *(j, k)*. The fluid temperature is measured by means of a thermocouple positioned at the location of the wire-mesh sensor (see Fig. 2). The temperature correction results in the following relation:

$$\varepsilon_{i,j,k} = \frac{u_{i,j,k} - u_{G_{j,k}}}{u^0_{L_{j,k}} - u_{G_{j,k}}} \frac{aT_0 + b}{aT + b} \qquad (2)$$

where $u^o_{Lj,k}$ is the liquid conductivity measured at the reference temperature T_0 and a and b are the coefficient of the linear regression.

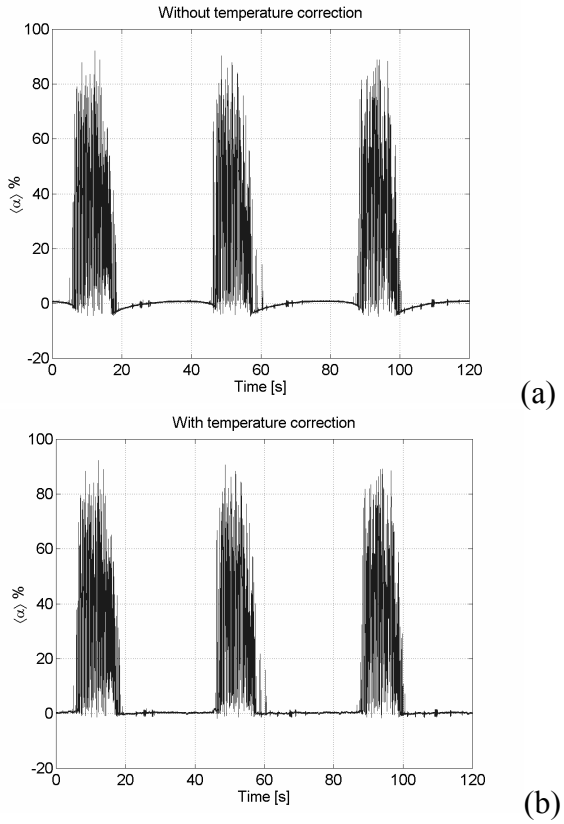

Fig. 3 Effect of temperature correction on void-fraction measurements.

As an example, in Fig. 3 the cross-section-averaged void fraction measured by the wire-mesh during a flashing-induced flow oscillation is shown. If the temperature variation is not taken into account (i.e. a constant liquid conductivity is assumed for the conversion from fluid conductivity to void fraction) the void fraction exhibits also negative values during a flashing cycle, while it shows positive values between two successive flashing cycles even though only liquid is present in the riser. This is due to the fact that the liquid temperature varies in time and exhibits a local maximum during a flashing cycle and a local minimum between two successive cycles. Since the liquid conductivity decreases with decreasing temperature, a decrease (increase) of temperature is erroneously interpreted as an increase (decrease) of void fraction. The effect vanishes when the described temperature calibration is applied (see Fig. 3.b).

Note that for the evaluation of the cross-section-averaged void fraction a weighting factor is needed to take into account whether the measurement area associated to a given crossing point *(j, k)* contributes completely (central meshes) or only partially (meshes at the periphery) to the pipe cross-section [23].

4. BUBBLE RECONSTRUCTION ALGORITHM

The algorithm used to identify bubbles starting from the wire-mesh signal has been developed by Prasser et al. [26]. Starting point of the algorithm is the three-dimensional matrix of local void-fractions ε_{ijk} measured by the wire-mesh sensor.

A bubble-object is defined as a region of connected elements *(i, j, k)* containing gas phase surrounded by elements containing liquid phase. Each element *(i, j, k)* belonging to the same bubble-object is assigned with a common number (so-called bubble identifier n_B) that is unique for each bubble.

However, due to the finite size of the measuring volume, a sharp distinction between elements filled with gas or liquid phase cannot be obtained. As a matter of fact, the local void fraction ε_{ijk} can take all values between zero (liquid) and unity (steam), since it can happen that steam only partially covers the measurement area defined by two crossing wires. Moreover a certain level of noise has also to be taken into account. Consequently, a threshold ε_{MIN} has to be used to distinguish between gas- and liquid-containing elements [26]. Without such a threshold, bubbles very close to each other might be erroneously unified. On the other hand, a high threshold may lead to the division of a bubble into unrealistic fragments.

The algorithm for the bubble identification

first searches for local void-fraction maxima ε_{MAX}. Then, for each of these maxima a recursive subroutine (*FILL* subroutine) is started to assign to all neighbouring elements *(i, j, k)* belonging to the same bubble the same bubble identifier n_B (the flow chart of the subroutine is shown in Fig. 4). When the *FILL* procedure for the bubble n_B is terminated, the bubble identifier n_B is increased to the next integer value and the procedure is repeated until no new start-element can be found in the data array. Result of the algorithm is a three-dimensional array of elements b_{ijk} having the same dimensions as the void-fraction array and containing the identifier of the bubble to which the element *(i, j, k)* belongs. Before starting the *FILL* procedure, all the elements b_{ijk} are set to zero. In the case in which a given element *(i, j, k)* is occupied by liquid, the corresponding array element b_{ijk} is not assigned to any bubble, so that its value remains equal to zero. For local void-fraction below the threshold ε_{MIN} the FILL subroutine is not executed. Prasser et al. [26] have shown that an optimum is achieved when a differential threshold $\Delta\varepsilon_{LEVEL}$ is used to terminate the FILL procedure. In this case, the threshold ε_{MIN} is set equal to ε_{MAX} - $\Delta\varepsilon_{LEVEL}$.

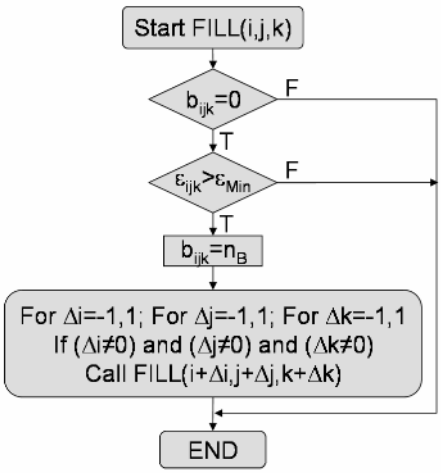

Fig. 4 Flow chart of the *FILL* subroutine for bubble identification

The elements that surround bubbles and have not been assigned yet by the FILL subroutine (because their void-fraction is lower than the threshold ε_{MIN}) are treated by means of an agglomeration algorithm that associates these elements to the bubbles that have already been identified. This subroutine does not create new bubble identifiers n_B. In the present work, a minimum value of 50 % was chosen for the local void-fraction maxima ε_{MAX} that define a bubble element and the differential threshold $\Delta\varepsilon_{LEVEL}$ was set equal to 20 %.

An example of the result of the bubble reconstruction algorithm is shown in Fig. 5. The two columns are derived from the lower and upper wire-mesh sensors respectively and represent virtual side cross-section views obtained by stacking one on top of each other the signals measured by each wire-mesh sensor along one pipe diameter at different time instants. Different colours are associated to different bubbles as identified by the bubble identification algorithm.

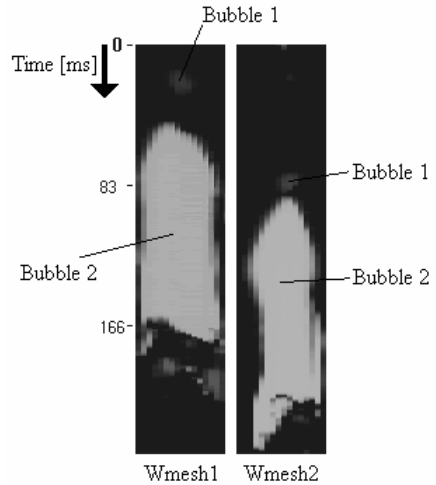

Fig. 5 Virtual sectional side views extracted from wire-mesh sensors data.

It is clear that for a complete three-dimensional reconstruction of the bubbles, the bubble velocity is needed. In first approximation, it can be assumed that all the elements *(i,j,k)* belonging to a given bubble move with the same velocity. For stationary flow it is generally assumed that the bubble velocity equals the gas superficial velocity divided by the cross-sectional-averaged void fraction. Unfortunately, the steam superficial velocity is not known a priori for steam-water flows because of the mass transfer between liquid and vapour phase (the mass transfer between phases is of particular importance in flashing flows). To overcome this problem, the steam velocity can be assessed by means of cross-correlation techniques based on local

[27-30] or cross-sectional-averaged [31-33] void-fraction signals. The latter method is used in this study.

Once the steam velocity w_G is known, the volume of a bubble can then be calculates as:

$$V_B = w_G \Delta x \Delta y \Delta t \sum_{i,j,k \in B} \varepsilon_{i,j,k} \quad (3)$$

and the bubble equivalent diameter as:

$$D_{eq,B} = 3\frac{\sqrt{6}}{\pi} V_B \quad (4)$$

5. THREE_DIMENSIONAL FLOW PATTERN VISUALIZATION

As mentioned in paragraph 4, once the bubble velocity is known it is possible to transform the time coordinate in the spatial coordinate perpendicular to the measurements plane.

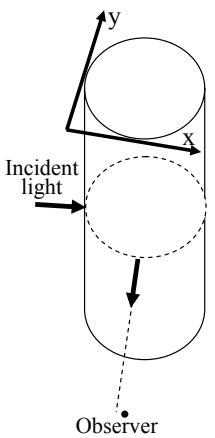

Fig. 6 Scheme for the 3D flow visualization.

To visualize the three-dimensional array of instantaneous local void-fractions delivered by the wire-mesh sensors a simplified ray-tracing algorithm is used [34].

Let's suppose that white light arrives from one side of the pipe in direction parallel to the x-axis, as schematically indicated in Fig. 6, and that the observation is performed from the direction parallel to the y-axis. Indicating with Φ_x the vector of light intensity, the boundary conditions at the pipe wall $x = 0$ ($j = - n_{el}/2$ in the discrete coordinate system, where n_{el} specifies the number of wire-mesh electrodes) can be written as:

$$\vec{\Phi}_{x_{j=0,k}} = \vec{\Phi}_{white} = \left(\varphi_{red_{white}}, \varphi_{green_{white}}, \varphi_{blue_{white}}\right) \quad (5)$$

On each point of the measurement domain, the light intensity vector Φ_x will have three components quantifying the red, green and blue content of the incident light. These components will be partially absorbed when the light beam will propagate through the steam and liquid present in the column characterized by the matrix of void-fractions $\varepsilon_{i,j,k}$. To evaluate the light intensity in each point of the measurement plane, it is first necessary to define vectors of absorption coefficients Λ_G and Λ_L for the steam and the liquid phase respectively. These vectors represent the absorption coefficients for the three light components of red, green and blue. For a given time instant, at each point *(j, k)* of the measuring plane the light intensity becomes:

$$\vec{\Phi}_{x_{j,k}} = \vec{\Phi}_{x_{j-1,k}} \cdot \left[1 - \vec{\Lambda}_G \cdot \varepsilon_{j,k} - \vec{\Lambda}_L \cdot \left(1 - \varepsilon_{j,k}\right)\right] \quad \text{for } j \geq -\tfrac{n_{el}}{2} \text{ and } j \leq \tfrac{n_{el}}{2} \quad (6)$$

where $n_{el}/2$ specifies the outer boundary of the measurements domain. Finally, to reconstruct the image, the intensity of the light that is scattered toward the observer (see Fig. 6) in the direction of the y-axis has to be calculated. For this aim, scattering coefficients Ω_G and Ω_L of steam and liquid respectively for the three light components have to be defined. The intensity of light that is scattered toward the observed (i.e. in the y-direction) at each point *(j, k)* is expressed by:

$$\vec{Q}_{j,k} = \vec{\Phi}_{x_{j,k}} \cdot \left[\vec{\Omega}_G \cdot \varepsilon_{j,k} - \vec{\Omega}_L \cdot \left(1 - \varepsilon_{j,k}\right)\right] \quad (7)$$

This light will be partially absorbed while passing through the two-phase mixture in the y-direction.

The light intensity Φ_y that travels in the y-direction will thus be a combination of source terms and absorption:

$$\vec{\Phi}_{y_{j,k}} = \vec{\Phi}_{y_{j,k-1}} \cdot \left[1 - \vec{\Lambda}_G \cdot \varepsilon_{j,k} - \vec{\Lambda}_L \cdot \left(1 - \varepsilon_{j,k}\right)\right] + \vec{Q}_{j,k} \quad \textit{for } k \geq -\tfrac{n_{el}}{2} \textit{ and } k \leq \tfrac{n_{el}}{2} \quad (8)$$

with "black" as initial value:

$$\vec{\Phi}_{y_{j,k=0}} = \vec{\Phi}_{black} = \left(\varphi_{red_{black}}, \varphi_{green_{black}}, \varphi_{blue_{black}}\right) \quad (9)$$

The value of Φ_y found for $k = n_{el}/2$ represents the light intensity that reaches the observer. The above described procedure is repeated for successive time frames *i*. The three dimensional flow visualization is obtained by plotting one below each other in the vertical direction the vector $\Phi_{y,j,k}$ calculated for $k =$

$n_{el}/2$ at each time instant $i\Delta t$. The vertical axis of the image is scaled by means of the steam velocity. A time-dependent steam velocity can be considered as well.

A clear advantage of the described method is a more realistic picture of the three-dimensional flow pattern that contains information of the entire three-dimensional void-fraction distribution. Such information would be lost if only a virtual sectional side view (as the one shown in Fig. 5) along the axis of the pipe is shown.

6. CHARACTHERISTICS OF "STATIONARY" FLASHING FLOW

A series of experiments was performed at atmospheric pressure in condition of forced circulation [35]. The use of forced circulation was necessary to ensure a constant flow rate at the inlet of the test section for a wide operational range. This in view of the fact that, as mentioned in the introduction, a natural-circulation two-phase system may exhibit flow oscillations when operated at low pressures.

Data from the wire-mesh sensors were recorded for 200 s. From the series, two sets of measurements are selected at constant superficial liquid velocity and increasing superficial vapour velocity to be discussed here. The main variables are reported in Table 2. The last column in the table indicates the distance in length over pipe-diameter between the measurement points (where the lowest wire-mesh sensors is located) and the lowest axial location at which flashing occurs (flashing front). Below the flashing front, flashing does not propagate in the liquid bulk. The temperature at the inlet of the heated section T_{inl}, the power and the superficial liquid velocity J_L are the controlling parameters during the experiments. The superficial steam velocity J_G is determined a posteriori as the product of the steam bubble velocity obtained by means of cross-correlation techniques and the cross-section-averaged void fraction measured by means of the lower wire-mesh sensor.

The flow patterns visualization obtained with technique described in paragraph 4 is shown in Fig. 7 for the two sets of measurements. The picture is scaled such that the length of the column is twenty times the pipe diameter (20 *47 = 940 mm). The flow pattern transits from bubbly to slug flow when the superficial vapour velocity increases. The corresponding distributions of bubble length and equivalent diameter are presented in Fig. 8 and Fig. 9 respectively. The equivalent diameter is calculated according to eq. (4). To evaluate the bubble length, first the time instants $t_{B,front}$ and $t_{B,back}$ at which the front and the back of the bubble touch the wire-mesh sensor are determined. The bubble length is then calculated as the product of the steam velocity and the time interval ($t_{B,back}$ - $t_{B,front}$). The distributions represent the part of the void fraction that is carried by bubbles of a given length or equivalent diameter. In this way, the area under the distribution gives the cross-section-averaged void fraction $<\varepsilon>$. The class width for calculating these histograms was 0.5 mm for bubbles length/equivalent-diameter lower than 10 mm. For larger bubbles the class width was increased exponentially. This was necessary to achieve smooth distributions because large bubbles are rare but carry a large quantity of void.

Table 2 Measurements in forced circulation conditions

	T_{inl} [°C]	Power [kW]	J_L [m/s]	J_G [m/s]	L/D Flashing front
SET 1					
A1	92	8.80	0.11	0.005	0.5
B1	92	9.12	0.11	0.030	4
C1	92	9.84	0.11	0.240	15
D1	92	10.4	0.11	0.590	32
E1	92	10.9	0.11	0.830	54
SET 2					
A2	96.2	7.20	0.14	0.018	1
B2	96.6	7.60	0.14	0.627	17
C2	96.4	7.88	0.14	0.775	28
D2	96.4	8.20	0.14	0.902	34
E2	96.6	8.64	0.14	1.100	52
F2	96.8	8.96	0.14	1.270	54

In Fig. 8 the flow pattern is indicated for each case according to the Mishima-Ishii flow map [36]. Confronting the predicted flow pattern with the visualization presented in Fig. 7 good agreement is found. This finding is quite remarkable since the Mishima-Ishii flow map has not been developed for flashing flow and

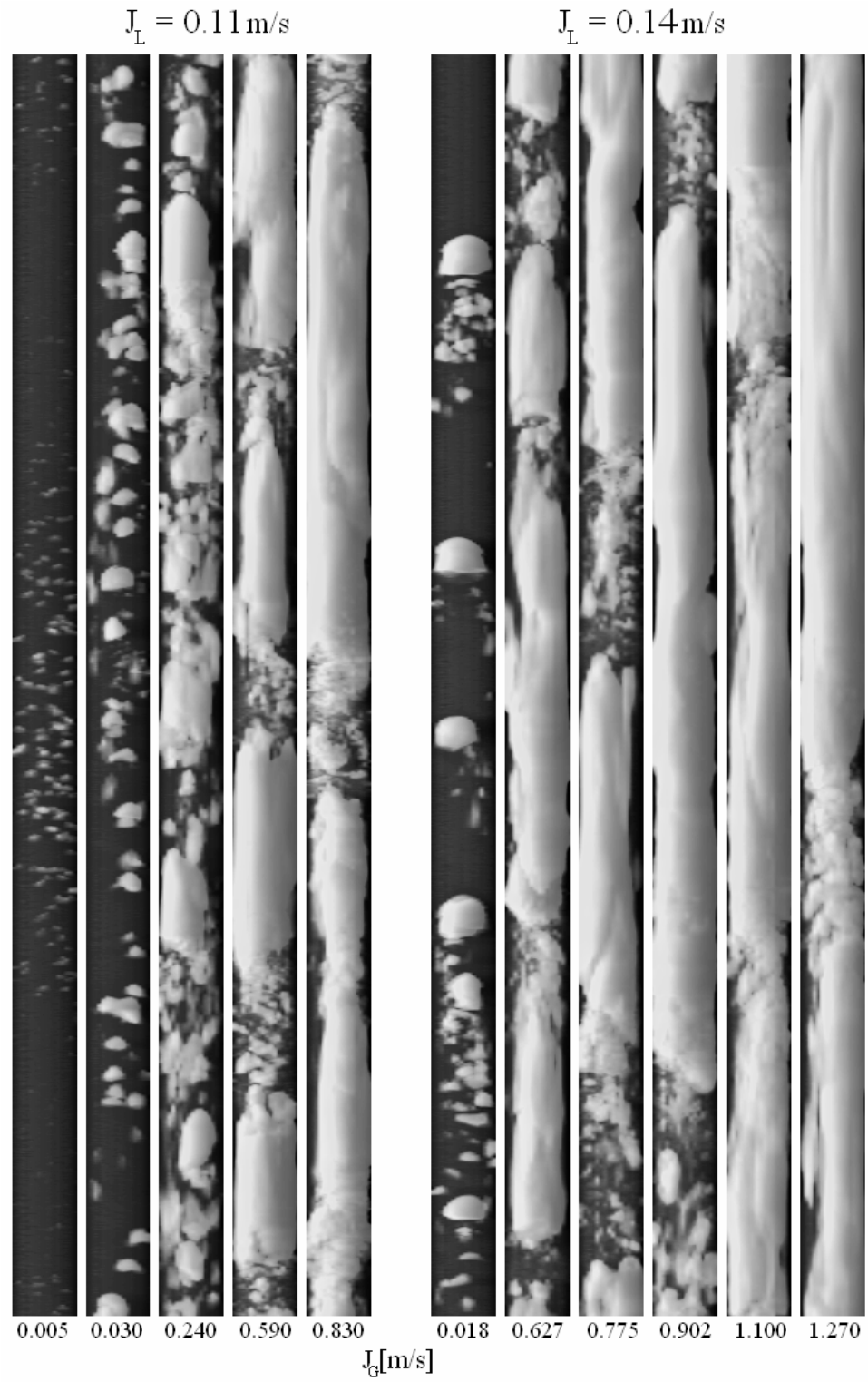

Fig. 7 Series of flow-pattern visualizations at constant liquid superficial velocity and increasing steam superficial velocity. The columns have a length of 20 times the pipe diameter, the latter being 47 mm.

in particular for flows in which void production takes place along the test section. In this specific case it is not possible to define a development length as for the air-water experiments where a constant air flow is injected in the test section or as for the steam-water experiments in which steam is produced by heaters below an adiabatic test section and no further production of steam takes place in the test section itself. Analyzing Fig. 8 and Fig. 9 it can be seen that the transition from bubbly to slug flow is characterized by the well known transition from unimodal to bimodal bubbles size distribution.

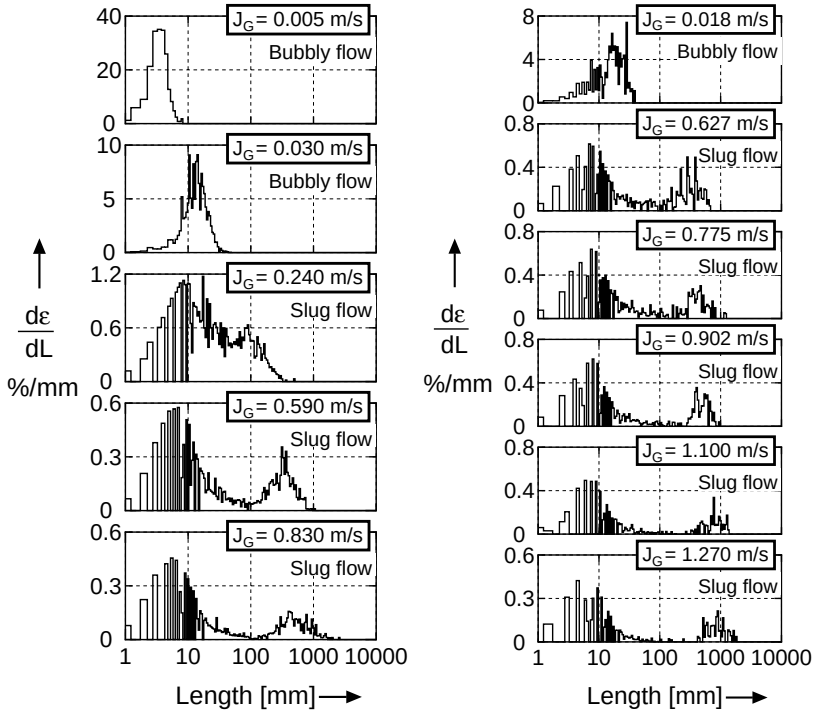

Fig. 8 Bubble length distributions for increasing gas superficial velocity J_G and constant liquid superficial velocity J_L equal to 0.11 m/s (left) and 0.14 m/s (right). The flow pattern according to the Mishima-Ishii flow map is reported for each case.

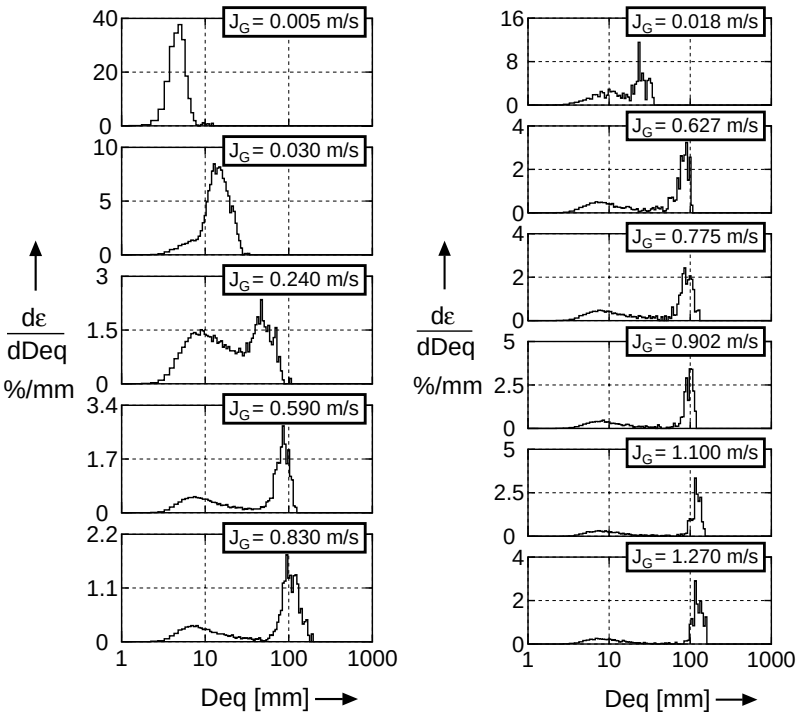

Fig. 9 Bubble equivalent diameter distributions for increasing gas superficial velocity J_G and constant liquid superficial velocity J_L equal to 0.11 m/s (left) and 0.14 m/s (right).

The unimodal distribution exhibits a tail toward lower bubbles sizes when cup bubbles are present in the flow. An increase of superficial steam velocity gives rise to longer Taylor bubbles, while an increase of the superficial liquid velocity yields shorter Taylor bubbles.

6.1. Void fraction profiles and decomposition according to bubble size classes

Tomiyama and co-workers [37, 38] stated that for a bubble radius corresponding to a critical

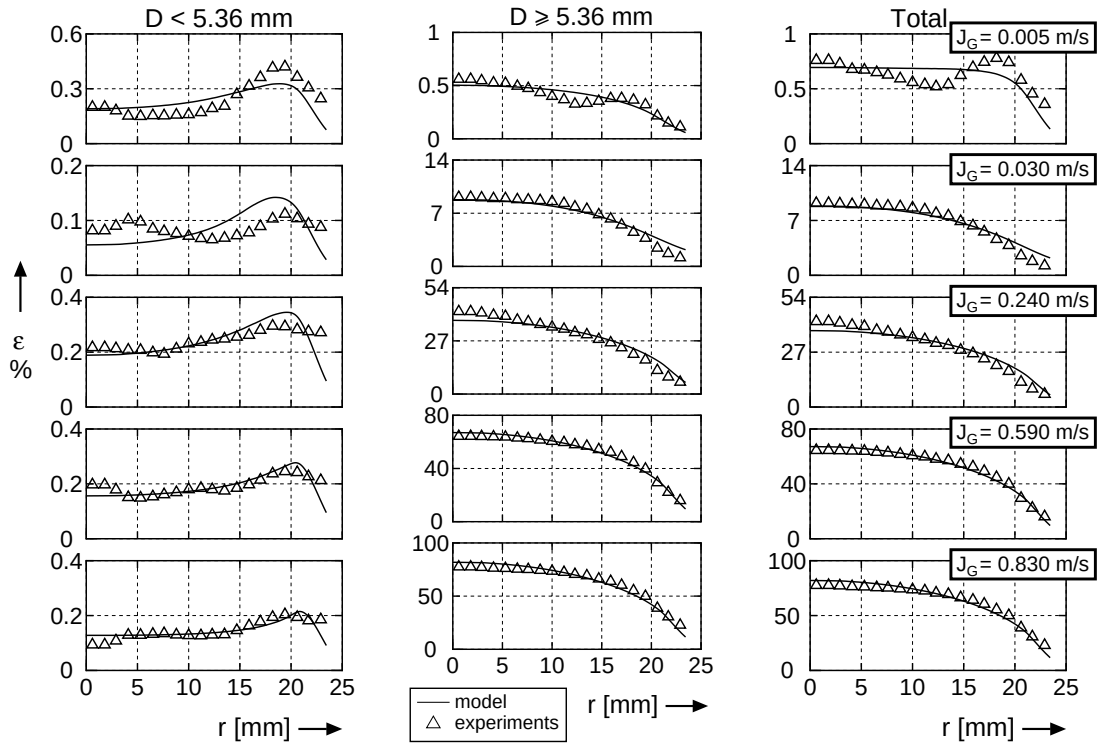

Fig. 10 Decomposition of void-fraction radial profile in two bubble size classes (J_L = 0.11 m/s). Experimental results and model predictions.

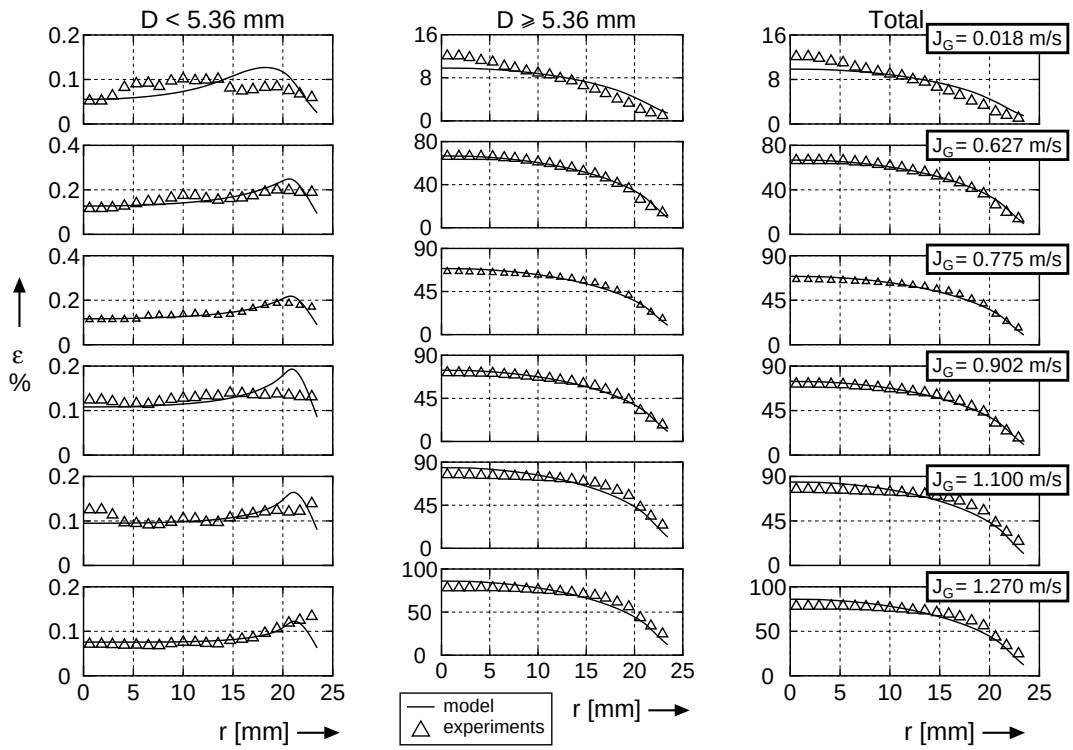

Fig. 11 Decomposition of void-fraction radial profile in two bubble size classes (J_L = 0.14 m/s). Experimental results and model predictions.

modified Eötvös number given by:

$$Eo_{\mathrm{mod}} = \frac{g\left(\rho_L - \rho_G\right)}{\sigma} d_{xy}^2 \qquad (10)$$

an inversion of the direction of the lift force occurs, which pulls the bigger bubbles towards the centre of the pipe. In the formula above d_{xy} represents the maximum bubble-diameter in the cross section. In case of steam/water mixture at atmospheric pressure the critical equivalent bubble diameter (evaluated from the bubble volume assuming

spherical shape) is about 5.36 mm. A method to check this finding in the case of flashing flows consists in decomposing the void-fraction radial profile in a series of partial void-fraction profiles associated to given bubble size classes. In this way it is possible to see where bubbles of a given size tend to accumulate.

Time-averaged void-fraction profiles can be obtained easily by averaging the local instantaneous void fractions ε_{ijk} over a given period (200 s in the present study). It has been pointed out that the bubble identification algorithm described in paragraph 4 allows to identify the set of elements (i,j,k) belonging to a given bubble (via the matrix of elements b_{ijk}). This information can be used to decompose the void-fraction profile in partial void-fraction profiles [39].

Two bubble size classes are used for the decomposition and the critical equivalent diameter of 5.36 mm is used as threshold between the two classes.

The results of the decomposition are shown in Fig. 10 and Fig. 11 for the two sets of stationary experiments. In agreement with the findings of Tomiyama et al. [37, 38] small bubbles are located preferentially close to the pipe wall, while bigger bubbles tend to be located toward the centre of the pipe.

To check whether the bubble radial distribution is in equilibrium with the forces acting on the bubbles, a model developed by Lucas et al. [40] has been applied. The model is based on a radial balance of the forces acting on the bubbles. The radial balance is solved separately for several bubble classes and the feedback between void fraction profile and velocity profile is taken into account as well. The forces considered in the models are:

1. Lift force: this force occurs if a particle is subjected to a shear flow. According to Zun [41] the lift force related to the unit volume can be calculated as :

$$\vec{F}_{lift} = -C_{lift}\rho_L(\vec{w}_G - \vec{w}_L)\times rot(\vec{w}_L) \qquad (11)$$

   For a spherical bubble in an upwards pipe flow the coefficient C_{lift} is positive and the force acts toward the pipe wall. Tomiyama et al. [37] found the force acting towards the pipe centre for large, non spherical bubbles. Based on experimental data they developed a correlation for the coefficient of the lift force C_{lift}, which depends on the modified Eötvös number (see eq. 10). It changes sign at the previously mentioned critical modified Eötvös number. The correlation is used in the model.
2. Lubrification force: it was introduced by Antal et al. [42] and is responsible for driving the bubbles away from the pipe wall. A modified expression for this force by Tomiyama et al. [37] is implemented in the model.
3. Turbulence dispersion force: it takes into account the smoothing of the void-fraction profiles caused by turbulence [43].
4. Eötvös number dependent dispersion force: this force has been introduced by Lucas et al. [40] to take into account that the fluctuating motions of large bubbles (Eo>1) caused by bubbles deformation produce an additional smoothing of the void-fraction profiles.

An equilibrium of the forces is assumed. The radial profile of the liquid velocity, which is required for the calculation of the lift force, is obtained using the model from Sato et al. [44]. They consider the inherent wall turbulence as well as the turbulence caused by the bubbles. This sub-model needs the radial void fraction profile as an input. For this reason, the radial profile of the liquid velocity and the radial profile of the gas fraction are calculated iteratively. There is a strong feedback between the two profiles.

The model allows the prediction of radial bubble distributions in a vertical two-phase flow once bubble size distributions are provided. The experimental bubble size distributions shown in Fig. 9 are given as input to the model and calculations are performed using 50 bubble classes and 100 radial nodes. To compare the results with the experimental data, the 50 bubble classes are reduced to two bubbles classes separated by the threshold defined by the equivalent critical diameter of 5.36 mm. For the reduction, it is sufficient to sum all the partial profiles of the bubble classes that have to be condensed together.

The model, successfully applied to air-water flows, is used here for the first time to study steam/water flow and no tuning of the original

model in ref. [40] has been performed to match the experimental results presented in this work.

The comparison with the experimental void-fraction profiles is shown in Fig. 10 and Fig. 11. Fair agreement is found for the two bubble classes considered (with diameter respectively smaller and larger than the critical diameter in correspondence of which Tomiyama et al. predict an inversion of the direction of the lift force [37]). This finding suggests that the equilibrium of forces acting on the bubbles is established fast enough in radial direction (perpendicularly to the flow), so that the equilibrium model is in good agreement with the measured results even for a flow not fully developed in axial direction (strictly speaking it is not possible to define a development length for flashing flow because bubbles are created along the entire length of the adiabatic section above the flashing front).

At low superficial steam velocity, close to the wall, a slight over-estimation of the void-fraction profile is found for large bubbles. This may be caused by a too large dispersion force. For the small bubbles the general trend is predicted reasonably well, though there are some deviations on the absolute values of the void fractions. Such deviations are in any case very small.

7. CHARACTERISTICS OF TRANSIENT FLASHING FLOWS DURING FLASHING-INDUCED FLOW OSCILLATION IN NATURAL CIRCULATION CONDITIONS

Under specific conditions of power and inlet subcooling, flashing-induced flow-oscillations can be observed [8]. Flashing taking place in the adiabatic section of the loop leads to an unbalance between the driving force and the pressure drops in the loop, giving rise to a flow-rate increase. This will cause a decrease of the temperature at the outlet of the heated section. Thus, colder water will enter the adiabatic section suppressing flashing. When flashing stops the driving force becomes small, yielding a low flow rate. This in turn will give a subsequent increase of the fluid temperature at the inlet of the adiabatic section. Eventually, a new flashing cycle will start. In this way so-called flashing-induced flow oscillations originate.

The evolution of the flow pattern and of the bubble size distribution during a typical flashing-induced flow oscillation is discussed in the next paragraphs. For this scope, the flow pattern visualization described in paragraph 5 is for the first time applied to time-dependent velocity. The first problem to be solved is to derive a time-dependent steam bubbles velocity. No literature has been found with regards to this problem (the studies published in the field mainly refer to stationary two-phase flows).

7.1. Bubble velocity measurement and 3D reconstruction in transient conditions

To evaluate the bubble velocity, being the superficial steam velocity unknown, the following methods can be applied:

a) by cross-correlating the cross-sectional-averaged void fractions measured by the two wire-mesh sensors;

b) by using a drift-flux model. The GE-Ramp model [45] is selected. This has been proven to give the best results in case of flashing flow [35];

c) by identifying the time delay that it takes for each bubble to touch the two sensors;

d) by “manually” identifying the time delay that it takes for each bubble to touch the two sensors.

The application of cross-correlation techniques and of drift-flux models is straightforward, but both methods lead to an approximated result since it is necessary to assume that all bubbles present in a given time interval have the same velocities.

The direct identification of time delays would give the possibility of associating to each bubble its “true” velocity, identified as the velocity of the bubble front. In the case presented in Fig. 5, for example, it is clear that the velocities of the two bubbles represented significantly differ from each other. Unfortunately, if this method is performed via a computer algorithm, extreme care has to be taken for the choice of the selection conditions used to find the same bubble in the data arrays measured by the two wire-mesh sensors. This task becomes particularly difficult in presence of high bubble density and bubble coalescence, break-up and expansion.

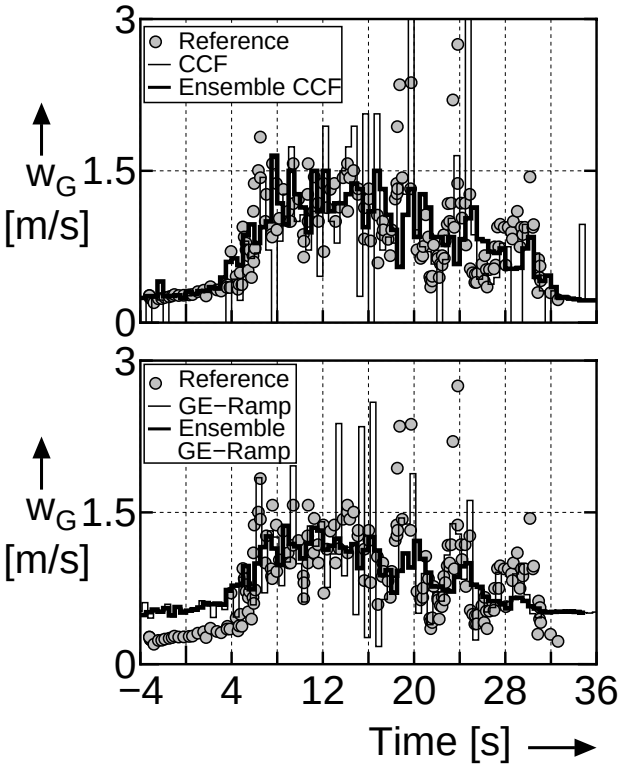

Fig. 12 Comparison between steam velocity estimations

The last method (d) is taken as reference for the assessment of the soundness of the other methods since judged to be the most reliable. A visualization program has been developed to allow the user to manually select and associate bubbles passing through the two wire-mesh sensors. Once the same bubble is identified in the three-dimensional data arrays delivered by the two wire-mesh sensors, the velocity of the bubble is evaluated on the basis of the time instants at which the bubble front touches successively the two sensors.

Method (a): to apply the cross-correlation method, the cross-correlation function (CCF) has to be calculated over a limited time window if the temporal variations of the steam velocity have to be derived. It is recommendable that the steam velocity is evaluated with a time step not larger than 0.5 – 1 s. The same limitation holds for the time window over which the cross-correlation is performed. Unfortunately, a small time window goes at the expenses of the accuracy of the CCF. To overcome this problem and reduce the uncertainty on the estimation of the steam velocity a second method based on ensemble-averaged CCF is applied. First, a longer measurement is performed (600s) in comparison with the stationary measurements in order to record a significant number of flashing cycles. Then individual flashing cycles are discriminated on the basis of the signal of the lower wire-mesh sensor. The beginning of a flashing cycle is determined as the time instant at which the wire-mesh sensor measures a cross-section-averaged void fraction of at least 10 %. The instantaneous cross-section-averaged void fractions measured by the two wire-mesh sensors are cross-correlated with a time step of 0.5 s. Ensemble averaging is performed over all flashing cycles in order to guarantee sufficient statistical accuracy. The steam velocity is calculated on the basis of the ensemble-averaged cross-correlation with a time step of 0.5 s. Ensemble averaging is also done for the liquid velocity and for the void fraction, in order to obtain a representative time-dependent flashing cycle. Details on the ensemble averaging technique are given in ref. [35].

Method (b): the Ge-ramp drift-flux model allows to calculate the steam velocity on the basis of the cross-section-averaged void fraction. As for the cross-correlation technique, it can be chosen to derive a time-dependent steam velocity for the first flashing cycle (for which the reference measurement "d" holds) or for the ensemble-averaged flashing cycle. In the latter case the ensemble-averaged void fraction has to be filled in the drift-flux model.

The comparison between the steam velocity estimations is presented in Fig. 12. The upper figure shows the performance of the cross-correlation technique applied to the first flashing cycle (CCF) and of the ensemble-averaged cross-correlation technique (ensemble CCF). The general trend of the time-dependent steam velocity is caught fairly well by both methods. As expected, the first method catches better the velocity fluctuations, while the second method delivers a smoother velocity distribution. In the lower graph the performance of the selected drift-flux model is shown.

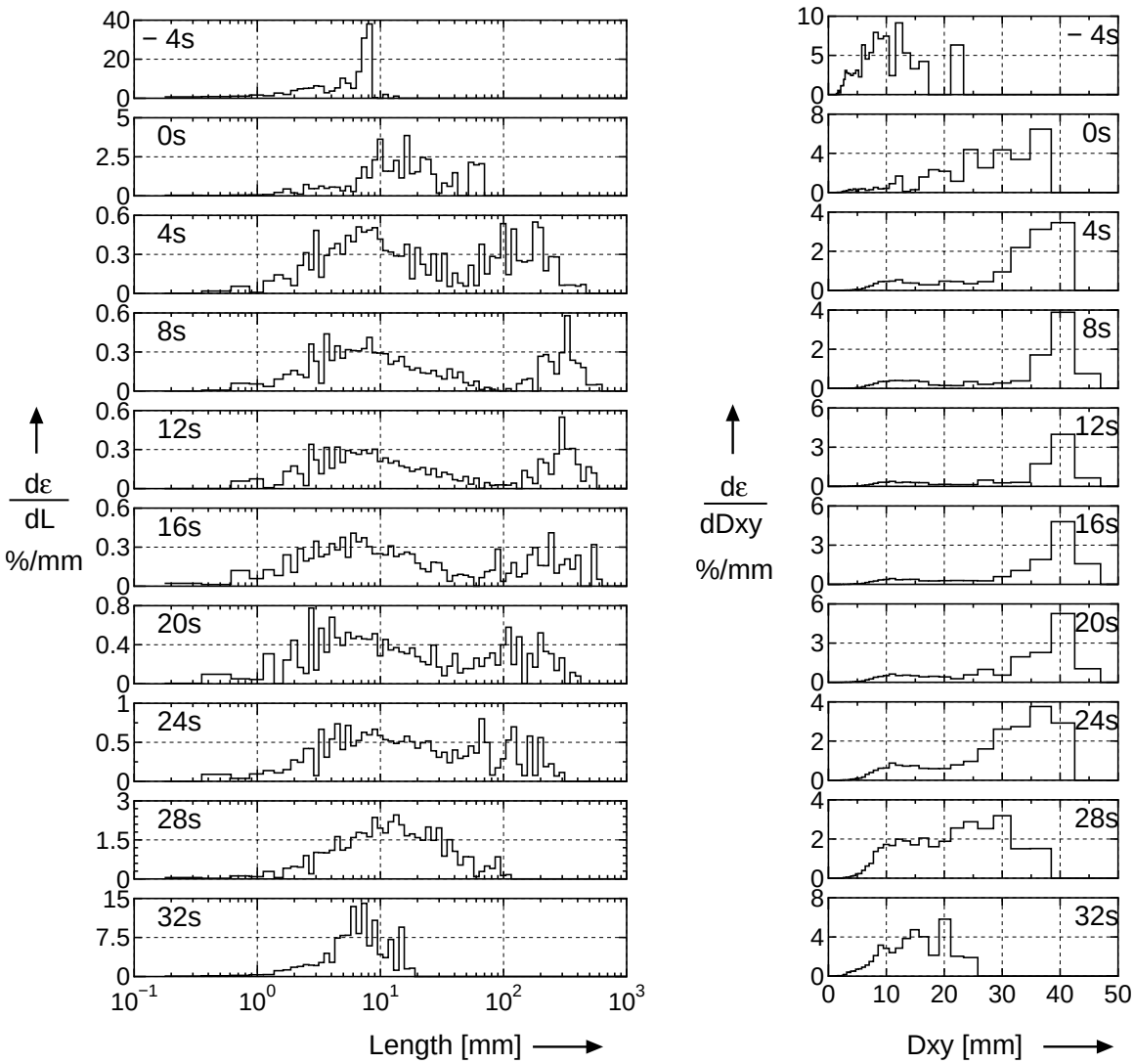

Fig. 13 Temporal evolution of bubbles length and diameter during a flashing-induced flow oscillation.

The curve "Ge-ramp" has been obtained on the basis of the time-dependent cross-section-averaged void-fraction measured during the first flashing cycle, while the curve "ensemble Ge-ramp" has been obtained on the basis of the ensemble-averaged void fraction over all the measured flashing cycles. The predictions of the drift-flux model are quite satisfactory. The bubble velocity is over-estimated at the beginning and at the end of the flashing cycle, when only small bubbles are present in the flow.

7.2. Temporal evolution of bubble size distribution and flow visualization during a flashing cycle

For the study of the temporal evolution of bubble size distributions and for the flow visualization, the steam velocity derived by the ensemble-averaged cross-correlation technique is used. The transient working point for the ensemble-averaged flashing cycle of the case considered is reported in Fig. 14 in the J_L-J_G phase space. The time increases from points A (0.25 s in the time axis of Fig. 12) to B (32.25 s). The flow maps according to Taitel et al. [46] and Mishima-Ishii [47] are reported as well in the figure. As it can be seen, during a flashing cycle the flow pattern transits from bubbly-flow to slug/churn flow (between 4.25 and 4.75 s) and ends as bubbly flow again (between 29.75 and 30.25 s). This can be also seen by visual inspection of the test section and by bubbles reconstruction and flow pattern visualization, as it is demonstrated in Fig. 13 and Fig. 15.

In Fig. 13 the bubble size distributions are shown at different time instants (namely, the bubble length distributions and the bubble diameter D_{xy} distributions are presented. D_{xy}

is defined as the maximum bubble diameter in the pipe cross-section). For each distribution all the bubbles found in a time interval of 4 s are considered. All flashing cycles in the 600 s measurement are taken into account. This is possible thanks to the fact that, with the synchronisation technique described in paragraph 7.1, a common time axis can be defined for all flashing cycles. This common time-axis has been used in Fig. 12 as well.

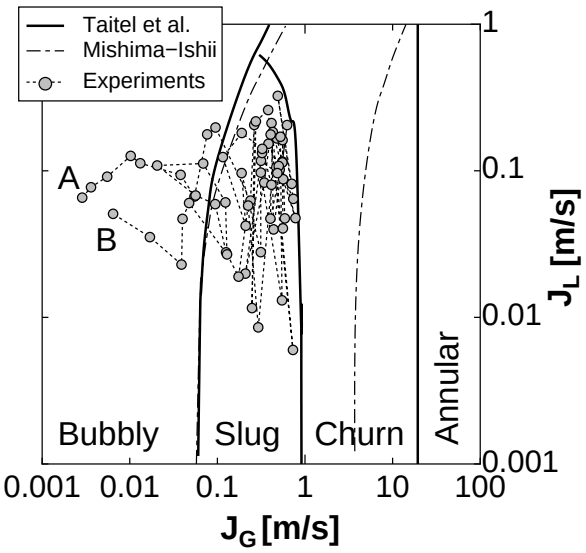

Fig. 14 Localization of transient working point in the JL-JG flow map. The time increases from point A to point B.

As for the stationary case the transition from spherical to cup bubbles is characterized by a unimodal distribution tailed towards lower bubble sizes. During the transition from cup bubbles to slug flow the unimodal distribution becomes symmetric but with a very large spreading in bubbles length. When the transition is completed the bimodal distribution typical of slug flow is found. Initially, the length of the Taylor bubbles gradually increases with time. The production of steam causes an increase of the buoyancy in the loop and consequently an increase of the liquid superficial velocity. Subsequently the length of the Taylor bubbles decreases until bubbly flow is reached again and the bubbles length distribution switches back again to unimodal. Similar conclusions can be drawn looking at the evolution of the maximum bubbles diameter D_{xy} in the cross section (note that this quantity can be measured exactly in the limits of the wire-mesh sensor spatial resolution and it is not biased by errors in the bubbles velocity measurement).

The flow visualization at different time instants for one of the flashing cycles of the considered case is shown in Fig. 15. Two successive columns correspond to the measurements performed by the two wire-mesh sensors respectively. The picture is in scale, the length of the column being twenty times the pipe diameter (20 *47 = 940 mm). The time instants corresponding to the beginning and the end of different columns are indicated for each column separately (again the same time axis as in Fig. 12 and Fig. 13 is used).

Note that if the “correct” bubble velocity is used for each bubble in the flow-pattern visualization, the distance between the bubble fronts of a given bubble as seen from the two wire-mesh sensors should be exactly equal to the distance of 27.5 mm existing between the two sensors (the distance between the two wire-mesh sensors is reported in scale in Fig. 15). Thus, a larger or smaller distance gives an idea of the velocity under-estimation or over-estimation respectively that is caused by the use of an approximate velocity.

As mentioned previously, on the basis of the flow map presented in Fig. 14 and from visual inspection of the test section, the flow pattern transits from bubbly to slug/churn flow and back to bubbly flow in the last instants of the flashing cycle.

The flow patterns agree quite well with the prediction of the Mishima-Ishii flow maps even in transient conditions. It is important to recall that in such conditions, not only the steam is generated along the adiabatic section, but also the flashing front changes location with time. Moreover, it has to be pointed out that also the time instants at which the flow pattern transitions occurs agree quite well with the flow map shown in Fig. 14 (between 4.25-4.75 s for the bubbly to slug flow transition and between 29.75-30.25 s for the slug to bubbly flow transition). This is remarkable in view of the fact that flow maps are meant for stationary developed flows, and also because in Fig. 14 the ensemble-averaged flashing cycle is considered, while the visualization in Fig. 15 obviously shows a single flashing cycle.

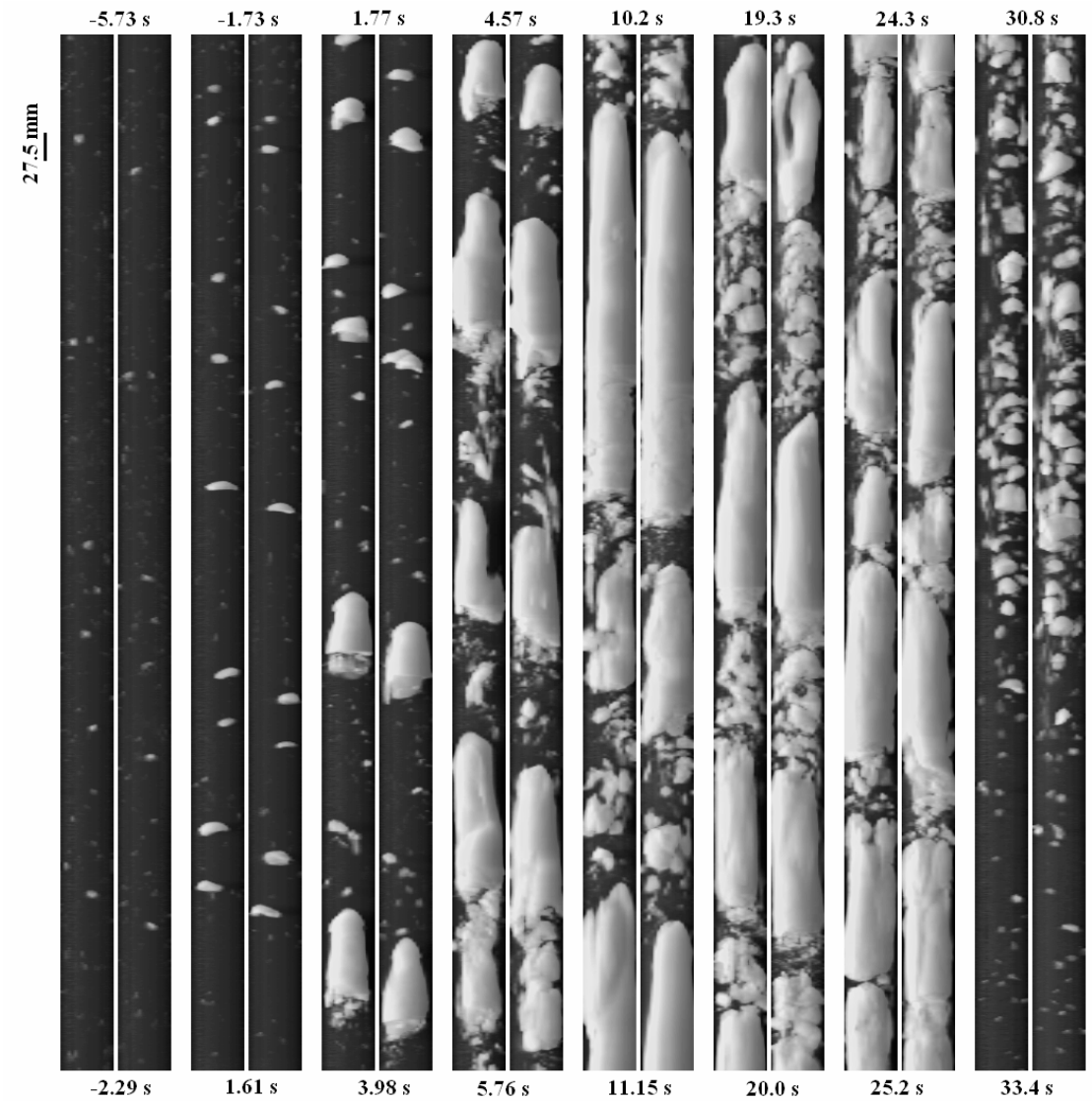

Fig. 15 Flow pattern visualization reconstructed from wire-mesh data. The same time axis as in Fig. 12 is used. Two successive columns correspond to the measurements extracted from the two wire-mesh sensors respectively. The columns have a length of 20 times the pipe diameter, the latter being 47 mm. The time corresponding to the beginning and the end of each column is indicated. The scaled distance between the two wire-mesh sensors (27.5 mm) is reported as well.

CONCLUSIONS

The characteristics of flashing flow in a vertical pipe have been studied for the first time in stationary and transient conditions (during so-called flashing-induced flow oscillations). Advanced instrumentation, namely wire-mesh sensors, has been used for detailed void-fraction and steam velocity measurements. Appropriate treatment of the data delivered by the wire-mesh sensor allows a reconstruction of the three-dimensional flow pattern visualization and helps revealing the structure of the flashing flow. Bubble size distributions have been obtained both in stationary and transient conditions.

The stationary bubbles size distributions have been used as input for a stationary model that calculates radial void-fraction profiles assuming equilibrium between the forces acting on the bubbles. The partial void-fraction profiles calculated for different bubble size classes have been compared with the experimental profiles and fair agreement has been found. This finding suggests that equilibrium in the radial direction (i.e. perpendicularly to the flow direction) is reached fast enough, so that good agreement is found between experimental radial bubbles distributions and the equilibrium model.

For the transient flashing flow different methods have been proposed to evaluate the time-dependent steam velocity. These

methods are based on cross-correlation techniques and on the use of drift-flux models. Methods based on ensemble-averaging techniques considering several flashing cycles have been applied. Reasonable agreement is found when comparing the proposed methods to the actual bubble velocities.

NOMENCLATURE

D	diameter	m
Eo	Eötvös number	-
J	superficial velocity	m s^{-1}
L	length	m
r	radial coordinate	m
t	time	s
T	temperature	^{o}C
V	volume	m^3
w	velocity	m s^{-1}
Greek symbols		
ε	void fraction	-
Subscripts		
G	vapour	
inl	inlet	
L	liquid	

ACKNOWLEDGMENT

This work has been partially sponsored within the EU Framework Program, NACUSP project, FIKS-CT2000-00041.

REFERENCES

1. F. INADA, M. FURUYA, A. YASUO, "Thermo-hydraulic Instability of Boiling Natural Circulation Loop Induced by Flashing (Analytical Consideration)," *Nucl. Eng. Des.,* **200**, 187, (2000).
2. D.D.B. VAN BRAGT, W.J.M. DE KRUIJF, A. MANERA, T.H.J.J. VAN DER HAGEN, H. VAN DAM, "Analytical modelling of flashing-induced instabilities in a natural circulation cooled boiling water reactor", *Nucl. Eng. Des.*, **215**, pp. 87-98, 2002.
3. M. ARITOMI, J.H. CHIANG, T. NAKAHASHI, M. WATARUM, M. MORI, "Fundamental Study on Thermo-hydraulics During Start-up in Natural Circulation Boiling Water Reactors (I)," *J. Nucl. Sci. Technol.,* **29**, *7*, 631, (1992).
4. M. FURUYA, F. INADA, A. YASUO, "A Study on Thermalhydraulic Instability of a Boiling Natural Circulation Loop with a Chimney (Part II. Experimental Approach to Clarify the Flow Instability in Detail)," *Heat Transfer - Japanese Research,* **24**, *7*, 577, (1995).
5. S.Y. JIANG, YAO, J.H. BO, S.R. WU, "Experimental Simulation Study on Start-up of the 5 MW Nuclear Heating Reactor," *Nucl. Eng Des.,* **158**, 111, (1995).
6. T.H.J.J. VAN DER HAGEN, A.J.C. STEKELENBURG, "The Low-Power Low-Pressure Flow Resonance in a Natural Circulation Boiling Water Reactor," *Nucl. Eng. Des.,* **177**, 229 (1997).
7. C. SCHUSTER, A. ELLINGER, J. KNORR, "Analysis of Flow Instabilities at the Natural Circulation Loop DANTON with regards to Non-linear Effects," *Heat and Mass Transfer,* **36**, 557, (2000).
8. A. MANERA, T.H.J.J. VAN DER HAGEN, "Stability of Natural-circulation-cooled Boiling Water Reactors during Startup: Experimental Results," *Nuclear Technology*, **143** (2003).
9. J.G.M. ANDERSEN, F. INADA, L.A. KLEBANOV, "TRACG Analyses of Flashing Instability During Start-up," *Proc. of 3rd Int. Conf. on Nucl. Eng. ICONE-3*, April 23-27, Kyoto, Japan (1995).
10. H.S. CHENG, H.J. KHAN, U.S. ROHATGI, "Simulation of SBWR Startup Transient and Stability", BNL-65535 (1998).
11. J. PANIAGUA, U.S. ROTHAGI, V. PRASAD, "Modeling of Thermal Hydraulic Instabilities in Single Heated Channel Loop During Startup Transients," *Nucl. Eng. Des.*, **193**, 207 (1999).
12. Y.K. CHEUNG, A.S. RAO, "Startup Simulation of a Natural Circulation Plant - ESBWR," *Proc. of 8th Int. Conf. on Nucl. Eng. ICONE-8*, April 2-6, Baltimore, MD, USA (2000).
13. I. TISELJ, G. CERNE, "Some Comments on the Behaviour of RELAP5 Numerical Scheme at Very Small Time Step", *Nucl. Eng. Des.*, **134**, 3 (2000).
14. T. SENGSTAG, "Pre-test calculations MONA-2-2 on the CIRCUS tests", NACUSP FIKS-CT-2000-00041, report D9a (2002).
15. G. TH. ANALYIS, D. LÜBBESMEYER, "Pre-test calculations on flashing-induced instability experiments in PANDA with TRAC-BF1/v2001.2 and RELAP5/MOD3.3./beta", EU project NACUSP, FIKS-CT-2000-00041, D09c (2002).
16. J.V. RIZNIC, M. ISHII, "Bubble number density and vapour generation in flashing flow", *Int. J. Heat Mass Transfer*, **32**, 10, 1821-1833 (1989).
17. J. DOMNICK, F. DURST, "Measurement of bubble size, velocity and concentration in flashing flow behind a sudden constriction", *Int. J. Multiphase flow*, **21**, 6, 1047-1062 (1995).
18. P. DOWNAR-ZAPOLSKI, Z. BILIKI, L. BOLLE, J. FRANCO, "The non-equilibrium relaxation model for one-dimensional flashing liquid flow", *Int. J. Multiphase flow*, **22**, 3, 473-483 (1996).
19. E. HAHNE, G. BARTHAU, "Evaporation waves in flashing processes", *Int. J. Multiphase flow*, **26**, 531-547 (2000).
20. E. ELIAS, P.L. CHAMBRÉ, "Bubble transport in flashing flow", *Int. J. Multiphase flow* **26**, 191-206 (2000).
21. H.-M. PRASSER, A. BÖTTGER, J. ZSCHAU, T. GOCHT, "Needle-shape conductivity probes with integrated micro-thermocouple and their application in rapid condensation experiments with

non-condensable gases", *Kerntechnik*, **68**, 114 (2003).
22. W.J.M. DE KRUIJF, A. MANERA, D.W. DE HAAS, J.G.F. SCHUT, T.H.J.J. VAN DER HAGEN, R.F. MUDDE, H.-M. PRASSER, *"Description of CIRCUS Including Test Matrix,"* EU project NACUSP, FIKS-CT-2000-00041, D08a (2001).
23. H.-M. PRASSER, A. BÖTTGER, J. ZSCHAU, "A New Electrode-Mesh Tomograph for Gas-Liquid Flows," *Flow Measurement and Instrumentation,* **9**, 111 (1998).
24. S. RICHTER, "Study on multidimensional characteristics of developing bubbly flow in a rectangular channel," Ph.D. thesis, Tokyo Institute of Technology (2001).
25. A. MANERA, H.-M. PRASSER, T.H.J.J. VAN DER HAGEN, R.F. MUDDE AND W.J.M. DE KRUIJF, "A comparison of void-fraction measurements during flashing-induced instabilities obtained with a wire-mesh sensor and a gamma-transmission set-up, " *Proc. 4th International Conference on Multiphase Flow (ICMF-2001)*, May 27 - June 1, New Orleans (2001).
26. H.-M. PRASSER, D. SCHOLZ, C. ZIPPE, "Bubble size measurements using wire-mesh sensors," *Flow Measurement and Instrumentation,* **12**, 299 (2001).
27. A. OHNUKI, H. AKIMOTO, "Experimental study on transition of flow pattern and phase distribution in upward air-water two-phase flow along large vertical pipe," *Int. J. Multiphase Flow,* **26**, 367 (2000).
28. R.P. ROY, V. VELIDANDLA, S.P. KALRA, P. PETURAUD, "Local measurements in the two-phase region of turbulent subcooled boiling flow," *Trans. ASME,* **116**, 660 (1994).
29. G. WANG, C.Y. CHING, "Measurements of multiple gas-bubble velocities in gas-liquid flows using hot-film anemometry," *Experiments in Fluids,* **31**, 428-439 (2001).
30. R. VAN HOUT, D. BARNEA, L. SHEMER, "Evolution of statistical parameters of gas-liquid slug flow along vertical pipes," *Int. J. Multiphase Flow ,* **27**, 1579 (2001).
31. G. COSTIGAN, P.B. WHALLEY, "Slug flow regime identification from dynamic void fraction measurements in vertical air-water flows," *Int. J. Multiphase Flow,* **23**, 263 (1997).
32. H. CHENG, J.H. HILLS, B.J. AZZOPARDI, "A study of the bubble-to-slug transition in vertical gas-liquid flow in columns of different diameter," *Int. J. Multiphase Flow,* **3**, 431 (1998).
33. Y. MI, M. ISHII, L.H. TSOUKALAS, "Investigation of vertical slug flow with advanced two-phase flow instrumentation," *Nucl. Eng. Des.,* **204**, 69 (2001).
34. H.-M. PRASSER ET AL., "Influence of the pipe diameter on the structure of the gas-liquid interface in a vertical two-phase pipe flow," *Proc. 10th Int. Top. Meetg. on Nuclear Reactor Thermal Hydraulics (NURETH-10)*, October 5-9, Seoul, Korea (2003).
35. A. MANERA, H.-M. PRASSER, U. ROHDE, T.H.J.J. VAN DER HAGEN, "Assessment of void-fraction correlations and drift-flux models applied to stationary and transient flashing flow in a vertical pipe", *to be submitted*.
36. K. MISHIMA, M. ISHII, "Flow regime transition criteria for upward two-phase flow in vertical tubes," *Int. J. Heat Mass Transfer,* **27**,723-737 (1984).
37. A TOMIYAMA, A. SOU, I. ZUN, N. KATANAMI, T. SAKAGUSHI, "Effects of Eötvös number and dimensionless liquid volumetric flux on lateral motion of a bubble in a laminar duct flow," *Advances in Multiphase Flow,* **10**, 3-15 (1995).
38. A TOMIYAMA, H. TAMAI, H. SHIMOMURA, S. HOSOKAWA, "Spatial evolution of developing air-water bubble flow in a vertical pipe," *Proc. 2nd Int. Symp. on Two-Phase Flow Modelling and Experimentation*, May 23-26, Pisa, Italy, Vol. 2, pp. 1027-1034 (1999).
39. H.-M. PRASSER, E. KREPPER, D. LUCAS, "Evolution of the two-phase flow in a vertical tube – decomposition of gas fraction profiles according to bubble size classes," *Int. J. Therm. Sci.,* **41**, 17-28 (2002).
40. D. LUCAS, E. KREPPER, H.-M. PRASSER, "Prediction of radial gas profiles in vertical pipe flow on the basis of bubble size distribution," *Int. J. Therm. Sci.,* **40**, 217-225 (2001).
41. I. ZUN, "The transverse migration of bubbles influenced by walls in vertical bubbly flow," *Int. J. Multiphase Flow,* **6**, 583-588 (1980).
42. S.P. ANTAL, R.T. LAHEY, J.E. FLAHERTY, "Analysis of phase distribution in fully developed laminar bubbly two-phase flow," *Int. J. Multiphase Flow,* **7**, 635-652 (1991).
43. R.T. LAHEY, M. LOPEZ DE BERTODANO, O.C. JONES, "Phase distribution in complex geometry conduits," *Nucl. Eng. Des.,* **141**, 177-201 (1993).
44. Y. SATO, M. SADATOMI, K, SEKOGUCHI, "Momentum and heat transfer in two-phase bubble flow - I," *Int. J. Multiphase Flow,* **7**, 167-177 (1981).
45. "Thermal-hydraulic relationships for advanced water cooled rectors", IAEA-TECDOC-1203, April 2001.
46. Y. TAITEL, D. BORNEA, A.E. DUKLER, "Modelling flow pattern transitions for upward gas-liquid flow in vertical tubes," *AIChE J.,* **26**,345-354 (1980).
47. K. MISHIMA, M. ISHII, "Flow regime transition criteria for upward two-phase flow in vertical tubes," *Int. J. Heat Mass Transfer,* **27**, 723-737 (1984).

STABILITY OF NATURAL-CIRCULATION–COOLED BOILING WATER REACTORS DURING STARTUP: EXPERIMENTAL RESULTS

THERMAL HYDRAULICS

KEYWORDS: *startup, natural circulation, stability analysis,*

ANNALISA MANERA* and TIM H. J. J. VAN DER HAGEN
Delft University of Technology, Interfaculty Reactor Institute
Mekelweg 15, 2629 JB, Delft, The Netherlands

Received September 17, 2002
Accepted for Publication January 9, 2003

The characteristics of flashing-induced instabilities, which are of importance during the startup phase of natural-circulation boiling water reactors, are studied. Experiments at typical startup conditions (low power and low pressure) are carried out on a steam/water natural-circulation loop. The flashing and the mechanism of flashing-induced instability are analyzed. The effect of system pressure and steam volume in the steam dome is investigated as well.

The instability region is found as soon as the operational boundary between single-phase and two-phase operation is crossed. Increasing pressure has a stabilizing effect, reducing the operational region in which instabilities occur. Nonequilibrium between phases and enthalpy transport are found to play an important role in the instability process. In contrast with results reported in the literature, instabilities can occur independently of the position of the flashing boundary in the adiabatic section of the loop. The period of the oscillation is found to be about twice the fluid transit time in the system.

I. INTRODUCTION

Natural-circulation–cooled boiling water reactors (BWRs) are promising candidates for more economic energy production due to their relatively simple design and their passive safety characteristics that make them more easily acceptable by the public. An item of concern is the susceptibility of these systems to exhibit thermal-hydraulic instabilities during the startup phase, as originally pointed out by Aritomi et al.[1]

*E-mail: manera@iri.tudelft.nl

The occurrence of instabilities as soon as the operation mode of this type of reactor passes from single-phase to two-phase natural circulation has been proved experimentally[2–7] and by means of simplified analytical models.[8–9] In particular, experiments performed on the DANTON facility[4] have shown that the pressure increase caused by the steam produced in the reactor vessel is not sufficient to suppress completely the flow oscillations and that without external pressurization, an instability region between single-phase and two-phase operation has necessarily to be crossed. Unstable behavior at low power and low pressure has also been encountered at specific conditions explored in an experimental campaign at the Dutch natural-circulation BWR Dodewaard.[10]

The instabilities in the region between single-phase and stable two-phase natural-circulation mode are mainly induced by flashing in the riser, i.e., steam production in the long adiabatic section present above the core to enhance the flow rate. Flashing causes an unbalance between driving force and pressure losses in the natural-circulation loop, giving rise to flow oscillations. These flow oscillations make the operation of the reactor during startup rather difficult and could cause strong mechanical vibrations of the reactor's internal components.

Well-defined startup procedures are therefore needed to cross the instability region during the transition from single-phase to two-phase flow conditions. Unfortunately, the computer codes available are not fully reliable at low-pressure and low-power conditions; thus, they cannot be used to predict the behavior of natural-circulation–cooled BWRs during startup conditions and to simulate startup procedures with reasonable confidence.

As a matter of fact, numerical simulations carried out with state-of-the-art thermal-hydraulic codes have given contradictory and not always fully satisfactory results. Cheung and Rao[11] performed simulations of the startup of the European Simplified Boiling Water

Reactor (ESBWR) with TRACG code and claim that no instabilities are found at all during the startup procedure; Paniagua et al.[12] used RAMONA-4B and an improved version of the code, which includes local pressure dependencies and an explicit numerical scheme to avoid numerical damping of the solution; their simulations with the original and with the improved code show the occurrence of geysering-type instabilities, but the quantitative comparison with experimental results from Wang et al.[13] gives an underprediction of the amplitude of the flow rate oscillation. They do not report about flashing-induced instabilities. Andersen et al.[14] reproduced flashing-induced instabilities with TRACG and found excellent qualitative agreement with the different kinds of flow oscillations obtained experimentally at the Central Research Institute of Electric Power Industry (CRIEPI) Japan test facility. In the cases they examined, the amplitude of flow oscillations is always underestimated, but no systematic quantitative comparison is reported. Although experiments on flashing-induced instabilities have been performed in the last few years,[2,3,15–18] the experimental database is still poor, and the characteristics of the different instabilities remain unclear.

Within the European Union Fifth Framework Program, a project, NACUSP, was started in December 2000, having as one of its main aims the understanding of the physics of the phenomena involved during the startup phase of natural-circulation–cooled BWRs. The development of the experimental database and the validation of state-of-the-art thermal-hydraulic codes in the low-pressure, low-power operational region of these reactors are an integral part of the project. This paper reports on the experimental work related to flashing-induced instabilities that has been performed within the framework of the NACUSP project. Experiments have been carried out on the CIRCUS facility, built at the Delft University of Technology in The Netherlands. The mechanism of flashing-induced instability and void production during flashing has been examined in detail. The transition from unstable to stable operational conditions has been demonstrated. Stability boundaries have been measured as a function of heat flux and core inlet temperature at different system pressures and with different steam volumes in the steam dome.

II. TEST FACILITY

The experimental facility (CIRCUS) is a natural-circulation water/steam loop. The heated section (1.95 m) consists of four parallel heated channels and four bypass channels. The latter ones were closed during the experiments presented in this work. On top of the heated channels, a long adiabatic section (length of 3 m) is present. In the following discussion this part will be referred to as the "riser section." The steam possibly produced in the heated channels and in the riser section is condensed in the heat exchangers. A pressure vessel containing air and water separated by a membrane is used to pressurize the loop before starting the set of experiments. A steam dome, in which a mixture of water and steam is at saturation conditions, is used to simulate the steam dome of a reactor; here, a small heater compensates for heat losses. A buffer vessel is used to damp temperature oscillations at the outlet of the heat exchanger, which ensures a constant temperature at the inlet of the heated section. A simplified scheme of the facility is shown in Fig. 1, and the main characteristics are reported in Table I. The inlet flow rate is measured by means of a magnetic flowmeter. The temperature along the riser section is measured by means of thermocouples equidistantly located along the riser vertical axis (see Fig. 1) and positioned in the center of the pipe section. Needle-probes[19] are located at the same positions of the thermocouple to measure the void fraction distribution along the riser (sampling frequency of 500 Hz). Their function is based on a local detection of the instantaneous electrical conductivity of the fluid. The measuring error on the void fraction[20] is always

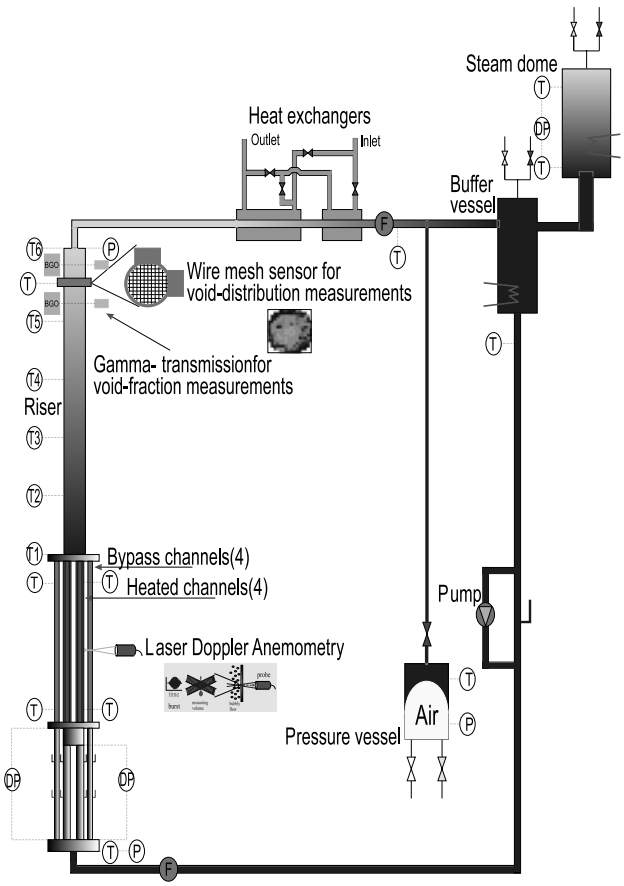

Fig. 1. Scheme of the CIRCUS Facility.

TABLE I

Main Characteristics of CIRCUS Facility

Power range per rod	0 to 3 kW
Pressure range	1 to 5 bar
Fuel channel diameter	20.4 mm
Fuel rod diameter	12.5 mm
Bypass channel diameter	10 mm
Heated section length	1.95 m
Riser diameter	47 mm
Riser length	3 m

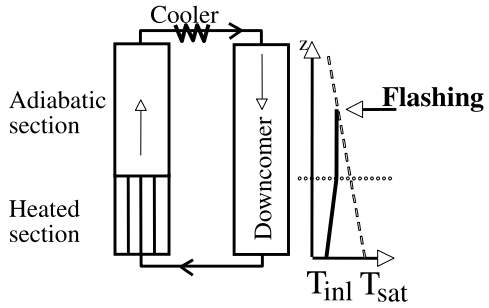

Fig. 2. Flashing in the riser section.

<10%. A more detailed description of the facility and its instrumentation is reported in Ref. 21.

II.B. Experimental Procedure

To perform the experiments, the facility is first pressurized to the desired value of pressure using the pressure vessel, and steam is created in the steam dome by means of a heater. The facility is heated up, and once the desired condensed water level is reached in the steam dome, the pressure vessel is disconnected from the loop. During the phase of heating up, the facility is operated in forced circulation to avoid the occurrence of flow oscillations. Once the inlet temperature stabilizes at the required value, the circulation pump is disconnected. Data acquisition is started after a stationary state is reached (stable or unstable). The achievement of a stationary state can take several minutes. After increasing the inlet temperature or the total heating power, a certain amount of condensed water level is discharged from the steam dome to take into account the variation of water density as a function of temperature. In this way all experiments can be performed at the same conditions of system pressure and available expansible volume.

III. MECHANISM OF THE INSTABILITY

The flow instability stems from flashing in the riser. This phenomenon is schematically illustrated in Fig. 2. When the power is low, the coolant temperature increases in the heated section without reaching saturation conditions. The coolant temperature remains constant in the adiabatic section if heat losses are neglected. Since at low pressure the saturation temperature is strongly dependent on pressure, the saturation temperatures at core-exit and at riser-exit locations, respectively, can differ by several degrees due to the decrease of pressure head along the axis of the system. Therefore, even if no boiling occurs in the core, void production can take place in the adiabatic section.

It is clear that flashing-induced instabilities are possible in a natural-circulation system only if the coolant temperature at the exit of the heated section is larger or equal to the saturation temperature at the exit of the riser.

As a consequence of flashing, the natural-circulation flow rate will increase as a result of the increased buoyancy of the loop. Due to the increase in flow rate, the fluid temperature at the exit of the core will decrease, so that flashing in the riser will be suppressed. The flow rate will then decrease, and the temperature at the core exit will consequently increase, giving rise to a new flashing cycle. In this way a self-sustained flow oscillation can take place. Therefore, the fluid traveling time in the heated section and the traveling time of enthalpy perturbations in the adiabatic section of the loop play a role in determining the period of the oscillation. This will be discussed quantitatively in Sec. V.

The occurrence of flashing will also cause an increase of the condensed water level in the steam dome, so that the pressure in the system will increase, leading to a decrease of the void production in the riser. Hence, the presence of the steam dome has a feedback effect that reduces the flow-oscillation amplitude, as will be demonstrated in Sec. IV.B.

III.A. Phenomenological Classification of Instabilities

Typical time traces of the flow rate measured on the CIRCUS facility are reported in Fig. 3. Eight cases with different water inlet temperature are presented. For all cases the system pressure was 1 bar, and a constant heating power of 2 kW per channel was applied. Four main types of behavior can be observed: stable single-phase circulation (Fig. 3a), intermittent natural circulation (Figs. 3b through 3f), unstable two-phase natural circulation (Fig. 3g), and stable two-phase circulation (Fig. 3h).

In single-phase circulation conditions, the liquid temperature always remains below saturation. The driving force is small because of the low density difference between downcomer section and heated channels/riser sections; therefore, a very low flow rate circulates in the system. As soon as the system passes from single-phase

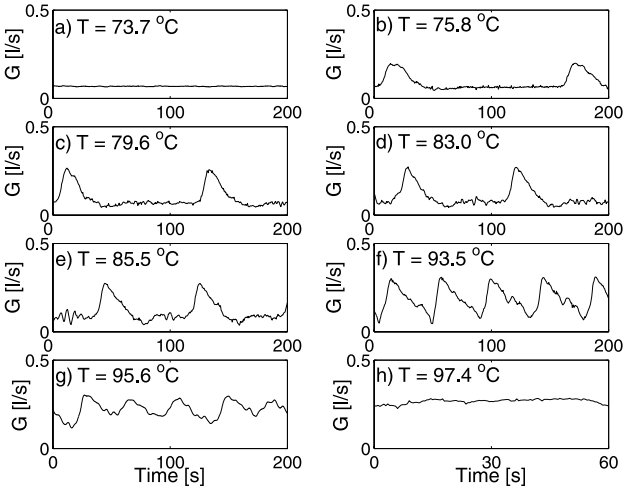

Fig. 3. Typical experimental flow time traces.

to two-phase operation, intermittent natural circulation takes place, which is characterized by an alternate presence of liquid and two-phase mixture in the riser section. Within a cycle, a certain time is needed for the liquid to reach saturation conditions (incubation period). The incubation period becomes shorter and shorter with increasing inlet temperature and disappears in the unstable two-phase natural-circulation region. In the latter condition, two-phase mixture is always present in the riser section due to flashing, but the location at which flashing starts (flashing boundary) oscillates, giving rise to an oscillatory driving force in the system, i.e., to a flow instability. Finally, when the flashing boundary stabilizes, stable two-phase circulation takes place. In this case a much higher flow rate is achieved with respect to single-phase natural circulation due to the large density difference between liquid in the downcomer and two-phase mixture in the riser.

Note that the intermittent natural circulation is often referred to as geysering instability, generating some confusion with the geysering instability extensively studied by Aritomi et al.,[1,22] Chiang et al.,[23] Downar-Zapolski et al.,[24] Dimmik et al.,[25] and Chiang et al.,[26] which is characterized by a high frequency and caused by production of steam bubbles in the heated section and their successive condensation in the upper plenum.

A similar phenomenological trend as reported in Fig. 3 can be observed if the inlet temperature is kept constant and the heating power is increased instead.

III.B. Detailed Transient Analysis of the Instability

In order to clarify the mechanism involved in the instability, the time evolution of temperature and void fraction along the riser is analyzed during one oscillation cycle. The void fraction and temperature profiles along the vertical axis of the riser are reported in Figs. 4a and 4b, respectively, at different times, together with the flow rate time trace (small window in Fig. 4a). The case considered corresponds to a pressure of 1 bar, heating power of 1.4 kW per channel, and an inlet temperature of 85°C.

Initially (see curves at 45 s), the flow rate is low, and no void is present in the riser section (single-phase circulation), although the liquid temperature is already higher than the saturation temperature (solid line in Fig. 4b) in the first 2 m of the riser section. Note that the saturation temperature is shown only for the cases in which the whole riser is single phase.

At 50 s, while the temperature profile has not changed significantly, voids start to be produced somewhere near the middle of the riser (Fig. 4a). The temperature in the lower part of the riser remains constant, while it increases in the upper part due to enthalpy transport upward in the system. The extent of superheat needed for the liquid before flashing is triggered in the adiabatic section is consistent with the findings of other researchers[25] who reported a superheating of ~2 to 3°C.

Once flashing occurs, the void fraction increases rapidly (see curves corresponding to 55 s). Void production is triggered both upward and downward. Void production downward in the system occurs also due to the sudden decrease in pressure head. The flow rate increases, causing a decrease of the temperature at the inlet of the riser section. At the outlet of the riser, the temperature keeps increasing due to enthalpy transport.

At 60 s the temperature drops below saturation in the lower part of the riser, and the void fraction decreases in the middle of the riser. At the riser exit the void fraction keeps increasing since voids are transported upward by the flow. The transport of low enthalpy liquid becomes dominant on the void productions.

Finally, voids are not produced any longer but only transported upward by the flow (see the curves corresponding to 75 s, when the temperature is high enough to allow presence of voids only at the very upper part of the riser). At the riser outlet voids are present without the need of superheated liquid because bubbles have been already produced at superheated conditions somewhere lower in the riser, and they trigger void production in the liquid saturated zone acting as nucleation sites.

At 85 s all the voids have been transported out of the riser, and single-phase circulation takes place again despite the fact that the temperature at the riser exit is still above saturation.

Together with the initial temperature profiles at which flashing starts, this shows that void production during flashing is a nonequilibrium process.

The wavy character of traveling enthalpy variations is also evident. It is interesting to note that temperature variations at the inlet and at the outlet of the riser are out of phase[2,18] (the inlet temperature increases when the outlet temperature decreases and vice versa), indicating

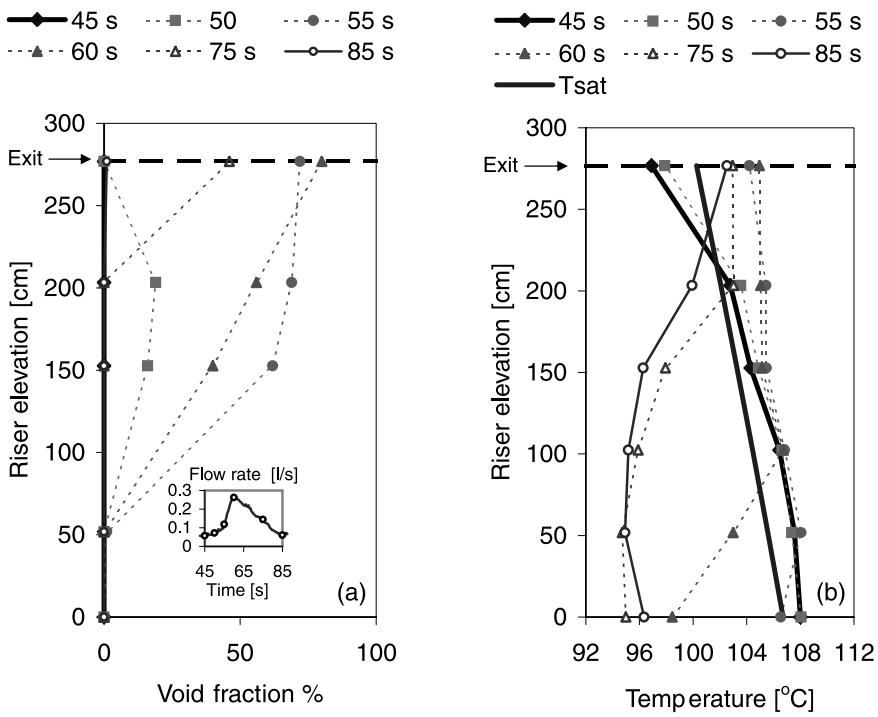

Fig. 4. Time evolution of void fraction (a) and temperature (b) profiles along the riser axis. The corresponding flow rate time trace is shown in the small window inside Fig. 4a.

that the enthalpy transport along the riser section plays a major role in determining the period of the self-sustained oscillation. This will be discussed quantitatively in Sec. V.

To complete the picture on void-fraction production during flashing, the time and spatial development of the void fraction in the riser section is given in Fig. 5 for different inlet temperatures at a pressure of 1 bar and a heating power of 2 kW per channel. The corresponding flow rate time traces are reported in Fig. 3.

At high subcooling (Fig. 5a) flashing starts relatively high in the riser and expands successively upward and downward. When the inlet temperature is increased (Fig. 5b), voids are generated in the heated section below the riser inlet. These voids collapse in the riser but contribute to the heating up of the liquid. Their contribution becomes stronger when the inlet temperature is further increased (Figs. 5c and 5d), so that flashing is triggered soon after the condensation of steam bubbles coming from the heated section. At even lower subcooling (Fig. 5e) the temperature in the riser is high enough that bubbles coming from the heated section are able to trigger flashing in the riser without being first condensed. In Fig. 5f a stable case is reported: In this case the position of the flashing boundary does not change significantly. Bubble formation and condensation continue to take place in the riser, giving rise to local void fraction fluctuations[27] with a frequency between 2 and 4 Hz.

The findings discussed above are in contrast with results reported in the literature, which state that flashing starts first at the riser exit[3] and that flashing instabilities occur only when the void fraction is produced in the very vicinity of the riser exit.[28]

In the following paragraphs details on the characteristics of flashing-induced oscillations and the effects of pressure and steam-dome compressible volume on the stability of the system will be discussed.

IV. STABILITY MAPS

The so-called Zuber-subcooling plane[29] is often used to represent stability maps for a natural-circulation system. Here, operational points are described by the subcooling number (proportional to the subcooling at the inlet of the heated section) and the Zuber number (proportional to the heating power and inversely proportional to the mass flow rate). Representation of stability maps in this plane has the advantages that each point on the map represents an operational condition of the system, that stability maps are pressure-independent at relatively high pressure[30] (when flashing is not important), and that the bisector of the plane corresponds to the transition from single-phase to two-phase operation. Unfortunately, this kind of representation also has

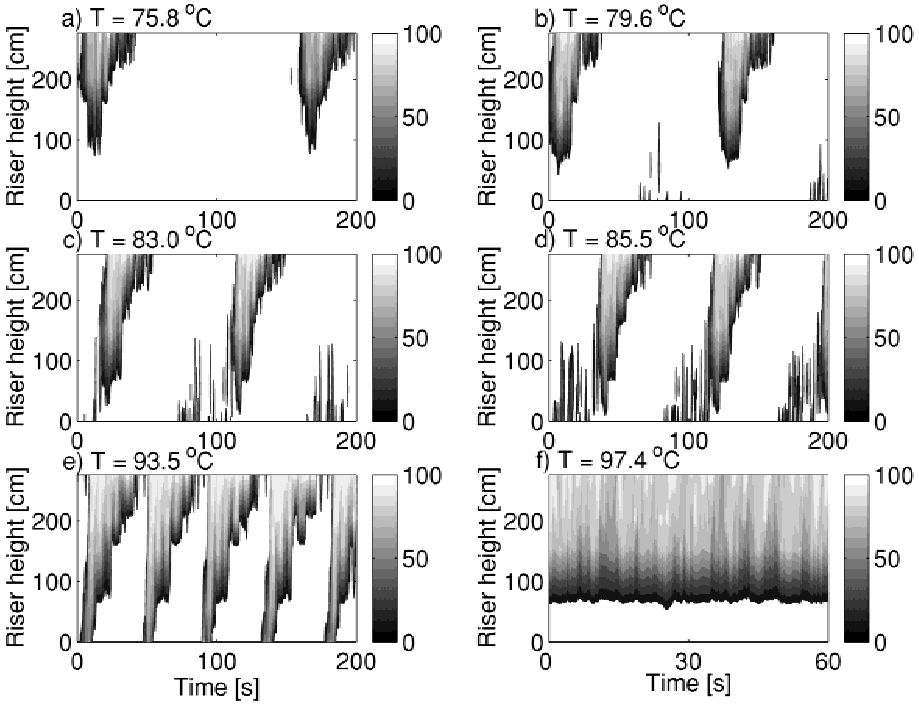

Fig. 5. Time- and spatial-dependent void fraction in the riser section for different inlet subcoolings. Vertical bars give the gray-scale coding for void fraction (in percent).

disadvantages: Since the flow rate is a dependent variable, it is not possible to know a priori how a given operational point will move on the map after a change of inlet subcooling or power. Secondly, if one has to report experimental data on such maps, the problem of how to define the Zuber number for an oscillatory behavior arises, since a single value of the flow rate cannot be defined. The use of an average flow rate gives results of dubious interpretation, as can be seen in Ref. 28. Hence, stability maps will be represented in the subcooling-power plane in the following discussion.

IV.A. Effect of System Pressure on Flow Stability

Three sets of experiments have been carried out to study the effects of pressure and steam volume in the steam dome on flashing-induced instabilities. The experimental stability boundaries are presented in Fig. 6; in Fig. 7 the relative flow-oscillation amplitude is reported (corresponding to a heating power of 2 kW per channel). From the results obtained it can be deduced, in agreement with other experimental results reported in the literature,[2,6,16] that the range of inlet subcoolings for which instabilities occur increases with power and decreases with pressure. Increasing system pressure has a stabilizing effect, both in reducing the amplitude of flow oscillations and in diminishing the region of subcoolings for which instabilities occur (see also Fig. 7). In Fig. 8 the minimum and the maximum flow rate are shown as a function of subcooling, corresponding to a pressure of 1 bar, a steam-cushion height of 18 cm, and a power level of 2 kW per channel. Both the maximum and the minimum values of the flow rate increase with decreasing subcooling. At very low subcooling the maximum flow rate decreases due to friction. The transition from stable single-phase circulation to intermittent circulation (point A) and the transition from intermittent circulation to unstable two-phase circulation (point B) can be seen.

IV.B. Effect of Compressible Volume in the Steam Dome

The effect of compressible steam volume in the steam dome does not influence the behavior of the system in steady-state conditions since in this case no variation of the compressible volume in the steam dome occurs. In dynamic conditions, however, flashing in the riser will cause a larger pressure increase when a smaller compressible volume is available in the steam dome. The pressure increase in its turn will lead to void collapse and to an increase of saturation temperature. This feedback limits the amplitude of the flow oscillation. This can be seen in Fig. 7: At a given subcooling, the relative amplitude of flow oscillations corresponding to a steam-cushion height of 18 cm is smaller in comparison with the one obtained with a height of 26 cm. The reason why at lower subcooling (i.e., close to the stable two-phase

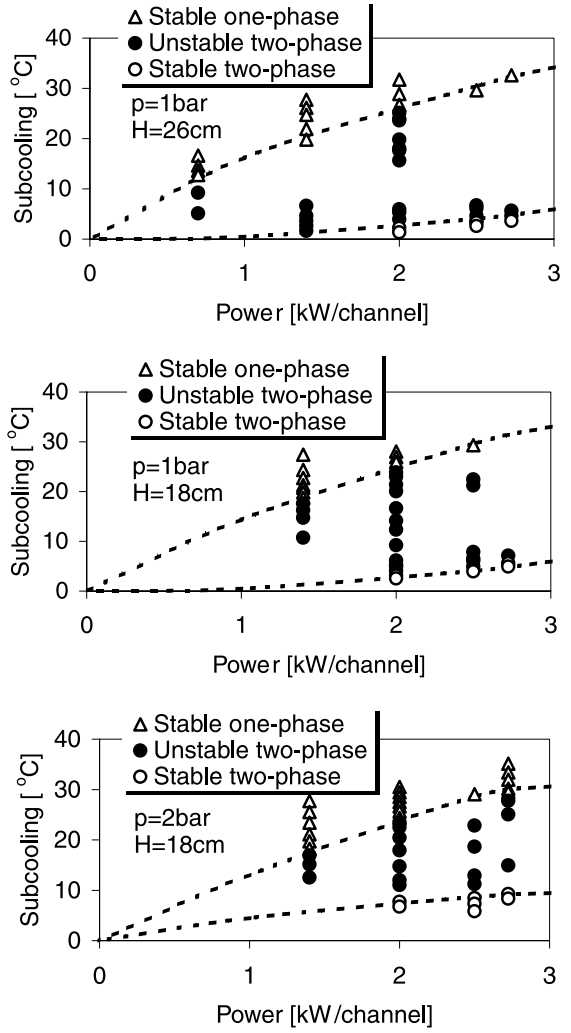

Fig. 6. Stability boundaries for different pressures p and steam volumes (H = steam-cushion height) in the steam dome.

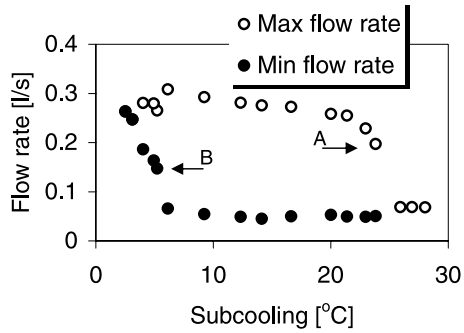

Fig. 8. Minimun and maximum flow rate as function of subcooling (pressure of 1 bar, steam-cushion height in the steam dome of 18 cm, heating power of 2 kW per channel).

operational region) the difference is less significant is not straightforward. First, it is necessary to examine the dependence of the amplitude of the spatially averaged void fraction in the riser as a function of subcooling and examine how the average flow rate changes with the void fraction.

The amplitude of the spatially averaged void fraction in the riser section during a flow oscillation as a function of subcooling is reported in Fig. 9 for the two different configurations of steam-cushion height in the steam dome. The amplitude of the spatially averaged void fraction corresponding to the smallest compressible volume in the steam dome is always the lowest. This is due to the fact that for a given decrease of the steam volume in the steam dome caused by a void-fraction increase in the riser, the pressure increase due to the steam compression in the steam dome is then larger.

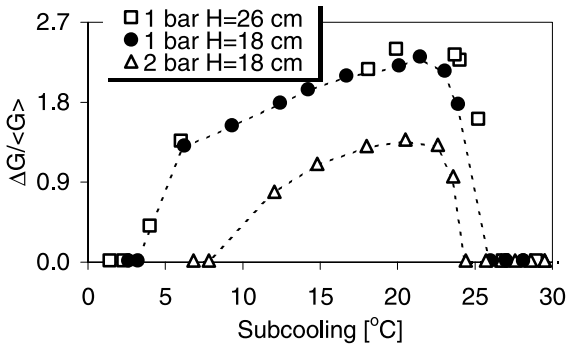

Fig. 7. Relative amplitude of flow oscillation as function of inlet subcooling (heating power equal to 2 kW per channel); H = steam-cushion height.

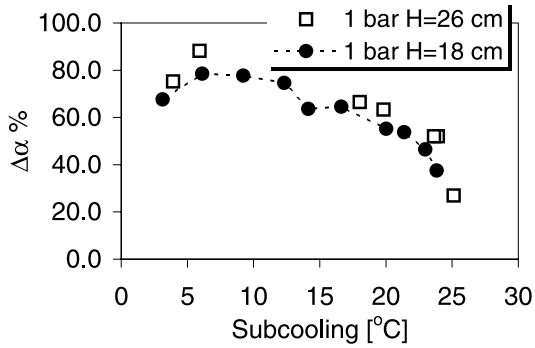

Fig. 9. Amplitude of spatially averaged void fraction in the riser section as function of subcooling, for two heights of the steam cushion in the steam dome.

The average flow rate increases with the void fraction present in the riser section due to the increase of buoyancy in the loop (see Fig. 10). Increasing the pressure, the relation between average flow rate and void fraction does not change considerably because the decrease in pressure head is compensated by a decrease of two-phase frictional pressure drops due to the smaller density ratio between liquid and gas. It is important to note that at high void fractions, the average flow rate does not change strongly because of the increase of friction in the riser.

Combining the two effects explained above, it is possible to understand why the effect of the compressible volume in the steam dome is larger at high subcoolings and becomes insignificant at low subcoolings. At high subcoolings the void fraction in the riser is small; thus, small variations of void fraction give rise to strong variations of flow rate. Since the increase of pressure in the steam dome limits the amplitude of the void fraction variations in the riser (see Fig. 9), the amplitude of the flow oscillation is also limited.

At low subcooling the time-dependent spatially averaged void fraction in the riser is on average very high (~40%) and can reach values of ~80 to 90% during an oscillation period. In this region of high void fraction, the flow rate amplitude is strongly limited by the friction in the riser section, and it does not change considerably with the void fraction. Also, at low subcooling, the steam dome will have a feedback effect on the void fraction in the riser but will not affect significantly the flow oscillation because in these conditions the flow rate is not strongly dependent on the void fraction, as it was in the case of high subcooling. Hence, at low subcooling, the total effect of the compressible volume in the steam dome becomes not significant.

In Fig. 11 the dependency of relative flow-oscillation amplitude is presented as a function of the average void fraction in the riser section. The highest values of relative flow-oscillation amplitudes are found at lower void fractions, i.e., in the low quality region where small changes of two-phase mixture quality give rise to considerable changes of void fraction, creating a stronger pressure drop unbalance in the loop to be compensated by flow readjustment. At higher void fractions the flow-oscillation amplitude decreases since the feedback quality–void fraction has a lower gain. The same occurs, for a given value of the void fraction, if the system pressure is higher.

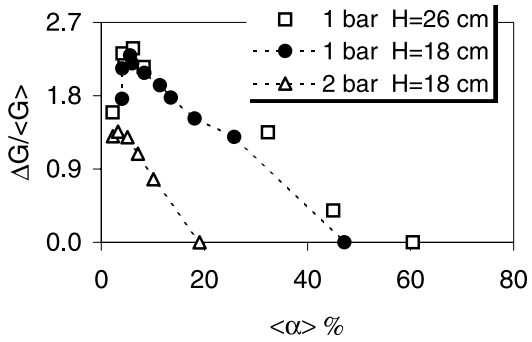

Fig. 11. Relative amplitude of flow oscillation as a function of average void fraction in the riser section.

V. CHARACTERISTICS OF INSTABILITIES

The physical origin of the instability observed suggests that the transit times of the mixture through the core and the riser play a major role in determining the oscillation period. The relation between oscillation period and average flow rate is shown in Fig. 12. It is remarkable that the oscillation period decreases monotonically with increasing average flow rate, although Fig. 12 contains cases with different subcoolings, heating power, and system pressure. Clearly, the relation between oscillation period and average flow rate depends only on the geometrical characteristics of the system. The relation also supports the idea that the faster the

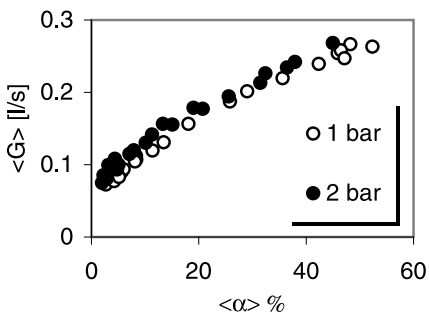

Fig. 10. Average flow as a function of average void fraction in the riser section.

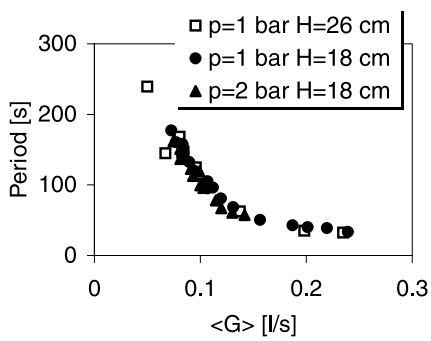

Fig. 12. Oscillation period as a function of average flow rate.

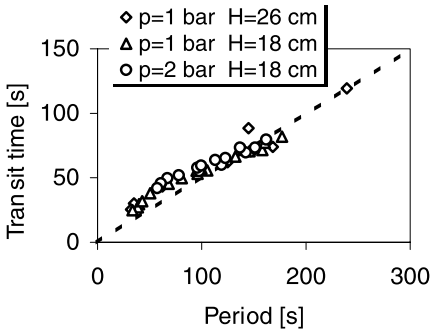

Fig. 13. Relation between oscillation period and transit time in heated and riser sections.

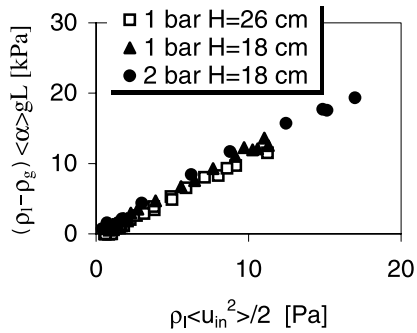

Fig. 14. Average driving pressure as a function of average kinetic pressure.

propagation of enthalpy perturbations, the shorter the period of the oscillation.

For a quantitative comparison between oscillation period and traveling time of enthalpy perturbations transported by the flow, the transit time is plotted against the oscillation period in Fig. 13. The transit time has been evaluated as the sum of the transit time in the riser section plus half of the transit time in the heated section. The factor $\frac{1}{2}$ for the heated section appears due to the fact that a perturbation of the inlet flow rate produces a perturbation of the enthalpy at the section outlet with an average phase lag corresponding to a traveling time equal to half of the transit time from the inlet to the outlet of the section (it can be derived by calculating the phase of the transfer function between enthalpy and flow rate perturbations after Laplace-transforming the energy balance).

Although the transit time is a time-dependent variable[31] in case of flow oscillations, for the sake of simplicity, the transit time is evaluated on the basis of the average flow rate during an oscillation period. From Fig. 13 it can be seen that all measurement points at unstable conditions are well correlated, regardless of the system pressure, steam-cushion height in the steam dome (denoted by H), inlet subcooling, and heating power. The oscillation period is very close to twice the transit time into the system, typical of density-wave–type instabilities. The time necessary for transport of enthalpy perturbations into the system gives the major contribution to the determination of the oscillation period. This is also confirmed by the fact that variations of inlet and outlet temperatures in the adiabatic section have ~180-deg phase shift.

Furuya et al.[2] have shown that the relationship between driving pressure in the loop and kinetic pressure can be approximated by a straight line passing through the origin and that the static characteristics are well correlated regardless of whether the flow condition is stable or unstable. This is also found for the experimental set presented in this work (see Fig. 14). Both stable and unstable cases are reported in the picture. The fact that stable points lie on a straight line indicates that driving pressure and friction are the major terms in the momentum balance of the loop. Since unstable points also lie on the same line, it means that on average during an oscillation period, inertia plays a small role in the determination of flow magnitude. Inertia is still important because it causes a phase lag between void fraction in the riser and flow rate as can be seen in Fig. 15, where typical time traces of flow rate and corresponding driving pressure are presented (pressure of 1 bar, 1.4 kW per channel, inlet temperature of 85°C). The departure from the

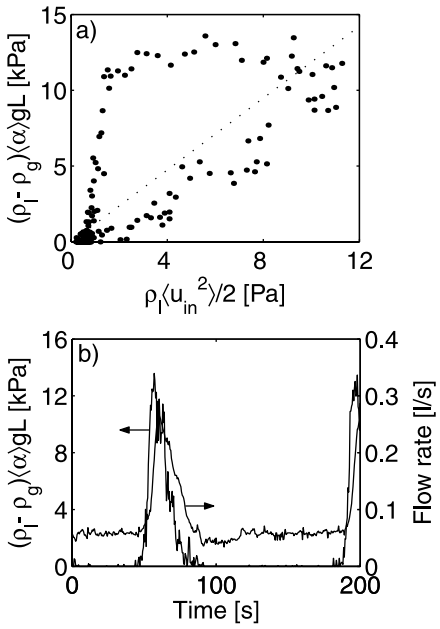

Fig. 15. (a) Typical time evolution of driving pressure versus kinetic pressure and (b) corresponding time traces of driving force and flow rate.

straight line in dynamic conditions can be seen from the phase-space in Fig. 15a.

VI. CONCLUSIONS

Experiments on flashing-induced instabilities, which are of importance in the startup phase of natural-circulation BWRs, have been carried out at low powers and low pressures. The following findings are reported:

1. An unstable operational region exists between stable single-phase and two-phase operation for natural-circulation systems; flashing is the main cause of these instabilities and has a nonequilibrium character.

2. In contrast with results reported in the literature, instabilities can occur independently on the position of the flashing boundary in the riser section.

3. Increasing the system pressure has a stabilizing effect, reducing both the extension of the unstable region and the magnitude of the flow oscillations amplitude. The feedback effect of the steam dome, caused by steam compression, reduces the amplitude of flow oscillations.

4. The oscillation period is twice the fluid transit-time in the system, typical of density-wave–type instabilities.

5. Frictional and gravitational pressure drops are the major terms in the momentum balance of the loop. Inertia is important in dynamics conditions since it causes a phase lag between driving pressure and flow rate.

Measurements on the details of flashing in an adiabatic vertical pipe were performed by means of wire-mesh sensors[32]; preliminary results are presented in Ref. 27. A study on the suitability of drift-flux models and slip models, bubble size and bubble velocity distributions, and flow pattern visualization during stable and unstable flashing flow will be published separately.

Further research will be carried out on the effect of bypass channels on stability, an issue that has not yet been discussed in the literature, with the final aim of developing optimal startup procedures for natural-circulation BWRs.

NOMENCLATURE

G = volumetric flow rate (ℓ/s)

H = steam-cushion height (m)

L = riser length (m)

u = velocity (m/s)

Subscripts

g = gas

in = inlet

l = liquid

sat = saturation

Greek

α = void fraction

ρ = density (kg/m^3)

Operators

$\langle\ \rangle$ = time/spatial average

Δ = amplitude

ACKNOWLEDGMENT

The work presented has been partially sponsored within the European Union Fifth Framework Program, NACUSP project, FIKS-CT2000-00041.

REFERENCES

1. M. ARITOMI, J. H. CHIANG, T. NAKAHASHI, M. WATARUM, and M. MORI, "Fundamental Study on Thermo-Hydraulics During Start-Up in Natural Circulation Boiling Water Reactors (I)," *J. Nucl. Sci. Technol.*, **29**, *7*, 631 (1992).

2. M. FURUYA, F. INADA, and A. YASUO, "A Study on Thermalhydraulic Instability of a Boiling Natural Circulation Loop with a Chimney (Part II. Experimental Approach to Clarify the Flow Instability in Detail)," *Heat Transfer—Jpn. Res.*, **24**, *7*, 577 (1995).

3. S. Y. JIANG, YAO, J. H. BO, and S. R. WU, "Experimental Simulation Study on Start-Up of the 5 MW Nuclear Heating Reactor," *Nucl. Eng. Des.*, **158**, 111 (1995).

4. C. SCHUSTER, A. ELLINGER, and J. KNORR, "Analysis of Flow Instabilities at the Natural Circulation Loop DANTON with Regards to Non-Linear Effects," *Heat Mass Transfer*, **36**, 557 (2000).

5. J. M. KIM and S. Y. LEE, "Experimental Observation of Flow Instability in a Semi-Closed Two-Phase Natural Circulation Loop," *Nucl. Eng. Des.*, **196**, 359 (2000).

6. S. R. WU, H. J. JIA, S. Y. JIANG, and Y. J. ZHIANG, "Investigation on Two-Phase Flow Stability in a Natural Circulation System," *Kerntechnik*, **65**, *5–6*, 222 (2000).

7. A. MANERA, W. J. M. DE KRUIJF, T. H. J. J. VAN DER HAGEN, and R. F. MUDDE, "Experiments with the CIRCUS-Facility on Flashing-Induced Instabilities During Startup of Natural-Circulation-Cooled BWRs," *Proc. Advances Reactor Physics, Mathematics and Computation into the Next Millennium (PHYSOR 2000)*, Pittsburgh, Pennsylvania, May 7–11, 2000, American Nuclear Society (2000) (CD-ROM)).

8. D. D. B. VAN BRAGT, W. J. M. DE KRUIJF, A. MANERA, T. H. J. J. VAN DER HAGEN, and H. VAN DAM, "Analytical Modeling of Flashing-Induced Instabilities in a Natural Circulation Cooled Boiling Water Reactor," *Nucl. Eng. Des.*, **215**, 87 (2002).

9. F. INADA, M. FURUYA, and A. YASUO, "Thermo-Hydraulic Instability of Boiling Natural Circulation Loop Induced by Flashing (Analytical Consideration)," *Nucl. Eng. Des.*, **200**, 187 (2000).

10. T. H. J. J. VAN DER HAGEN and A. J. C. STEKELENBURG, "The Low-Power Low-Pressure Flow Resonance in a Natural Circulation Boiling Water Reactor," *Nucl. Eng. Des.*, **177**, 229 (1997).

11. Y. K. CHEUNG and A. S. RAO, "Startup Simulation of a Natural Circulation Plant—ESBWR," *Proc. 8th Int. Conf. Nuclear Engineering (ICONE-8)*, Baltimore, Maryland, April 2–6, 2000 (2000).

12. J. PANIAGUA, U. S. ROTHAGI, and V. PRASAD, "Modeling of Thermal Hydraulic Instabilities in Single Heated Channel Loop During Startup Transients," *Nucl. Eng. Des.*, **193**, 207 (1999).

13. S. B. WANG, J. Y. WU, C. PAN, and W. K. LIN, "Thermal-Hydraulic Oscillations in a Low Pressure Two-Phase Natural Circulation Loop at Low Pressures and High Inlet Subcoolings," *Proc. 4th Int. Topl. Mtg. Nuclear Thermal Hydraulics, Operations and Safety*, Taipei, Taiwan, April 3–6, 1994 (1994).

14. J. G. M. ANDERSEN, F. INADA, and L. A. KLEBANOV, "TRACG Analyses of Flashing Instability During Start-Up," *Proc. 3rd Int. Conf. Nuclear Engineering (ICONE-3)*, Kyoto, Japan, April 23–27, 1995 (1995).

15. Y. MASUHARA, H. USTUNO, Y. BESSHO, O. YOKOMIZO, and T. FUKAHORI, "Research on Geysering Phenomena in the Natural Circulation BWR," *Proc. 2nd Int. Conf. Nuclear Engineering*, Vol. 1, American Society of Mechanical Engineers (1993).

16. F. INADA and Y. YASUO, "The Boiling Flow Instability of a Natural Circulation BWR with a Chimney at Low Pressure Start-Up," *Proc. Int. Conf. Design and Safety of Advanced Nuclear Power Plants (ANP'92)*, Tokyo, Japan, October 25–29, 1992, Vol. 3, p. 25.3.1 (1992).

17. S. Y. JIANG, X. X. WU, and Y. J. ZHANG, "Experimental Study of Two-Phase Flow Oscillation in Natural Circulation," *Nucl. Eng. Des.*, **135**, 177 (2000).

18. A. MANERA, H. HARTMANN, W. J. M. DE KRUIJF, T. H. J. J. VAN DER HAGEN, R. F. MUDDE, and D. W. DE HAAS, "Experimental Observations on Flashing-Induced Oscillations in a Water/Steam Natural Circulation Loop," *Proc. 4th Int. Conf. Multiphase Flow (ICMF-2001)*, New Orleans, Louisiana, May 27–June 1, 2001 (2001).

19. H.-M. PRASSER, R. LOTZMANN, G. UHLMANN, L. MAROTI, and P. WINDBERG, "Beobachtung des Loop-Seal-Clearings in der Integralanlage PMK-NVH des KFKI Budapest mit Nadelsonden," *Kernenergie*, **34** (1991).

20. V. N. CHOCHLOV, A. D. DUNCEV, V. V. IVANOV, V. V. KONTELEV, V. I. MELNIKOV, L. K. STOPPEL, H.-M. PRASSER, W. ZIPPE, J. ZSCHAU, and R. ZBORAY,"Local and Integral Ultrasonic Gauges for Two-Phase Flow Instrumentation in Nuclear Reactor and Safety Technology," FZR-303, Forschungszentrum Rossendorf (2000).

21. W. J. M. DE KRUIJF, A. MANERA, D. W. DE HAAS, J. G. F. SCHUT, T. H. J. J. VAN DER HAGEN, R. F. MUDDE, and H.-M. PRASSER, "Description of CIRCUS Including Test Matrix," Euratom 5th Framework Program 1998–2002, EVOL-NACUSP-D8a, European Commission (2001).

22. M. ARITOMI, J. H. CHIANG, and M. MORI, "Geysering in Parallel Boiling Channels," *Nucl. Eng. Des.*, **141**, 111 (1993).

23. J. H. CHIANG, M. ARITOMI, and M. MORI, "Fundamental Study on Thermo-Hydraulics During Start-Up in Natural Circulation Boiling Water Reactors (II)," *J. Nucl. Sci. Technol.*, **30**, *3*, 203 (1993).

24. P. DOWNAR-ZAPOLSKI, Z. BILICKI, L. BOLLE, and J. FRANCO, "The Non-Equilibrium Relaxation Model for One-Dimensional Flashing Liquid Flow," *Int. J. Multiphase Flow*, **22**, 3 (1996).

25. G. R. DIMMIK, V. CHATOORGON, H. F. KHARTABIL, and R. F. DUFFEY, "Natural-Convection Studies for Advanced CANDU Reactor Concepts," *Nucl. Eng. Des.*, **215** (2002).

26. J. H. CHIANG, M. ARITOMI, R. INOUE, and M. MORI, "Thermo-Hydraulics During Start-Up in Natural Circulation Boiling Water Reactors," *Nucl. Eng. Des.*, **146**, 241 (1994).

27. A. MANERA, H.-M. PRASSER, W. J. M. DE KRUIJF, T. H. J. J. VAN DER HAGEN, and R. F. MUDDE, "A Comparison of Void-Fraction Measurements During Flashing-Induced Oscillations Obtained with a Wire-Mesh Sensor and a Gamma-Transmission Set-Up," *Proc. 4th Int. Conf. Multiphase Flow (ICMF-2001)*, New Orleans, Louisiana, May 27–June 1, 2001 (2001).

28. F. INADA, M. FURUYA, and A. YASUO, "Thermo-Hydraulic Instability of a Boiling Natural Circulation Loop with a Chimney (an Analytical Study of Instability at Low and High Pressure)," *Proc. 7th Int. Conf. Nuclear Engineering (ICONE-7)*, Tokyo, Japan, April 11–15, 1999 (1999).

29. M. ISHII and N. ZUBER, "Thermally Induced Flow Instabilities in Two-Phase Mixtures," *Proc. 4th Int. Heat Transfer Conf.*, Paris, France, August 31–September 5, 1970, Vol. 5 (1970).

30. D. D. B. VAN BRAGT and T. H. J. J. VAN DER HAGEN, "Stability of Natural Circulation Boiling Water Reactors: Part II—Parametric Study of Coupled Neutronic-Thermohydraulic Stability," *Nucl. Technol.*, **121**, 52 (1998).

31. A. MANERA, T. H. J. J. VAN DER HAGEN, W. J. M. DE KRUIJF, and H. VAN DAM, "On the Determination of Transit Time During Flow Oscillations," *Proc. Int. Mtg. Reactor Noise (IMORN 28)*, Athens, Greece, October 11–13, 2000 (2000).

32. H.-M. PRASSER, A. BÖTTGER, and J. ZSCHAU, "A New Electrode-Mesh Tomograph for Gas-Liquid Flows," *Flow Meas. Instrum.*, **9**, 111 (1998).

Annalisa Manera (MS, nuclear engineering, University of Pisa, Italy, 1999) is a PhD student at the Reactor Physics Department of the Interfaculty Reactor Institute in Delft. Her research interests include experimental and analytical study of natural-circulation two-phase flow systems, flashing flows, and application of noise-analysis techniques to boiling water reactor (BWR) stability investigation.

Tim H. J. J. van der Hagen (MS, Eindhoven University of Technology, The Netherlands, 1984; PhD, Delft University of Technology, The Netherlands, 1989) is head of the Department of Reactor Physics at the Interfaculty Reactor Institute in Delft. He is a full professor in the Faculty of Applied Sciences of the Delft University of Technology. He has explicit experience in BWR dynamics and a specific interest in the interaction between neutronics and thermal hydraulics.

MODELLING OF FLASHING-INDUCED INSTABILITIES IN THE START-UP PHASE OF NATURAL-CIRCULATION BWRS USING THE TWO-PHASE FLOW CODE FLOCAL

A. MANERA[1], U. ROHDE[2], H.-M. PRASSER[2], T.H.J.J. VAN DER HAGEN[1,3]
[1]Interfaculty Reactor Institute, Delft University of Technology, Mekelweg 15, 2629 JB, Delft, The Netherlands
[2]Forschungzentrum Rossendorf e.V., Institute of Safety Research, P.O.B. 510119, D-01314 Dresden, Germany
[3]Kramers Laboratorium voor Fysische Technologie, Delft University of Technology, The Netherlands

This paper reports on the modelling and simulation of flashing-induced instabilities in natural circulation systems, with special emphasis on natural circulation Boiling Water Reactors (BWRs). For the modelling the 4-equation two-phase model FLOCAL [1], developed at the Forschungzentrum Rossendorf (FZR, Germany), has been used. The model allows for the liquid and vapour to be in thermal non-equilibrium and, via drift-flux models, to have different velocities.
The phenomenology of the instability has been studied and the dominating physical effects have been determined. The results of the simulations have been compared qualitatively and quantitatively with experiments [2] that have been carried out within the framework of a European project (NACUSP) on the CIRCUS facility. The facility, built at the Delft University of Technology in The Netherlands, is a water/steam 1:1 height-scaled loop of a typical natural-circulation-cooled BWR.

1. INTRODUCTION

The issue concerning flashing-induced instabilities in natural circulation systems is getting increasing degree of attention due to its relevance during the start-up phase of the ESBWR (European Simplified Boiling Water Reactor) [3]. The design of this type of reactor, which is cooled by means of natural circulation, considers a long adiabatic pipe (so-called riser) on the top of the core in order to enhance the flow rate. During the start-up phase of the reactor both pressure and power are relatively low and flashing in the riser (i.e. void production in adiabatic conditions) is very likely to occur while in the heated core the coolant has not yet reached saturation. The feedback between void generation in the riser and buoyancy of the natural-circulation loop may, under specific conditions, give rise to flow oscillation. This type of instability was first pointed out by the pioneering work of Wissler and colleagues [4], who reported about flashing-induced instabilities in a natural circulation steam/water loop in 1956. Since then, several experimental studies have addressed stability at low pressure of natural circulation two-phase flow systems [2, 5-10] emphasizing that well-defined start-up procedures are needed to cross the instability region during the transition from single-phase to two-phase flow operation.
Unfortunately, no computer code has been proved to be reliable enough at low-pressure and low-power conditions to predict the behaviour of the ESBWR during the start-up procedure with reasonable confidence. As a matter of fact, very few codes have been found to be able to reproduce the physics behind flashing-induced flow oscillations. Even numerical simulations carried out with state-of-the-art thermal-hydraulic codes have given contradictory and not always fully satisfactory results.
Inada et al. [11] reported a simplified model based on HEM formulation, which includes pressure-dependent thermodynamic properties along the vertical axis of the system but excludes single-phase natural circulation (i.e. in their model the flow rate is different from zero only when steam is present in the system). Though the model is able to predict stability boundaries fairly well compared with experimental results, the code cannot be used to simulate start-up procedures since it has been developed in frequency domain. Van Bragt et al. [12] extended the model by Inada et al. in time-domain, but the differential equation that determines the position of the boiling boundary has been derived by linearisation and Laplace transformation of the energy equation. In this way, important non-linear effects are excluded. Moreover, single-phase circulation is excluded as in the

original model from Inada et el. Consequently, far from the stability boundary, where alternation between single- and two-phase flow circulation and non-linear effects become important, the code cannot reproduce correctly flashing-induced instabilities.

Sawai et al. [13] developed a time-domain model also based on HEM formulation. Despite the authors claim that the model was developed for low-pressure conditions, they do not consider pressure changes along the axis of the system, which are fundamental for the reproduction of flashing-induced instabilities. As a consequence of the strong simplification Sawai et al. do not find any flashing-type flow oscillations, but they find unstable behaviour related to flow pattern transition from churn/annular to slug flow. This transition however is not observed experimentally during the start-up phase of natural-circulation systems [14, 15].

Chatoorgoon [16] developed a simple time-domain code SPORT, also based on HEM formulation, which includes single-phase circulation and pressure-dependent thermodynamic properties along the axis of the system. Chatoorgoon shows that the code is able to reproduce flashing instabilities at low pressure and low power, but no systematic parametric study is performed and no comparison with experimental results is shown.

About so-called best-estimate thermal-hydraulic codes Cheng et al. report on RAMONA-4B [17] applied to the start-up transient of the SBWR and do not find flashing-induced instabilities. However, the inability of finding flashing-induced oscillation is not surprising since in this code local physical properties are evaluated on system averaged transient pressure without taking into account the effect of local pressure. A modified version of RAMONA-4B was developed by Paniagua et al. [18] which includes local pressure dependencies and an explicit numerical scheme to avoid numerical damping of the solution. Their simulations with the improved code show occurrence of geysering-type instabilities, but the quantitative comparison with experimental results from Wang et al. [19] gives an under-prediction of the flow-rate oscillation amplitude. They do not report about flashing-induced instabilities. The 7-equations thermal-hydraulic code MONA-2.2 developed by Studsvik-Scandpower [20] has been proven to be unable to reproduce any flashing at low pressure due to numerical problems [21]. Cheung and Rao [22] performed simulations of the start-up of the ESBWR with TRACG code and claim that no instabilities are found during the all start-up procedure. Andersen et al. [23] reproduced flashing-induced instabilities with TRACG and found excellent qualitative agreement with the different types of flow oscillations obtained experimentally at the CRIEPI (Central Research Institute of Electric Power Industry, Japan) test facility. In the cases they examined the amplitude of flow oscillations is always underestimated, but no systematic quantitative comparison is reported. In addition, they do not find any unstable region at low power in contradiction with experimental results. Tiselj and Cerne [24] showed that RELAP5 cannot deal with flashing, in which case the results become strongly dependent on the integration time step used for the simulations.

There is thus a clear need for models development and testing in the low-power low-pressure operational region of natural circulation two-phase systems, if reliable simulations of start-up procedures for the ESBWR are to be achieved and to develop guidelines for the reactor operation.

This paper addresses the improvement and application of the 4-equation two-phase flow model FLOCAL [1], developed at the FZR (Germany), to the simulation of flashing-induced instabilities in natural circulation two-phase systems. The model allows for the liquid and vapour to be in thermal non-equilibrium and, via drift-flux models, to have different velocities. The results of the simulations have been compared qualitatively and quantitatively with experiments that have been carried out, within the framework of the EU NACUSP project, on the CIRCUS facility [2]. CIRCUS, built at the Delft University of Technology in The Netherlands, is a water/steam 1:1 height-scaled loop of a typical natural-circulation-cooled BWR.

2. DESCRIPTION OF THE TWO-PHASE CODE FLOCAL

FLOCAL is a 1-D two-phase thermal-hydraulic code originally developed to model the dynamic behaviour of the AST-500 reactor, a Russian design district reactor based on natural circulation. The core is modelled as a series of parallel coolant channels associated to one or more fuel assemblies. On top of the core both individual (parallel) risers and a common riser can be modelled. The parallel channels are coupled by a boundary condition of equal pressure drops over their total length. Four balance equations are used for the coolant: a momentum balance, an energy balance and a mass balance equation for the two-phase mixture with in addition a separate mass balance equation for the vapour phase. The coupling between the two mass balance equations is done by means of additional evaporation and condensation models, allowing thermodynamic non-equilibrium between the two phases. The difference in velocity between vapour and liquid phase is taken into account in the common momentum balance equation by means of a drift-flux model. The set of four PDEs (partial differential equations) is transformed into a set of ODEs (ordinary differential equations) after subdivision of the heated and adiabatic sections into user-defined number of axial nodes. Time-dependent boundary conditions can be given for inlet temperature and system pressure.

2.1. The system of PDEs and model assumptions

The starting set of PDEs for two-phase thermalhydraulics in the 4-equations approach can be written as following:

$$\begin{cases} \frac{\partial}{\partial t}\left[\varphi\rho_G+(1-\varphi)\rho_F\right]+\frac{\partial}{\partial z}\left[u_G\rho_G\varphi+u_F\rho_F(1-\varphi)\right]=0 & \text{Mixture mass balance} \\ \frac{\partial}{\partial t}(\rho_G\varphi)+\frac{\partial}{\partial z}(u_G\rho_G\varphi)=\mu & \text{Vapour mass balance} \\ \frac{\partial}{\partial t}\left[\varphi\rho_G u_G+(1-\varphi)\rho_F u_F\right]+\frac{\partial}{\partial z}\left[u_G^2\rho_G\varphi+u_F^2\rho_F(1-\varphi)\right]+ \\ \qquad +\frac{\partial p_R}{\partial z}+g\left[\varphi u_G+(1-\varphi)u_F\right]+\frac{\partial p}{\partial z}=0 & \text{Mixture momentum balance} \\ \frac{\partial}{\partial t}\left[\varphi h_G\rho_G+(1-\varphi)h_F\rho_F\right]+\frac{\partial}{\partial z}\left[h_G u_G\rho_G\varphi+h_F u_F\rho_F(1-\varphi)\right]=Q & \text{Mixture energy balance} \end{cases} \tag{1}$$

The unknowns for the two-phase flow are the vapour and liquid velocities u_G and u_F, the enthalpies h_G and h_F, the densities ρ_G and ρ_F, the void fraction φ and the pressure p. The four balance equations are completed by a quasi-stationary relation for the phase-slip $S=u_G/u_F$, as well by the thermodynamic state equations $h_G=h''(p)$, $\rho_G=\rho''(p)$, $\rho_F=\rho(h_F, p)$. Moreover, constitutive relations are used for the distributed and concentrated frictional pressure drops and for the evaporation/condensation rate μ.

Using the following definitions:

$$\begin{cases} h\equiv xh_G+(1-x)h_F \\ G\equiv\varphi\rho_G u_G+(1-\varphi)\rho_F u_F \\ \rho\equiv\varphi\rho_G+(1-\varphi)\rho_F \\ u\equiv\varphi u_G+(1-\varphi)u_F \\ \rho^*\equiv\frac{\partial\varphi}{\partial x}\left[x\rho_f+(1-x)\rho_g\right] \\ \frac{1}{\rho_m}\equiv\frac{1}{\rho_G}\frac{x^2}{\varphi}+\frac{1}{\rho_F}\frac{(1-x^2)}{(1-\varphi)} \end{cases} \tag{2}$$

where x is the two-phase mixture quality, the system of PDEs can be rewritten as:

$$\begin{cases} \frac{\partial G}{\partial t}+\frac{\partial}{\partial z}\left(\frac{G^2}{\rho_m}\right)+\frac{\partial p_{R,ev}}{\partial z}+\rho g+\frac{\partial p}{\partial z}=0 \\ \rho\frac{\partial h}{\partial t}+G\frac{\partial h}{\partial z}=Q+\frac{\partial\chi}{\partial t} \\ \frac{\partial\rho}{\partial t}+\frac{\partial G}{\partial z}=0 \\ \rho^*\frac{\partial x}{\partial t}+G\frac{\partial x}{\partial z}=\mu \end{cases} \tag{3}$$

where h is the enthalpy, G the mass flux, u the velocity, ρ the density and ρ_m the density for the momentum balance. All this quantities are related to the two-phase mixture.

The system of PDEs in the form (3) has the advantage that the equations appear to be formally equal to the balance equation set for homogeneous flow. The non-homogeneity of the flow is in the definition of the flow parameters (2) and the non-equilibrium between the phases is expressed by means of the condensation/evaporation rate μ and by the source term $\partial\chi/\partial t$ in the energy balance, where:

$$\chi = \left(h_G - h_F\right)\left[\left(1-\varphi\right)x\rho_F - \varphi\left(1-x\right)\rho_G\right] \quad (4)$$

Although this term is small compared to the heating source term Q, it plays a role in adiabatic conditions (i.e in the riser section). The term

$$\frac{\partial p}{\partial t} + u\frac{\partial p}{\partial z},$$

has been neglected in the energy balance, since it is not important for quasi-isobaric processes.

The unknowns are ρ, G, h, p, x and implicitly φ. For the evaluation of the quality and the enthalpy at the inlet of the common adiabatic section perfect mixing is assumed:

$$\begin{cases} x_{R,in} = \dfrac{\sum_k x_k m_k}{\sum_k m_k} \\ h_{R,in} = \dfrac{\sum_k h_k m_k}{\sum_k m_k} \end{cases} \quad (5)$$

The summation is performed over all parallel channels k, where x_k, h_k and m_k are the quality, the fluid enthalpy and the mass flow rate at the exit of the k-th coolant channel respectively. In the downcomer the flow is considered to be incompressible and the pressure drops in this section are evaluated as:

$$\Delta p_{FS} = g\sum_i H_i\rho_i - \sum_i \frac{H_i}{A_i}\frac{dm}{dt} \quad (6)$$

where m is the total coolant flow, H_i and A_i the height and the flow area in the different sections of the downcomer, ρ_i the average fluid density in each section. The water entering the downcomer is supposed to be at saturation temperature without carry-under of steam. The downcomer contains a heat exchanger for cooling down the water, but the heat exchanger is not modeled. Instead, the water temperature at the core inlet must be given. To evaluate the heat transfer between fuel and coolant the heat balance for the fuel and the cladding is solved:

$$\rho c_p \frac{\partial T}{\partial t} = \frac{1}{r}\frac{\partial}{\partial r}\left(\lambda r \frac{\partial T}{\partial r}\right) + Q_B, \quad (7)$$

where Q_B is the source term of power density in the fuel. The temperature jump between fuel and cladding is described with an effective heat transfer coefficient α_{SP}. Constant values are assumed for the density ρ, the heat capacity c_p, and the conductivity λ of fuel and cladding. The heat flux between coolant and cladding is then calculated as:

$$\underline{q}'' = \alpha_{W,KM}\left(T_W - T_{KM}\right) \quad (8)$$

where $\alpha_{W,KM}$ is the heat transfer coefficient from cladding to coolant, T_W is the cladding wall temperature and T_{KM} the coolant temperature. This is evaluated as $T_{KM} = T_F(h_F, p)$.

2.2. Main constitutive relations

Drift-flux relations

In drift-flux relations the ratio between vapour and liquid velocity depends on the so-called drift velocity (velocity of the gas relative to the liquid) and on the distribution of the two-phases (by means of the distribution parameter C_0). Different drift-flux models have been implemented in FLOCAL. The GE-Ramp drift-flux model [25] has been selected for the study presented in this paper, since this model has been found to give the best void-fraction predictions in case of flashing flow [26].

Evaporation/condensation term in steam mass balance (THERMIT model)

The model developed by Kelly and Kazimi [27] is used for the evaporation/condensation term which couples the two mass balance equations:

$$\mu = \frac{3\varphi}{R_{B0}}\mathrm{F}\left(\varphi\right)\mathrm{k}\left(T_F - T'\right) \quad (9)$$

with:

$$R_{B0} = \frac{0.45}{1+1.34\left[(1-\varphi)u_F\right]^{1/3}}\sqrt{\frac{\sigma}{(\rho_F-\rho_G)g}}$$

$$F(\varphi) = \begin{cases} \left(\dfrac{9\varphi}{1-\varphi}\right)^{-1/3} & \text{for } \varphi > 0.1 \\ 1 & \text{for } \varphi \le 0.1 \end{cases} \qquad (10)$$

$$\mathrm{k} = \begin{cases} \dfrac{\lambda_F}{\delta_F R_{B0}} & \text{for } T_G \le T_F \\ \left(\dfrac{\delta_G}{\lambda_G}+\dfrac{\delta_F}{\lambda_F}\right)^{-1} R_{B0}^{-1} & \text{for } T_G > T_F \end{cases}$$

where R_{B0} is the bubble radius and the function F(φ) is a correction term for the coalescence of bubbles for $\varphi > 0.1$. The vapour is assumed to be at saturation, so that $T_G = T''(p)$.

2.3. The model for heat structures (pipe walls)

During the analysis of flashing-induced instabilities, it has been found that heat structures play an important role in the determination of the oscillation period (this issue is discussed in section 4).

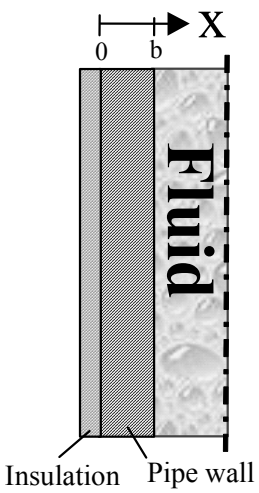

Fig. 1 Scheme of an axial node of the adiabatic section.

To consider the dynamics of the heat structures of core and adiabatic sections, a model for pipe walls has been included in the FLOCAL code. The glass pipes of the CIRCUS facility are approximated as flat walls. This approximation is acceptable because the ratio between wall tickness and pipe radius is small (< 0.1). A scheme of an axial node of the adiabatic section is illustrated in Fig. 1.

The heat conduction equation expressed by:

$$\frac{\partial \mathrm{T}}{\partial \mathrm{t}} = \frac{\lambda}{\rho\, c_p}\frac{\partial^2 \mathrm{T}}{\partial \mathrm{x}^2}, \qquad (11)$$

is solved with the following boundary conditions:

$$\begin{cases} \lambda \dfrac{\partial \mathrm{T}}{\partial \mathrm{x}} = -q''_{wall} & x = b \\ \dfrac{\partial \mathrm{T}}{\partial \mathrm{x}} = 0 & x = 0 \end{cases} \qquad (12)$$

A zero heat flux is assumed as boundary condition for the external wall surface (x=0) because of the presence of insulation material in the experimental set-up. For the surface at contact with the fluid (x=b) it holds:

$$q''_{wall} = \alpha\left(T_{wall} - T_{fluid}\right) \qquad (13)$$

For the heat transfer coefficient α the Guerrieri's model [28] is used, which is basically a Dittus-Bolter type correlation extended to the case of two-phase mixture.

To solve the PDE (11) the temperature distribution in the wall is expanded in eigenfunctions. After appling the boundary conditions (12) and truncating the expansion to N for practical applications, the PDE can be expressed as a system of *N+1* ODEs:

$$\begin{cases} \dfrac{\partial \Delta T_{wall,0}}{\partial t} = \dfrac{q''}{b\,\rho\, c_p} \\ \dfrac{\partial \Delta T_{wall,n}}{\partial t} = \dfrac{2q''}{b\,\rho\, c_p} - \dfrac{\lambda}{\rho\, c_p}\left(\dfrac{n\pi}{b}\right)^2 \Delta T_{wall,n} \quad \text{n=1,2,...N} \end{cases} \qquad (14)$$

with

$$T_{wall}(t) = T_{wall}(t=0) - \sum_{n=0}^{N} \Delta T_{wall,n}(t) \qquad (15)$$

The system of equations (14) is solved for each axial node of the adiabatic and heated sections. An explicit Euler scheme is used for the numerical integration. To ensure numerical stability a much smaller time step is needed with respect to the one used for the solution of the PDEs in (3). Therefore a separate time-step controlled routine has been added to the code.

At the beginning of the dynamic calculation, it is assumed that walls and fluid have the

same temperature as calculated from the steady-state module of the code FLOCAL.
The iterative schemes of the FLOCAL code are described in appendix.

3. EXPERIMENTAL SET-UP AND NODALIZATION ADOPTED

An experimental campaign on flashing-induced instabilities has been carried out at the CIRCUS facility [2], at the Delft University of Technology, within the framework of the EU project NACUSP.
The experimental facility (see scheme in Fig. 2.a) is a steam/water natural-circulation loop built to simulate the behaviour of a natural-circulation BWR at low-pressure conditions. Demineralised water is used as working fluid. The test section consists of an insulated adiabatic pipe (3 m length, 47 mm diameter), so-called riser, made of glass built on top of four parallel heated channels (1.95 m length). The steam produced in the heated and in the adiabatic sections is condensed by a heat exchanger. The pressure can be set higher than the atmospheric pressure by means of a steam dome where liquid and steam are kept at saturation conditions (in this case the loop is pressurised by means of a pressure vessel containing air and water separated by a membrane. After the pressurization the vessel is disconnected from the loop). A buffer vessel is used to damp temperature oscillations at the outlet of the heat exchanger in order to ensure a constant temperature at the inlet of the heated section.
The flow rate at the inlet of the heated section is measured by means of a magnetic flowmeter, the temperature along the riser section is measured by means of six equidistant thermocouples, while the void fraction is measured along the central axis of the riser by means of conductivity needle probes with integrated thermocouple [29] developed by Forschungzentrum Rossendorf (FZR, Germany). These probes allow measuring the local conductivity (sampling frequency of 500 Hz) and the fluid temperature (thermocouple time response of 17 ms) at the same location, thus it is possible to detect possible temperature differences between the liquid and the vapour phases.

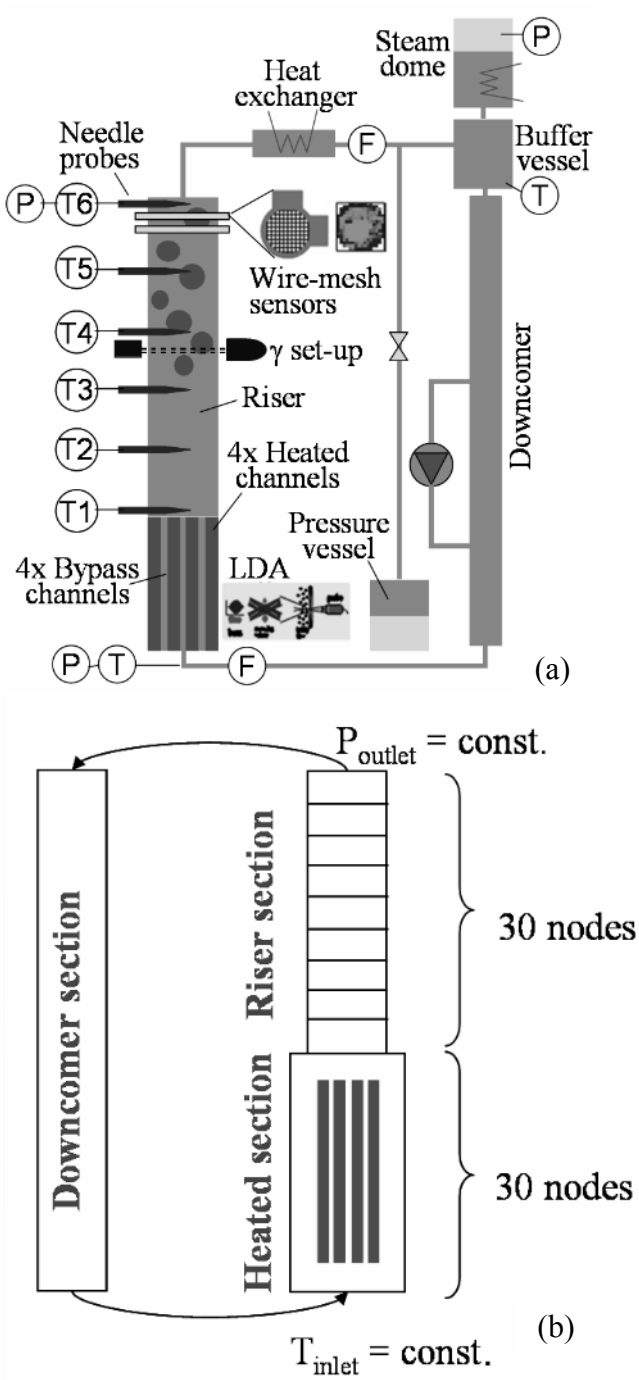

Fig. 2 Scheme of the experimental set-up CIRCUS (a) and its corresponding nodalization (b) for FLOCAL simulations.

The nodalization used to simulate the CIRCUS facility is schematically represented in Fig. 2.b. Both heated and riser sections have been divided into 30 axial nodes for the spatial integration of the system of PDEs. As boundary conditions, the coolant temperature at the inlet of the heated section and the pressure at the outlet of the adiabatic section are kept constant. The boundary condition on the coolant temperature is exact, since the inlet temperature is kept constant also during

the experiments. This is not the case for the condition on the outlet pressure. In the experimental set-up the loop is connected to a steam dome, where a mixture of steam and water is present. During flow instabilities, the production of steam in the adiabatic section causes an equivalent volume of water to enter the steam dome leading to a compression (and partially condensation) of the steam cushion in the steam dome itself. This has as effect a temporary increase of the system pressure that limits the void production and expansion in the adiabatic section and therefore the amplitude of the flow oscillations. Since the feedback of the steam dome is not considered in this analysis with the code FLOCAL, one should expect higher amplitude of the flow oscillation in the simulations. In any case, neglecting the feedback of the steam dome does not affect the reproducibility of the phenomenology of flashing-induced instabilities.

The k-factors that define the concentrated frictional pressure drops have been evaluated on the basis of standard geometry-based correlations [31]. The k-factor corresponding to the valve at the inlet of the heated section has been determined experimentally.

4. RESULTS AND DISCUSSION

The comparison between experimental and calculated flow rate in stationary single-phase conditions is shown in Fig. 3. Good agreement is found, giving confidence that the friction k-factors have been well evaluated.

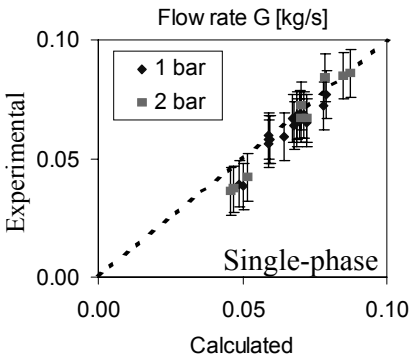

Fig. 3 Comparison between experimental and predicted flow rate in stationary single-phase conditions.

The results for transient conditions are reported in Fig. 4, where the time-dependent flow rates calculated with FLOCAL are compared with the experimental time-traces recorded at the CIRCUS facility. The time-traces were collected at a total heating power of 8 kW and to a system pressure of 1 bar. The temperature at the inlet of the heated section is gradually increased. As expected, FLOCAL slightly over-estimates the maximum flow rate achieved during the flow oscillations. As mentioned previously, this is due to the neglect of the feedback from the compressible volume in the steam dome. Despite this approximation, the general phenomenology and trends seem to be reproduced very well.

Increasing the inlet temperature, the model correctly predicts the transition from stable single-phase circulation (Fig. 4.a) to stable two-phase circulation (Fig. 4.h) passing through an intermediate unstable region (Fig. 4.b-g). As from the experiments, two main types of instabilities are predicted by the code: a first type, so-called intermittent natural circulation, in which single-phase and two-phase natural circulation alternate periodically (Fig. 4.b-f) and a second type of oscillation, so-called unstable two-phase circulation, during which the two-phase mixture is always present in the system and a sinusoidal-type flow oscillation is established (Fig. 4.g). The existence of an incubation period between two successive flow-rate peaks (Fig. 4.b-d) is also predicted by the model, though it is under-estimated. This issue will be discussed in more details in the following paragraph. In agreement with the experimental trend, the period of the oscillation predicted by the model decreases with increasing inlet temperature.

In Fig. 5 the time evolution of the void fraction along the vertical axis of the riser section is reported. Again the time traces were recorded at a total heating power of 8 kW and a system pressure of 1 bar. Different cases are shown corresponding to different temperatures at the inlet of the heated section. The magnitude of the void fraction is represented by means of contour plots. In Fig. 5 both simulated (left picture) and experimental (right picture) time traces are reported. The experimental void fraction is measured by means of conductive needle-probes [29] located at position T1 to T6 as

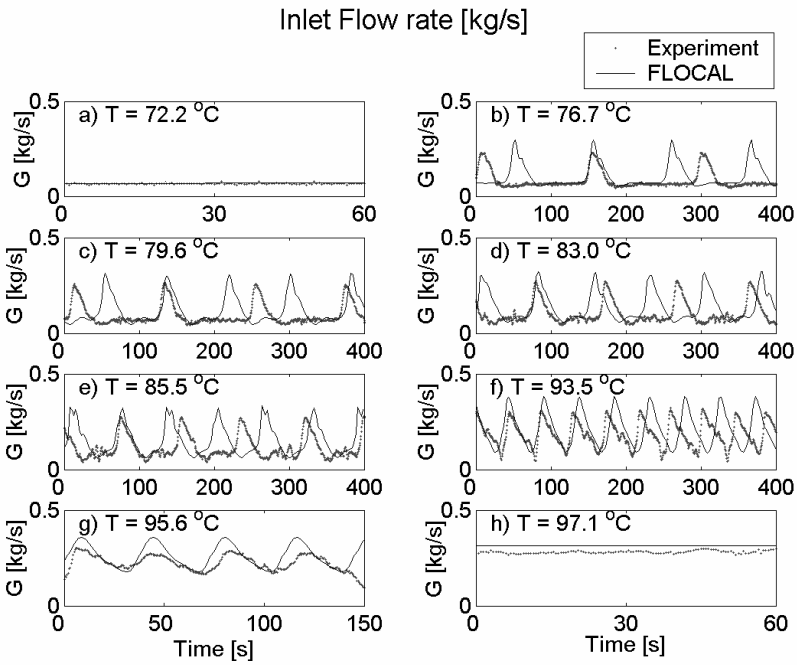

Fig. 4 Comparison between experimental flow-rate time traces and FLOCAL simulations (1 bar, 8 kW).

shown in Fig. 2. Also with regard to the void fraction good agreement is found between the model prediction and the experiments and the phenomenology is reproduced very well.

At low inlet temperatures (Fig. 5.a) flashing starts relatively high in the riser and later on the flashing front expands and propagates both in the upward and downward directions. As soon as the inlet temperature increases, voids are generated first in the heated section (subcooled boiling) below the riser inlet. These voids collapse in the riser (contributing to the heating up of the fluid) before flashing starts (Fig. 5.b-c). Increasing the inlet temperature flashing in the riser is directly triggered by the voids coming from the heated section (Fig. 5.d-e).

Experimental evidence of thermal non-equilibrium between liquid and vapour phase, as shown in (Fig. 5.b-d), can be verified even better by a careful analysis of the needle-probes' signals. As already mentioned, these sensors are able to measure at the same location void fraction (sampling frequency of 500 Hz) and fluid temperature (time constant of 17 ms).

In Fig. 6 the instantaneous local void fractions measured by the needle-probes along the vertical axis of the riser section are presented together with the corresponding temperatures. From the enlargement at the right side of the picture it is evident that temperature peaks occur concurrent with the passage of steam bubbles (detected as peaks in the void fraction).

Steam bubbles transported upwards encounter liquid which can be even more than 2°C colder than the steam. The thermal non-equilibrium between liquid and vapour phase is very pronounced when flashing is not yet developed. The magnitude of the temperature difference between liquid and vapour decreases during the development of void production due to flashing until thermal-equilibrium is reached.

A quantitative comparison between experimental and model results is shown in Fig. 7 to Fig. 10. In Fig. 7 (left) the oscillation period is reported against the average flow rate. Here H indicates the height of the steam cushion present in the steam dome during the experiments. The findings of the experimental campaign at the CIRCUS facility support the idea that the relation between the two variables is merely a function of the geometry of the system and it is not influenced by pressure, heating power or inlet subcooling. This trend seems to be confirmed by the FLOCAL calculations.

In Fig. 7 (right) the relation between the driving pressure in the loop and the kinetic pressure is shown. All experimental points, both stable and unstable, lie approximately on a straight line passing through the origin.

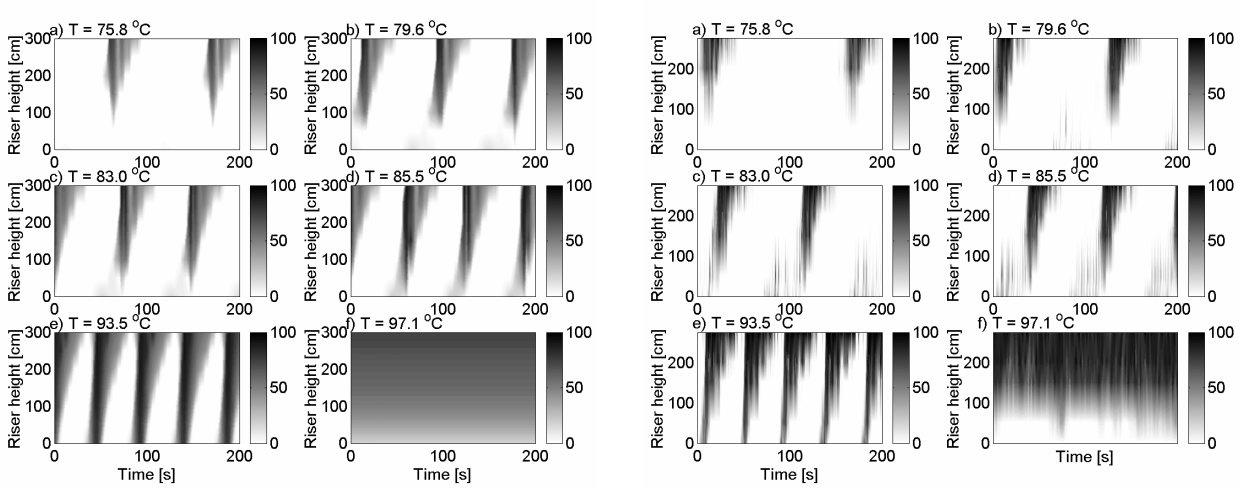

Fig. 5 Void-fraction evolution from FLOCAL simulations (left) and as measured with needle-probes at the CIRCUS facility (right). Vertical bars give the grey-scale coding for the void fraction (in percent).

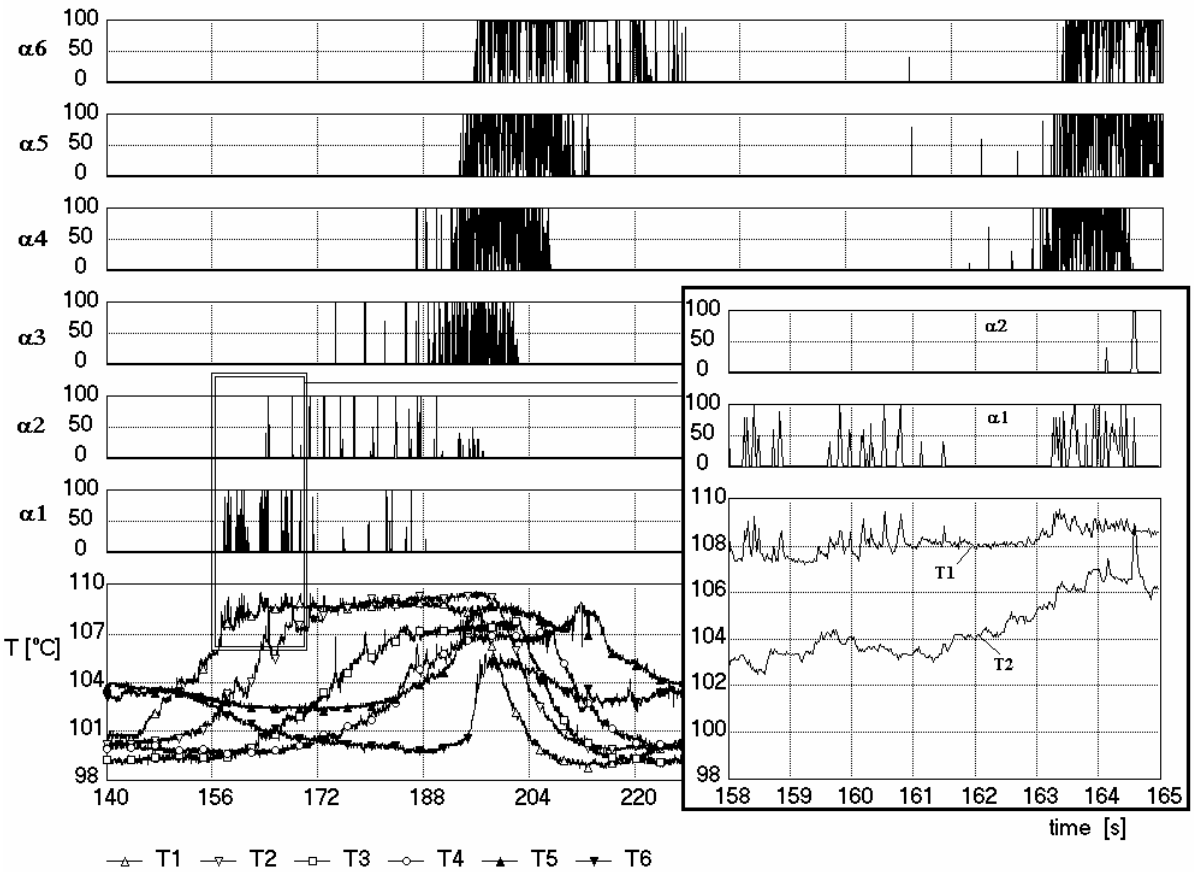

Fig. 6 Experimental evidence of thermal non-equilibrium between liquid and vapour phase.

In ref. [2] it was argued that the reason for this behaviour lies in the fact that driving pressure and friction are the major terms in the momentum balance of the loop, while inertia and acceleration pressure drops play a small role in the determination of flow magnitude. This argument has been confirmed by the FLOCAL calculations, since it is found that inertia and acceleration pressure drops are orders of magnitude smaller with respect to frictional and gravitational pressure drops. This effect is even more prominent at low inlet subcooling (i.e. high void fraction).

In Fig. 8 (left) the relation between minimum and maximum flow rate during a flashing-induced flow oscillation and the inlet subcooling is shown for the experiments and the model results (8 kW power, 1 bar system pressure). The calculated minimum flow rate

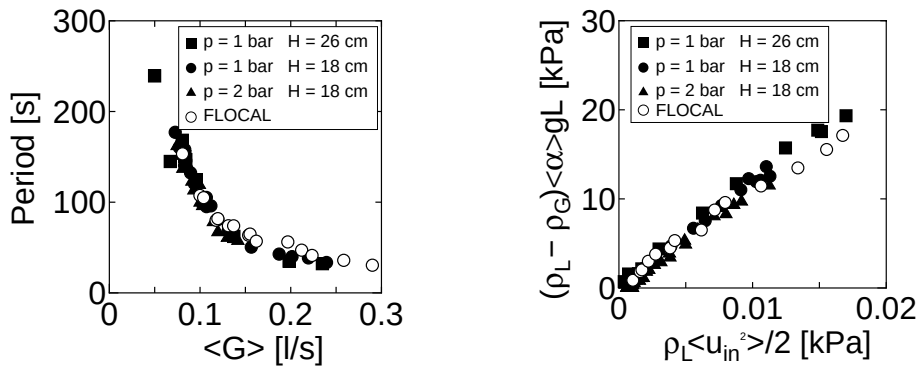

Fig. 7 Relation between oscillation period and average flow rate (left) and between driving and kinetic pressure (right).

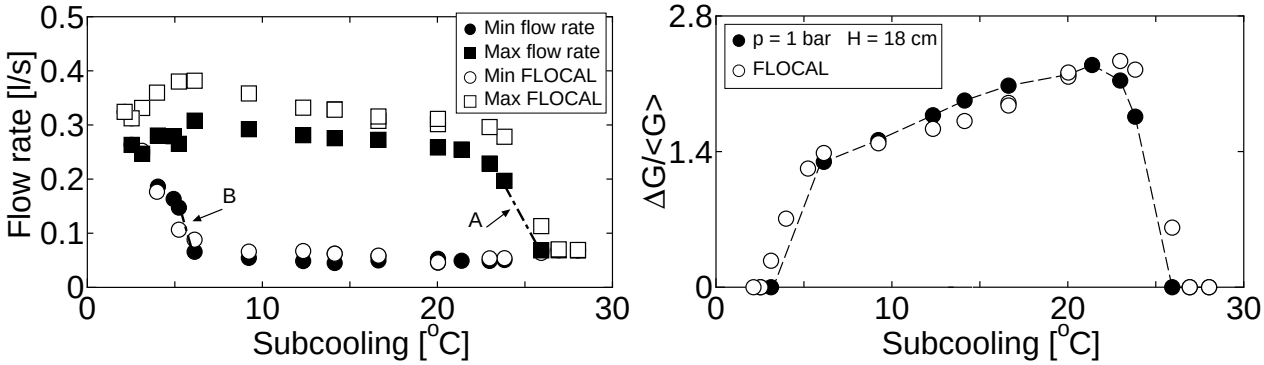

Fig. 8 Relation between maximum and minimum flow rate vs inlet subooling (left) and between relative amplitude of the flow oscillation and inlet subcooling.

matches very well the experimental values. The maximum flow rate is overestimated, this effect being caused by the boundary condition of constant pressure at riser outlet. Nevertheless, the transition A, from stable single-phase to unstable circulation, and the transition B, from intermittent circulation to unstable two-phase circulation, are well reproduced.

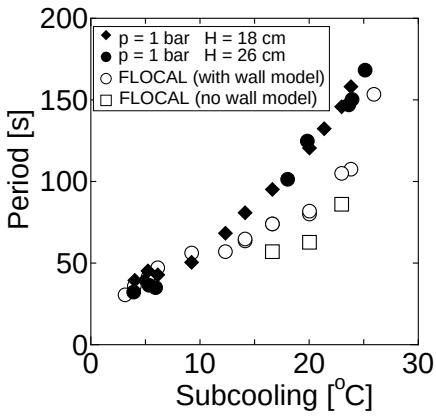

Fig. 9 Oscillation period vs subcooling.

In Fig. 8 (right) the relation between the relative amplitude of the flow oscillation and the inlet subcooling is reported, always for a total power of 8 kW and a system pressure of 1 bar. The subcooling range of instabilities (from 3°C to 25°C) is predicted perfectly. On the other hand, the very good agreement in predicting the relative amplitude of oscillation ΔG/<G> is misleading since it is due to the combination of the overestimation of maximum flow rate and underestimation of the oscillation period.

The relation between oscillation period and inlet subcooling is presented in Fig. 9 (8 kW, 1 bar). As already pointed out, in many cases the model under-estimates the oscillation period (from Fig. 3 it can be seen that is mainly the incubation period which is under-estimated rather than the duration of the flow peak caused by the flashing transient).

In particular, the oscillation period is very well predicted at low subcoolings (i.e. high flow rates and absence of single-phase circulation) and underestimated at high subcoolings (i.e. at low flow rates and presence of alternate single-phase/two-phase circulation). The reason could lie in both heat losses to the environment, neglected in the calculation presented here, and in the smearing of the temperature front during the single-phase circulation. This latter effect is caused by turbulent diffusion in presence of a

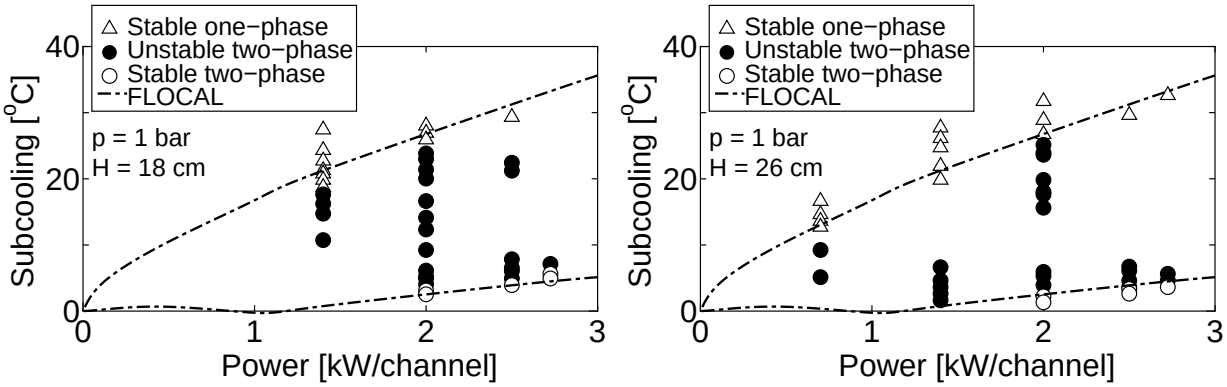

Fig. 10 Comparison between experimental and FLOCAL stability boundary.

negative temperature gradient along the vertical axis of the adiabatic section and it will be discussed in the next paragraph.

Calculations including heat losses have been performed with FLOCAL but, though they cause an increased incubation period, they do not justify the extent of under-estimation of the incubation period.

The strong effect of the energy accumulated in the heat structures, namely the walls of riser and heated section is clearly visible (Fig. 9, "no wall" calculations). Finally, in Fig. 10 the comparison between experimental and calculated stability boundary in the subcooling-power plane is reported. Good agreement is found.

5. TURBULENT DIFFUSION DUE TO TEMPERATURE GRADIENT

The energy balance considered in the original FLOCAL model has the form:

$$\frac{\partial \rho h}{\partial t} + \frac{\partial \rho u h}{\partial z} = q \tag{16}$$

In the adiabatic section $q=0$ (if heat transfer to the structures is not considered), thus in the single-phase region the temperature front is simply transported upward with velocity u. In reality, during the incubation period that precedes the occurrence of flashing, liquid at higher temperature coming from the heated section moves upward toward a region at lower temperature. The negative temperature gradient can cause turbulent mixing between the liquid layers because of buoyancy effects. This phenomenon is more significant at low velocities when the turbulent diffusive processes play an important role with respect to convective processes.

Experimental evidence of the smearing of the temperature front during flashing experiments at the CIRCUS facility can be deduced by analysing thermocouples signals. As shown in Fig. 2, the temperature is measured at six axial locations in the riser section. To study how the temperature front propagates along the riser section we first define a virtual z axis for each i-th temperature measurement:

$$z_i^*(t) = \int_{t_0}^{t} u_{inl}(t')\,dt' - z_i \tag{17}$$

where $u_{inl}(t)$ is the liquid velocity at the inlet of the test section and z_i is the distance of the i-th thermocouple from the inlet of the riser section (where the temperature T1 is measured. See Fig. 2). The time t_0 can be chosen arbitrarily. Assuming the liquid to be incompressible, the fluid velocity can be considered only time-dependent so that the virtual axis z^* in eq. (17) represents the space that would be travelled by a temperature wave moving with a velocity $u_{inl}(t)$. In Fig. 11 the temperatures measured along the riser section during a flashing cycle are presented (left) together with the corresponding void fraction (right) measured by means of needle-probes. Instead of the time-axis, the virtual z^*-axis is used. In case of pure transport, all the temperatures in the new reference system should rise and decrease in the same way (since the time shift due to transport has been eliminated by means of the change of coordinate system). On the contrary, from Fig. 11 (left) it is observed that the slope of the temperature rise is progressively decreasing along the riser (from T1 to T6). This slope change is observed when the temperature gradient is negative. During the

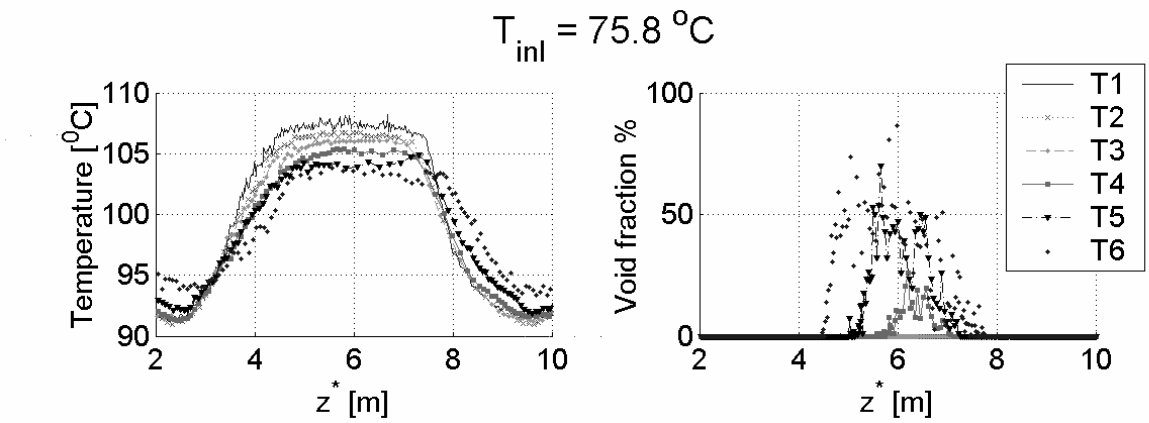

Fig. 11 Experimental evidence of mixing between temperature layers (power of 8 kW, pressure of 1 bar).

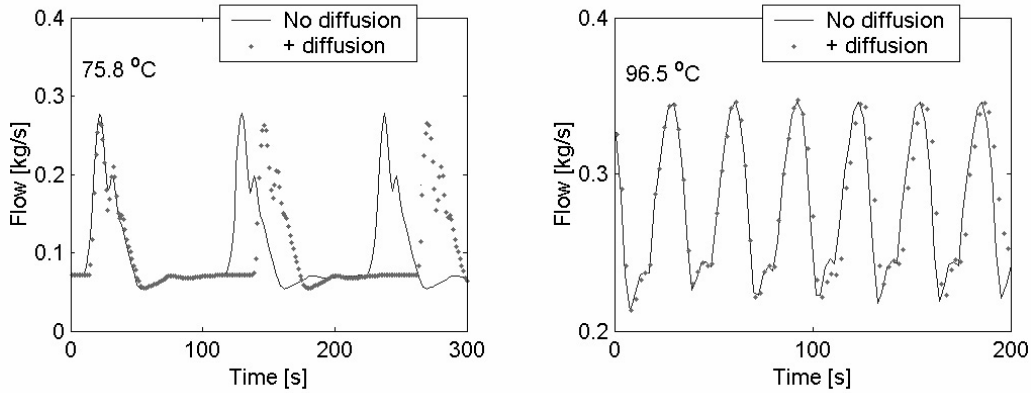

Fig. 12 Effect of diffusive term in the energy balance equation.

temperature drop instead, when the temperature gradient is positive, all the temperature measurements are superimposed with the exception of measurements T5 and T6 and in minor extent of T4. This is due to the fact that at location 4 to 6 void fraction has been produced (see Fig. 11 right) in which case the assumption of space-independent velocity does not hold and the definition of the virtual axis z^* loses its meaning.

The effect of turbulent mixing due to buoyancy effects in presence of a positive temperature gradient has been found also by CFD simulations at conditions representative of the measurements carried out at the CIRCUS facility. A very simple way to model this effect is to include a diffusive term in the energy balance (16) of the FLOCAL model as follows:

$$\frac{\partial \rho h}{\partial t} + \frac{\partial \rho w h}{\partial z} = q + \frac{\partial}{\partial z}\left(\nu \frac{\partial h}{\partial z} \right), \qquad (18)$$

The diffusive term will cause a smearing of the temperature front moving from the heated to the adiabatic section, causing a time delay in the flashing occurrence. The effect should become negligible when the convective term in the equation plays a major role.

A simple estimation for the diffusivity coefficient ν is given by [32]:

$$\nu \approx L^2 \sqrt{\frac{1}{T}\frac{\partial T}{\partial z} g}\ , \qquad (19)$$

where L is an appropriate scale length. At conditions typical of the CIRCUS facility the diffusivity is of the order of about $5*10^{-3}$ m^2/s.

The diffusivity is not constant, being a function of the temperature gradient, but an exact modelling of this effect goes beyond the scope of this work. Thus, a constant value of $5*10^{-3}$ m^2/s has been used in the FLOCAL model to study the effect of diffusivity on the period of flashing-induced flow oscillations. The coefficient is set to zero when void is present (in this case the diffusion term can be neglected with respect to the transport term) or when the temperature gradient is positive.

In the latter case, low-density fluid is above high-density fluid and the mixing of temperature layers will not occur because of density differences. The effect on the oscillation period is shown in Fig. 12 for high and low inlet subcooling.

As it can be seen, at high subcooling (Fig. 12 left) a considerable increase of the incubation period (i.e. of the oscillation period) is achieved if the diffusion term is considered in the energy balance. At low subcooling (Fig. 12 right) the effect is negligible. Thus, this phenomenon explains why the original FLOCAL model under-estimates the oscillation period at high inlet subcoolings, while it gives good predictions at low inlet subcoolings (see Fig. 9).

6. CONCLUSIONS

In the present paper a two-phase flow model has been presented which is able to cope with flashing-induced flow instabilities in natural circulation systems at low pressure conditions. Phenomena that had to be taken into account are:

- dependency of the thermodynamic properties on the local pressure;
- thermal non-equilibrium between liquid and vapour phases (i.e. subcooled boiling and liquid superheating);
- velocity slip between the two phases;
- thermal structures: they are found to play an important role for the correct determination of the incubation period between two consecutive flashing cycles;
- turbulent diffusion due to temperature gradient: it is found (both experimentally and by means of CFD and FLOCAL simulations) to play an important role in the determination of the incubation period at high subcooling.

In full agreement with experiments it is found that:

- the flashing front propagates simultaneously upward and downward, but with decreasing subcooling the downward propagation becomes less significant;
- temperature propagation in the riser section has a wavy character and inlet and outlet temperature in the riser are out-of-phase;
- two main types of instabilities occur: the first in which two-phase flow alternates with single-phase flow; the second in which two-phase flow is always present in the system, but the point of flashing onset changes periodically;
- the relation between oscillation period and average flow rate is geometry-dependent and independent of inlet subcooling, power or pressure. The relation found is in agreement with the experimental one;
- the relation between gravitational pressure head and inlet kinetic pressure is linear; the relation is also in good agreement with the experiments.

The onset of instability between single-phase and two-phase operation and the onset of two-phase flow stable circulation are well predicted.

Since the feedback mechanism of the steam dome has not been taken into account in the simulations, the maximum flow rate is slightly overestimated.

Gravitational and frictional pressure drops are found to be the major terms in the momentum balance for the determination of the amplitude of the flow oscillations, the acceleration and inertia pressure drops being orders of magnitude smaller.

The incubation period, which occurs at high subcoolings between two consecutive flashing cycles, is underestimated. The error is significantly reduced if heat structures are modelled for the core and the riser section and if turbulent diffusion due to negative temperature gradients is taken into account.

APPENDIX: NUMERICAL SCHEMES IN FLOCAL

The system of PDEs is reduced to a set of ODEs by dividing the heated and adiabatic section in axial meshes. All parameters are evaluated at the meshes borders and the heat sources for the energy equations are averaged values in the given mesh. The outlet of the heated section and the inlet of the riser form a single mesh point at which jump conditions are given. The downcomer is not discretized, as already mentioned, but is described by means of a lumped-parameter model.

The same time step is used for all equations and iterations and it is kept constant during the all calculation. Limitations on the time step are given by the characteristic times and period of the instabilities (the time step has to be smaller than these characteristic times) while the stability and accuracy of the solution are guaranteed by the iteration schemes and spatial discretization.

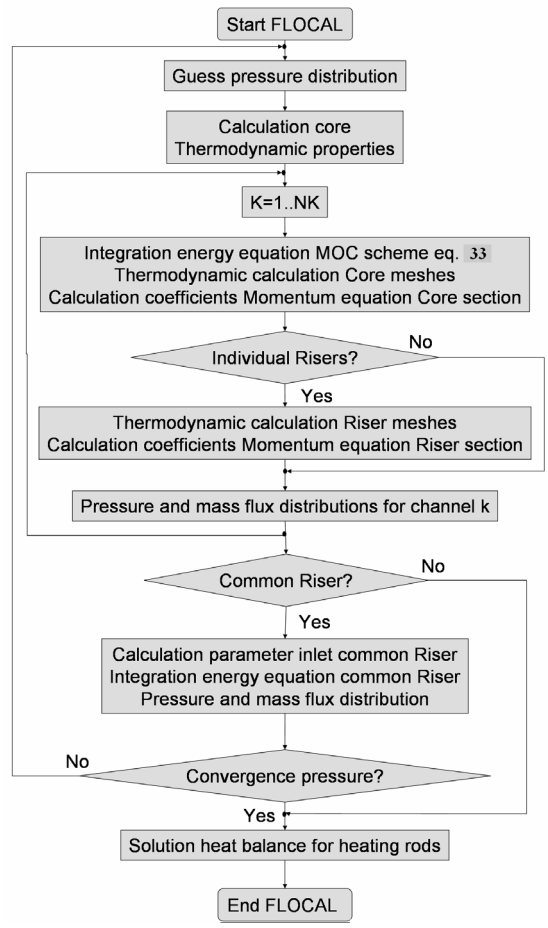

Fig. 13 Iterative scheme of the FLOCAL solver.

Pressure iteration

The calculation of mass flow and pressure distributions in the loop is performed iteratively in two steps. First the integral pressure drops balance is solved in the so-called external iteration. Then, in the so-called inner iteration, the mass flow distribution is calculated for the given pressure drop distribution.

In the external iteration the following set of non-linear equations has to be solved:

$$\Delta p_K\left(\dot{m}_K\right)+\Delta p_{ZS}\left(\dot{m}_1,...,\dot{m}_K,...\dot{m}_{NK}\right)=\Delta p_{FS} \qquad (20)$$

K=1,...NK

where Δp_{ZS} is the pressure drop across the common riser and Δp_K is the pressure drop across each coolant channel K (including individual riser section). This pressure drop has to be the same for each channel (transversal pressure gradients at inlet and outlet are neglected). The calculation of the pressure drop Δp_{FS} follows from equation (6).

In the external iteration a prediction value for the pressure drop $\Delta\tilde{p}_K$ is given, with which the mass flow distribution in the coolant channels is calculated (inner iteration) and on this basis Δp_{ZS} and Δp_{FS} are then evaluated. The iterative process continues until $\Delta\tilde{p}_K$ converges to Δp_K calculated from equation (20). For the iterative solution of the balance equation (20) in the non-stationary case, a good initial condition for the iteration is already available from the previous time step. The guess for the (m+1)-th iteration is based on:

$$\Delta\tilde{\mathrm{p}}_K^{(m+1)}=\theta\Delta\mathrm{p}_K^{(m)}+\left(1-\theta\right)\Delta\tilde{\mathrm{p}}_K^{(m)} \qquad (21)$$

and the iteration stops when the guessed pressure drop converges to the pressured drop calculated from equation (20). High efficiency of the iterative scheme is achieved with θ equal to 0.8 [1].

During the inner iteration the mass flow distribution inside the coolant channels is calculated for a given pressure drop Δp_K (solution of the momentum balance equation for each coolant channel). In stationary conditions the mass flow m_K is calculated with the method of the secants, while in non-stationary conditions the mass flow and pressure distributions are calculated together. The iteration scheme of the FLOCAL solver is shown in Fig. 13.

By a given pressure drop balance, the momentum and continuity equations are solved simultaneously to give the mass flow distribution. For the parallel heated sections the pressure drops across the section itself is given as boundary condition. For the riser section the mass flow at the inlet and the pressure at the outlet are given as boundary conditions; the iteration results in a new pressure drop and the pressure drop balance has to be verified again. In steady-state

conditions the integrated momentum balance equation for the K-th coolant channel is:

$$G_K^2\left[v_{I,N}-v_{I,0}+\sum_{i=1}^{N}\left(\frac{R_i}{2\rho_{F,i}}+\frac{R_{i-1}}{2\rho_{F,i-1}}\right)\right]+\frac{g}{2}\sum_{i=1}^{N}\left(\rho_i+\rho_{i-1}\right)=\Delta p_K \tag{22}$$

where R_i is the effective friction coefficient at the i-th mesh point, including both distributed and concentrated friction losses. Since the coefficients in equation (22) depend on the mass flow, the equation has to be solved iteratively and the method of the secants is applied.

For the solution of the non-stationary momentum and continuity equations the Mironov implicit differential scheme is used. The mass flow is calculated from the momentum equation and a correction is then derived on the basis of the continuity equation. Moreover a quasi-linearization is used to treat the quadratic terms in the momentum equation, which are present in the friction and acceleration pressure drops terms:

$$G^{2(K)}\sim 2G^{(K-1)}G^{(K)}-G^{2(K-1)} \tag{23}$$

The continuity and momentum equations are approximated according to the following differentiating scheme:

$$\frac{\rho_{i-1/2}^{n}-\rho_{i-1/2}^{n-1}}{\Delta t}+\frac{G_i^{n(k)}-G_{i-1}^{n(k)}}{\Delta z}=0 \tag{24}$$

$$\frac{G_{i-1/2}^{n(k)}-G_{i-1/2}^{n-1}}{\Delta t}+\frac{p_i^n-p_{i-1}^n}{\Delta z}+g\rho_{i-1/2}^n+\frac{2G_i^{n(k-1)}G_i^{n(k)}-G_i^{2n(k-1)}}{\Delta z}\left(\frac{R_i^n}{2\rho_{F,i}^n}+v_{I,i}^n\right)+\frac{2G_{i-1}^{n(k-1)}G_{i-1}^{n(k)}-G_{i-1}^{2n(k-1)}}{\Delta z}\left(\frac{R_{i-1}^n}{2\rho_{F,i-1}^n}+v_{I,i-1}^n\right)=0 \tag{25}$$

in which n relates to the time-step, i to the spatial mesh and k is the index of the pressure-drop iteration. For the values in the mesh-middle point *i-1/2* a linear interpolation is used. The following algebraic system of equations can be therefore derived:

$$p_i^n=p_{i-1}^n-a_{1i}G_i^{n(k)}+a_{2i}G_{i-1}^{n(k)}+b_{1i} \tag{26}$$

$$G_i^{n(k)}=G_{i-1}^{n(k)}-b_{2i} \tag{27}$$

The coefficients can be derived from equations (24) and (25). Including the so-called Ricatti-transformation:

$$p=Gr+s \tag{28}$$

in the system of equations (26) and (27), the following recursive system of equations for the coefficients r and s is found:

$$\begin{cases} r_{i-1}=r_i+a_{1i}-a_{2i} \\ s_{i-1}=s_i-b_{1i}-b_{2i}\left(r_i+a_{1i}\right) \end{cases} \tag{29}$$

for which the following boundary conditions hold:

$$r_N=0;\quad s_N=p_N;\quad G_0=\frac{p_0-s_0}{r_0},$$

where N stands for outlet and 0 for inlet of the integration domain respectively. The system of equations gives simultaneously the pressure and mass-flux distribution.

For the riser section the boundary conditions are different: the pressure and mass-flux distributions are evaluated on the basis of the given values at the entrance of the riser section itself. This case can be solved by successive application of the discretized continuity and momentum equations (24) and (25).

Considerable mathematical difficulties arise from the strongly non-linear coupling between momentum and continuity equations introduced by phase-slip models. To cope with this problem a predictor-corrector method is applied.

Predictor step:

- $\rho_{i-1/2}^{n(k-1/2)}$ is calculated on the base of $G_{i-1/2}^{n-1}$;
- $G_i^{n(k-1/2)}=G_{i-1}^{n(k-1/2)}-\frac{\Delta z}{\Delta t}\left(\rho_{i-1/2}^{n(k-1/2)}-\rho_{i-1/2}^{n-1}\right)$

Corrector-step:

- $\rho_{i-1/2}^{n(k)}$ is calculated on the base of $G_{i-1/2}^{n(k-1/2)}$
- $G_i^{n(k)}=G_i^{n(k-1/2)}-\frac{\Delta z}{\Delta t}\left(\rho_{i-1/2}^{n(k)}-\rho_{i-1/2}^{n(k-1/2)}\right)$

Energy and steam mass balance

The energy balance and the vapour mass balance equations are expressed in the characteristic form:

$$\frac{\partial y}{\partial t} + u\frac{\partial y}{\partial z} = \underline{q} \tag{30}$$

where the velocity u and the source term q are a function of the solution y. This non-linearity can be treated iteratively. These iterations are particularly important for the vapour balance since the source term (especially the re-condensation rate) is very sensitive to the void fraction and the solution can be strongly influenced by this dependence. For the iterations of the source terms in the void-fraction equation the method of the secants is used, that converges within 5 iterations. From experience it is known that at each spatial and time-step φ has to be iterated sufficiently correct, otherwise unphysical oscillations of the void fraction can be generated.

For the solution of hyperbolic differential equations the method of characteristics (MOC) is often used. This method is implemented also in FLOCAL for the solution of the energy balance.

The equation (30) is integrated inside a mesh along the characteristic function $u=dz/dt$:

$$y_{i+1}^{n+1} = y^* + \int_{t^*}^{t+\Delta t} \underline{q}_i(t')dt' \tag{31}$$

Applying a linear interpolation for y^* and substituting the integral of the source by means of the product between average and time interval:

$$\int_{t^*}^{t+\Delta t} \underline{q}_i(t')dt' = \begin{cases} \frac{\Delta t}{2}\left(\underline{q}_i^{n+1} + \underline{q}_i^{n}\right) & \mathrm{r} \le 1 \\ \frac{\Delta z_i}{u_{i+½}^{n+1}}\frac{1}{2}\left[\left(1 - \frac{\Delta z_i}{u_{i+½}^{n+1}\Delta t}\right)\underline{q}_i^{n+1} + \frac{\Delta z_i}{u_{i+½}^{n+1}\Delta t}\underline{q}_i^{n} + \underline{q}_i^{n+1}\right] & \mathrm{r} > 1 \end{cases} \tag{32}$$

the MOC for the equation (30) in the finite-difference approximation becomes:

$$\begin{cases} y_{i+1}^{n+1} = (1-r)\,y_{i+1}^{n} + r y_i^{n} + \frac{\Delta t}{2}\left(\underline{q}_i^{n+1} + \underline{q}_i^{n}\right) & r \le 1 \\ y_{i+1}^{n+1} = \frac{r-1}{r}y_i^{n+1} + \frac{1}{r}y_i^{n} + \frac{\Delta t}{2r}\left(\frac{2r-1}{r}\underline{q}_i^{n+1} + \frac{1}{r}\underline{q}_i^{n}\right) & r > 1 \end{cases} \tag{33}$$

This scheme can be seen as a 4-points-MOC. The scheme has good characteristics when the Courant number, defined as:

$$r = u_{i+½}^{n+½}\frac{\Delta z}{\Delta t}$$

is close to unity. However, if the velocity undergoes large changes, for fixed Δt and Δz, the parameter r can significantly differ from unity.

From numerical investigations [1] it has been shown that large deviations of the Courant number from unity, using the 4-points MOC, can give rise to accuracy problems (the perturbations at the inlet of the channel are strongly damped) and can lead to a wrong evaluation of the stability behaviour of a system.

One possibility to avoid this problem is to control the spatial- or time-steps such that r~1 is always satisfied. In FLOCAL an artificial control of the spatial step is applied (Lagrange-MOC). For each time step a Δz* is calculated, so that

$$r^* \equiv u\frac{\Delta t}{\Delta z^*} = 1$$

The algorithm proceeds as follows:

1) integration of equation (30) in a spatial mesh along the characteristic function

$$\begin{cases} y_{i+1}^{n+1} = y_i^* + \frac{t^{n+1} - t_i^*}{2}\left(\underline{q}_i^{n+1} + \underline{q}_i^*\right) \\ t_i^* = t^{n+1} - \frac{\Delta z}{u_{i+½}^{n+1}} \end{cases}$$

in which the source term is linearly interpolated:

$$\underline{q}_i^* = \frac{t^{n+1} - t_i^*}{\Delta t}\underline{q}_i^{n} + \frac{t_i^* - t^{n}}{\Delta t}\underline{q}_i^{n+1}$$

2) for the successive mesh point it follows:

$$\begin{cases} y_i^* = y_{i-1}^* + \dfrac{t_i^* - t_{i-1}^*}{2}\left(\underline{q}_i^* + \underline{q}_{i-1}^*\right) \\ t_{i-1}^* = t_i^* - \dfrac{\Delta z}{u_{i-1/2}^*} \\ u_{i-1/2}^* = \dfrac{t^{n+1} - t_{i-1}^*}{\Delta t} u_{i-1/2}^n + \dfrac{t_i^* - t^n}{\Delta t} u_{i-1/2}^{n+1} \end{cases}$$

3) at the beginning of the characteristic function and in correspondence with r<1 the Lax-Wendroff scheme is used. This is a scheme of the second order that leads to:

$$y_i^{n+1} = y_i^n + \Delta t \left(\frac{\partial y}{\partial t}\right)_i^n + \int_{t^n}^{t^{n+1}} \underline{q}_i dt$$

With the transformations:

$$\begin{cases} \dfrac{\partial y}{\partial t} = -u \dfrac{\partial y}{\partial z} \\ \dfrac{\partial^2 y}{\partial t^2} = -\dfrac{\partial}{\partial t}\left(u \dfrac{\partial y}{\partial z}\right) = -\dfrac{\partial u}{\partial t}\dfrac{\partial y}{\partial z} - u \dfrac{\partial}{\partial z}\dfrac{\partial y}{\partial t} = \\ \qquad -\dfrac{\partial u}{\partial t}\dfrac{\partial y}{\partial z} + u \dfrac{\partial}{\partial z} u \dfrac{\partial y}{\partial z} \end{cases}$$

the following expression is obtained:

$$y_i^{n+1} = y_i^n - u_i^n \frac{1}{2}\frac{\Delta t}{\Delta z}\left(y_{i+1}^n - y_i^n\right) - \frac{1}{4}\frac{\Delta t}{\Delta z}\left(u_i^{n+1} - u_i^n\right)\left(y_{i+1}^n - y_{i-1}^n\right)$$
$$+ \frac{1}{2}\left(\frac{\Delta t}{\Delta z}\right)^2 u_i^n \left[u_{i+1/2}^n\left(y_{i+1}^n - y_i^n\right) - u_{i-1/2}^n\left(y_i^n - y_{i-1}^n\right)\right] + \Delta t \underline{q}_i^{n+1/2}$$

that can be written as:

$$\begin{cases} y_i^{n+1} = a_i^n y_{i+1}^n + b_i^n y_i^n + c_i^n y_{i-1}^n + \Delta t \underline{q}_i^{n+1/2} \\ a_i^n = \dfrac{1}{4}\left[\left(\dfrac{\Delta t}{\Delta z}\right)^2 u_i^n\left(u_{i+1}^n + u_i^n\right) - \dfrac{\Delta t}{\Delta z}\left(u_i^n + u_i^{n+1}\right)\right] \\ b_i^n = 1 - \dfrac{1}{4}\left(\dfrac{\Delta t}{\Delta z}\right)^2 u_i^n\left(u_{i+1}^n + 2u_i^n + u_{i-1}^n\right) \\ c_i^n = \dfrac{1}{4}\left[\left(\dfrac{\Delta t}{\Delta z}\right)^2 u_i^n\left(u_i^n + u_{i-1}^n\right) + \dfrac{\Delta t}{\Delta z}\left(u_i^n + u_i^{n+1}\right)\right] \end{cases} \tag{34}$$

The Lax-Wendroff scheme has a higher order of accuracy and is stable also for r<1. Combining it with the methods of characteristics in case of r>1 a stable and sufficiently accurate solution is guaranteed even when the criterion r~1 is not satisfied.

NOMENCLATURE

A	flow area	m^2
c_p	heat capacity	$J\ kg^{-1}\ K^{-1}$
C_0	distribution parameter	-
g	gravity acceleration	$m\ s^{-2}$
G	mass flux	$kg\ m^{-2}\ s^{-1}$
h	enthalpy	$J\ kg^{-1}$
H	height	m
L	length	m
m	mass flow	$kg\ s^{-1}$
p	pressure	$kg\ m^{-1}\ s^{-2}$
Q	source of power density	$W\ m^{-3}$
S	slip-ratio	-
t	time	s
u	velocity	$m\ s^{-1}$
x	quality	-
z	spatial coordinate	m
Greek symbols		
α	heat transfer coefficient	$W\ m^{-2}\ K^{-1}$
φ	void fraction	-
λ	thermal conductivity	$W\ m^{-1}\ K^{-1}$
μ	condensation/evaporation rate	$kg\ m^{-3}\ s^{-1}$
ν	thermal diffusivity	$m^{-2}\ s^{-1}$
ρ	density	$kg\ m^{-3}$

Subscripts

G	vapour
F	liquid
R	riser
W	wall

ACKNOWLEDGMENT
The work presented has been partially sponsored within the EU Framework Program, NACUSP project, FIKS-CT2000-00041.

REFERENCES

1. U. ROHDE, "Ein teoretisches Modell fur Zweiphasen-stromungen in wassergekulthen Kernreaktoren und seine Anwendung zur Analyse des Naturumlaufs im Heizreaktor AST-500", Ph.D. dissertation, Akademie der Wissenschaften der DDR, Dresden (1986).
2. A. MANERA, T.H.J.J. VAN DER HAGEN, 2002, "Stability of natural-circulation-cooled Boiling Water Reactor during Startup: Experimental Results", *Nuclear Technology*, **143** (2003).
3. Y.K. CHEUNG, B.S. SHIRALKAR, A.S. RAO, "Design Evolution of Natural circulation in ESBWR", *6th Int. Conf. on Nuclear Engineering ICONE-6*, May 10-15, San Diego, USA (1998).
4. E. WISSLER, H.S. ISBIN, N.R. AMUDSON, "Oscillatory Behavior of a Two-phase Natural-circulation Loop", *A.I.Ch.E.J.* Vol. **2**, No. 2, pp. 157-162 (1956).
5. C. SCHUSTER, A. ELLINGER, J. KNORR, "Analysis of Flow Instabilities at the Natural Circulation Loop DANTON with regards to Non-linear Effects," *Heat and Mass Transfer,* **36**, 557 (2000).
6. M. ARITOMI, J.H. CHIANG, T. NAKAHASHI, M. WATARUM, M. MORI, "Fundamental Study on Thermo-hydraulics During Start-up in Natural Circulation Boiling Water Reactors (I)," *J. Nucl. Sci. Technol.,* **29**, *7*, 631 (1992).
7. M. FURUYA, F. INADA, A. YASUO, "A Study on Thermalhydraulic Instability of a Boiling Natural Circulation Loop with a Chimney (Part II. Experimental Approach to Clarify the Flow Instability in Detail)," *Heat Transfer - Japanese Research,* **24**, *7*, 577 (1995).
8. S.Y. JIANG, YAO, J.H. BO, S.R. WU, "Experimental Simulation Study on Start-up of the 5 MW Nuclear Heating Reactor," *Nucl. Eng. Des.,* **158**, 111 (1995).
9. J.M. KIM, S.Y. LEE, "Experimental Observation of Flow Instability in a Semi-closed Two-phase Natural Circulation Loop," *Nucl. Eng. Des.,* **196**, 359 (2000).
10. S.R. WU, H.J. JIA, S.Y. JIANG, Y.J. ZHIANG, "Investigation on Two-phase Flow Stability in a Natural Circulation System," *Kerntechnik.,* **65**, *5-6*, 222 (2000).
11. F. INADA, M. FURUYA, A. YASUO, "Thermo-hydraulic instability of boiling natural circulation loop induced by flashing (analytical consideration)," *Nucl. Eng. Des.,* **200**, 187-199 (2000).
12. D.D.B. VAN BRAGT, W.J.M. DE KRUIJF, A. MANERA, T.H.J.J. VAN DER HAGEN, H. VAN DAM, "Analytical modeling of flashing-induced instabilities in a natural circulation cooled boiling water reactor," *Nucl. Eng. Des.*, **215**, 87-98 (2002).
13. T. SAWAI, M. KAJI, S. NAKANISHI, S. YAMAUCHI, "Stability and non-linear dynamics in natural circulation loop at low pressure condition", 2nd *Int. Symp. on Two-Phase Flow Modelling and Experimentation*, May 23-26, Pisa, Italy, 363-369 (1999).
14. M. FURUYA, F. INADA, A. YASUO, "A Study on Thermalhydraulic Instability of a Boiling Natural Circulation Loop with a Chimney (Part II. Experimental Approach to Clarify the Flow Instability in Detail)," *Heat Transfer - Japanese Research,* **24**, *7*, 577 (1995).
15. A. MANERA, H.-M. PRASSER, U. ROHDE, T.H.J.J. VAN DER HAGEN, "Assessment of void-fraction correlations and drift-flux models applied to stationary and transient flashing flow in a vertical pipe", *to be submitted* (2003).
16. V. CHATOORGOON, 1986, "SPORTS – A simple non-linear thermalhydraulic stability code", *Nucl. Eng. Des.*, **93**, 51-67 (1986).
17. H.S. CHENG, H.J. KHAN, U.S. ROHATGI, "Simulation of SBWR Startup Transient and Stability", BNL-65535 (1998).

18. J. PANIAGUA, U.S. ROTHAGI, V. PRASAD, "Modeling of Thermal Hydraulic Instabilities in Single Heated Channel Loop During Startup Transients," *Nucl. Eng. Des.*, **193**, 207 (1999).
19. S.B. WANG, J.Y. WU, C. PAN, W.K. LIN, "Thermal-hydraulic Oscillations in a Low Pressure Two-phase Natural Circulation Loop at Low Pressures and High Inlet Subcoolings," *Proc. of 4th Int. Topical Meetg. Nuclear Thermal Hydraulics, Operations and Safety*, April 5-8, Taipei, Taiwan (1994).
20. N. HOYER, 1994, "MONA, a 7-Equation Transient Two-Phase Flow Model for LWR Dynamics," *Proc. of Int. Conf. on New Trends in Nuclear System Thermohydraulics,* May 30-June 2, Pisa, Italy (1994).
21. T. SENGSTAG, "Pre-test calculations MONA-2-2 on the CIRCUS tests", NACUSP FIKS-CT-2000-00041, report D9a (2002).
22. Y.K. CHEUNG, A.S. RAO, "Startup Simulation of a Natural Circulation Plant - ESBWR," *Proc. of 8th Int. Conf. on Nucl. Eng. ICONE-8*, April 2-6, Baltimore, MD, USA (2000).
23. J.G.M. ANDERSEN, F. INADA, L.A. KLEBANOV, "TRACG Analyses of Flashing Instability During Start-up," *Proc. of 3rd Int. Conf. on Nucl. Eng. ICONE-3*, April 23-27, Kyoto, Japan (1995).
24. I. TISELJ, G. CERNE, "Some Comments on the Behaviour of RELAP5 Numerical Scheme at Very Small Time Step", *Nucl. Eng. Des.*, **134**, 3 (2000).
25. "Thermal-hydraulic relationships for advanced water cooled reactors", IAEA-TECDOC-1203 (2001).
26. A. MANERA, H.-M. PRASSER, U. ROHDE, T.H.J.J. VAN DER HAGEN, "Assessment of void-fraction correlations and drift-flux models applied to stationary and transient flashing flow in a vertical pipe", *to be submitted* (2003).
27. J.E. KELLY, M.S. KAZIMI, *Nucl. Sci. Eng.* **81**, 3 (1982).
28. J.HUHN, J.WOLF, "Zweiphasen-strömung", VEB Fachbuchverlag Leipzig (1975).
29. H.-M. PRASSER, A. BÖTTGER, J. ZSCHAU, T. GOCHT, "Needle-shape conductivity probes with integrated micro-thermocouple and their application in rapid condensation experiments with non-condensable gases", *Kerntechnik* **68**, 114 (2003).
30. G.B. WALLIS, J.H. HEASLY, "Oscillations in Two-Phase Flow Systems", *J. Heat Transfer*, **83**, 363-369 (1964).
31. I.E. IDELCHIK, "Handbook of hydraulic resistance", 2nd ed., Washington Hemisphere (1986).
32. E.E.. ZUKOSKI, "A review of flows driven by natural convection in adiabatic shafts," NIST-GCR-95-679, Caltech (1995).

ELSEVIER

Nuclear Engineering and Design 215 (2002) 87–98

Nuclear Engineering and Design

www.elsevier.com/locate/nucengdes

Analytical modeling of flashing-induced instabilities in a natural circulation cooled boiling water reactor

D.D.B. Van Bragt, W.J.M. De Kruijf *, A. Manera, T.H.J.J. Van Der Hagen, H. Van Dam

Interfaculty Reactor Institute, Delft University of Technology, Mekelweg 15, 2629 JB Delft, The Netherlands

Abstract

A dynamic model for natural circulation boiling water reactors (BWRs) under low-pressure conditions is developed. The motivation for this theoretical research is the concern about the stability of natural circulation BWRs during the low-pressure reactor start-up phase. There is experimental and theoretical evidence for the occurrence of void flashing in the unheated riser under these conditions. This flashing effect is included in the differential (homogeneous equilibrium) equations for two-phase flow. The differential equations were integrated over axial two-phase nodes, to derive a nodal time-domain model. The dynamic behavior of the interface between the one and two-phase regions is approximated with a linearized model. All model equations are presented in a dimensionless form. As an example the stability characteristics of the Dutch Dodewaard reactor at low pressure are determined.

1. Introduction

The stability of natural circulation BWRs under start-up conditions has been recognized in recent years as an important issue that needs to be considered in the design of new reactor types. The key issue under low-pressure startup conditions is the phenomenon of void 'flashing' in the riser. The term 'flashing' refers to the occurrence of boiling in a natural circulation BWR, due to the decrease of hydrostatic pressure and saturation enthalpy along the flow path, when the coolant flows upwards through the core and riser sections. Since the saturation enthalpy is strongly dependent on the pressure at pressures lower than 20 bar, see Fig. 1, the influence of flashing becomes especially important under low-pressure conditions.

Dynamic instabilities can be induced by flashing under these circumstances, since the slope of the void fraction-flow quality curve is very steep under low power and pressure conditions, i.e. a small increase of the flow quality induces a large increase of the riser void fraction. As a result, the driving force of the convection and the natural circulation flow increase. The flow quality in the core and the riser will consequently decrease, this way providing a thermohydraulic feedback mechanism that can cause self-sustained oscillations. Since void flashing in the riser directly affects the gravitational pressure drop over this section, it

* Corresponding author.
E-mail address: kruijf@iri.tudelft.nl (W.J.M. De Kruijf).

0029-5493/02/$ - see front matter
PII: S0029-5493(02)00043-2

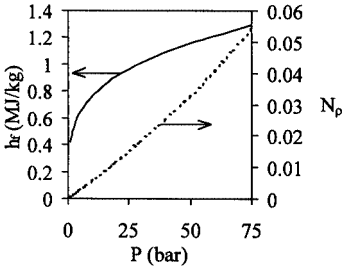

Fig. 1. Influence of the pressure level on the saturated liquid enthalpy h_f and the vapor to liquid density ratio N_ρ.

can be classified as a 'Type-I' density-wave instability phenomenon (Fukuda and Kobori, 1979).

2. Previous research on flashing

The impact of void flashing on reactor stability is the incentive to recent studies of the stability of natural circulation BWRs under low-pressure start-up conditions. A short summary of the main research activities in this new and quickly developing field is provided in this section.

The Central Research Institute of Electric Power Industry (CRIEPI) in Japan has constructed a low-pressure thermohydraulic test facility, which has been used to simulate the startup of the Simplified BWR (SBWR) concept of General Electric (GE) (Inada et al., 1995; Furuya et al., 1995; Andersen and Klebanov, 1995).

The Chinese Institute of Nuclear Energy and Technology (INET) has developed a 5 MW nuclear test reactor for district heating, which is in operation since 1989 (Wang et al., 1990). This natural circulation reactor operates at a low pressure (15 bar), low steam quality (less than 1% at the core exit), and is cooled by natural circulation. A test loop (HRTL-5), simulating the design and geometry of this reactor, was built at INET to simulate the thermohydraulic stability of the nuclear test reactor (Jiang and Emendörfer, 1993; Jiang et al., 1997; Jiang and Emendörfer, 1996).

The first in-core measurements of the startup stability of a natural circulation BWR were performed in the Dutch Dodewaard BWR. A team of specialists from several Dutch institutes has performed measurements during the startup phase of this reactor at the beginning of cycles 23–26 (Van der Hagen et al., 1996). The Dodewaard start-up of cycle 23 was simulated successfully with the TRACG code by Wouters et al. (1996). However, during this particular measurement session only minor oscillations were measured (and predicted by TRACG). The first significant decrease of low-pressure stability was observed during the startup of cycle 25 (Van der Hagen et al., 1997), but these experimental data have not yet been analyzed quantitatively with a BWR stability code that includes a flashing model.

At the Delft University of Technology, the test facility CIRCUS has been built to study the startup stability of a natural circulation BWR. The design parameters for this facility have been based on the Dodewaard reactor. The first results obtained with this facility have been presented (De Kruijf et al., 1999; Manera et al., 2000). Previously, a stability model for natural circulation BWRs had been developed (Van Bragt and Van der Hagen, 1998a; Van Bragt, 1998). This model is now extended with a description of the flashing effect. This extended model can be used as a powerful analytical tool to gain more physical insight into the complicated flashing phenomenon.

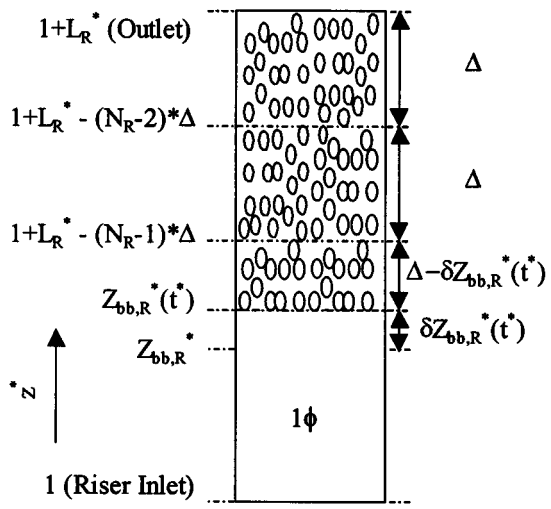

Fig. 2. Nodalization scheme for the riser section, if out-of-core boiling occurs. A three-node scheme ($N_R = 3$) is shown.

3. Model

Our theoretical flashing model is developed using the one-dimensional homogeneous equilibrium mixture (HEM) equations for two-phase flow. We also employed these equations in the development of the high-pressure model (Van Bragt and Van der Hagen, 1998a). The decrease of the liquid saturation enthalpy along the flow path in the core and riser is, however, neglected in that model. Inada and Ohkawa (1994) included flashing effects in the HEM model for two-phase flow by assuming that the liquid saturation enthalpy is linearly dependent on the local pressure. All other fluid properties were assumed to be independent of the pressure. The non-dimensional differential equations which Inada and Ohkawa used, based on these assumptions, are the starting point of our flashing model. Precise definitions of pressure-dependent dimensionless numbers and variables, like the Zuber number and the subcooling number, are provided in Appendix B. Dimensionless variables are denoted with an asterisk. If time-dependence is not indicated, the steady-state value of a variable is denoted. The axial power profile is assumed to be flat, to simplify the analysis.

The dimensionless continuity equation for the two-phase region is (Inada and Ohkawa, 1994):

$$\frac{\partial}{\partial t^*}\,[1\ -\alpha(z^*,t^*)+N_\rho\alpha(z^*,t^*)]+\frac{\partial M^*(z^*,t^*)}{\partial z^*}=0 \tag{1}$$

The dimensionless energy equation for homogeneous two-phase flow can be written as:

$$\begin{aligned}&\frac{\partial}{\partial t^*}\{(1-N_\rho)\alpha(z^*,t^*)\\&-N_{\text{flash}}h_{\text{f}}^*(z^*,t^*)[1-\alpha(z^*,t^*)]\}\\&+\frac{\partial}{\partial z^*}\left\{\frac{1-N_\rho}{N_\rho}\chi(z^*,t^*)M^*(z^*,t^*)\right.\\&\left.-N_{\text{flash}}h_{\text{f}}^*(z^*,t^*)[1-\chi(z^*,t^*)]M^*(z^*,t^*)\right\}\\&=N_{\text{Zu}}q'^*(t^*)\end{aligned} \tag{2}$$

The void production due to flashing is incorporated in the dimensionless flashing number N_{flash}. This number is equal to the difference between the dimensionless subcooling of the inlet fluid with respect to the saturated liquid enthalpy at the *core inlet* and the dimensionless subcooling of the inlet fluid with respect to the saturated liquid enthalpy at the *riser exit*, see Appendix B. When flashing is neglected, i.e. when the saturated liquid enthalpy is constant over the assembly height, these two dimensionless numbers are equal and the flashing number becomes equal to zero. The differential momentum equation for the boiling region becomes:

$$\begin{aligned}&\frac{\partial M^*(z^*,t^*)}{\partial t^*}+\frac{\partial}{\partial z^*}\{[1+(1/N_\rho-1)\chi(z^*,t^*)]M^{*2}(z^*,t^*)\}+\frac{1}{N_{\text{Fr}}}[1-\alpha(z^*,t^*)+N_\rho\alpha(z^*,t^*)]\\&+\Lambda[1+(1/N_\rho-1)\chi(z^*,t^*)]M^{*2}(z^*,t^*)+\frac{\partial}{\partial z^*}\sum_j\left\{\frac{1}{2}k_j[1+(1/N_\rho-1)\chi(z^*,t^*)]M^{*2}(z^*,t^*)\delta(z^*-z_j^*)\right\}\\&=-\frac{\partial P^*(z^*,t^*)}{\partial z^*}\end{aligned} \tag{3}$$

The left hand side of Eq. (3) consists respectively of the differential inertial, accelerational, gravitational, frictional and local pressure losses. The differential momentum Eq. (3) is identical to the equation previously used in the model without flashing. The pressure drop terms used in the model without flashing (Van Bragt and Van der Hagen, 1998a) are, therefore, equally valid in this flashing model[1].

The following axial nodalization scheme is used in this low-pressure model. If the coolant reaches the boiling point before the core exit, the two-phase region in the core is treated as a single node

[1] The (small) accelerational and frictional pressure drops over the downcomer are added to the pressure losses at the core inlet, to simplify the analysis. Therefore a factor $\frac{1}{2}\frac{k_{D,i}}{A_{d,i}^{*2}}+\frac{1}{2}\left(\frac{1}{A_{d,e}^{*2}}-\frac{1}{A_{d,i}^{*2}}\right)$ is added to the core inlet friction coefficient $k_{\text{C,i}}$.

with a dimensionless length $1 - Z^*_{\mathrm{bb,C}}(t^*)$. The riser section is divided in N_{R} axial nodes of equal length $L^*_{\mathrm{R}}/N_{\mathrm{R}}$ if $Z^*_{\mathrm{bb}}(t^*) \leq 1$. Neglecting the flashing effect, this condition is always satisfied, and the same nodalization scheme as used in the model without flashing is applied. If $Z^*_{\mathrm{bb}}(t^*) > 1$, only out-of-core boiling occurs. The nodalization scheme shown in Fig. 2 is adopted in this case.

As an example, a three-node scheme is considered here. Applying another number of nodes is straightforward. The height of the first riser node in Fig. 2 is dependent on the transient position of the boiling boundary:

$$L^*_{\mathrm{R},1}(t^*) = \Delta - [Z^*_{\mathrm{bb,R}}(t^*) - Z^*_{\mathrm{bb,R}}],$$
$$\Delta \equiv \frac{1 + L^*_{\mathrm{R}} - Z^*_{\mathrm{bb,R}}}{N_{\mathrm{R}}} \tag{4}$$

A large increase of the boiling boundary position causes a significant reduction of the height of this node. It is important, therefore, to check whether $L^*_{\mathrm{R},1}(t^*)$ remains positive at all time during the transient calculations[2]. All other riser nodes in Eq. (2) have a fixed height Δ. The advantage of this nodalization scheme becomes clear when we integrate Eq. (1) over an arbitrary boiling node with boundaries $z^*_{n-1}(t^*)$ and $z^*_n(t^*)$ and with a dimensionless length $L^*_n(t^*) = z^*_n(t^*) - z^*_{n-1}(t^*)$:

$$\frac{\mathrm{d}\langle\alpha(t^*)\rangle_n}{\mathrm{d}t^*} = \frac{M^*_n(t^*) - M^*_{n-1}(t^*)}{L^*_n(t^*)(1-N_\rho)} - \frac{\langle\alpha(t^*)\rangle_n}{L^*_n(t^*)}\frac{\mathrm{d}L^*_n(t^*)}{\mathrm{d}t^*} + \frac{\alpha(z^*_n(t^*))}{L^*_n(t^*)}\frac{\mathrm{d}z^*_n(t^*)}{\mathrm{d}t^*} - \frac{\alpha(z^*_{n-1}(t^*))}{L^*_n(t^*)}\frac{\mathrm{d}z^*_{n-1}(t^*)}{\mathrm{d}t^*} \tag{5}$$

The quantities with a subscript $n-1$ are evaluated at the node 'inlet', while a subscript n denotes the node 'outlet'. Because either the node boundary is fixed or the local void fraction is zero, the third and fourth term on the right hand side of Eq. (5) are zero for all riser nodes. Because their node heights are fixed, the second term on the right hand side of Eq. (5) is zero for all riser nodes, except the first one, assuming that $Z^*_{\mathrm{bb}}(t^*) > 1$. If $Z^*_{\mathrm{bb}}(t^*) < 1$, all riser nodes have a fixed height, and the second term on the right hand side becomes zero for all riser nodes.

Integrating the differential energy Eq. (2) over a two-phase node, and simplifying the result by substituting Eq. (5), with the third and fourth term on the right hand side equal to zero, leads to:

$$M^*_n(t^*) = \frac{\left\{1 + \frac{N_{\mathrm{flash}}}{1-N_\rho}[\langle h^*_{\mathrm{f}}(t^*)\rangle_n - (1-N_\rho)h^*_{\mathrm{f},n-1}(t^*)] + \left[\frac{1-N_\rho}{N_\rho} + N_{\mathrm{flash}}h^*_{\mathrm{f},n-1}(t^*)\right]\chi_{n-1}(t^*)\right\}M^*_{n-1}(t^*) + \Gamma^*_n(t^*)}{1 + \frac{N_{\mathrm{flash}}}{1-N_\rho}[\langle h^*_{\mathrm{f}}(t^*)\rangle_n - (1-N_\rho)h^*_{\mathrm{f},n}(t^*)] + \left[\frac{1-N_\rho}{N_\rho} + N_{\mathrm{flash}}h^*_{\mathrm{f},n}(t^*)\right]\chi_n(t^*)},$$

$$\text{with } \Gamma^*_n(t^*) = q'^*(t^*)L^*_n(t^*)N_{\mathrm{Zu}} + N_{\mathrm{flash}}L^*_n(t^*)[1 - \langle\alpha(t^*)\rangle_n]\left(\frac{\mathrm{d}\langle h^*_f(t^*)\rangle_n}{\mathrm{d}t^*}\right) + N_{\mathrm{flash}}(\langle h^*_f(t^*)\rangle_n - h^*_{\mathrm{f},n-1}(t^*))\frac{\mathrm{d}L^*_n(t^*)}{\mathrm{d}t^*} \tag{6}$$

The saturation enthalpy $h^*_{\mathrm{f}}(t^*)$ in Eq. (6), defined in Eq. (B.1), is assumed to be linearly dependent on the local pressure (Inada and Ohkawa, 1994):

$$h^*_{\mathrm{f}}(t^*) = \frac{P^*(t^*) - P^*_{\mathrm{C,i}}(t^*)}{P^*_{\mathrm{R,e}}(t^*) - P^*_{\mathrm{C,i}}(t^*)} \tag{7}$$

This approximation is used because the pressure difference between the core inlet and the riser exit is smaller than 0.5 bar. A linear approximation of the saturation-enthalpy function over such a small pressure range is quite accurate, even in the low-pressure regime, see Fig. 3.

[2] If this restriction causes problems, an alternative nodalization scheme, for instance using N_{R} time-dependent riser nodes with equal length $(1 + L^*_{\mathrm{R}} - Z^*_{\mathrm{bb,R}}(t^*))/N_{\mathrm{R}}$ might be used.

The influence of the inertial pressure losses on the saturation enthalpy is neglected in this model. The pressure difference $P^*_{\mathrm{R,e}}(t^*) - P^*_{\mathrm{C,i}}(t^*)$ between the riser exit and core inlet is then equal to the gravitational pressure drop over the downcomer, when the minor frictional, local and accelerational pressure losses over the downcomer are also neglected. Assuming that the down-coming fluid is subcooled, as has been done in the model without flashing (Van Bragt and Van der Hagen, 1998a), this pressure difference becomes:

$$P^*_{\mathrm{R,e}}(t^*) - P^*_{\mathrm{C,i}}(t^*) = -\frac{1 + L^*_{\mathrm{R}}}{N_{\mathrm{Fr}}} \tag{8}$$

As a boundary condition, the pressure at the riser exit is assumed to be kept constant by the reactor pressure controller, so using Eq. (8) $P^*_{\mathrm{C,i}}(t^*)$ can be calculated.

The local pressure at the boiling boundary (the 'inlet' of the first boiling node) is then determined by integrating Eq. (3) over the one-phase regions in the core and the riser. Since the pressure drop over each two-phase node is a function of two-phase variables as the flow quality, the saturation enthalpy at the node 'exit' becomes a function of these variables, whereas according to Eq. (6) these variables are in their turn dependent on the saturation enthalpy. This leads to recursive equations, which are rather cumbersome in the numerical analysis. Therefore, it is assumed that the saturation enthalpy is a linear function of the axial position between the boiling boundary and the riser exit.

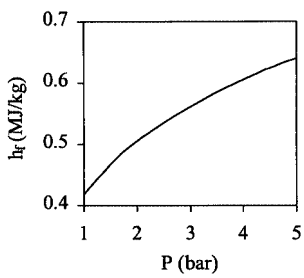

Fig. 3. The saturated liquid enthalpy h_{f} as a function of the pressure level, for pressures below 5 bar (cif. Fig. 1). A linear approximation of the h_{f}-function (over a pressure range of ~ 0.4 bar) is used in the model.

The local quality in Eq. (6) is assumed to increase or decrease linearly between the node inlet and outlet (this approximation has been applied as well in the model without flashing). The nodal void fraction then becomes:

$$\langle \alpha(t^*) \rangle_n = \frac{1}{1 - N_\rho} \left\{ 1 - \frac{1}{(1/N_\rho - 1)[\chi_n(t^*) - \chi_{n-1}(t^*)]} \times \ln\left[\frac{(1/N_\rho - 1)[\chi_n(t^*) - \chi_{n-1}(t^*)]}{1 + (1/N_\rho - 1)\chi_{n-1}(t^*)} + 1 \right] \right\} \tag{9}$$

A Taylor approximation of the logarithmic term in Eq. (9) is recommended to avoid a singularity in the steady state.

Finally, the complexity of Eq. (6) is reduced further by neglecting the term containing the time derivative of the nodal saturation enthalpy $h^*_{\mathrm{f}}(t^*)$. The magnitude of this term is proportional to the flashing number, and its importance, therefore, increases at lower pressures. The impact of this neglect is investigated numerically by Van Bragt, 1998(pp. 100–101).

The dimensionless length of the lowest two-phase node is determined by the instantaneous position of the boiling boundary. An evaluation of the one-phase region is necessary to determine the dynamic behavior of this boiling boundary. In fact, we can employ Eqs. (1)–(3) for the one-phase region as well, if we set the void fraction and flow quality equal to zero in these equations. Eq. (1) then shows that $M^*(Z^*_{\mathrm{bb,C}}, t^*) = M^*_{\mathrm{C,i}}(t^*)$, if $Z^*_{\mathrm{bb}} < 1$. Due to conservation of mass at the junction of the core and the riser we also find that $M^*(Z^*_{\mathrm{bb,R}}, t^*) = M^*_{\mathrm{C,i}}(t^*)/A^*_{\mathrm{R}}$, if $Z^*_{\mathrm{bb}} > 1$. Applying Eq. (2), the differential energy equation for the one-phase region becomes:

$$\frac{\partial h^*_{\mathrm{I}}(z^*, t^*)}{\partial t^*} + M^*(z^*, t^*) \frac{\partial h^*_{\mathrm{I}}(z^*, t^*)}{\partial z^*} = -\frac{N_{\mathrm{Zu}}}{N_{\mathrm{flash}}} q'^*(t^*) \tag{10}$$

Eq. (10) is used to determine whether the equilibrium position of the boiling boundary is lo-

cated in the core or in the riser section. *Assuming* that the saturation temperature is reached in the *core* section ($Z^*_{bb} < 1$), and neglecting the time-dependent term in Eq. (10), we integrate this equation from the core inlet to the boiling boundary:

$$h^*_l(Z^*_{bb}) = h^*_{l,C,i} - \frac{N_{Zu}}{N_{flash}} Z^*_{bb} \tag{11}$$

Integrating Eq. (3) over the one-phase region in the core, and substituting the pressure differential between the core inlet and the boiling boundary in Eq. (7), then yields the saturation enthalpy at the boiling boundary:

$$h^*_f(Z^*_{bb}) = \frac{N_{Fr}}{1 + L^*_R}[P^*_{C,i} - P^*(Z^*_{bb})] = \frac{N_{Fr}}{1 + L^*_R}\left(\frac{k_{C,i}}{2} + Z^*_{bb}\Lambda_C + \frac{Z^*_{bb}}{N_{Fr}}\right) \tag{12}$$

With the new parameter b_R, Eq. (11) and Eq. (12) can be generalized for an arbitrary position of the boiling boundary:

$$h^*_l(Z^*_{bb}) = h^*_{l_{C,i}} - \frac{N_{Zu}}{N_{flash}}[b_R + Z^*_{bb}(1 - b_R)], \quad \text{and}$$

$$h^*_f(Z^*_{bb}) = \frac{N_{Fr}}{1 + L^*_R}\left\{\frac{k_{C,i}}{2} + b_R\frac{k_{C,e}}{2} + \Lambda_C[b_R + (1 - b_R)Z^*_{bb}] + b_R\frac{(Z^*_{bb} - 1)\Lambda_R}{L^*_R A^{*2}_R} + \frac{Z^*_{bb}}{N_{Fr}}\right\} \tag{15}$$

Equating the liquid enthalpy with the saturation enthalpy in Eq. (15), and solving for the boiling boundary position, we arrive at:

$$Z^*_{bb} = \frac{N_{sub,C,i} - b_R N_{Zu} - (N_{Fr}/(1 + L^*_R))N_{flash}[((k_{C,i}/2) + b_R((k_{C,e}/2) + \Lambda_C - (\Lambda_R/(L^*_R A^{*2}_R)))]}{(1 - b_R)N_{Zu} + (N_{Fr}/(1 + L^*_R))N_{flash}[\Lambda_C(1 - b_R) + b_R(\Lambda_R/(L^*_R A^{*2}_R)) + (1/N_{Fr})]} \tag{16}$$

If the boiling boundary is indeed located in the core section (as has been assumed!), the fluid reaches the saturation enthalpy before the core outlet:

$$h^*_l[Z^*_{bb}(t^*)] = h^*_f[Z^*_{bb}(t^*)] \tag{13}$$

Substituting Eq. (11) and Eq. (12) in Eq. (13) then implies that:

$$0 \le \frac{N_{sub,C,i} - (k_{C,i}/2)(N_{Fr}/(1 + L^*_R))N_{flash}}{N_{Zu} + (\Lambda_C + (1/N_{Fr}))(N_{Fr}/(1 + L^*_R))N_{flash}} \le 1 \tag{14}$$

when the coolant starts to boil in the core. We now introduce the parameter b_R, which is equal to zero when Eq. (14) is satisfied, and equal to one if the condition in Eq. (14) is violated. The equilibrium position of the boiling boundary is thus located in the core section if $b_R = 0$, while $b_R = 1$, if only boiling in the riser occurs. We assume here that two-phase flow is present in at least part of the system. The occurrence of single-phase convection, when $h_{l,R,e} < h_{f,R,e}$ can be predicted with a simple criterion, which will be derived below.

Note that even when $b_R = 1$, the outcome of Eq. (16) can be smaller than unity. This apparent paradox occurs when the coolant temperature is slightly below the saturation temperature just before the core outlet, and starts to boil at the core exit, due to local core outlet pressure losses. These local core outlet pressure losses are not taken into account in Eq. (14). The boiling boundary position Z^*_{bb} is equal to unity in this particular case.

The boundary between the one- and two-phase regions in the operational N_{Zu}, N_{sub} space can be determined easily using Eq. (16). At the onset of boiling, the boiling boundary position will be located at the very end of the riser. Furthermore, the coolant flow rate (and, therefore, the Froude number) will diminish if the length of the two-phase region decreases. Setting $Z^*_{bb} = 1 + L^*_R$ and letting N_{Fr} approach zero in Eq. (16), we find that the boundary between the one- and two-phase regions is located at $N_{Zu} = N_{sub,C,i} - N_{flash}$. Two-phase flow will thus exist if $N_{Zu} > N_{sub,C,i} - N_{flash}$. This criterion suggests that two-phase flow can exist if the power level and, therefore, the Zuber number, is equal to zero, provided that $N_{sub,C,i} < N_{flash}$. This apparent paradox is avoided, however,

because the latter condition is never satisfied. Assume, for instance, that the coolant enthalpy at the *core inlet* is equal to the saturated liquid enthalpy at the *riser exit*. The core-inlet subcooling is then equal to $(h_{\mathrm{f,C,i}} - h_{\mathrm{f,R,e}})(\rho_{\mathrm{f,C,i}} - \rho_{\mathrm{g,C,i}})/(h_{\mathrm{fg,C,i}}\rho_{\mathrm{g,C,i}}) = N_{\mathrm{flash}}$. Taking the effect of the added feedwater into account, it is clear that $N_{\mathrm{sub,C,i}} \geq N_{\mathrm{flash}}$. The influence of the system pressure and the feedwater flow on the core inlet subcooling has been taken into account in a parametric study (Van Bragt, 1998, pp. 93–98).

The dynamic behavior of the boiling boundary is approximated with a linearized model. Perturbing and Laplace transforming Eq. (10) yields:

$$s^*\delta h_{\mathrm{l}}^*(z^*, s^*) + M^*(z^*, s^*)\frac{\partial \delta h_{\mathrm{l}}^*(z^*, s^*)}{\partial z^*} = \frac{N_{\mathrm{Zu}}}{N_{\mathrm{flash}}}[\delta M^*(z^*, s^*) - \delta q'^*(z^*, s^*)] \tag{17}$$

Integrating Eq. (17) from $z^* = 0$ to Z_{bb}^*, and assuming that $\delta h_{\mathrm{l}}^*(z^* = 0, s^*) = 0$, results in:

$$\delta h_{\mathrm{l}}^*(Z_{\mathrm{bb}}^*, s^*) = \frac{N_{\mathrm{Zu}}}{N_{\mathrm{flash}}}\frac{1 - \exp(-s^*\tau_{1\phi,\mathrm{C}}^*)}{s^*}\exp(-s^*\tau_{1\phi,\mathrm{R}}^*)[\delta M_{\mathrm{C,i}}^*(s^*) - \delta q'^*(s^*)] \tag{18}$$

The dimensionless transit time $\tau_{1\phi,\mathrm{C}}^*$ of the one-phase fluid, introduced in Eq. (18), is equal to:

$$\tau_{1\phi,\mathrm{C}}^* = Z_{\mathrm{bb,C}}^*, \quad \text{and} \quad \tau_{1\phi,\mathrm{R}}^* = (Z_{\mathrm{bb,R}}^* - 1)A_{\mathrm{R}}^* \tag{19}$$

Perturbing the pressure difference between the core inlet and the boiling boundary, and applying Eq. (7) leads to:

$$\delta h_{\mathrm{f}}^*(Z_{\mathrm{bb}}^*, s^*) = \frac{\partial \delta h_{\mathrm{f}}^*(Z_{\mathrm{bb}}^*, s^*)}{\partial \delta Z_{\mathrm{bb}}^*, (s^*)}\delta Z_{\mathrm{bb}}^*(s^*) + \frac{\partial \delta h_{\mathrm{f}}^*(Z_{\mathrm{bb}}^*, s^*)}{\partial \delta M_{\mathrm{C,i}}^*(s^*)}\delta M_{\mathrm{C},i}^*(s^*), \quad \text{with}$$

$$\frac{\partial \delta h_{\mathrm{f}}^*(Z_{\mathrm{bb}}^*, s^*)}{\partial \delta Z_{\mathrm{bb}}^*, (s^*)} = \frac{N_{\mathrm{Fr}}}{1 + L_{\mathrm{R}}^*}\left[(1 - b_{\mathrm{R}})\Lambda_{\mathrm{C}} + \frac{1}{N_{\mathrm{Fr}}} + b_{\mathrm{R}}\frac{\Lambda_{\mathrm{R}}}{L_{\mathrm{R}}^* A_{\mathrm{R}}^{*2}}\right] \quad \text{and}$$

$$\frac{\partial \delta h_{\mathrm{f}}^*(Z_{\mathrm{bb}}^*, s^*)}{\partial \delta M_{\mathrm{C},i}^*(s^*)} = 2\frac{N_{\mathrm{Fr}}}{1 + L_{\mathrm{R}}^*}\left\{\Lambda_{\mathrm{C}}[(1 - b_{\mathrm{R}})Z_{\mathrm{bb}}^* + b_{\mathrm{R}}] + \frac{k_{\mathrm{C,i}}}{2} + b_{\mathrm{R}}\frac{k_{\mathrm{C,e}}}{2} + b_{\mathrm{R}}\frac{(Z_{\mathrm{bb}}^* - 1)\Lambda_{\mathrm{R}}}{L_{\mathrm{R}}^* A_{\mathrm{R}}^{*2}}\right\} \tag{20}$$

Perturbing Eq. (13) relates the fluctuations of the liquid and saturation enthalpy at the boiling boundary:

$$\frac{\partial h_{\mathrm{l}}^*(Z_{\mathrm{bb}}^*, 0)}{\partial Z_{\mathrm{bb}}^*}\delta Z_{\mathrm{bb}}^*(s^*) + \delta h_{\mathrm{l}}^*(Z_{\mathrm{bb}}^*, s^*) = \delta h_{\mathrm{f}}^*(Z_{\mathrm{bb}}^*, s^*), \quad \text{where}$$

$$\frac{\partial h_{\mathrm{l}}^*(Z_{\mathrm{bb}}^*, 0)}{\partial Z_{\mathrm{bb}}^*} = -(1 - b_{\mathrm{R}})\frac{N_{\mathrm{Zu}}}{N_{\mathrm{flash}}} \tag{21}$$

according to Eq. (10). Substituting Eq. (18) and Eq. (20) in Eq. (21), and solving for the boiling boundary perturbation, leads to:

$$\delta Z_{\mathrm{bb}}^*(s^*) = \frac{N_{\mathrm{Zu}}((1 - \exp(-s^*\tau_{1\phi,\mathrm{C}}^*))/s^*)\exp(-s^*\tau_{1\phi,\mathrm{R}}^*)[\delta M_{\mathrm{C},i}^*(s^*) - \delta q'^*(s^*)] - N_{\mathrm{flash}}[\partial\delta h_{\mathrm{f}}^*(Z_{\mathrm{bb}}^*, s^*)/\partial\delta M_{\mathrm{C},i}^*(s^*)]\delta M_{\mathrm{C},i}^*(s^*)}{(1 - b_{\mathrm{R}})N_{\mathrm{Zu}} + N_{\mathrm{flash}}[\partial\delta h_{\mathrm{f}}^*(Z_{\mathrm{bb}}^*, s^*)/\partial\delta Z_{\mathrm{bb}}^*(s^*)]} \tag{22}$$

A first-order Padé approximation (Brezinski, 1996) for the exponential function, having a second-order accuracy, is useful to reduce the order of Eq. (22):

$$\exp(-s^*\tau^*) \approx \frac{1 - (\frac{1}{2}\tau^* s^*)}{1 + (\frac{1}{2}\tau^* s^*)} \tag{23}$$

The exponential terms in Eq. (22) are now rewritten, applying Eq. (23):

$$\frac{1 - \exp(-s^*\tau_{1\phi,\mathrm{C}}^*)}{s^*}\exp(-s^*\tau_{1\phi,\mathrm{R}}^*) \approx \frac{\tau_{1\phi,\mathrm{C}}^* - \frac{1}{2}\tau_{1\phi,\mathrm{C}}^*\tau_{1\phi,\mathrm{R}}^* s^*}{1 + \frac{1}{2}(\tau_{1\phi,\mathrm{C}}^* + \tau_{1\phi,\mathrm{R}}^*)s^* + \frac{1}{4}(\tau_{1\phi,\mathrm{C}}^*\tau_{1\phi,\mathrm{R}}^*)s^{*2}} \tag{24}$$

Eq. (24), in combination with Eq. (22), shows that the boiling boundary transfer function is a first-order system, when boiling occurs in the core ($\tau_{1\phi,\mathrm{R}}^* = 0$ in this case). The first-order transfer function that was used in the model without

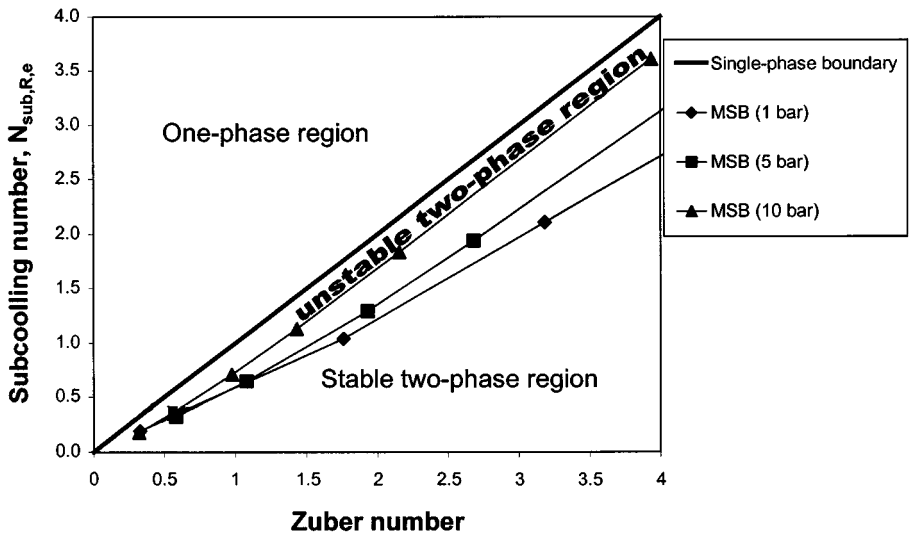

Fig. 4. Stability characteristics of the Dodewaard reactor in the dimensionless Zuber-subcooling plane as predicted by our model. The subcooling number, $N_{\mathrm{sub,R,e}}$, is defined with respect to the pressure at the riser exit.

flashing is derived when we set N_{flash} equal to zero in Eq. (22) and apply Eq. (23):

$$\frac{\delta Z^*_{\mathrm{bb}}(s^*)}{\delta M^*_{\mathrm{C},i}(s^*)} = -\frac{\delta Z^*_{\mathrm{bb}}(s^*)}{\delta q'^*(s^*)} = \frac{\tau^*_{1\phi,\mathrm{C}}}{1+\frac{1}{2}\tau^*_{1\phi,\mathrm{C}}s^*} \tag{25}$$

The boiling boundary transfer function becomes of order two, when the coolant is subcooled in the entire core region and starts boiling in the riser. Substituting Eq. (24) into Eq. (22) and transforming back to the time domain results in a second-order ordinary differential equation for the boiling boundary position:

$$C_{\mathrm{Z},2}\frac{\mathrm{d}^2 Z^*_{\mathrm{bb}}(t^*)}{\mathrm{d}t^{*2}} + C_{\mathrm{Z},1}\frac{\mathrm{d}Z^*_{\mathrm{bb}}(t^*)}{\mathrm{d}t^*} + C_{\mathrm{Z},0}(Z^*_{\mathrm{bb}}(t^*) - Z^*_{\mathrm{bb}})$$
$$= C_{\mathrm{M},2}\frac{\mathrm{d}^2 M^*_{\mathrm{C,i}}(t^*)}{\mathrm{d}t^{*2}} + C_{\mathrm{M},1}\frac{\mathrm{d}M^*_{\mathrm{C,i}}(t^*)}{\mathrm{d}t^*} + C_{\mathrm{M},0}(M^*_{\mathrm{C,i}}(t^*) - 1) + C_{\mathrm{Q},1}\frac{\mathrm{d}q'^*(t^*)}{\mathrm{d}t^*} + C_{\mathrm{Q},0}(q'^*(t^*) - 1) \tag{26}$$

The coefficients of this equation are provided in Appendix C.

4. Stability characteristics of the Dodewaard natural circulation BWR

As an example, the model has been implemented in a code (Manera and De Kruijf, 2000) and the stability characteristics of the Dutch Dodewaard reactor at low pressure have been calculated. The Dodewaard reactor was a small natural circulation BWR with a thermal power of 183 MW. This reactor has been in operation from 1968 to 1997. We use the data for this reactor as presented by Van Bragt and Van der Hagen (1998b). Fig. 4 shows the stability of the reactor as predicted by our analytical model in the plane of the dimensionless Zuber number and subcooling number. The subcooling number in Fig. 4 is defined with respect to the saturation conditions at the riser exit (i.e. $N_{\mathrm{sub,R,e}}$ is plotted, see Appendix B). The diagonal in Fig. 4 is the boundary between one- and two-phase flow in this dimensionless plane. The unstable region is the narrow region between the diagonal and the marginal stability boundaries (MSBs) shown in Fig. 4.

Fig. 4 clearly shows that when the pressure

increases the size of the instability region *decreases*. This is to be expected since flashing becomes more important at lower pressures. Note, however, that stability is characterized in terms of the dimensionless Zuber and subcooling numbers. In Fig. 5 exactly the same data are shown as a function of the power level and the degree of subcooling of the fluid (again with respect to the saturation temperature at the riser exit). In Fig. 5, the size of the instability region for 10 bar is the smallest, but the size of the instability region is actually *larger* for 5 bar than for 1 bar. This may seem surprising, since the size of the unstable region decreases with increasing pressure in the dimensionless plane shown in Fig. 4. Note, however, that the Zuber and subcooling numbers used in Fig. 4 are strongly depending on the actual pressure level themselves. This explains the different effect of changing the pressure on the size of the unstable zones in Figs. 4 and 5. These results show that one should be careful in quantifying instability regions with respect to dimensionless numbers.

Note that the dynamical model described in this paper neglects single-phase convection. We expect single-phase convection to become important at low power levels, however. A simple steady-state model in which single-phase density differences are taken into account shows for example that the boundary between one- and two-phase flow at 5 K subcooling is located at about 28 MW (i.e. close to the MSB as predicted by our dynamical model in case of a pressure of 10 bar). So, it would be very interesting to extend our dynamical model with single-phase convection in order to have a more accurate determination of the instability region.

5. Conclusions

The developed theoretical model for flashing-induced oscillations in natural circulation BWRs can be summarized at this point. The two-phase flow dynamics is governed by Eqs. (5) and (6), stating the conservation of mass and energy in the two-phase nodes. Conservation of momentum in a natural circulation system implies that the total pressure drop over the core, the riser, and the downcomer sections is equal to zero.

A time-domain expression for the (linearized) boiling boundary dynamics is provided by Eq. (26). The models for neutron kinetics and fuel dynamics that have been used previously in the

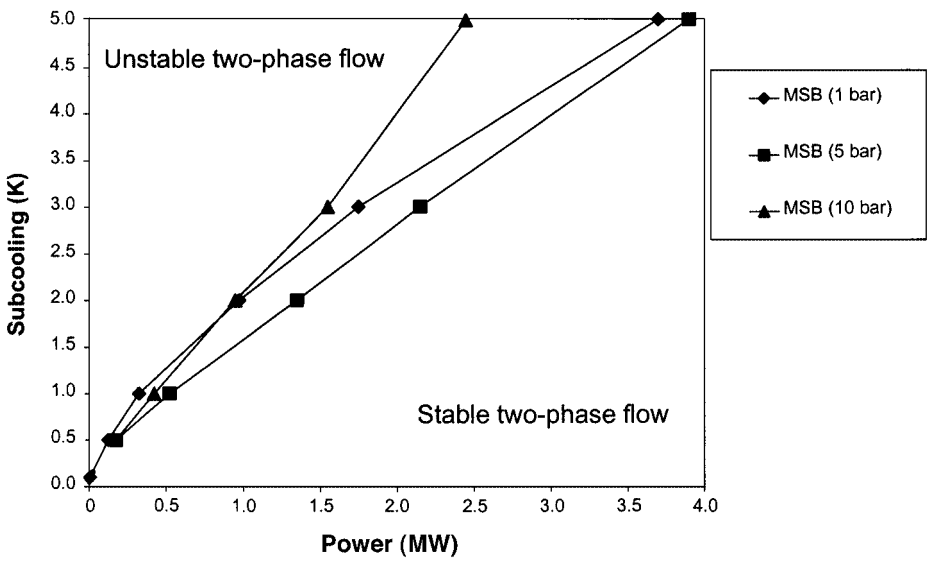

Fig. 5. Stability characteristics of the Dodewaard reactor in the power-subcooling plane as predicted by our model. The subcooling is again defined with respect to the pressure at the riser exit.

natural circulation BWR model without flashing, can be coupled directly with this thermohydraulic model. However, nuclear feedback effects are important only when the coolant reaches the boiling point before the core outlet, and can be neglected if ex-core boiling occurs due to flashing in the riser.

The model can be used for parameter studies in the low-power, low-pressure operating range of a natural circulation BWR. As an example the stability characteristics of the Dodewaard reactor have been determined at low pressure. The size of the instability region in the dimensionless plane decreases as the pressure increases. However, in the power-subcooling plane this dependence is not straightforward. Some comparisons with a steady-state model for single-phase convection show that it would be very interesting to take single-phase density differences into account in our model.

Appendix A. Nomenclature

A	cross-sectional flow area (m^2)
b_R	determines whether boiling occurs in the core ($b_R = 0$) or in the riser ($b_R = 1$)
C	coefficients for Eq. (26), defined in Appendix C
g_c	gravitational acceleration ($m\ s^{-2}$)
h	enthalpy ($J\ kg^{-1}$)
k	local pressure drop coefficient
L	length (m)
M	mass flux density ($kg\ m^{-2}\ s^{-1}$)
N_R	number of nodes in the riser
P	pressure ($kg\ m^{-1}\ s^{-2}$)
q'	linear power transferred from fuel to coolant ($J\ s^{-1}\ m^{-1}$)
s	Laplace variable (s^{-1})
t	time (s)
Z_{bb}	boiling boundary position (m)
z	axial position (m)

Greek

α	void fraction
$\delta(z)$	Dirac's delta function
Δ	(steady-state) riser node height
Λ	frictional number
ρ	density ($kg\ m^{-3}$)
τ	transit time (s)
χ	quality

Subscripts and superscripts

1ϕ	one-phase fluid
C	core
D	downcomer
e	exit
f	saturated liquid
fg	difference between vapor and (saturated) liquid properties
g	vapor
i	inlet
l	liquid
R	riser
*	normalized

Operators

δ	fluctuating part
$\langle\rangle$	average

Dimensionless numbers

N_{Fr}	Froude number
N_{flash}	flashing number
N_{sub}	subcooling number
N_{Zu}	Zuber number
N_ρ	density ratio number

Appendix B. Dimensionless numbers and variables

The dimensionless numbers and variables in the BWR model are given by Van Bragt and Van der Hagen (1998a) and in this Appendix. The vapor and liquid densities (ρ_l and ρ_g) and the evaporation enthalpy (h_{fg}) are assumed to be constant in the flow loop. These properties are evaluated at the core inlet. However, alternative definitions, for instance with respect to the local pressure at the riser exit, are also possible. Since the pressure dependence of the saturation enthalpy is accounted for in the low-pressure model, the dimensionless subcooling of the fluid with respect to the riser exit, $N_{sub,R,e}$ will differ from the core-inlet subcooling $N_{sub,C,i}$. The difference between $N_{sub,C,i}$ and $N_{sub,R,e}$ is equal to the flashing number N_{flash}. This number is assumed to be zero in the high-pressure model (i.e. $N_{sub,R,e} = N_{sub,C,i}$).

$$N_{\mathrm{Zu}} \equiv \frac{L_{\mathrm{C}} q'_{\mathrm{C}}}{A_{\mathrm{C}} M_{\mathrm{C,i}} h_{\mathrm{fg,C,i}}} \frac{\rho_{\mathrm{f,C,i}} - \rho_{\mathrm{g,C,i}}}{\rho_{\mathrm{g,C,i}}},$$

$$N_{\mathrm{Fr}} \equiv \frac{(M_{\mathrm{C,i}}/\rho_{\mathrm{f,C,i}})^2}{g_{\mathrm{c}} L_{\mathrm{C}}}, \qquad N_{\rho} \equiv \frac{\rho_{\mathrm{g,C,i}}}{\rho_{\mathrm{f,C,i}}},$$

$$N_{\mathrm{sub,C,i}} \equiv \frac{h_{\mathrm{f,C,i}} - h_{\mathrm{l,C,i}}}{h_{\mathrm{fg,C,i}}} \frac{\rho_{\mathrm{f,C,i}} - \rho_{\mathrm{g,C,i}}}{\rho_{\mathrm{g,C,}i}},$$

$$N_{\mathrm{sub,R,e}} \equiv \frac{h_{\mathrm{f,R,e}} - h_{\mathrm{l,C,i}}}{h_{\mathrm{fg,C,i}}} \frac{\rho_{\mathrm{f,C,i}} - \rho_{\mathrm{g,C,i}}}{\rho_{\mathrm{g,C,i}}},$$

$$N_{\mathrm{flash}} \equiv N_{\mathrm{sub,C,i}} - N_{\mathrm{sub,R,e}} = \frac{h_{\mathrm{f,C,i}} - h_{\mathrm{f,R,e}}}{h_{\mathrm{fg,C,i}}} \frac{\rho_{\mathrm{f,C,i}} - \rho_{\mathrm{g,C,i}}}{\rho_{\mathrm{g,C,i}}},$$

$$h^*(t^*) = \frac{h(t^*) - h_{\mathrm{f,C,i}}}{h_{\mathrm{f,R,e}} - h_{\mathrm{f,C,i}}} \tag{B.1}$$

Appendix C. Coefficients of Eq. (26)

The coefficients of the ordinary differential Eq. (26) for the boiling boundary are listed in this appendix. The partial derivatives of the saturation enthalpy, see Eq. (20), are used to simplify the expressions for these coefficients:

$$C_{\mathrm{Z,0}} = (1 - b_{\mathrm{R}}) N_{\mathrm{Zu}} + N_{\mathrm{flash}} \frac{\partial \delta h_{\mathrm{f}}^*(Z_{\mathrm{bb}}^*, s^*)}{\partial \delta Z_{\mathrm{bb}}^*(s^*)},$$

$$C_{\mathrm{Z,1}} = C_{\mathrm{Z,0}} \frac{1}{2} (\tau_{1\phi,\mathrm{C}}^* + \tau_{1\phi,\mathrm{R}}^*),$$

$$C_{\mathrm{Z,2}} = C_{\mathrm{Z,0}} \frac{1}{4} \tau_{1\phi,\mathrm{C}}^* \tau_{1\phi,\mathrm{R}}^*, \qquad C_{\mathrm{Q,0}} = -N_{\mathrm{Zu}} \tau_{1\phi,\mathrm{C}}^*,$$

$$C_{\mathrm{Q,1}} = N_{\mathrm{Zu}} \frac{1}{2} \tau_{1\phi,\mathrm{C}}^* \tau_{1\phi,\mathrm{R}}^*,$$

$$C_{\mathrm{M,0}} = N_{\mathrm{Zu}} \tau_{1\phi,\mathrm{C}}^* - N_{\mathrm{flash}} \frac{\partial \delta h_{\mathrm{f}}^*(Z_{\mathrm{bb}}^*, s^*)}{\partial \delta M_{\mathrm{C},i}^*(s^*)},$$

$$C_{\mathrm{M,1}} = \frac{1}{2} (\tau_{1\phi,\mathrm{C}}^* + \tau_{1\phi,\mathrm{R}}^*)(C_{\mathrm{M,0}} - N_{\mathrm{Zu}} \tau_{1\phi,\mathrm{C}}^*) - N_{\mathrm{Zu}} \frac{1}{2} \tau_{1\phi,\mathrm{C}}^* \tau_{1\phi,\mathrm{R}}^*,$$

$$C_{\mathrm{M,2}} = \frac{1}{4} \tau_{1\phi,\mathrm{C}}^* \tau_{1\phi,\mathrm{R}}^* (C_{\mathrm{M,0}} - N_{\mathrm{Zu}} \tau_{1\phi,\mathrm{C}}^*) \tag{C.1}$$

References

Andersen, J.G.M., Klebanov, L.A., 1995. TRACG Analyses of Flashing Instability During Start-Up, Proc. 3rd Int. Conf. Nuclear Engineering (ICONE-3).

Brezinski, C., 1996. Extrapolation algorithms and padé approximations: a historical survey. Appl. Numer. Math. 20, 299.

De Kruijf, W.J.M., Van der Hagen, T.H.J.J., Mudde, R.F., 1999. CIRCUS, a Natural Circulation Two-Phase Flow Facility, Proc. Eurotherm Seminar No. 63.

Fukuda, K., Kobori, T., 1979. Classification of two-phase flow instability by density wave oscillation model. J. Nucl. Sci. Technol. 16 (2), 95–108.

Furuya, M., Inada, F., Yasuo, A., 1995. Density wave oscillations of a boiling natural circulation loop induced by flashing, Proc. 7th Int. Mtg. Nuclear Reactor Thermal-Hydraulics (NURETH-7), p. 923.

Inada, F., Ohkawa, T., 1994. Thermo-hydraulic instability of natural circulation BWRs (explanation on instability mechanisms at start-up by homogeneous and thermo-dynamic equilibrium model considering flashing effect), Proc. Int. Conference on New Trends in Nuclear System Thermohydraulics, p. 187.

Inada, F., Furuya, M., Yasuo, A., Tabata, H., Yoshioka, Y., Kim, H.T., 1995. Thermo-hydraulic instability of natural circulation BWRs at low pressure start-up: experimental estimation of instability region with test facility considering scaling law, Proc. 3rd Int. Conf. Nuclear Engineering (ICONE-3), p. 173.

Jiang, S.Y., Emendörfer, D., 1993. Subcooled boiling and void flashing in a natural circulation system at heating reactor conditions. Kerntechnik 58, 273.

Jiang, S.Y., Emendörfer, D., 1996. Analysis of flow oscillations in a natural circulation system taking account of non equilibrium boiling and void flashing. Kerntechnik 61, 23.

Jiang, S.Y., Wu, X.X., Wu, S.R., Bo, J.H., Zhang, Y.J., Han, P., 1997. Experimental study on flashing concerned instability in a natural circulation system at nuclear heating conditions. Kerntechnik 62, 148.

Manera, A., De Kruijf, W.J.M., 2000. User Manual Time Domain Model for Low Pressures, DAVID_LP version 99_2, IRI-131-99-010 (Rev. 1), Interfaculty Reactor Institute, Delft University of Technology.

Manera, A., De Kruijf, W.J.M., Van der Hagen, T.H.J.J. Mudde, R.F., 2000. Experiments with the CIRCUS-facility on flashing-induced instabilities during start-up of natural-circulation-cooled BWRs, Proc. PHYSOR 2000 (CDROM)

Van Bragt, D.D.B., 1998. Analytical Modeling of Boiling Water Reactor Dynamics, Delft University Press, (ISBN: 90-407-1719-2).

Van Bragt, D.D.B., Van der Hagen, T.H.J.J., 1998a. Stability of natural circulation boiling water reactors. Part I—description stability model and theoretical analysis in terms of dimensionless groups. Nucl. Technol. 121, 40.

Van Bragt, D.D.B., Van der Hagen, T.H.J.J., 1998b. Stability of natural circulation boiling water reactors. Part II—

parametric study of coupled neutronic-thermohydraulic stability. Nucl. Technol. 121, 52.

Van der Hagen, T.H.J.J., Stekelenburg, A.J.C., Kaart, S., Schouten, J.C., 1996. Investigations on start-up flow oscillations in natural circulation BWRs. Proc. Natl. Heat Transfer Conf. 9, 188.

Van der Hagen, T.H.J.J., Van Bragt, D.D.B., Van der Kaa, F.J., Karuza, J., Killian, D., Nissen, W.H.M., Stekelenburg, A.J.C., Wouters, J.A.A., 1997. Exploring the Dodewaard type-I and type-II stability; from start-up to shut-down, from stable to unstable. Ann. Nucl. Energy 24, 8.

Wang, D.Z., Ma, C.W., Dong, D., Ling, J.G., 1990. A 5-MW Nuclear Heating Reactor. Trans. Am. Nucl. Soc. 61, 468.

Wouters, J.A.A., Morales, J.B., Kim, H.T., 1996. TRACG Simulation of the February 1992 Startup of the Dodewaard Natural Circulation BWR, Proc. 4th Int. Conf. Nuclear Engineering (ICONE-4), p. 149.